UNIVERSIDADE DE BRASÍLIA – UnB

INSTITUTO DE GEOCIÊNCIAS – IG

PROGRAMA DE PÓS-GRADUAÇÃO EM GEOLOGIA

ESTUDOS PETROLÓGICOS DO COMPLEXO DE MAURICE EWING BANK

Mateus Rodrigues de Vargas

Dissertação de Mestrado Nº437

Orientador: Prof° Dr. Farid Chemale Júnior (UnB)

Banca Examinadora: Profª Drª Maria Emília S. Della (UnB)

Profº Dr. Leo Afrâneo Hartmann (UFRGS)

Suplente: Profº Dr. Reinhardt Adolfo Fuck (UnB)

Brasília – DF

Maio de 2019

AGRADECIMENTOS

Marina Kirsch, agradeço pelo amor, paciência, suporte, companheirismo, *coaching,* silêncio, carinho, amizade e inúmeras outras faculdades morais relacionadas a ti. Te amo. Tu és meu maior tesouro.

Agradeço ao afeto silencioso de meus filhos felinos, com muito amor: Oby Fabiane e Charlly.

Agradeço ao meu orientador, Faridão, pelo suporte intelectual e logístico dado a este trabalho e pelos sábios conselhos e puxões de orelha relacionados à vida profissional e ao *Homo geologensis.*

À minha mãe, Bernadete, por ser sempre um exemplo de força de vontade, superação e amor Ágape. Obrigado por ser minha mãe.

À grande amiga (e poderosa chefona) Ariane Santos da Silveira, agradeço teus conselhos sobre a vida e ao teu suporte *Giganewtoniano* à minha carreira profissional.

André e Bruna, meus queridos irmãos, obrigado pelo amor e carinho. Sei que sempre posso contar com vocês. Nossas diferenças nos fazem mais fortes. Amo-os.

À família Kirsch Ohlweiler (e agregados), minha família em lei, Ana, Raul, Claudio, July, Augusta, Débora, Jessé, Bruno, Songa, Nina, Chico, Filó e Boris, obrigado pelo amor.

Agradeço aos meus antepassados.

Aos meus colegas de trabalho Zeca, Gustavo, Vanessa, Fran, Felipe, Lucas e Dante, obrigado pela paciência.

Aos amigos de longa jornada, direto do grande reino: Rafael, Duko's, Paulu's, Ananá e Marlon. Nenhuma noitada foi em vão.

Aos geólogos de peso (em termos de massa) Tiago Girelli e Henrique Serratt pelas discussões sobre o estado da arte, métodos, aquisição de dados e (principalmente) pela amizade.

Agradeço a equipe técnica dos laboratórios de DRX-UnB e Microssonda eletrônica-UnB em especial a Isabella e Gabriela. Obrigado pela paciência!

Ao pai Walmor, obrigado pelos 23 pares de cromossomos.

Aos professores e colegas da UnB.

A Wegener e Du Toit

RESUMO

Mateus Rodrigues de Vargas, 2019. Estudos Petrológicos do Complexo de Maurice Ewing Bank. Dissertação de Mestrado, Programa de Pós-Graduação em Geologia, Universidade de Brasília, 167 pp. Data 17/05/2019. Orientador Farid Chemale Júnior.

A evolução do Rodínia ainda possui diversas questões que permanecem incógnitas, afetando diretamente as interpretações paleotectônicas dos eventos geológicos contemporâneos e posteriores. Este é o caso, por exemplo, do papel da crosta Mesoproterozóica não aflorante ou, ainda, de terrenos remanescentes como Maurice Ewing Bank e suas relações com o evento formador do Rodínia. Este trabalho visa refinar, definir e interpretar as rochas do Complexo de Maurice Ewing Bank (CMEB) com aplicação de estudos petrológicos e geoquímicos. Para assim definir sua trajetória de recristalização/deformação, comparar CMEB com as principais unidades da orogenia de Natal-Maud e tecer considerações sobre os blocos envolvidos no processo. CMEB consiste de um terreno metamórfico polifásico com três ciclos de recristalização. O ciclo formador do Rodínia (R) tem um episódio de deposição e quatro episódios de recristalização e/ou deformação progressiva identificados: [1] deposição de paraderivados, em ambiente de back-arc, próximo à área fonte (R0); [2 e 3] período de longa exposição à alta temperatura e pressão, relacionado com cinturão de cavalgamento e dobramento (R1 e R2); [4] fim do evento colisional, caracterizado pela ocorrência de granitóides pós-orogênicos (R4). Nós interpretamos que R1 e R2 coincidem com a mais velha idade adquirida nos granitoides sin- a tardi-deformacionais de 1068 ± 28 Ma. Um evento de exumação tectônica, em R3, é relacionado com a idade dos granitóides sin- a tardi-deformacionais em 1032 ± 12 Ma. Subsequentemente, o evento R4 é relacionado com delaminação crustal em 1006 ± 13 Ma. O reset nos sistemas Rb-Sr e K-Ar foi gerado por um ciclo metamórfico posterior, na facies Xisto Verde. Nós o interpretamos como causado por anomalias termais distais associadas com eventos Neoproterozóicos-Paleozóicos como orogenias Panantárticanas-Panafricanas-Gondwanides. O ciclo anquimetamórfico, abaixo de 300ºC, é relacionado com eventos ainda incompreendidos de rifteamento na região, de idade Juro-Cretáceo. CMEB, na transição Meso- Neoproterozóico constitui a frente deformacional da orogenia Natal-Maud, estando entre dos terrenos Margate e Heimefrontfjella. Sugerimos que a colisão entre os crátons de Kaapvaal e Coats-Patagônia geraram não somente as rochas Mesoproterozóicas de Dronning Maud Land Oeste, mas também as de CMEB, Província Natal, Complexo de Cape Meredith e as rochas que geraram a anomalia de Beattie-A. O bloco de Patagônia consiste de apêndice entre Laurentia e Coats-Land. Portanto, a orogenia de Natal-Maud deve ser considerada como Grenviliana.

Palavras-chave: DSDP Sítio 330; Cráton Kalahari; Ilhas Falkland-Malvinas; Bloco Falkland-Malvinas Maurice; F2MT; Orogenia Natal-Maud, Orogenia Grenville; Supercontinente Rodínia.

ABSTRACT

Mateus Rodrigues de Vargas, 2019. Petrological Studies of Maurice Ewing Bank Complex. Master Thesis, Programa de Pós-Graduação em Geologia, Universidade de Brasília, 167 pp. Date 05/17/2019. Thesis Advisor: Farid Chemale Júnior.

The evolution of Rodinia still have several questions that remain *incognito,* which directly impact the paleotectonic interpretation of coeval and posterior events. That is the case, for example, the role of either the unexposed Mesoproterozoic crust or remnant micro-terranes such as Maurice Ewing Bank and its relationship with the Rodinia-forming orogens. This works aims to characterize and interpret the igneous-metamorphic basement of Maurice Ewing Bank Complex (MEBC), using petrology and geochemistry. Thereby defining their recrystallization/deformation time path, comparing with the main units from Natal-Maud belt orogeny, and extrapolating the blocks involved in the regional metamorphism process. MEBC consist of a polyphasic metamorphic terrane with three recrystallization cycles. The Rodinia-forming cycle (R) has one episode of deposition and four episodes of recrystallization and/or progressive deformation identified: [1] deposition of immature sediments, in a back-arc environment, close to the source rock (R0); [2 and 3] long-lasting high-temperature, high-pressure metamorphic condition, related with a fold-and-thrust belt (R1-R2). [4] metamorphic climax up-to granulite facies metamorphism (R3). [4] end of the collisional event, characterized by post-deformational granitoids (R4). We interpret that R1-R2 coincides with the older syn-deformational granitoid age of 1068 ± 28 Ma. A tectonic exhumation in R3 is related to syn- to tardi-granitoids at 1032 ± 12 Ma. It was followed by an R4 event of crustal delamination at 1006 ± 13 Ma. The reset in Rb-Sr and K-Ar systems were due to posterior metamorphic cycle, in the greenschist facies. We interpret that as caused by far-field thermal anomalies of Neoproterozoic-Paleozoic orogenic events, such as Panantarctican-Pananfrican-Gondwanides. The anchimetamorphic cycle, below 300ºC, is related to still uncomprehended Jurassic-Cretaceous events of rifting in the region. MEBC constituted the deformational front of Natal-Maud orogeny by the end of Mesoproterozoic, standing right on the middle of Margate and Heimefrontfjella terranes. We suggest that the collision of Kaapvaal and Coats-Patagônia cratons generated not only Dronning Maud Land Mesoproterozoic rocks, but also MEBC, Natal Province, Cape Meredith Complex, and rocks that generates Beattie-A anomaly. Coats-Patagônia consisted of a Laurentian appendix. Thus, MEBC and Natal-Maud should also be addressed as Grenvillian.

Keywords: DSDP Site 330; Kalahari Craton; Falkland-Malvinas Islands; Falkland-Malvinas-Maurice Block; F2MT; Grenville Orogeny; Natal-Maud Orogeny, Rodinia Supercontinent.

LISTA DE FIGURAS

LISTA DE FIGURAS DO MANUSCRITO

LISTA DE TABELAS

1

SUMÁRIO:

1 INTRODUÇÃO

Rodínia é uma palavra russa polissêmica. De maneira geral, significa *to beget* ou ainda *to grow* (Li et al., 2008; McMenamin e McMenamin, 1990). Isto é, representa não apenas crescimento, mas também o desenvolvimento natural da maturidade. Seu sentido foi incorporado à geologia, representando uma configuração hipotética de massas continentais com ápice entre a transição Meso-Neoproterozóico. Durante este período, diversos blocos se amalgamaram para formar um supercontinente através de um processo chamado “orogeneses formadoras do Rodínia” (a.k.a. *Rodínia-forming orogens*; Li et al., 2008; Roberts et al., 2015). No entanto, diversas “crias” continentais de menor escala ainda são consideradas “bastardas”. Isto é, unidades geológicas que ainda não são consideradas em reconstruções paleotectônicas, devido à pouca representatividade em área ou ainda desconhecimento geral acerca da área (Fuck et al., 2008; Li et al., 2008).

Nesse contexto emerge o embasamento ígneo-metamórfico recuperado ao oeste do Platô de Falkland, mais precisamente no Banco de Maurice Ewing (*Maurice Ewing Bank*), durante a campanha de perfuração do *Deep-Sea Drilling Project* (DSDP) 330, foco deste estudo. Os dados geológicos, geoquímicos e geocronológicos e interpretações iniciais foram apresentados em Barker et al. (1977a, 1977b) e Beckinsale et al. (1977). Mais recentemente, Chemale Jr. et al. (2018) realizam estudos geocronológicos com maior precisão e exatidão, que serviram de base para o presente estudo. As rochas recuperadas foram inicialmente datadas por método Rb-Sr e K-Ar em rocha total como representativas do período Ediacarano-Fortuniano por Beckinsale et al. (1977). No entanto, Chemale Jr. et al. (2018), com aplicação do método U-Pb e Lu-Hf em zircão, reinterpreteram-nas como metamorfizadas e, quando aplicado, geradas por um evento regional de idade Esteniano com contribuição de crosta juvenil e retrabalhada. Este fato levou a reinterpretação tectônica da região, relacionando as rochas do embasamento de Maurice Ewing Bank com as rochas de Cape Meredith Complex (Ilhas Falkland; Chemale Jr. et al., 2018). Os aspectos petrográficos, no entanto, foram estudados unicamente por Tarney (1977), que identificou um evento metamórfico de alto grau. Desde os estudos pioneiros de Tarney, as rochas de MEBC não foram revisitadas.

1.1 Objetivos

Este trabalho visa estudar, definir e interpretar as rochas Mesoproterozóicas advindas do embasamento de Maurice Ewing Bank (Maurice Ewing Bank Complex – MEBC; Chemale Jr. et al., 2018), usando petrografia e geoquímica. Para que, deste modo, defina-se o ambiente da formação das rochas, bem como a trajetória de recristalização/deformação ao longo do tempo (PTt) para que se possa estabelecer com maior precisão os processos tectono-metamórficos envolvidos na geração do MEBC e, ao mesmo tempo, comparar com terrenos adjacentes da orogenia Natal-Maud (1.2-1.0 Ga).

2 GEOLOGIA REGIONAL

O Planalto das Malvinas é uma projeção submarina da margem continental da América do Sul que se extende por aproximadamente 1800 km a leste das Ilhas Malvinas. Ao norte, é limitado por uma escarpa transformante com tendência W-E, chamada de Zona de Falha de Malvinas/Agulhas (*Malvinas-Agulhas Fracture Zone* - MAF), que acomoda uma feição de 1400 km de extensão que limita a interface continente-oceano da Plataforma Argentina (Kimbell e Richards, 2008). Ao Sul, por outro lado, é diretamente limitado pelo *North Scotia Ridge* (NSR). Possui suave mergulho em direção leste. No entanto, em seu extremo leste, há uma estrutura morfológica chamada Maurice Ewing Bank (MEB; Barker, Dalziel e Wise, 1974; Ludwig, Krasheninnikov *et al*., 1983). O sítio 330, realizado nas coordenadas 50º55.19'S, 46º53.00'W, localiza-se a oeste desse alto morfoestrutural e consiste de dois *cores,* 16 e 17 (Figura 1).

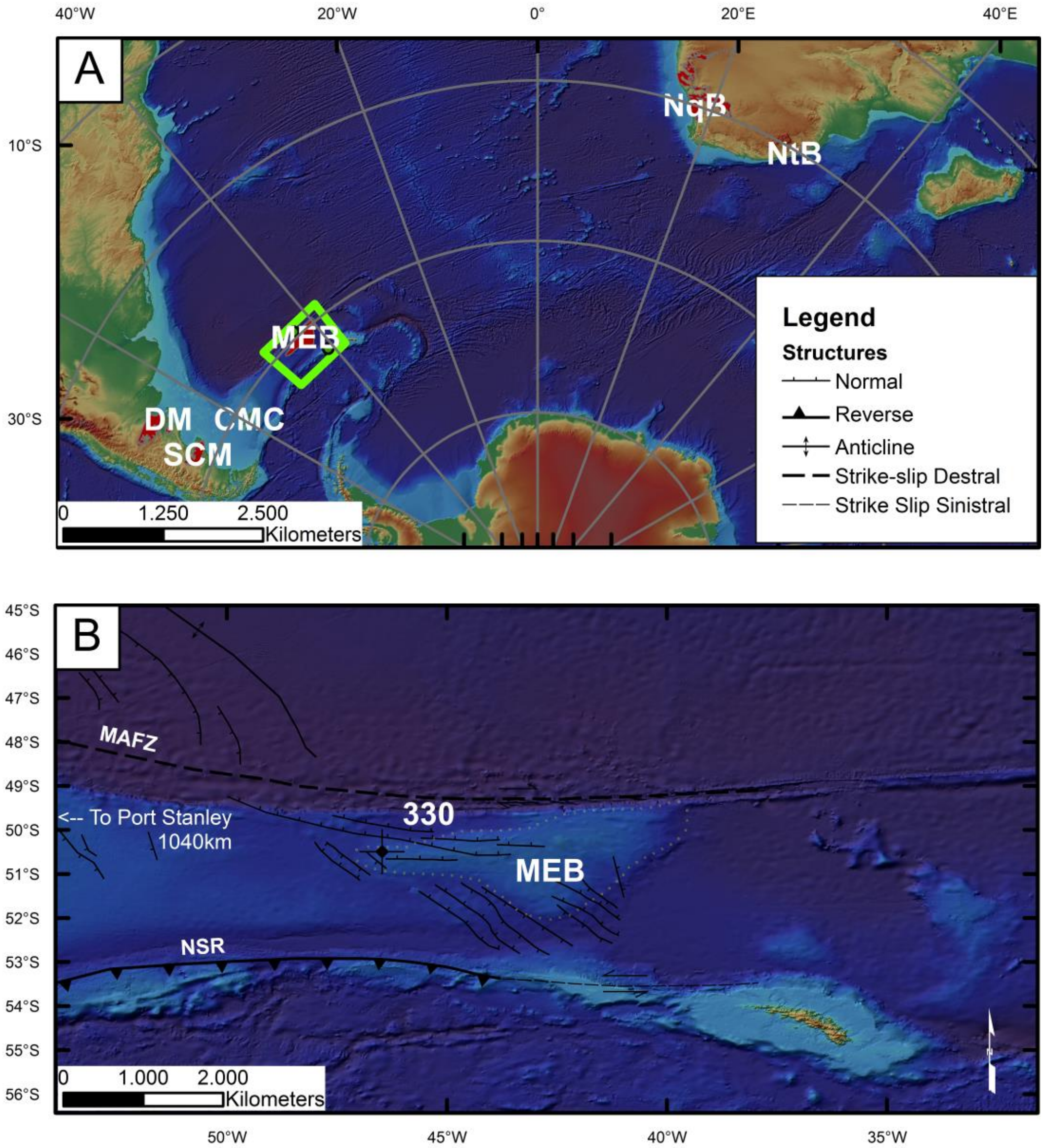

Figura 1 – A) Localização geográfica do Maurice Ewing Bank e terrenos com assinaturas isotópicas e/ou idades que remontam o Mesoproterozoico, utilizando a Projeção Antártica Cônica de Lambert; B) Localização do site 330 que engloba os *cores* 16-17. Legenda das abreviações: DM - Deseado Massif, SCM: Somun Cura Massif, CMC – Cape Meredith Complex, MEB - Maurice Ewing Bank, NqB - Namaqua Belt, NtB – Natal Belt. Estruturas: MAFZ – Malvinas-Agulha Fault Zone, NSR – North Scotia Ridge.

Após ultrapassar uma lâmina d’água de 2626 m, foram perfuradas, então, 550 m de rochas sedimentares que representaram, em sua maioria, um registro deposicional de idade sin- a pós-Jurássica. Após perfuração e testemunhagem do material sedimentar, 19,5 m de embasamento gnáissico-granítico foram atingidos, claramente representando a ínfima parcela de um complexo ígneo-metamórfico continental de idade Pré-Cambriana, afetado por eventos termais em diversos momentos durante o Eratema Paleozóico (Barker et al., 1977a). O material utilizado neste estudo derivará desta parcela do embasamento.

2.1 Bloco Falkland (Malvinas)

A única exposição Mesoproterozóica das Ilhas Malvinas consiste de delgada seção aflorante, encontrada na porção sul da *West Falkland (Malvinas) Islands* (Figura 2), chamada de Cape Meredith Complex. Thomas et al. (1997) mapearam e classificaram as rochas em duas unidades litoestratigráficas distintas. Subsequentemente, Jacobs et al. (1999) as dataram. As unidades, conforme Thomas et al. (1997), são: i) Big Cape Fm., principalmente composta de anfibolitos com idades ^{40}Ar-^{39}Ar Bt variando de 1009 ± 14 até 1015 ± 6 Ma intercalados com gnaisses félsicos de idade 1118 ± 8 Ma. Esta unidade representa uma sequência Vulcano-sedimentar que evoluiu durante a transição do Meso-Neoproterozóico (Jacobs et al., 1999); ii) Suite de Granitóides relacionada com três eventos de granitogênese distintos. O primeiro, nomeado G1, é principalmente composto por Bt-Granodioritos localmente deformados que sugerem gênese sin-deformacional, com idades em torno de 1090 Ma (U-Pb em zircão). O G2, composto *sensu latu* por augen-ortognaisses, possui uma idade de 1135 ± 11 Ma U-Pb nos núcleos de zircão, enquanto as bordas possuem idades de 1003 ± 14 Ma. O leucogranito G3 intrude as unidades mais velhas e possui uma idade de cristalização (U-Pb em zircão) que coincide com o evento metamórfico de G2 (1003 ± 14 Ma) (Jacobs et al., 1999). Portanto, o evento metamórfico de G2 e a granitogênese de G3 são resultados de um evento anatético regional (Jacobs et al., 1999; Thomas et al., 2000). ^{40}Ar-^{39}Ar em muscovita e biotita com idades de 989 ± 3 Ma e 989 ± 7 Ma para G2 e G3, respectivamente, sugerindo que Cape Meredith Complex provavelmente foi submetido a um resfriamento abaixo dos ~300ºC em apenas alguns milhões de anos (Jacobs et al., 1999). Não há evidências direta de metamorfismo relacionado com orogenias pós Mesoproterozóicas (Thomas et al., 2000, 1997). Diversos diques lamprofíricos cortam o complexo, com idades que variam do Paleozóico ao Mesozóico (Cingolani e Varela, 1976; Thistlewood et al., 1997; Thomas et al., 2000, 1998).

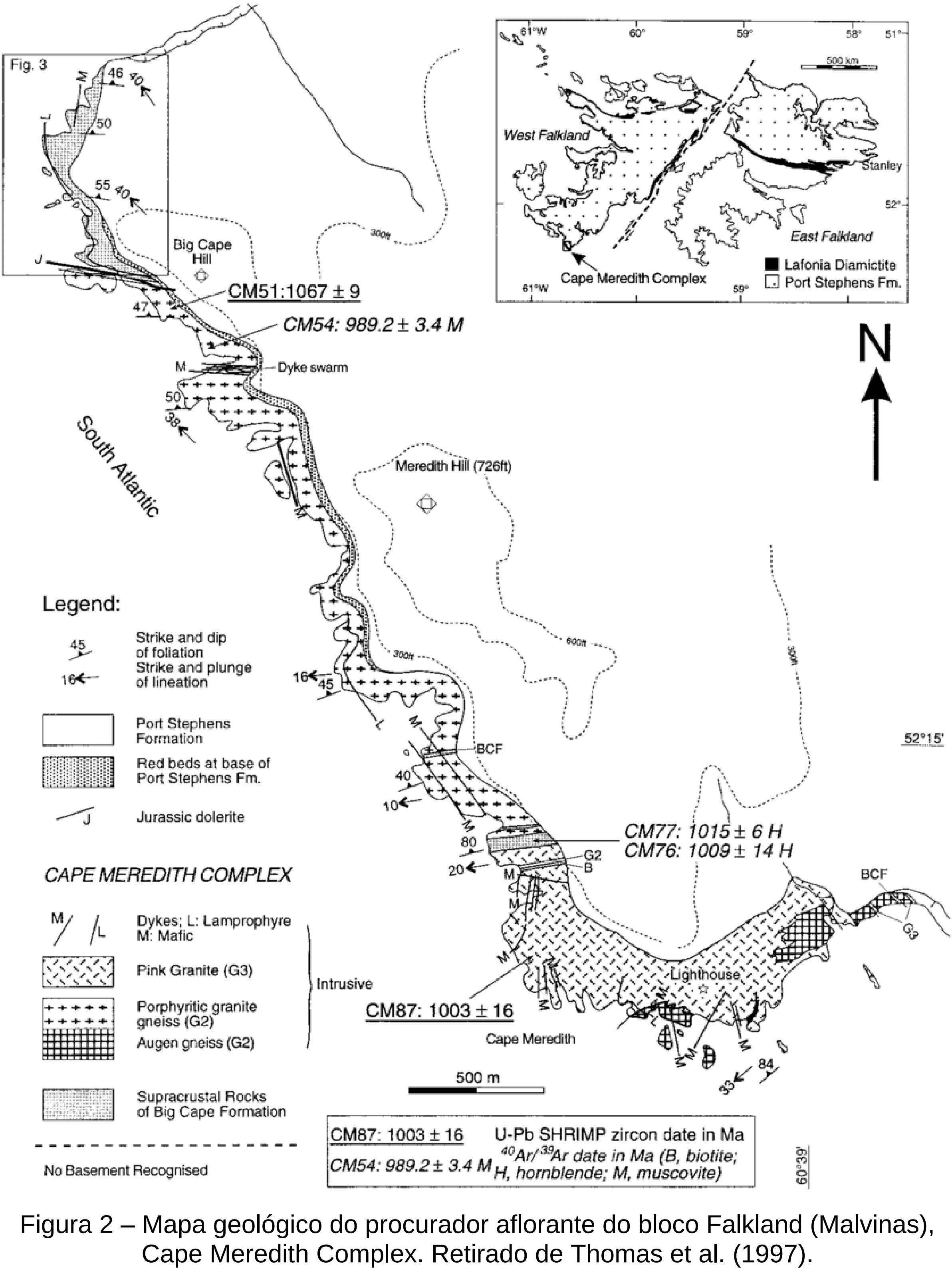

Figura 2 – Mapa geológico do procurador aflorante do bloco Falkland (Malvinas), Cape Meredith Complex. Retirado de Thomas et al. (1997).

2.2 Bloco Agulhas

O Platô de Agulhas Plateau é um alto oceânico situado 500 km SE do Cabo da Boa Esperança, onde, em seu máximo, possui 700 km de comprimento e 400 km de largura (Parsiegla et al., 2008; Figura 3). Atualmente, Barrett (1977), Parsiegla et al. (2008) e Scrutton (1973) sugerem, através de modelagem geofísica reversa, que a porção norte do bloco tem uma composição de crosta oceânica, com idades variando de 80 a 100 Ma (Gohl e Uenzelmann-Neben, 2001; Uenzelmann-Neben et al., 1999). Na parte sul, Parsiegla et al. (2008) identificaram um padrão de crosta fina que pode conter fragmento de crosta continental, sugerindo deste modo um ambiente de crosta superextendida. As únicas rochas de embasamento testemunhadas na região foram descritas por Allen e Tucholke (1981), estando inseridas, na sua maioria, em um contexto de metamorfismo regional, indo de fácies xisto verde até eclogito. Eles dataram dois gnaisses, pelo sistema K-Ar em biotita, obtendo idades de 1074 ± 36 Ma e 1105 ± 36 Ma, respectivamente. Essas idades são relacionadas com o metamorfismo causado pelas orogenias formadoras do Rodínia (Roberts et al., 2015). No entanto, duas amostras resultaram em idades de 478 ± 17 e 498 ± 17 Ma, provavelmente resultado de um *reset* termal relacionado com as orogenias Panafricanas-PanAntárticanas que marcaram o final do Neoproterozóico. É importante enfatizar que os autores se opõem a ideia que as rochas foram transportadas por processos glaciotectônicos. Chemale Jr (pers. commut.) datou-as, através do método U-Pb em zircão, obtendo resultado que variam de 1.2 a 1 Ga, portanto, comprovando a similaridade das rochas com os eventos de amalgamação do Rodínia.

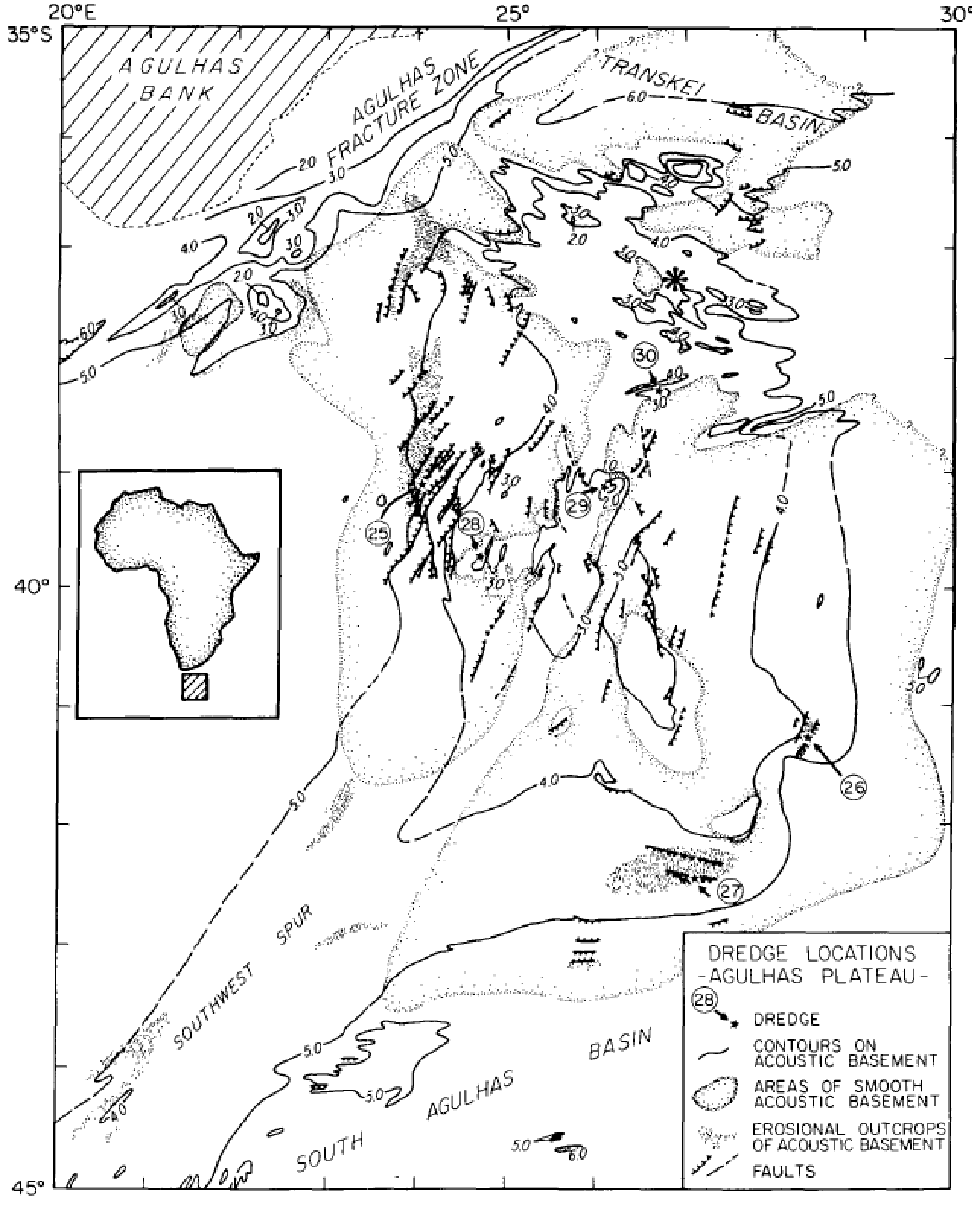

Figura 3 – Localização do Platô de Agulhas. As dragagens de número 25, 26, 27 e 28 possuem amostragem do embasamento Mesoproterozóico. Retirado de Allen e Tucholke (1981).

2.3 Província Natal

A Província Ígneo-Metamórfica Natal localiza-se ao leste da África do Sul e consiste de três terrenos acrescionados, produtos de diversos nappes com trend NE Figura 4. São eles: Tugela, Mzumbe e Margate (Cornell et al., 2006). Esses terrenos foram acrescionados na margem SE do cráton de Kaapval no final do Mesoproterozóico, sendo submetidos a metamorfismo na fácies anfibolito superior até granulito inferior. Posteriormente, foram submetidos a metamorfismo regressivo para a fácies xisto verde (Arima e Johnston, 2001; Cornell et al., 2006; Johnston et al., 2001). Os terrenos Tugela e Mzumbe registram um magmatismo de arco de ilhas entre 1200 Ma e 1160 Ma, seguido pela acresção na margem sul do cráton Kaapval, por volta de 1150 Ma (Arima e Johnston, 2001; Mendonidis et al., 2015). O terreno Margate é relacionado com magmatismo de arco continental até aproximadamente 1120 Ma. Em sucessão, ocorre um vulcanismo bimodal, resultado de eventos extensionais, antecedendo a acresção do terreno na porção sul de Mzumbe, por volta de 1090 Ma. Próximo à zona de sutura, devido a esta configuração colisional, ocorre um metamorfismo de alta temperatura e baixa pressão, com evento de anatexia regional, que levou a criação de grandes volumes de granitos derivados da fusão no limite arco-crosta (Cornell et al., 2006; Mendonidis et al., 2015; Mendonidis e Grantham, 2003; Spencer et al., 2015). Spencer et al. (2015) identificaram que após a acresção e amalgamação do terreno, por volta de 1085 Ma, ocorreu um colapso extensional, caracterizado pela intrusão de corpos máficos e suítes alcalinas intermediárias, produto de tanto *underplating* quanto delaminação da crosta. Isótopos de Nd e Hf sugerem que as rochas magmáticas do Cinturão Natal derivaram de crosta continental juvenil, inicialmente gerada por um magmatismo de arco de ilhas e, subsequentemente, retrabalhada por eventos acrescionários (Mendonidis et al., 2015a).

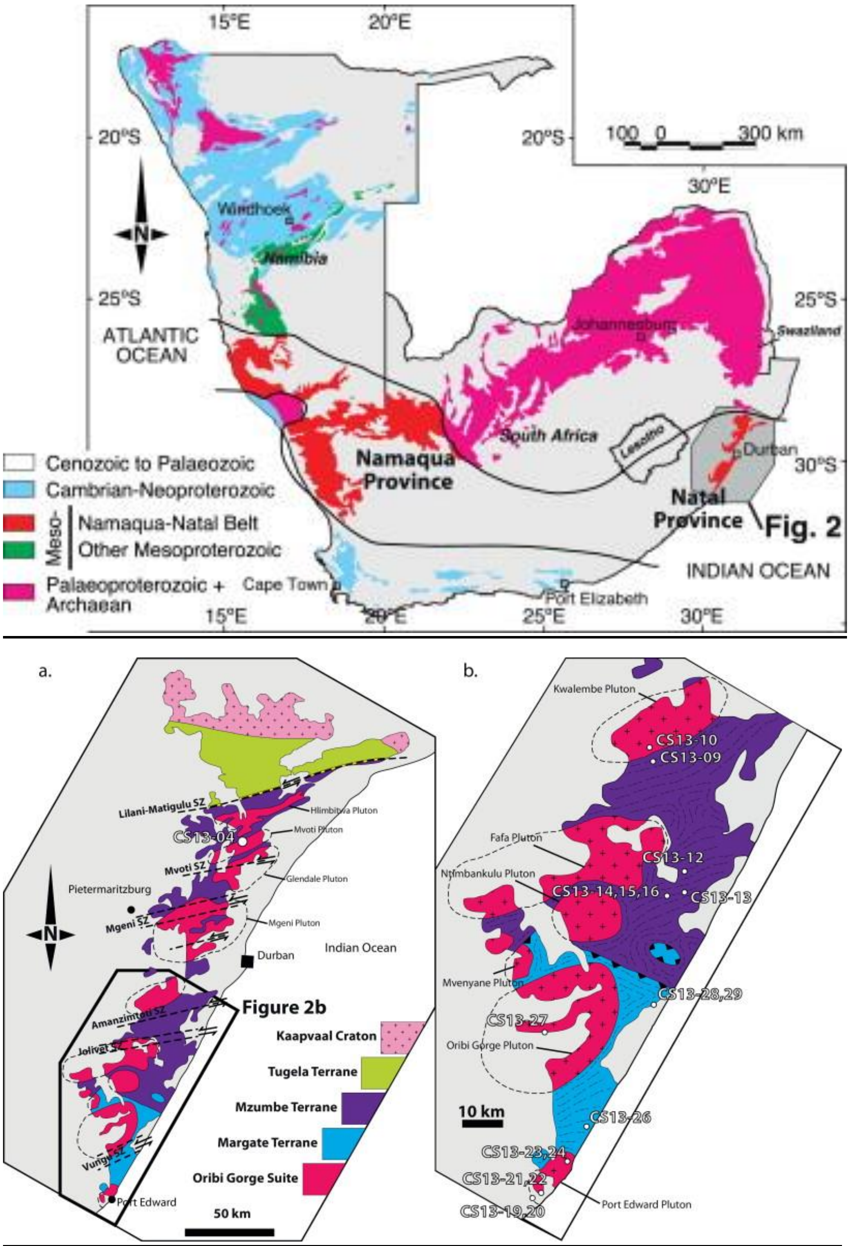

Figura 4 Superior - Localização da Província Natal em relação ao continente Africano. Inferior (a) – Divisão dos três terrenos: Tugela ao norte, Mzumbe no centro e Margata ao sul; (b) Detalhamento da porção sul da província. Retirada de Spencer et al. (2015)

2.4 *Dronning Maud Land* – Terras da Rainha Maud

Constituindo 1/6 da área total do continente Antártico, Dronning Maud Land é uma superprovíncia geológica formada por rochas dominantemente geradas durante o Mesoproterozóico-Neoproterozóico, de gênese complexa remontando acresção e posterior separação de diversos terrenos, simbolizando orogeneses e tafrogêneses de nível intracontinental, ímpares na evolução de supercontinentes como Rodínia, Gondwana e Pangea (Bisnath et al., 2006; Harris, 1999; Harris et al., 1995; Jacobs et al., 2015; Figura 5).

As Terras da Rainha Maud consistem, simplificadamente, de um núcleo Paleoproterozóico, Grunehogna Craton, na qual acredita-se ser um bloco pertencente ao Cráton Kalahari (Jacobs et al., 2008). Adicionalmente, são formadas, de oeste a leste, pelos terrenos Heimefrontfjella (Arndt et al., 1991), Kirwanveggen (Harris, 1999), Sverdrupfjella (Board et al., 2005), Gjelsviksfjella (Bisnath et al., 2006), Mühlig-Hofmannfjella (Owada et al., 2003), Central Dronning Maud Land (Jacobs et al., 2003b) e Sør Rondane (Masao et al., 1996). Genericamente, estes terrenos, com exceção dos dois últimos, representam principalmente a amalgamação, na transição Meso-Neoproterozóico, de um bloco continental desconhecido ao cráton de Kalahari, com metamorfismo regional de alta pressão associado à criação de expressivos volumes de magma (Jacobs et al., 2008). Os blocos Central Dronning Maud Land e Sør Rondane possuem rochas de assinatura isotópica juvenil, além de idades U-Pb mais jovens que os terrenos adjacentes (Jacobs et al., 2003a, 2003b, 2015). Jacobs et al (2015) atribuem estas rochas como pertencentes a um arco de ilhas, de idade Steniana.

A grande maioria destes blocos foram submetidos, no final do Neoproterozóico pelos processos decorrentes da orogenia Ross (Bisnath et al., 2006), tais como *overprint* metamórfico e geração de expressivos volumes de magma alcalino. Ainda, relacionado à abertura do Wedell Sea, já no Mesozóico, há a presença de diversos diques máficos de idade dominantemente Jurássica (Bauer et al., 2003a; Harris et al., 1991). Através do estudo de traços de fissão em apatita, titanita e zircão, além de isótopos do sistema U-Pb-He foi observado que as rochas passaram por um rápido soerguimento na transição Mesozóico-Cenozóico, interpretado como causado pela flexura isostática causada pela massa das geleiras do continente Antártico (Emmel et al., 2009, 2008).

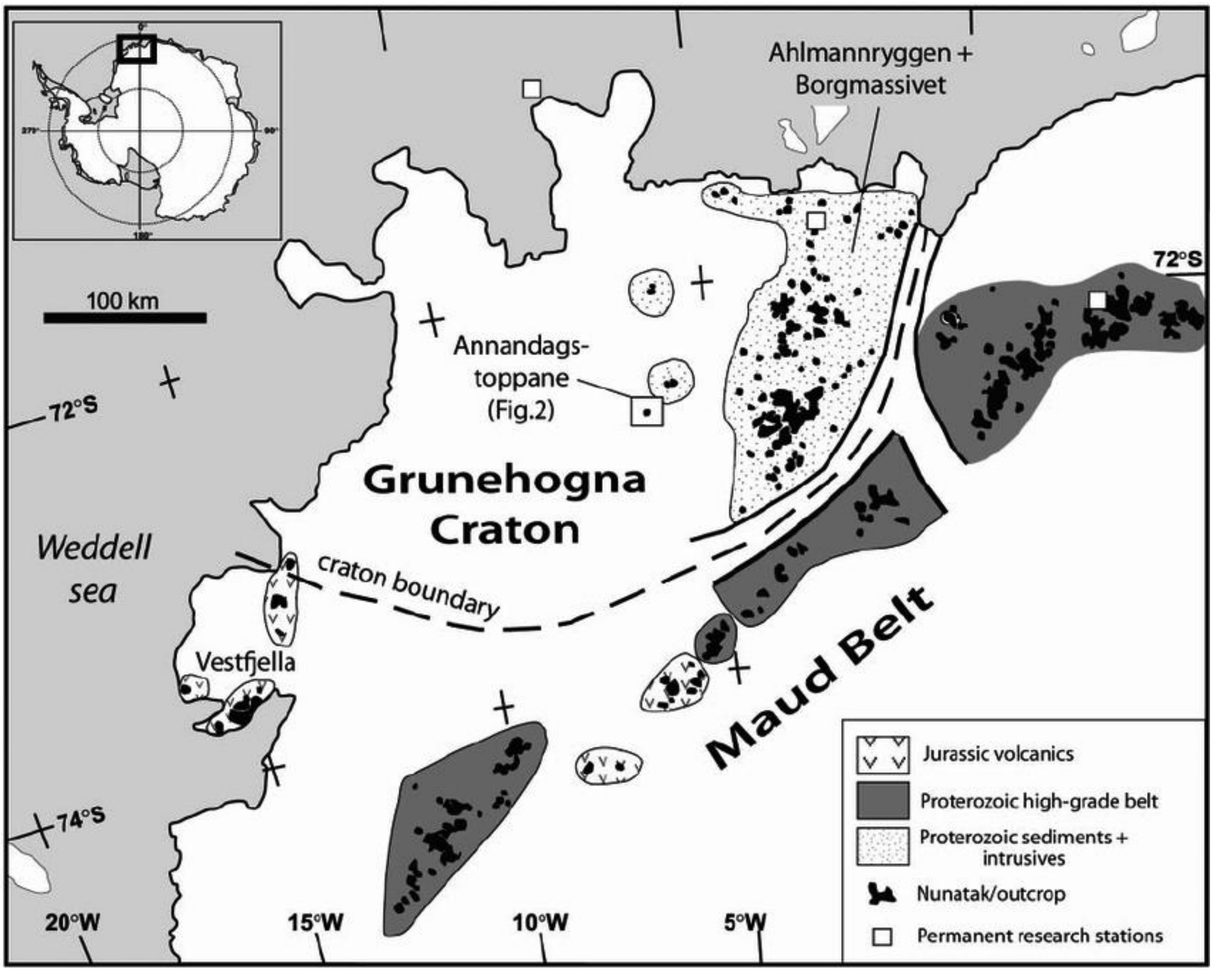

Figura 5 – Mapa de localização do *Dronning Maud Land* em relação à Antártica. Notar a relação de proximidade com o cráton de Grunehogna. Retirado de Board et al. (2005).

2.5 *Coats Land*

O bloco de *Coats Land* é uma entidade geológica distinta no domínio do Leste da Antarctica (Loewy et al., 2011; Figura 6). Apenas dois afloramentos são acessíveis, compostos de riolitos e granófiros não deformados com idade de 1112 ± 4 Ma (Gose et al., 1997). No entanto, sua expressão areal extende-se em subsuperfície até os limites do Dronning Maud Land Central. Jacobs et al. (2015, 2008) consideram que os eventos geológicos ocorridos no Dronning Maud Land são resultado da colisão entre *Coats Land* e cráton de Grunehogna. Loewy et al. (2011) identificaram que as rochas de Coats Land possuem similaridade isotópica com rochas da orogenia Grenviliana, no Laurentia. Ainda, os autores supracitados coletaram dados de paleomagnetismo, demonstrando que, de fato, os terrenos Grenville e Coats eram adjacentes. Da mesma forma, relacionam o terreno com duas unidades específicas: (i) embaiamento de Ouachita, no Texas-Novo México e <u>(ii) Terreno Cuyania, na Argentina.</u>

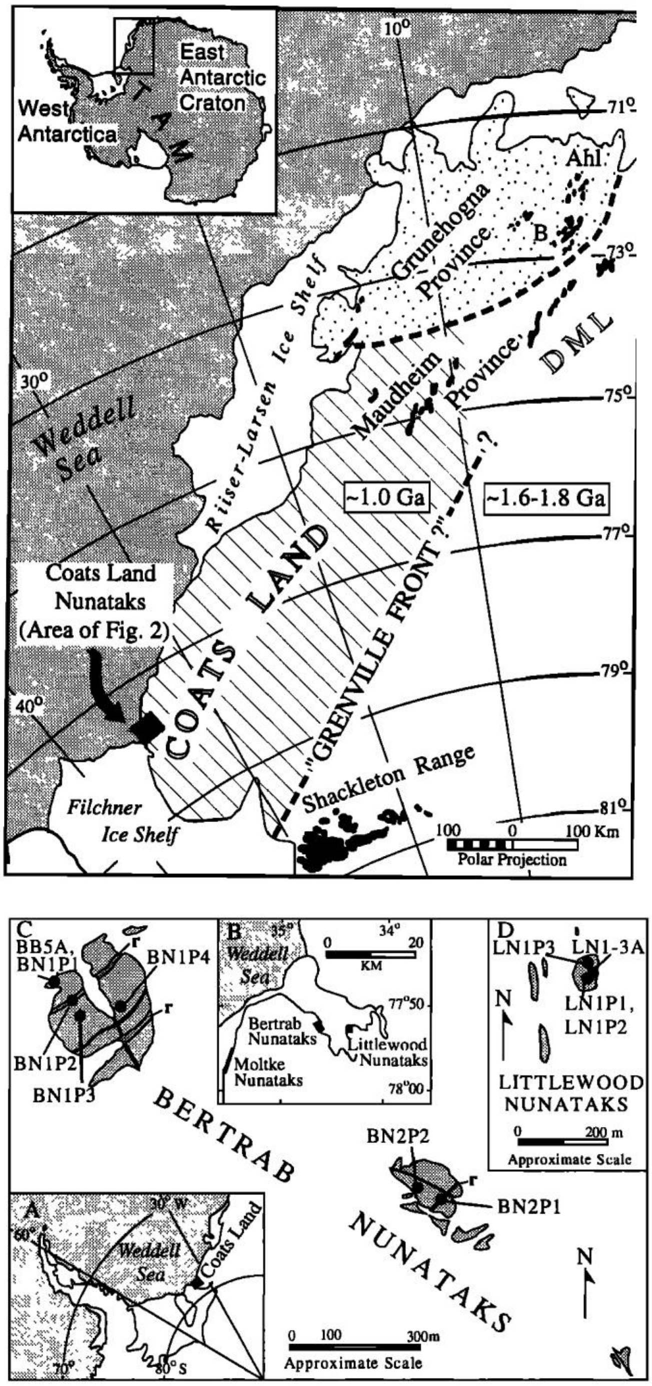

Figura 6 – Superior – Localização do terreno *Coats Land* em relação à Antártica. Inferior – Área aflorante do terreno de Coats, representando dois Nunataks da região: *Littlewood* e *Bertrab*. Retirada de Gose et al. (1997).

2.6 *Shackleton Range*

Shackleton Range é uma província na Antarctica Leste (Figura 7) composta por três terrenos distintos: i) o terreno sul possui zircões detriticos com idades em torno de 2850 Ma, magmatismo entre 1850-1810 Ma, sendo submetidas a eventos de metamorfismo de médio a alto grau em torno de 1700-1680 Ma, com reativação no Paleozóico, em 510 Ma; ii) terreno leste formado por granitóides com ca. 1060 Ma, com metamorfismo associado em torno de 600 Ma; iii) terreno norte, caracterizado por diorites e granitos com idade de 530 Ma, intrudidos sob paragneisses e rochas máfica-ultramáficas, onde, na passagem Neoproterozóico-Paleoproterozóico, foram submetidos a eventos metamórficos de médio a alto grau, com clímax em fácies eclogito (Will et al., 2010, 2009).

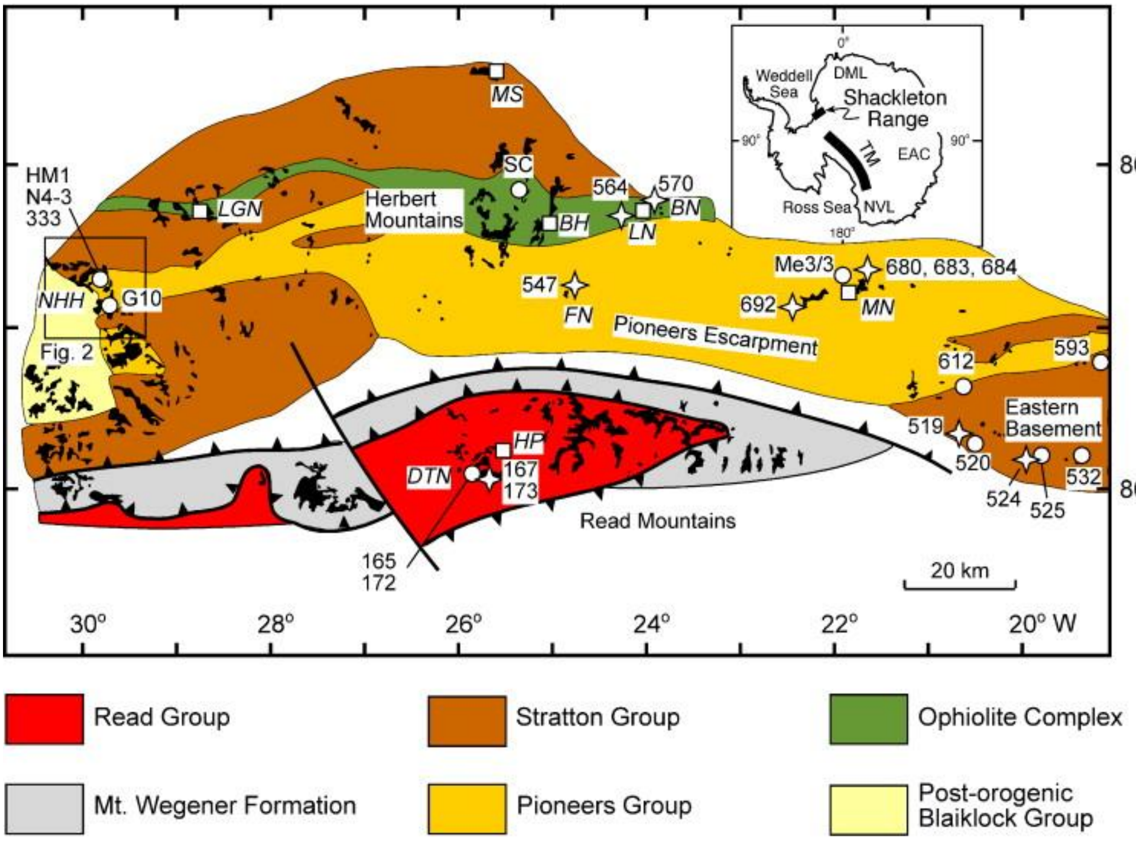

Figura 7 – Mapa geológico simplificado de *Shackleton Range*. Retirado de Will et al. (2009).

2.7 *West Antarctica*

As únicas rochas conhecidas de idade Proterozóica do oeste da Antártica são gnaisses granodioriticos intrudidos por diques máficos e camadas de microgranitos na região conhecida como *Haag Nunataks*. Isócronas de Rb-Sr em rocha inteira tiveram idades de 1176 ± 76 Ma para os gnaisses granodioritícos e 1058 ± 53 Ma para os micrograntios, respectivamente (Millar e Pankhurst, 1987). Conforme apontado por Millar e Pankhurst (1987), essas rochas permaneceram tectônica- e termicamente impertubáveis durante o tempo. As assinaturas de $^{87}Sr/^{86}Sr$ e εNd são típicas de crosta derivada de orogenias formadoras do Rodínia, demonstrando similaridades com unidades de, por exemplo, Cape Meredith Complex (Thomas et al., 2000).

Os granitóides do Jurássico que intrudem as rochas sedimentares do bloco Ellsworth-Whitmore possuem idades de T_{DM} entre 1370-1600 Ma. Esses valores são coerentes com os valores de T_{DM} encontrados nos granitóides Paleozóicos e Mesozóicos da Patagônia (Pankhurst et al., 2006).

Na Península Antártica há evidências estratigráficas que, abaixo das rochas predominantemente Paleozóicas e Mesozóicas, há um embasamento Proterozóico. As idades mais antigas atestadas nessa região são gnaisses de aproximadamente 640 Ma, 410 ± 15 Ma e 426 ± 12 Ma (Rb-Sr em rocha total). No entanto, elas possuem idades de T_{DM} entre 900-1200 Ma (Wareham et al., 1998). Também, em outras localidades da Península Antarctica há granodioritos e ortognaisses granodioriticos Triássicos com T_{DM} de 1100-1750 Ma.

2.8 Província Geológica Patagônia

De acordo com Ramos (2008) e Ramos et al. (2004), o embasamento da Patagônia é dividido em dois domínios tectônicos (Figura 8): (i) Maciço de Somun Cura (a.k.a. *Northern Patagonia Domain*, *basement*, etc) e (ii) Maciço de Deseado, localizado ao sul. De maneira geral, a Patagônia é delimitada ao norte com o terreno Chilenia e cinturão de dobramento Sierra de La Ventana. Ao Sul, é delimitada por bacias sedimentares Meso-Cenozóicas e rochas relacionadas à orogenia Andina. O maciço de Somun Cura é composto por rochas ígneo-metamórficas com um *trend* NW-WNW e idades que variam do Ordoviciano ao Permiano. O metamorfismo, quando presente, é até a fácies anfibolito (Basei et al., 1999; Llambías et al., 2002; Ramos, 2008; Varela et al., 1999; von Gosen, 2003). A Bacia de Colorado a separa do Maciço de Deseado. Genericamente, é composto de rochas ígneas que variam entre 420 e 380 Ma (Basei et al., 2005). O metamorfismo, quando presente, ocorreu por volta de 360 Ma (U-Pb em zircão) e 375-310 Ma (K-Ar em titanita; Pankhurst et al., 2006). As rochas geradas neste domínio são derivadas do processo tectono-termal que afetou um hipotético arco magmático durante o Eo-Paleozoíco (Pankhurst et al., 2006; Ramos, 2008).

Mesmo que a cristalização e idade de metamorfismo de ambos blocos de fato indicam variações de gênese e metamorfismo ao longo do Paleozóico, a unidade apresenta idades modelo T_{DM} entre 1.7 e 854 Ma. Este dado sugere que as rochas da Patagônia derivaram de uma crosta juvenil Mesoproterozoica, relacionada com os eventos de formação do Rodínia (Pankhurst et al., 2006; Roberts et al., 2015; Wareham et al., 1998). Além disso, métodos como $^{87}Sr/^{86}Sr$ e εNd também demonstram mesma derivação Mesoproterozóica (Pankhurst et al., 2006). Diversos trabalhos recentes fomentam este dado (e.g. Martínez Dopico et al. 2011; Mundl et al., 2015), correlacionando xenólitos mantélicos encontrados tanto no terreno norte, quanto no sul, com a crosta gerada no Rodínia e, ainda mais antiga, provavelmente relacionada com a orogenia Grenviliana (Mundl et al., 2015). Martínez Dopico et al. (2011) correlacionaram o maciço Somun-Cura com o terreno Cuyania, até então considerado alóctone à evolução sul-Americana, e relacionável, mais uma vez, com a orogênia Grenviliana, no Laurentia.

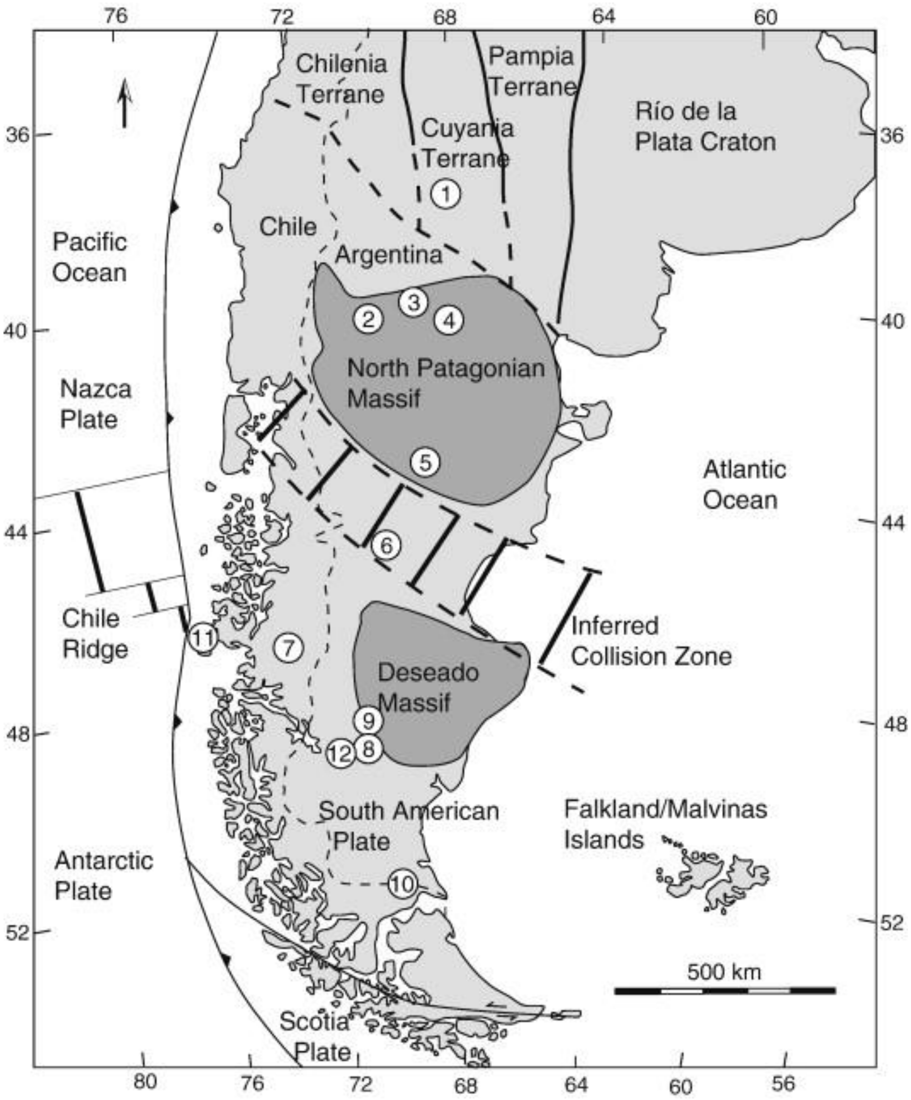

Figura 8 – Mapa simplificado dos maciços da Patagônia e terrenos sobrejacentes como Chilenia, Cuyania, Pampia e Río de la Plata. Retirado de Schilling et al. (2008)

2.9 Terreno Cuyania

O embasamento do terreno Cuyania é constituído de rochas com idade dos eventos formadores do Rodínia (Kay et al., 1996). Thomas e Astini (1996) sugerem que o embasamento é similar ao Sistema Grenvilliano do Laurentia (Figura 8). A idade U-Pb em zircão varia de ca. 1200 a 1000 Ma em diferentes setores do terreno (Casquet et al., 2001; Kay et al., 1996; Sato et al., 2004; Thomas e Astini, 1996). A presença de fauna típica do Laurentia e dado paleomagnético confirmam o carater alóctone do terreno (Benedetto, 2004; Rapalini e Astini, 1998). Ramos (2010) afirma que a ausência de eventos magmato-metamórficos Pampeano ou Brasiliano indica que o terreno não fez parte da amalgamação Neoproterozóica do Gondwana.

2.10 Terreno Chilenia

Conforme Ramos et al. (1986), este terreno foi definido sendo limitadamente aflorante seguindo a tendência de alinhamento axial da cordilheira (Figura 8; Figura 9). Ramos e Basei (1997) dataram rochas metamórficas de alto grau, adjacentes a uma zona ofiolítica, de idade desconhecida, que separa este terreno de seu vizinho a leste, Cuyania. Idades entre 1060 e 1080 Ma foram adquiridas na zona de Codon del Portillo, através de U-Pb em zircão, que são coincidentes com o metamorfismo existente, por exemplo no Western Dronning Maud Land (Arndt et al., 1991; Jacobs et al., 2003c), Província Natal (Mendonidis e Armstrong, 2016; Spencer et al., 2015b) e Falkland-Malvinas-Maurice Terrane (F2MT; Chemale Jr. et al., 2018; Jacobs et al., 1999).

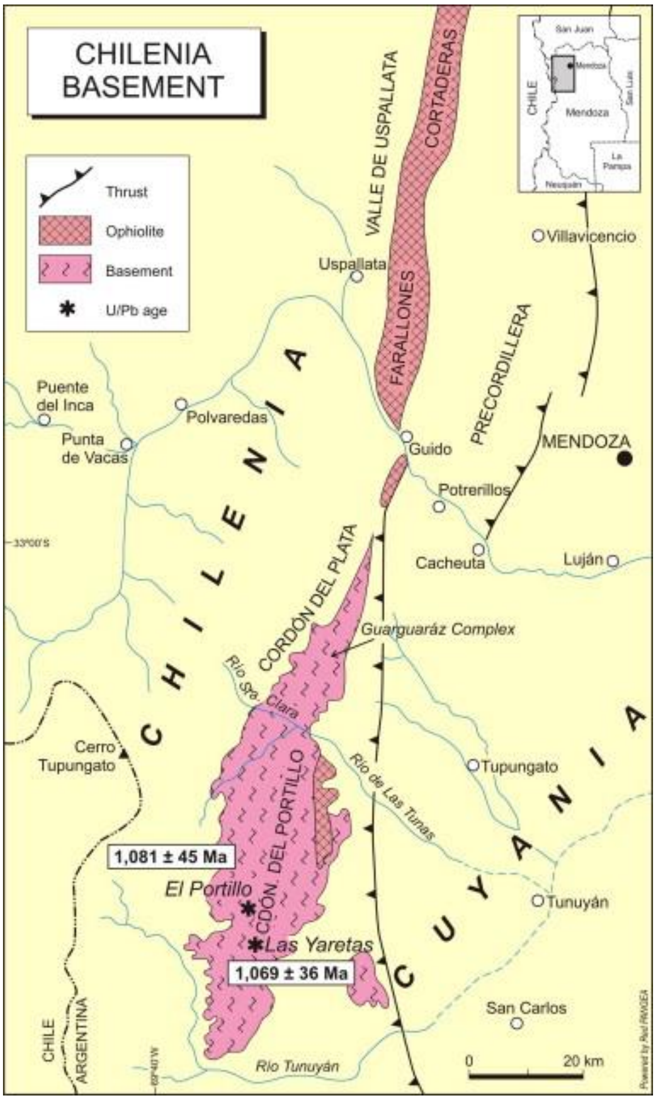

Figura 9 – Cordón del Portillo, formado por rochas de alto grau com idades coincidentes ao metamorfismo regional relacionado com o evento de formação do Rodínia. Retirado de Ramos (2010).

3 RODÍNIA: ORIGEM, NOME E EVOLUÇÃO

Rodínia é uma palavra derivado do russo “*rodit*”, usada de modo a homenagear o papel da pesquisa soviética no Pré-Cambriano(McMenamin e McMenamin, 1990, p. 95). Sua polissemia, em inglês, é incorporada a três verbos: *“to beget”*, *“to grow”* ou ainda *“to give birth” “To beget”* é um verbo de difícil tradução, significa gerar algo, normalmente uma criança, referindo-se especificamente ao papel dos pais. No entanto, não parece completa sem *“to give birth”*, dar à luz e *“to grow”*, o desenvolver natural da maturidade. Portanto, é ampla: Rodínia gerou os supercontinentes, dando à luz aos primeiros animais. Suas margens serviram como berço, um ambiente propício para a evolução da vida (McMenamin and McMenamin, 1990). No entanto, sua origem geológica é pretérita, advindo de Valentine e Moores (1970), que teorizaram um supercontinente, chamado Pangea I. De idade Pré-Cambriana, este supercontinente englobava todos os continentes da Terra, detendo os principais fatores para a diversificação das formas de vida.

Hoje uma verdade geológica em pleno desenvolvimento, o supercontinente Rodínia possui diversas teorias de evolução ao longo do tempo geológico. No entanto, a maior parte das reconstruções partem do pressuposto do Laurentia como centro do mundo. Os principais modelos em voga são SWEAT (Dalziel, 1991; Hoffman, 1991; Moores, 1991), Missing Link (Li et al., 1995), AUSWUX (Brookfield, 1993), SAMBA (Johansson, 2014, 2009) e WALahari (Pisarevsky et al., 2003; Powell et al., 2001). Todos os modelos possuem, em algum ponto, potencialidades e pontos fracos, haja visto nenhuma solução ser única (Li et al., 2008, Figura 10a).

3.1 Modelos da evolução do Rodínia

3.1.1 SWEAT – *SouthWest United-States East Antarctica*

A correlação estratigráfica, metalogenética e paleomagnética de rochas Pré-cambrianas do oeste do Canada e sul da Austrália levou Bell e Jefferson (1987) a proporem que estes dois blocos estavam originalmente conectados e, a partir de 1.2 Ga começaram um processo de rifteamento e desenvolvimento de margem passiva. Inspirado nessas similaridades, Dalziel (1991), Hoffman (1991) e Moores (1991), propuseram o modelo *Southwestern United States-East Antarctica* (SWEAT), sugerindo que as rochas, até então de origem controversa, de terrenos encontrados em *Nimrod Glacier*, *Pensacola Mountains* e *Maud Belt*, com idades entre ≈1.2-0.8 Ga, formavam uma extensão das província Grenviliana, região leste da América do Norte. Ênfase também foi dada para idades similares das rochas do *Shackeleton Range* e o terreno adjacente de *Coats Land* aquelas características da Província Yavapai-Mazatzal (Figura 10). Moores (1991) sugeriu que os crátons do norte e oeste australianos provavelmente não faziam parte da extensão SWEAT até a colisão do final do Mesoproterozóico, caracterizado pelo cinturão Albany-Fraser-Musgrave.

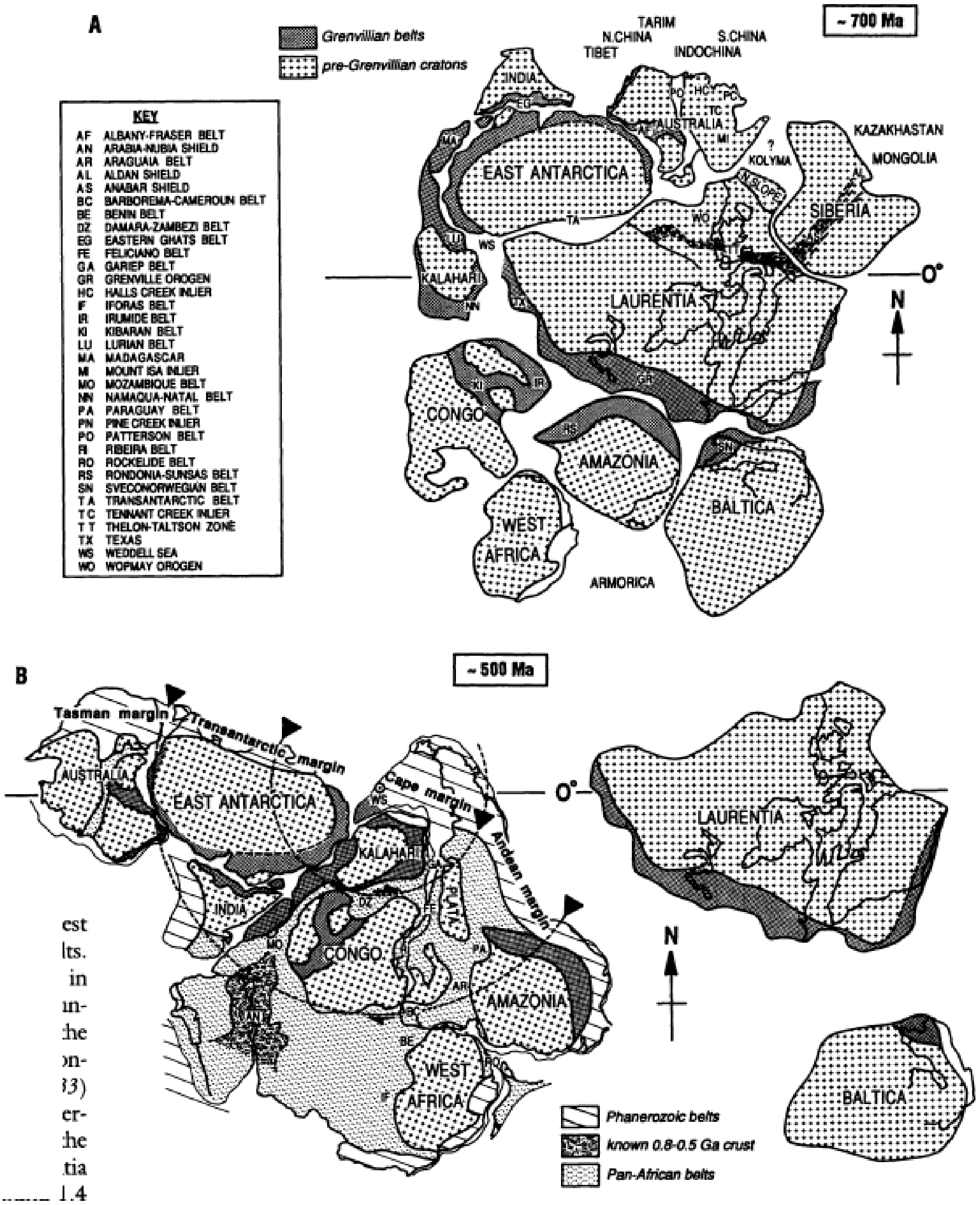

Figura 10 – Modelo SWEAT proposto por Hoffman (1991). A – Reconstrução dos grandes blocos continentais amalgamados, formando o primeiro mapa oficial do supercontinente Rodínia, com a posição dos continentes há aproximadamente 700 Ma. B – Idealização do *break-up* entre a margem Proto-andina e Laurentia ocorrido, conforme o autor, há aproximadamente 500 Ma.

Em uma visão minuciosa das províncias cristalinas e proveniência das bacias, Borg e DePaolo (1994), através da análise detalhada de dados isotópicos, cronológicos e geoquímicos, identificaram descontinuidades na conexão SWEAT. Como resultado, de modo a manter o modelo SWEAT viável, os autores sugeriram que os terrenos Mesoproterozóicos das Montanhas Transartáticas mais jovens que ca. 1000 Ma eram provavelmente alóctones, sendo acrescidos as margens do

Laurentia após a abertura do oceano proto-Pacífico. No entanto, conforme apontado por Li et al. (2008), não há evidência geológica para o *docking* destes terrenos, carecendo de deposição advinda de um período mais antigo que 668 ± 1 Ma (Goodge et al., 2002).

Li et al. (2008) apontaram outras evidências que não fomentam o modelo SWEAT, como: (i) falta de continuação da província magmática transcontinental do sul do Laurentia (1500-1350 Ma; até as *Transartarctic Mountains*; (ii) discrepâncias no evento de pluma mantélica do Neoproterozóico entre a conexão SWEAT (Li et al., 1999; Park et al., 1995; Wingate et al., 1998); (iii) bacias do oeste da América do Norte (e.g. *Belt Basin*) possuem áreas fonte com idades de 1786-1642 Ma, 1600-1590 Ma e 1244-1070 Ma, não identificadas no Leste da Antártica (Ross et al., 1992; Ross and Villeneuve, 2003); (iv) a conexão SWEAT, inicialmente proposta por Dalziel (1991) e Moores (1991), provou-se inatingível tanto paleomagneticamente (Gose et al., 1997), quanto geologicamente (Jacobs et al. 2003a; 2003b). No entanto, cabe ressaltar que, conforme Li et al. (2008), o Laurentia se conectou com o Kalahari em ca. 1090-1060 Ma, permanecendo deste modo até o *break-up* do Gondwanaland (Jacobs et al., 2003b, 2003a; J. Jacobs et al., 2008). Li et al. (2008) enfatizaram que se de fato houve cinturões orogênicos conectando Laurentia, Austrália e *East Antarctica*, ou se conexão SWEAT existiu, ela deve ser Grenviliana ou posterior. Há a possibilidade da comprovação do modelo SWEAT, através de dados paleomagnéticos, após ca. 1050 Ma (Powell et al., 1993). No entanto, essa conexão não é possível em ca. 1200 Ma (Pisarevsky et al., 2003). Portanto, Li et al. (2008) não aceitam uma conexão SWEAT em momentos tardi-Paleoproterozóico, isto é, ca. 1800-1600 Ma.

3.1.2 *Missing link*

Proposto inicialmente por Li et al. (1995), o modelo Missing Link coloca o *South China Block* entre os blocos Australia-Leste da Antártica (Li et al., 2008; Figura 11). O modelo foi concebido de modo a (i) preencher o vazio entre as províncias crustais da Austrália - *East Antarctica* e o Laurentia; (ii) devido às similaridades estratigráficas observadas por Eisbacher (1985) entre o sul da China, Austrália e oeste do Laurentia; (iii) similaridades entre províncias crustais do bloco Cathaysia e sul do Laurentia e (iv) a necessidade de uma área fonte para as Bacias cronocorrelatas do oeste norte-americano, com picos de idade de proveniência similares àquelas encontradas no terreno de Cathaysia (Ling et al., 2003; Ross e Villeneuve, 2003).

Por exemplo, há diversas similaridades entre os depósitos de rift encontrados na parte sul da China e o leste da Austrália. No entanto, dos 4 episódios de magmatismo-*rifting*, apenas os 2 mais jovens são documentados na Laurentia (ver Li et al., 2008). Ainda, é interpretado que a colisão entre a Laurentia-Cathaysia e bloco Yangtzie é limitada a, no máximo, 1140 Ma e durou até o circa de 900 Ma (Greentree et al., 2006; Li et al., 2003; Ling et al., 2003).

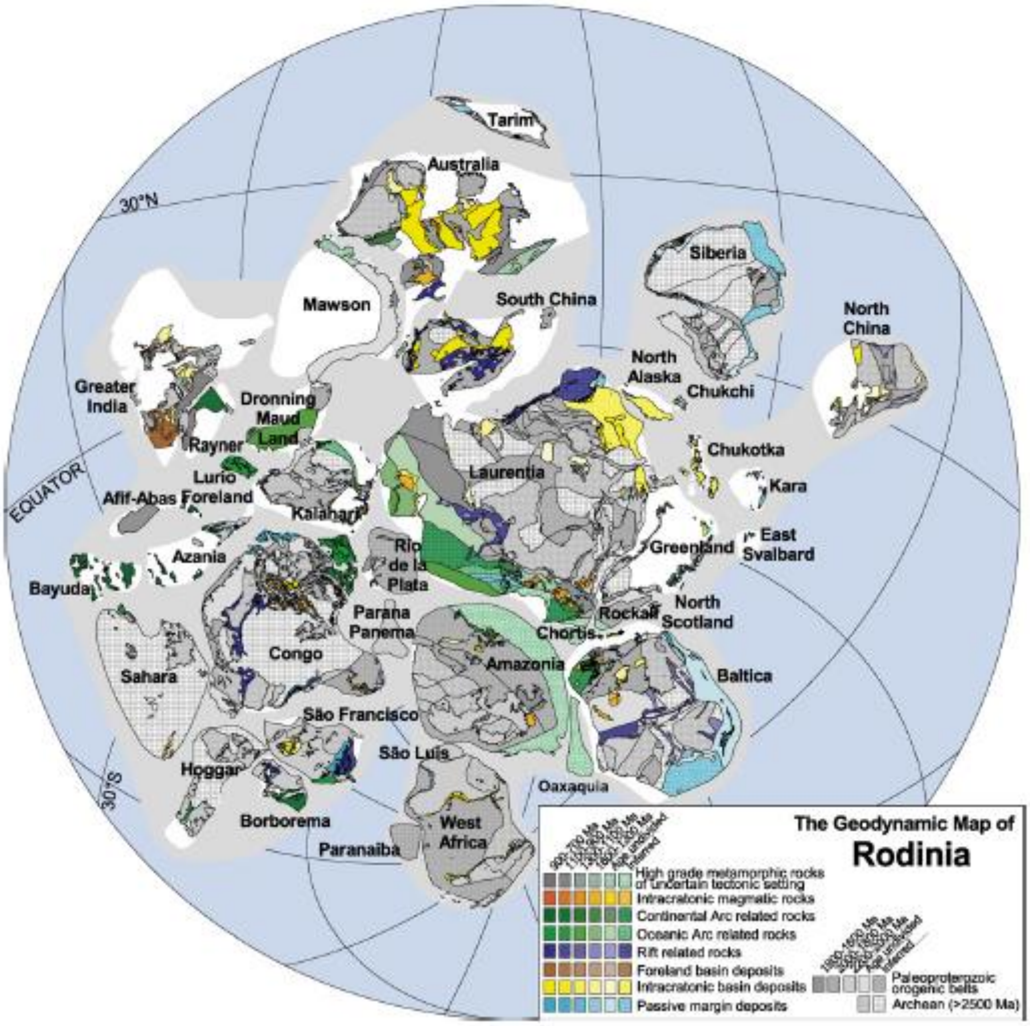

Figura 11 – O modelo Missing-link conforme concebido por Li et al (1995) e aprimorado por Li et al (2008).

De maneira geral, outra vantagem do modelo é que não necessita de um *apparent polar wander path* (APWP) entre os continentes relevantes entre 1 Ga e 900 Ma. Com os dados paleomagnéticos disponíveis atualmente é possível uma conexão entre os blocos da Austrália-sul da China-Laurentia durante 820-800 Ma; no entanto, a partir de 750 Ma, eles devem ser separados (Li et al., 2008).

3.1.3 AUSWUX – Australia-Southwest US

Inicialmente proposta por Brookfield (1993), o modelo Australia-Southwest US (AUSWUX) foi concebido na equivalência de fraturas lineares supostamente formadas durante o break-up do Rodínia nas margens leste do cráton da Austrália e oeste do Laurentia (Figura 12). O modelo foi revisitado por Burrett e Berry (2000) e Karlstrom et al. (1999), principalmente por correlação e províncias cristalinas e estudo de proveniência entre os blocos.

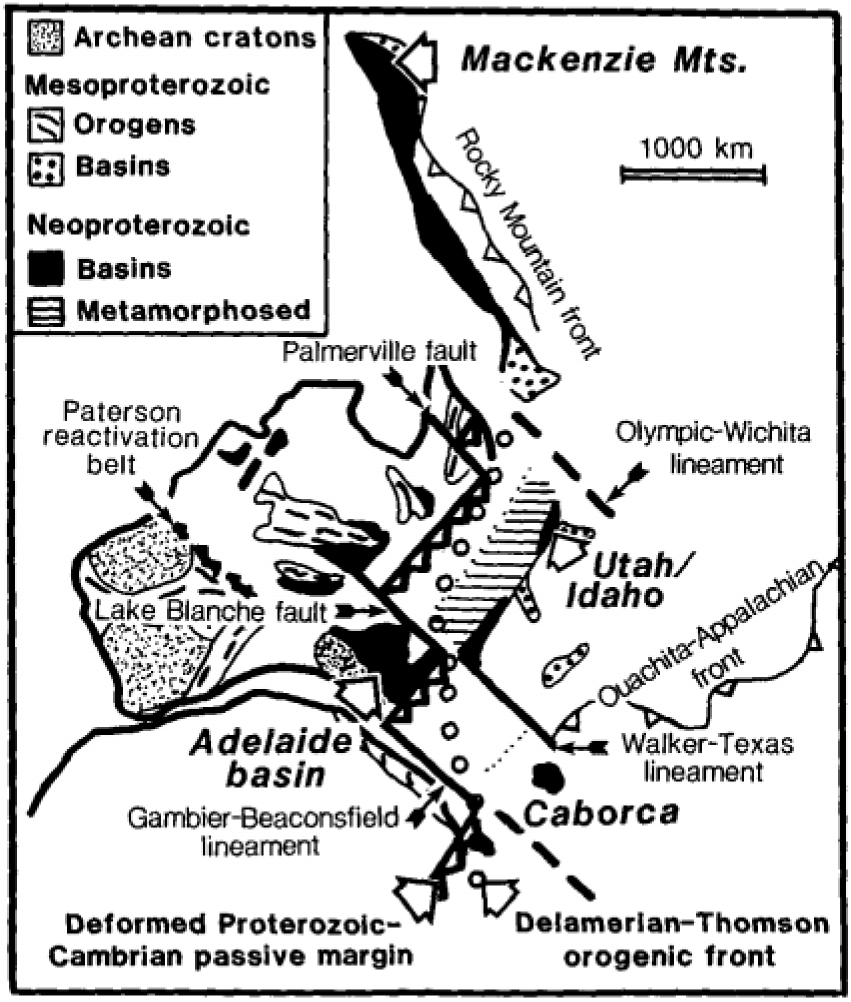

Figura 12 – Modelo AUSWUX, conforme concebido por Brookfield (1993).

No entanto, Direen e Crawford (2003) identificaram que os lineamentos que ocorrem na Austrália não são mais antigos que 600 Ma. Conforme Li et al. (2008), apesar de seus méritos, o modelo apresenta diversas dificuldades, tais como: (i) dificuldades em explicar os dados esparsos de metamorfismo Greenvilliano no oeste do Laurentia, norte de Queensland, Tasmania e orogenia Ross; (ii) ausência de rochas graníticas e riolíticas com ca. 1400 Ma na Austrália, como são encontradas no sul do Laurentia; (iii) o começo do rifte no Laurentia (ca. 750 Ma) é diferente do observado no leste da Austrália (ca. 825 Ma); (iv) há uma incoerência nos dados de paleomagnetismo de 1200 Ma com o modelo Pisarevsky et al. (2003). Em 1100-1050 Ma, entretanto, os paleopólos são coerentes.

3.1.4 SAMBA – South AMerica-BAltica

Através da interpretação de compilações de dados geológicos gerais e modelos de reconstrução de placas, foi proposto por Johansson (2014, 2009) um modelo onde correlaciona-se, durante o Rodínia, o bloco Baltica com o Amazonia. Esta correlação, conforme o já citado autor, ocorreu de 1.8 Ga até 0.8 Ga, onde, o cráton West Africa servia como conexão entre o nordeste da Amazonia e sudeste de Baltica. Deste modo, será considerado como SAMBA a amalgamação dos terrenos Amazonia, Baltica e *West Africa* (Figura 13).

De maneira geral, em consonância com boa parte das reconstruções já propostas, a parte noroeste do Baltica era conectada com o leste do Laurentia *(Greenland)* de 1.9 Ga até 1.3 Ga. Johansson (2014) sugere uma configuração como a proposta no modelo SWEAT (Moores, 1991). Deste modo, o cráton Kalahari era anexado ao sudoeste do Laurentia e junto com o *East Antarctica*, juntamente com o cráton do Congo, Tanzânia, São Francisco e Rio de la Plata.

Johansson (2009) sugere que para atingir o modelo padrão do Rodínia, o bloco Baltica deve ter se separado do Laurentia e, junto com o bloco Amazonia e *West Africa*, rotacionar aproximadamente 75º, em sentido horário, em relação ao Laurentia. De modo a encaixar no modelo proposto do Gondwana, exige-se a rotação de diversos crátons (e.g. Laurentia-Kalahari, *East Antarctica*) em ângulos maiores que 90º no sentido anti-horário (Johansson, 2014). A separação do Rodínia é interpretada como ocorrida por volta de 0.6 Ga, em resposta as rotações em escala global. Da mesma forma, a abertura do oceano Proto-Pacífico e as colisões Brasilianas/Panafricanas são relacionadas a este evento.

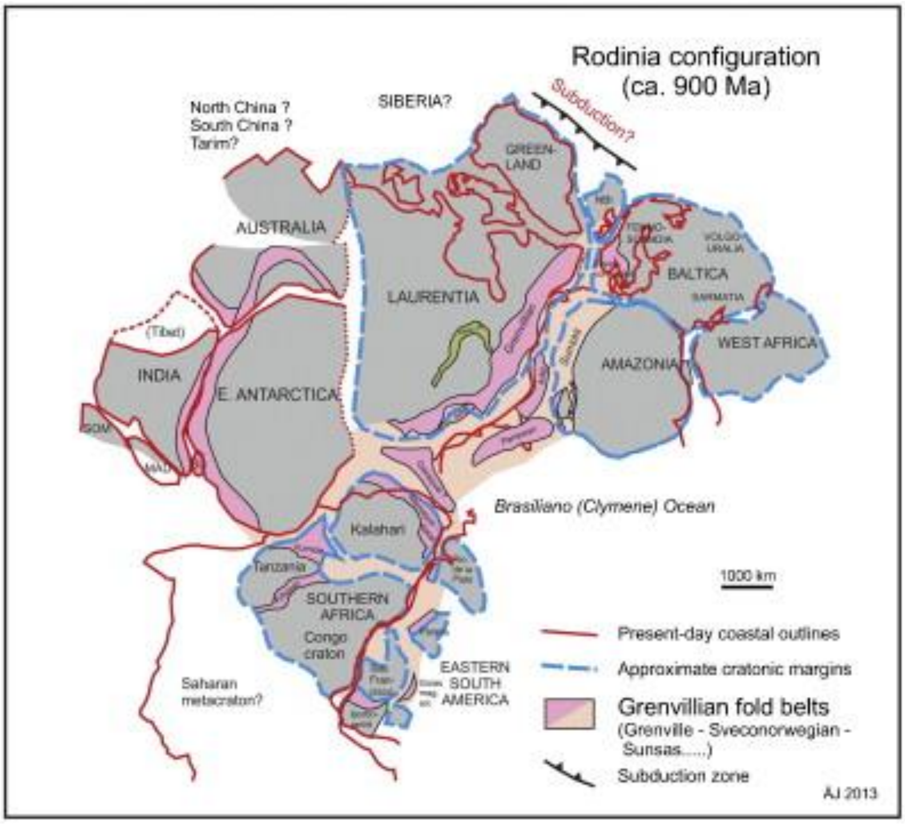

Figura 13 – Reconstrução do Rodínia (ca. 900 Ma) conforme modelo SAMBA (Johansson, 2014, 2009).

Fuck et al. (2008), ainda, sugeriram que as províncias Ventuari-Tapajós e Rio Negro-Juruena, chaves para a reconstrução do modelo, são truncadas ao norte por orogenias de idade Grenviliana. Este dado coloca em prova a estabilidade proposta pelo modelo do superbloco SAMBA durante 1.8 até 0.9 Ma (Pisarevsky et al., 2014).

Não são consideradas neste modelo as unidades formadoras do arco de Ilhas Steniano (TOAST; Jacobs et al., 2015 e Ruppel et al., 2018), localizadas tanto em terrenos como Central Dronning Maud Land e Sør Rondane (Jacobs et al., 2015; Ruppel et al., 2018) e Terreno Madagascan (Archibald et al., 2018).

3.1.5 WALahari – *Western Australia-KaLahari*

O modelo Western Australia-Kalahari (WALahari; Figura 14), inicialmente foi concebido por meio de dados paleomagnéticos de Pisarevsky et al. (2003), Powell et al. (2001) e Powell e Pisarevsky (2002). Subsequentemente, diversos dados geocronológicos deram suporte hipótese, como Fitzsimons (2002, 2003).

A concepção é de que o Kalahari estaria localizado junto ao oeste do *Western Australia block*, com o *Maud-Belt* adjacente à orogenia Pinjarra, de idade também

Grenviliana (Ksienzyk e Jacobs, 2015). A principal base teórica para a colisão entre o *Western Australia* e o Kalahari, no fim do Mesoproterozóico, foi a similaridade do espectro de idades e características estratigráficas observadas nos dois terrenos (Ksienzyk e Jacobs, 2015).

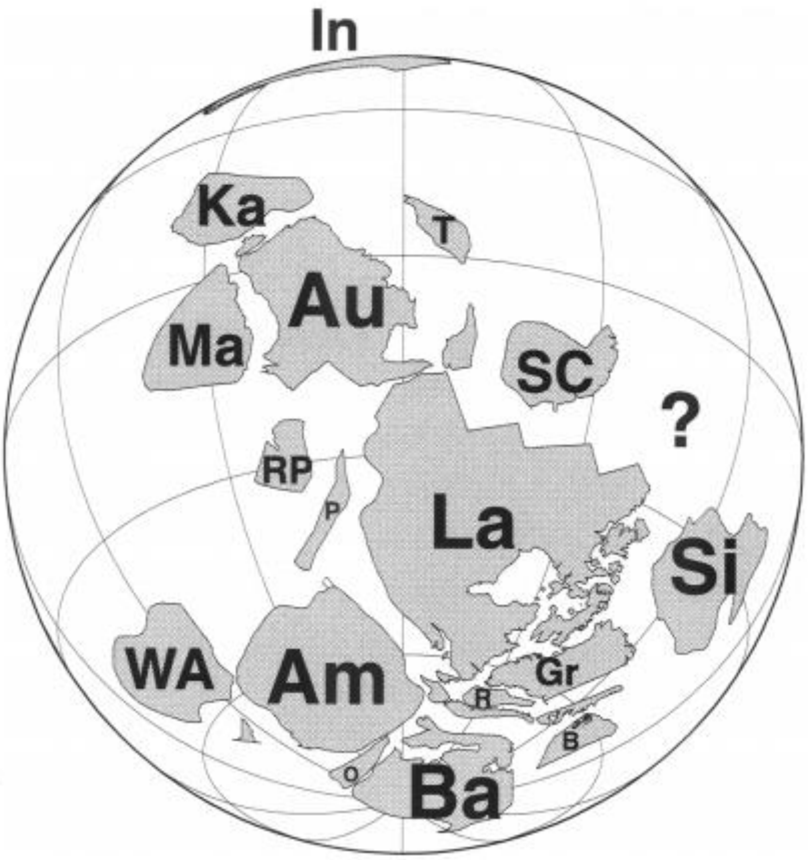

Figura 14 – Modelo WALahari, conforme concebido por Pisarevsky et al. (2003). Idealização do Rodínia há 900 Ma. Legenda: In – Índia; Ka – Kalahari, Au – Austrália; Ma – Mawson; T- Tarim; RP – Rio de La Plata; P – Pampean Terrane; SC – South China; La – Laurentia; Si – Sibéria; Am – Amazonia; WA – West Africa; B – Barentsia; Ba – Baltica; Ch – Chortis; Gr – Greenland; R – Rockall; O – Oaxaquia; Ba – Baltica.

Essencialmente, Fitzsimons (2002, 2003) comparou dados de proveniência e do *Maud Belt* de Arndt et al. (1991) e Harris (1999) e da orogenia Pinjarra do *Western Australia* de Bruguier et al. (1999) e Cobb et al. (2001). No entanto, Ksienzyk e Jacobs (2015b), com base em dados mais consistentes obtidos pelos autores, do leste da Antártica, e Ksienzyk et al. (2012), da orogenia Pinjarra, concluíram que a comparação direta dos metassedimentos das duas áreas demonstra uma incompatibilidade de área fonte, sugerindo diferentes sequências sedimentares.

Apesar disso, o espectro de idades dos grãos detríticos de zircão encontrados no metassedimento não elimina a possibilidade do modelo WALahari ser aceitável (Ksienzyk e Jacobs, 2015). De qualquer forma, os autores consideram a posição do Kalahari adjacente ao SW Laurentia com o Namaqua-Natal-Maud Belt como a contraparte colisional da orogenia Grenviliana.

3.1.6 TOAST – Tonian Oceanic Arc Super Terrane

Proposto inicialmente por Jacobs et al. (2015), o modelo TOAST (*Tonian Oceanic Arc Super Terrane*) postula que as rochas de Central Dronning Maud Land e Sør Rondane representam um amplo terreno de arco de ilhas, que, durante 1000-900 Ga não faziam parte do supercontinente Rodínia (Figura 15). Conforme apontado por Ruppel et al. (2018), a primeira evidência geológica do TOAST é relacionada a uma fase principal de subducção que formou rochas magmáticas de assinatura juvenile em torno de 995-975 Ma. É seguida por uma fase de gênese similar, mas tenuemente mais jovem (960-925 Ma) nos terrenos localizados a SW do Sør Rondane.

As unidades do TOAST, de maneira geral, possuem uma história de polimetamorfismo com geração de grandes volumes de magma, datados em ca. 630 até 500 Ma. De maneira geral, as idades do *overprint* metamórfico diminuem de oeste para o leste. Isto é interpretado por Jacobs et al (2015) como evidência que o TOAST colidiu com o Kalahari primeiro, antes de colidir com o terreno Rukerland e/ou Indo-Antártica em seu limite leste. Ainda, há um *overlap* de idades entre as rochas TOAST e as localizadas à leste, compreendendo rochas do *Rayner Complex*. No entanto, três principais diferenças emergem: i) longa história acrescional de arcos de ilha formadores do *Rayner Belt* (entre 1400-900 Ma) que culminam em ii) colisão continente-continente em ca. 950 Ma; iii) o TOAST possui uma pronunciada assinatura juvenil, carecendo de qualquer indicativo de herança e *overprint* metamórfico imediatamente após a formação da crosta (Figura 15).

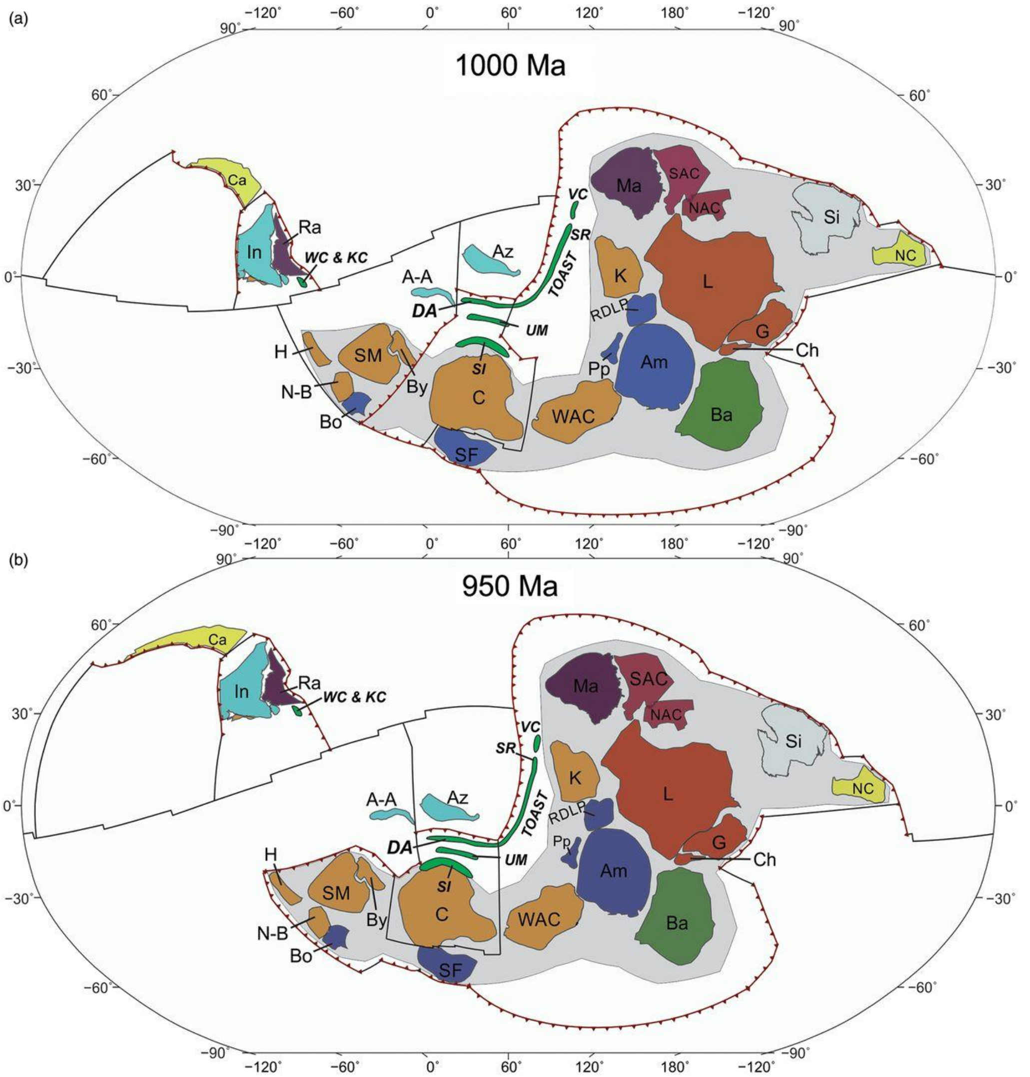

Figura 15 – Reconstrução tectônica em (a) 1000 Ma e (b) 950. North America, vermelho (Ch, Chortis; G, Greenland; L, Laurentia); South America, azul marinho; (Am, Amazonia; Bo, Borborema; Pp, Paranapanema; RDLP, Rio de la Plata; SF, São Francisco) Baltica, verde; (Ba, Baltica); Siberia, grey; (Si, Siberia); India, continentes do Indian Ocean e Middle East (oriente médio), azul claro (A-A, Afif–Abas Terrane; Az, Azania; In, India); China, amarelo (Ca, Cathaysia, South China; NC, North China); Africa, laranja (By, Bayuda; C, Congo–Tanzania–Bangweulu Block; H, Hoggar; K, Kalahari; N-B, Nigeria–escarlate (NAC, North Australian Craton; SAC, South Australian Craton); Antarctica, roxo (Ma, Mawson; Ra, Rayner); Arcos Meso-Neoproterozoic, verde escuro; (DA, Dabolava Arc; SI, Southern Irumide; SR, Sør Rondane; TOAST, Tonian Oceanic Arc Super Terrane; UM, Unango–Marrupa; VC, Vijayan Complex; WC, Wanni Complex; KC, Kadugannawa Complex). Retirada de Archibald et al. (2018).

A sutura TOAST-Dronning Maud Land é considerada por Jacobs et al (2015) como o limite TOAST-orogenias Grenvilianas na Antártica. Os limites sul e leste são meramente especulativos.

4 ROTAÇÃO DAS ILHAS FALKLAND (MALVINAS) NO MESOZÓICO

As Ilhas Falkland (Malvinas), localizadas na plataforma Argentina, 500 km a leste da costa da Patagônia, possuem ativa participação na consolidação da Teoria da Deriva Continental e evolução do Gondwana. Conforme Ramos et al. (2017), três hipóteses sobre evolução tectônica das ilhas foram inicialmente propostas: (i) Du Toit (1937) colocou a ilha entre a América do Sul e África do Sul, (ii) Adie (1952), em contra partida, inverteu a posição atual das ilhas, colocando-as na borda leste da África do Sul, como um apêndice dos terrenos dobrados e um importante evento de rotação ocorrido no Mesozóico; (iii) Borello (1963) teorizou que as ilhas se mantiveram em uma posição similar, em relação a América do Sul, conforme a configuração atual (Figura 16).

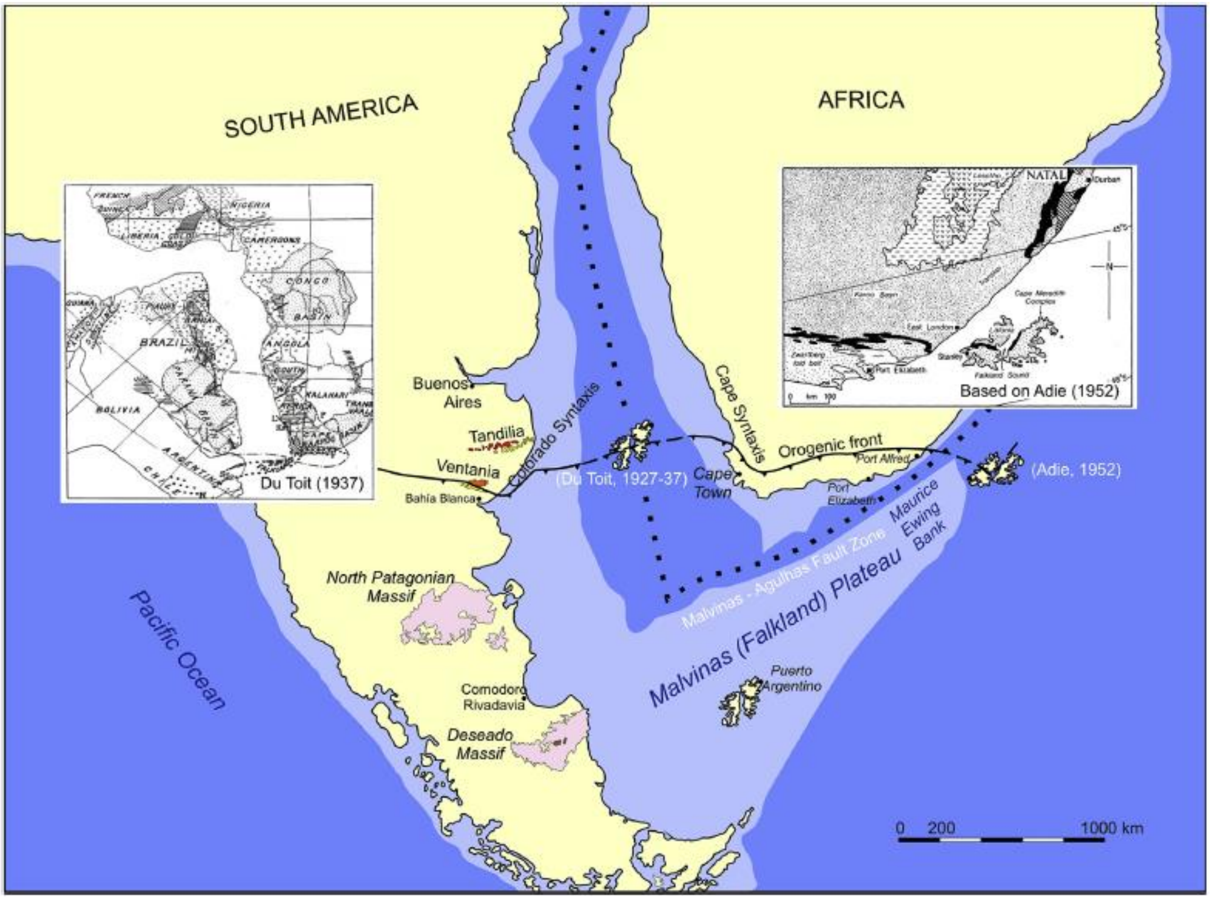

Figura 16 – Posição das Ilhas Falkland (Malvinas) no contexto pre-break up conforme Du Toit (1937), Borello (1956) e Adie (1952). Retirada de Ramos et al. (2017).

Diversas aproximações avaliaram / fomentaram / desvalidaram essas hipóteses. Estas aproximações incluíram reconstruções paleogeográficas, análises paleomagnéticas, análise geocronológica dos diques Juro-Cretáceos (Mitchell et al., 1986; Stone et al., 2009, 2008; Taylor and Shaw, 1989) e embasamento (Cingolani and Varela, 1976; Jacobs et al., 1999; Thomas et al., 2000, 1997), proveniência das sequências sedimentares (Ramos et al. 2017, dentre tantas outras). No entanto, ainda não há consenso sobre a posição das ilhas durante sua evolução entre o Mesoproterozóico e, principalmente, durante o Mesozóico. Assim sendo, serão abordadas as principais características de cada hipótese, da mais antiga para a mais recente.

3.4.1 Hipótese de Du Toit (1927)

As similaridades estratigráficas entre Sierra de La Ventana e Cape Fold Belt levaram (Du Toit, 1927) a postular que as Ilhas Falkland (Malvinas) encontravam-se na mesma latitude e no meio do caminho entre essas duas unidades. Conforme pontuado por Ramos et al. (2017) esta hipótese foi principalmente baseada nos estudos de Keidel (1916, 1913) e comprovada após a visita do pesquisador nos depósitos da América do Sul. O principal argumento baseava-se na correlação dos tilitos encontrados nessas três unidades, que além de mesma gênese deposicional, possuíam mesma idade.

Existem dois problemas na hipótese de Du Toit. O primeiro, relacionado com a vergência estrutural dos depósitos Paleozóicos das Ilhas Falkland (Malvinas), são opostas as da Ventania e Cape Fold (S-N). É conhecido que a vergência dos tilitos das ilhas tem sentido SW (Adie, 1952a; Baker, 1924). O segundo é relacionado com a falta de correlação entre a Patagônia e as Ilhas Falkland (Malvinas). O motivo principal baseia-se no fato de, no período em que o trabalho foi proposto, Du Toit não tinha conhecimento dos depósitos glaciais Eo-Paleozóicos com idade de deposição similar àqueles encontradas nos tilitos das Ilhas Falkland (Malvinas; Griffis et al., 2014).

3.4.2 Hipótese de Adie (1952)

A hipótese correlaciona as Ilhas Falkland (Malvinas) com o oeste da África do Sul. No entanto, baseia-se na rotação de 180º das ilhas para que haja uma maior consistência na correlação. É estruturada nas seguintes premissas: (i) a rotação de 180º facilita a associação das unidades Mesoproterozóicas das ilhas com o terreno

Natal; (ii) com a rotação, torna-se aceitável a correlação das unidades estratigráficas presente nas duas regiões; (iii) afinidades paleontológicas no mar Devoniano, identificadas na fauna Malvinokafrica (Richter e Richter, 1942); (iv) a partir da rotação as paleocorrentes das unidades glaciais do Eo-Paleozóico passam a ser iguais; (v) os diques basálticos presentes nas ilhas podem ser correlacionados com os diques doleríticos; (vi) estilo do padrão de dobras das ilhas se tornam similares ao do *Cape Fold Belt*.

Diversos estudos paleomagnéticos feitos nos enxames doleríticos das ilhas suportam a hipótese de Adie. Inicialmente, Mitchell et al. (1986) propuseram uma paleolatitude similar ao Transkei, permitindo, desta forma, a localização das ilhas ao leste da África do Sul. Um estudo mais consistente foi efetuado por Taylor e Shaw (1989), com resultados aproximados. Uma rotação de 120º ocorreu durante o Jurássico, seguida por uma rotação de 60º no Cretáceo durante a abertura do Atlântico Sul (Stone et al., 2009; Storey et al., 1999). Ben-Avraham et al. (1993), baseados nessas interpretações, propuseram a existência da Microplaca de Lafonia. Para acomodar os tensores necessários para a rotação desta microplaca, foi teorizada uma microplaca extra, chamada de Microplaca Patagônica. Esta microplaca Patagônica era provavelmente conectada com a Microplaca Lafonia através de uma grande zona de cisalhamento destral. Provavelmente, esta falha, chamada de Sistema de Gastre (Rapela et al., 1991; Rapela and Pankhurst, 1992), foi essencial agente de transporte da Microplaca de Lafonia. Marshall (1994), partindo desta premissa, propôs que ela deveria ser desconectada do Maurice Ewing Bank (Barker et al., 1977a) e então rotacionada. Diversos autores amarraram estes eventos entre 190 e 130 Ma (Barker, 1999; Stone et al., 2009; Storey et al., 1999; Thomson, 1998). No entanto, observando diversos padrões de rifteamento nas bacias de Outenika e *Northern Falkland (Malvinas) Basin*, Thomson (1998) limitou este período ao Valengiano (≈134 Ma).

Da mesma forma que o modelo de Du Toit, há ambiguidades neste modelo de reconstrução. A estratigrafia, incluindo suas descontinuidades, é similar entre as unidades expostas na Sierra Pillahuincó e Sierra de La Ventana (Pankhurst et al., 2006). Ainda, a assembléia Malvinokafrica se extende não somente nas Ilhas Falkland (Malvinas), mas também na Bacia do Paraná (Clarke, 1913), Patagônia (Manceñido and Damborenea, 1984), prisma acrescionário do Chile (Fortey et al., 1992), além do já citado *Cape Fold Belt*. As glaciações do Eo-paleozóico e a direção do fluxo das geleiras são similares aos depósitos glaciais do centro da Bacia de Tepuel-Genoa (Griffis et al., 2014). Além disso, a vergência observada nas ilhas é diferente da vergência catalogada tanto no Cape Fold Belt, quanto no Sierra de La Ventana Fold-belt; no entanto, conforme apontado por Ramos et al. (2017) possui o mesmo *trend* observado em quartzitos na Patagônia (von Gosen, 2003).

O principal ponto fraco da hipótese de Adie é a necessidade de uma rotação de 180º das ilhas em tempos pré-Jurássicos, de maneira a acomodar as similaridades já citadas. Ramos et al. (2017) apontaram que, apesar de robusta, a correlação entre as Ilhas Malvinas e África do Sul não consiste de única solução para a problemática da evolução da região e mostram que há similaridades importantes com a Patagônia que não devem ser descartadas.

3.4.3 Hipótese de Borello (1963)

Borello (1963) apontou diversas similaridades das Ilhas Falkland (Malvinas) com o terreno Patagônico. Ramos et al. (2017) mostraram, através de uma excelente revisão bibliográfica, seguida de um estudo isotópico e de proveniência, a importância de considerar o terreno setentrional sul-americano nas reconstruções.

É demonstrado, por exemplo, que o Sistema Gastre não possui evidências de cisalhamento destral. De maneira oposta, é um sistema de falhas reversas com um componente sinistral subordinado (Franzese e Martino, 1998; Ramos et al., 2017). Provavelmente, esta zona de falhas reversas dúcteis está restrita ao Paleozóico, não podendo ser mais jovens que o Permiano. Portanto, os dados de Franzese e Martino (1998) e von Gosen e Loske (2004) não corroboram à existência de um sistema de cisalhamento destral intracontinental, tal qual concebido por Rapela et al. (1991) e Rapela e Pankhurst (1992), que acomodasse os movimentos necessários à rotação das Ilhas Falkland (Malvinas; Ramos et al., 2017). Desta forma, Ramos et al. (2017) concordam com o inicialmente proposto por Rabinowitz e LaBrecque (1979), onde a zona de falha da Agulhas/Malvinas, transformante em essência, foi de vital importância à separação do Falkland (Malvinas) Plateau do Agulhas Plateau. Esta falha foi ativa durante a abertura do Atlântico Sul e, do lado sul-americano, desaparece em direção ao continente.

Ainda, há duas populações de diques doleríticos, com idades do Eo-Jurássico e Eo-Cretáceo, respectivamente (Cingolani e Varela, 1976; Hole et al., 2015; Mitchell et al., 1986; Mussett e Taylor, 1994; Richards et al., 2012; Stone et al., 2009, 2008). O mais antigo, Eo-Jurássico, possui um *trend* directional que sugere esforços extensionais de natureza NE-SW; enquanto que os Eo-Cretáceos possuem esforções de natureza E-W. Conforme apontado por Ramos et al. (2017), o evento Jurássico é provavelmente resposta à abertura do Mar de Wedell, enquanto que o evento Cretáceo ocorreu devido à abertura do Atlântico Sul. Evidências destes episódios são encontradas em bacias *offshore*, por exemplo *Southern Rift System* (NW-SE) e *North Falkland (Malvinas) Basin* (N-S; Richards et al., 2012). Assim sendo, os esforços Mesozóicos das ilhas são dominantemente puros e, devido a isso, podem ser associados a esforços de mesma natureza e idade encontrados na Patagônia. Desta forma, é possível relacionar a mudança de tensões a episódios tectônicos de escala continental distintos, ao invés da rotação do bloco.

De maneira a corroborar à hipótese de Borello (1963), Ramos et al. (2017), fazendo um estudo de proveniência de unidades Siluro-Devonianas pós desconformidade, identificaram uma assinatura Neo-Cambriana-Ordoviciana nos zircões. Esta assinatura é comum em quartzitos do sistema Sierra de La Ventana (Alessandretti et al., 2013). Provavelmente, são derivados de rochas ígneas de mesma idade advindas do Maciço Deseado (Moreira et al., 2013). Não há rochas com essas idades advindas do sistema *Cape Fold Belt*, nem de *Maud Belt*. A assinatura das rochas do Natal, no entanto, é marcada por zircões Neo-, Meso- e Paleoarqueanos (Ramos et al., 2017).

MANUSCRITO

MAURICE EWING BANK COMPLEX: NATAL-MAUD BELT MISSING FRAGMENT AND ITS IMPLICATIONS FOR RODINIA RECONSTRUCTIONS

Mateus Rodrigues de Vargas[1,2], Farid Chemale Junior[1,2], Tiago Girelli[2]

[1]Programa de Pós-Graduação em Geologia, Universidade de Brasília, Brasília-DF, 70904-970, Brazil
[2]Programa de Pós-Graduação em Geologia, Universidade do Vale do Rio dos Sinos, São Leopoldo-RS, 93022-000, Brazil

Highlights:

- Maurice Ewing Bank Complex underwent collisional granulite facies metamorphism, with associated partial melting, related to Rodinia-Forming orogeny;
- Paragneiss protolith deposited in a back-arc environment, with sediments transported from Margate-Maurice-Sivorg volcanic arc and Kaapvaal-Grunehogna craton;
- 4 episodes of recrystallization-partial melting are related to Rodinia forming orogens. The climax (R3) occurred close to the Stenian-Tonian boundary at 1 Ga, causing the peak metamorphism recrystallization event not only in Maurice Ewing Bank, but also in Natal Province, and Cape Meredith Complex;
- Maurice Ewing Bank constitutes a link between Natal and Maud belt. Therefore, it is part not only of Kalahari Craton but also of Grenville orogeny.
- Natal-Maud belt were generated due to the interaction of Patagonia-Coats land and Kaapvaal-Grunehogna margins;
- The complex underwent several thermal reactivations, up-to greenschist facies, related to Neoproterozoic and Paleozoic events such as Panantarctican-Panafrican, and Gondwanides.

Graphical Abstract:

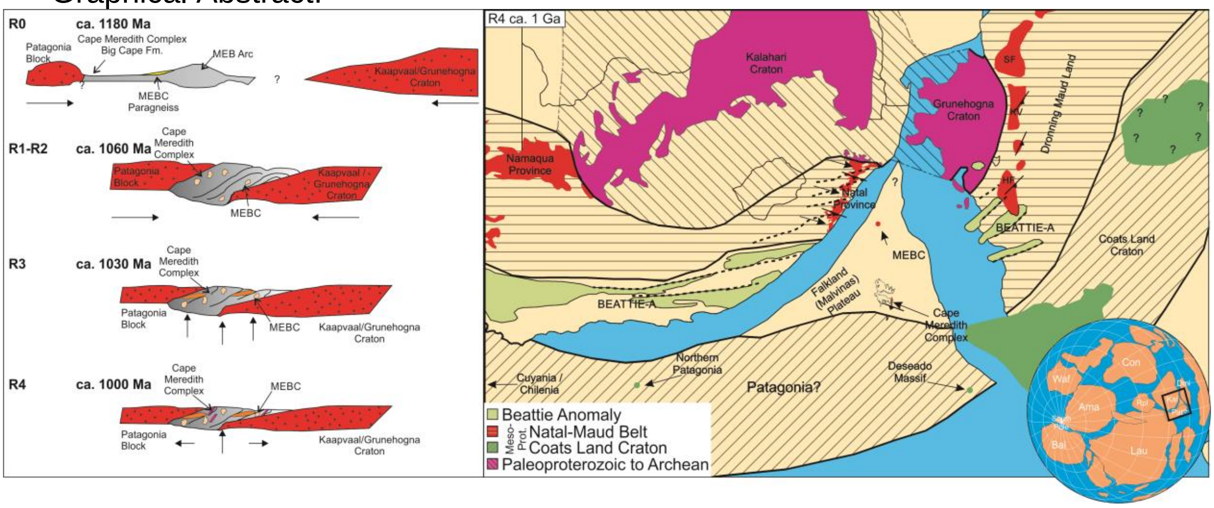

ABSTRACT

The evolution of Rodinia still have several questions that remain *incognito,* which directly impact the paleotectonic interpretation of coeval and posterior events. That is the case of the role of the unexposed Mesoproterozoic crust of remnant micro-terranes such as Maurice Ewing Bank and its relationship with the Rodinia-forming process at ca. 1 Ga. This works aims, by means of petrology and geochemistry, to unravel the metamorphic history of the Maurice Ewing Bank Complex (MEBC), and to determinate its role in the Laurentia-Kalahari evolution. MEBC consist of a polyphasic metamorphic terrane with three recrystallization cycles. The Rodinia-forming cycle (R) has one episode of deposition and four episodes of recrystallization/progressive deformation identified: [1] deposition of immature sediments, in a back-arc environment, close to the source rock (R0); [2 and 3] long-lasting high-temperature, high-pressure metamorphic condition, related with a fold-and-thrust belt (R1-R2). [4] granulite facies metamorphism (R3). [5] end of the collisional event, characterized by post-deformational granitoids (R4). We interpret that R1-R2 coincides with the older syn-deformational metagranitoid age of 1068 ± 28 Ma. A tectonic exhumation in R3 is related to syn- to tardi-metagranitoids at 1032 ± 12 Ma. It was followed by an R4 event of crustal delamination at 1006 ± 13 Ma. The reset in Rb-Sr and K-Ar systems were due to posterior metamorphic cycle, up to greenschist facies (<500ºC). We interpret that as caused by far-field thermal anomalies of Neoproterozoic-Paleozoic orogenic events, such as Panantarctican-Pananfrican-Gondwanides. The anchimetamorphic cycle (<300ºC) is related to uncomprehend Juro-Cretaceous rifting events. MEBC was part of Natal-Maud orogeny by the end of Mesoproterozoic, standing right in between Margate and Heimefrontfjella terranes. We suggest that the collision of Kaapvaal and Coats-Patagonia margins generated Natal-Maud belt, including MEBC. The true extension of the collision could be extrapolate far west the Beattie-A anomaly, ending close to the Chilenia-Cuyania-Llano at Laurentia.

Keywords: DSDP Site 330; Kalahari Craton; Falkland-Malvinas Islands; Falkland-Malvinas-Maurice Block; F2MT; Grenville Orogeny; Natal-Maud Orogeny, Rodinia Supercontinent.

1 INTRODUCTION

Rodinia is a powerful polysemic Russian word (McMenamin and McMenamin, 1990). It means what it means: *to beget* or even *to grow*. By doing so, this word represents not only procreation but also the natural development of maturity (Li et al., 2008). Notwithstanding, in Earth Sciences, Rodinia represents a hypothetic configuration of land masses that perpetuated from Mesoproterozoic (≈1.1 Ga) to Neoproterozoic (≈0.7 Ga; Nance et al., 2014; Roberts, 2013; Roberts et al., 2015). Rodinia-forming event had reached its apex around Stenian-Tonian period when several continental blocks amalgamate to form a supercontinent through continental-wide orogenic events (*a.k.a Grenville Event;* Li et al., 2008; Roberts et al., 2015). Today, several available reconstruction models represent this cycle. These models surround the threshold between creativity and scientific knowledge. Unfortunately, they only consider large cratonic areas. As expected, several units of geological relevance have not been considered in paleogeographical reconstructions whether their limited areal extent or complete geological unawareness (Fuck et al., 2008; Li et al., 2008). In other words, many of Rodinia continental *"heir"* is still considered *"bastards."*

Ignore these still illegitimate terranes, such as Falkland (Malvinas) Island, might lead to conflicting interpretations about Earth evolution. Despite its active role for the consolidation of Continental Drift Theory and Gondwana evolution (Du Toit, 1927, 1937), there is still no consensus about Falkland (Malvinas) Island position before Gondwana break-up. According to Ramos et al. (2017), there are three main hypotheses about the tectonic evolution of the island. Du Toit (1937) argued that the island was somewhere between South America and South Africa. Contrastingly, Adie (1952) inverted the position of the island, placing it as an appendix of Cape Fold Belt, in South Africa east side. Borello (1963) theorized that the island kept a similar position as seen today, standing fixed to the South American plate. However, as pointed out by Ramos et al. (2017), one effective way to reduce the several degrees of freedom related to all interpretations is increase the knowledge about Maurice Ewing Bank continental basement.

This feat has only made possible due to the *Deep-Sea Drilling Program* (DSDP), which was, coincidentally proposed by Dr. Maurice Ewing (Ewing and

Hayes, 1970). In 1974, DSDP leg 36 was planned to clarify the geologic history of the southwest Atlantic Ocean, and Falkland (Malvinas) Plateau (Barker et al., 1977b). During the expedition, lousy weather condition led to a re-evaluation of the selected sites, which ironically resulted in the drilling of site 330 (Barker et al., 1977b). After 2626 m of the water column, and 550 m of Mesozoic-Cenozoic sedimentation, 19.5 m of the gneissic and granitic continental basement were drilled that comprehend the only physical register of a whole crustal block (Tarney, 1977; Figure 1 - B). Beckinsale et al. (1977) had dated these rocks as Ediacarian-Fortunian (Rb-Sr, and K-Ar), and interpreted them as a thermal reactivation event during Paleozoic. Nonetheless, the scientific community considered those ages as crystallization events, which led to several misinterpretations about the Falkland (Malvinas) Plateau evolution. Recently, Chemale Jr. et al. (2018), using U-Pb in zircon, reinterpreted the age of Maurice Ewing basement rocks as metamorphosed and, when applicable, generated by a Stenian-Tonian age regional event. This fact led to a debunking of the region, relating Maurice Ewing Bank rocks with Cape Meredith Complex, located at Falkland (Malvinas) Islands (see Chemale Jr. et al., 2018 for more detail). The petrography aspects, however, were only studied by Tarney (1977), who identified a high-grade metamorphism event. Since Tarney's pioneer study, the rocks have not been revisited.

This work aims, by means of petrology and geochemistry, unravel the metamorphic history of the MEBC to determine its role in the Natal-Maud belt, and Greenville orogeny. Furthermore, after an extensive literature review, this work purposes to hypothesize the terranes involved in the Natal-Maud generation to diminish the degrees of freedom derived from Rodinia reconstructions.

2 REGIONAL FRAMEWORK

The Falklands (Malvinas) Plateau is a submarine projection of the South American continental margin that extends through approximately 1800 km east of the Falklands (Malvinas) Islands, where gently pinches out through the Georgia Basin (Figure 1 - A; Kimbell and Richards, 2008). Two continental-wide features bound the Plateau, Falkland-Malvinas Escarpment (FME) and North Scotia Fault Zone (NSFZ), both related with South Atlantic evolution and Pangea Breakup (Ludwig and Rabinowitz, 1982; Rabinowitz and LaBrecque, 1979). There are two remarkable morpho-structural highs located in the central part of the plateau: i) Falkland Islands and ii) Maurice Ewing Bank. Recently, Schimschal and Jokat (2018), after seismic refraction experiments, postulated that both highs are indeed continental crust separated by a rifting event that had caused oceanic spreading before the Mesozoic-Cenozoic filling of the Falkland Plateau Basin (Figure 1 – B).

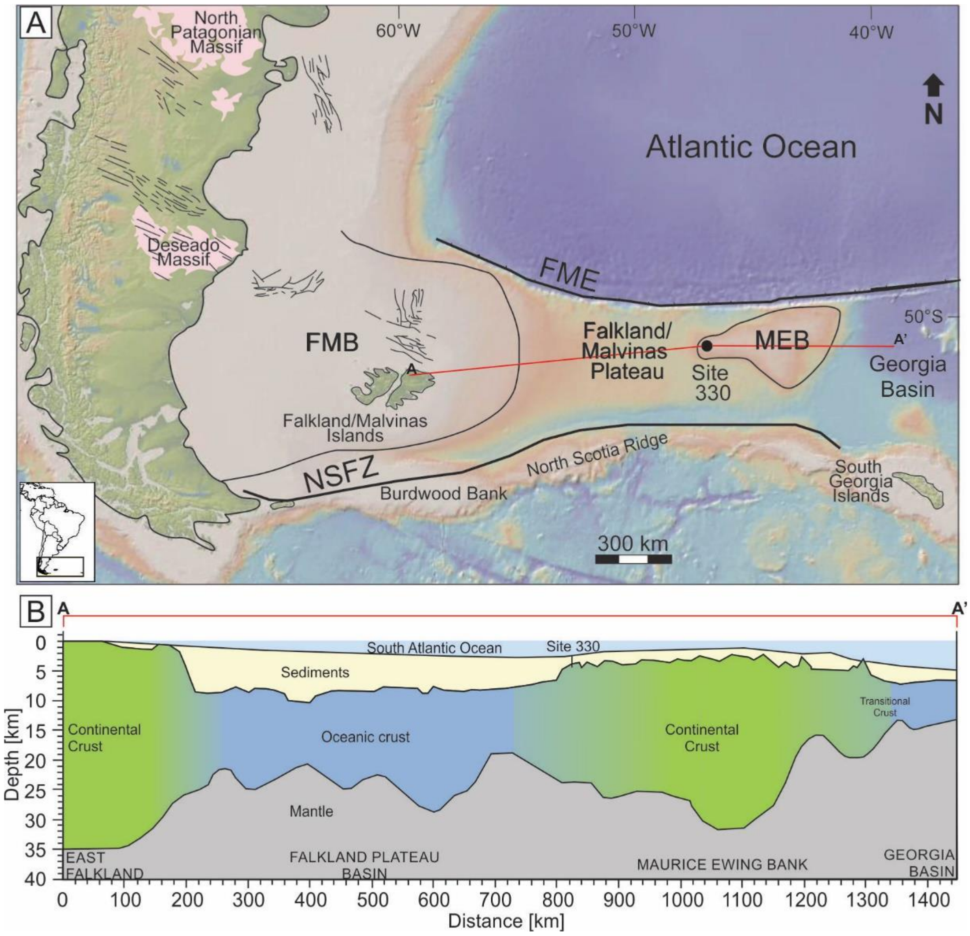

Figure 1 – Location of DSDP Site 330, Leg 36. A) Falkland-Malvinas Plateau map with the main geomorphological features (modified from Chemale Jr. et al., 2018); B) Simplified geological interpretation of A-A' section following Schimschal and Jokat (2019) scheme. Legend: FMB – Falkland-Malvinas Block, FME – Falkland-Malvinas Escarpment, MEB – Maurice Ewing Bank, NSFZ – North Scotia Fault Zone.

Both blocks have physical evidence of this continental crust signature. In the Falkland Islands side, there is a thin region located at West Island where these continental crust rocks outcrop. The Cape Meredith Complex (CMC; Adie, 1952; Baker, 1924) consists of a metamorphosed volcano-sedimentary sequence with ca. 1.1 to 1 Ga crosscut by several anatectic granites from Stenian-Tonian transition (Jacobs et al., 1999; Thomas et al., 2000, 1997). Similarly, there is a register of continental crust recovered at Maurice Ewing Bank block, during DSDP Site 330, leg 36 (Barker et al., 1977a). As CMC, MEBC rocks consist of a metamorphosed volcano-sedimentary complex, with ca. 1.1 to 1 Ga, crosscut by several anatectic granites from Stenian-Tonian (Beckinsale et al., 1977; Chemale Jr. et al., 2018; Tarney, 1977, and this work). These similarities led Chemale Jr. et al. (2018) to hypothesize that, before the Mesozoic extension, MEBC and CMC were the same crustal fragment, herein considered Falkland-Malvinas-Maurice Terrane (F2MT), following suggestions first proposed by Tarney (1977). The impact of these recent finds results in a critical review of the role of F2MT during supercontinent cycles associated with Rodinia amalgamation, and Gondwana breakup.

Several reconstructions (Bisnath et al., 2006; Bisnath and Frimmel, 2005; Frimmel, 2004; Jacobs et al., 2015; Joachim Jacobs et al., 2008) consider Falkland (Malvinas) Island, and therefore F2MT, as part of Namaqua-Natal-Maud belt (Jacobs et al., 1993). This belt forms a continental-wide continuum of Mesoproterozoic rocks, product of collisional tectonics along the southern portion of Proto-Kalahari Craton (Jacobs et al., 1993; Joachim Jacobs et al., 2008; Thomas et al., 1994). The Natal Province consists of three arc terranes of ca. 1250-1150 Ma, accreted and metamorphosed during 1150-1100 Ma with post-accretion extension at ca. 1080 Ma and post-tectonic magmatism of ca. 1050-1030 Ma (Cornell et al., 2006; Mendonidis et al., 2015a; Mendonidis and Grantham, 2003; Spencer et al., 2015a); Heimefrontfjella, the Dronning Maud Land proxy, represents a complete volcanic-arc system, composed by back-arc basin, volcanic rocks related to the arc itself, and forearc basin sediments with protolith, and maximum deposition ages varying from 1200-1100 Ma (Jacobs, 2009; Jacobs et al., 1996). The region underwent two high-grade metamorphism event, related to the orogenic event at ca. 1090- 1060 Ma and ca. 500 Ma (Arndt et al., 1991; Jacobs et al., 2003a; Schulze, 1992). Both provinces have post-deformational rocks from the Tonian-Stenian transition.

3 RESULTS

3.1 Petrography

The samples employed for this work consist of 7,2 m of the recovered basement from the DSDP expedition 330, leg 36, cores 16 – 17 (Barker et al., 1977a). After the mesoscale description, 22 thin polished sections were made to understand the relationship between minerals, textures, and their structural/spatial patterns (Passchier and Trouw, 2005 - more info about sampling, check Supplementary Material 1). We collected 300 points per sample, at regular intervals of 1 mm, to obtain the statistic mode (Table 1 – see Supplementary Material 2).

Petrographically, the MEBC rocks have five distinct and wide classes, hereafter considered *sensu latu* lithofacies: (Figure 2 - A) paragneisse, (B) pre-deformational metagranite, (C) syn- to tardi-deformational metagranite, (D) post-deformational granitoid, and (E) melanossome (Table 1 - to compare with Tarner, 1974 and Chemale Jr. et al 2018 interpretations Supplementary Material 3).

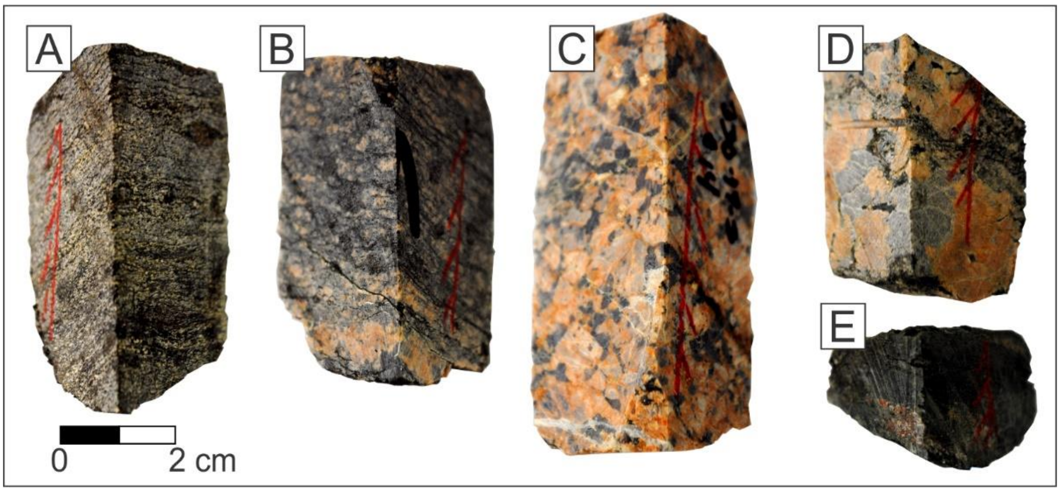

Figure 2 - – Lithofacies of Maurice Ewing Bank Complex. A - Paragneisse (#17R2-06; 0.33-0.40m); B – Pre-deformational metagranite (#16R2-08; 0.50-0.56m); C – Tardi-deformational granite (17R3-14; 0.83-0.90m); D – post-deformational granite (#16R2-18; 0.69-0.77m); E – Melanossome (#16R2-11; 0.69-0.77m).

The lithofacies has medium to coarse-grained crystals, primarily composed by quartz and feldspars in the quartzo-feldspatic (QF) domain, and biotites in the mafic (M) domain. The main structure is gneissose, and the main texture is granoblastic. The sum of these characteristics fits the definition of granulite rock, as suggested by

Coutinho et al. (2007). There is a subgroup of this lithofacies, herein classified as weathered paragneiss. In a broad sense, it contains euhedral diagenetic calcite, and tabular tourmaline, despite all paragneisses characteristics. As expected in this lithofacies, there are two main mineralogical domains i) quartz-feldspathic rich (QF), and ii) mafic rich (M) in a well-formed primary foliation. There is a posterior subtle foliation, mainly composed by platy biotite crystals, that crosscuts the main foliation. This feature is indicative of a C-S fabric as already noted by Chemale Jr. et al., (2018).

The granitoids were classified as pre- (Figure 2 - B), tardi- (Figure 2 - C), and post-deformational (Figure 2 – D). They vary from very fine to coarse-grained crystals. In pre-deformational, grains tend to be fine-grained. The dominant crystal size is medium in tardi-deformational; however, coarse-grained crystals can also occur. In post-deformational, the crystal size, dominated by alkali feldspars, tends to be coarse to very coarse.

The last unit has a brownish to black color, dominantly composed by relict biotites, today replaced by green chlorites (Tarney, 1977; Figure 2 – F). All units are cut to some extent by mm to cm thick subvertical to subhorizontal quartz or calcite veins. For a description of microtectonics, the reader is referred to Supplementary Material 4.

Table 1 – Summary of mineral assemblage and accessories according to each lithofacies.

Lithofacies	Paragenesis	Accessories
Paragneiss	Qtz + Kspar + Plag + Grt ± Sil ± Tour ± Cal	Rut + Ap + Zrc + Mon
Pre-deformational metagranite	Qtz + Kspar + Bt + Sil + Grt + Plag ± Cal ± Chl	Chl + Ap + Zrc + Mon
Syn- to Tardi-deformational metagranite	Kspar + Qtz + Plag + Bt + Grt ± Chl	Chl + Ap + Zrc + Mon
Post-deformational Granitoid	Kspar + Qtz + Bt	Chl + Ap + Zrc + Mon
Melanossome	Bt + Chl + Qtz	Rut

3.1.1 Paragneisses

The metasedimentary rocks were classified as paragneisses and weathered paragneisses, following the suggestions of Schmid et al. (2007). Generically, this unit is dominantly composed by quartz, alkali-feldspar, with minor plagioclase, and sillimanite in the QF domain. Biotite mainly composes the mafic domain. Garnet does also occur in the interface between QF, and M. Common accessories are zircon, tourmaline, rutile, ilmenite, and apatite.

The quartz crystals tend to be allotriomorphic and granoblastic; while the potassic feldspars are tabular and hypidiomorphic, being recurrently sericitized. The tabular plagioclase, usually sericitized and calcitized, forms a minor constituent. The overall plagioclase composition ranges from Ab_{10-20} (Beckinsale et al., 1977). This high albite content is usually related to retrometamorphism in green-schist facies (Moody et al., 1985).

The garnet porphyroblasts, usually located in the interface between QF and M domain, have a variance of textures and geometries. The dominant one consists of blastoid idiomorphic; nonetheless, some allotriomorphic minerals are present, as well as minerals with core-and-mantle texture. Moreover, some garnet crystals are relict, being partially or entirely substituted by biotite/chlorite. In a broad sense, they have a uniform grain size and are usually fractured, with sparse inclusions of quartz, rutile, biotite, ilmenite, and zircon. The occurrence of anomalous size grains is indicative of crystal amalgamation, and thus, rapid growth rate.

There are several occurrences of Al_2SiO_5 polymorph sillimanite and fibrolite, demonstrating two different stages of growth with distinctive stress fields. Sillimanite has a bladed geometry oriented according to mineral lineation. The fibrolite is either oriented according to the mineral lineation or randomly arranged in fabric, even occurring as a radiate pattern.

The M domain is composed of mm-thick layers mainly formed by idiomorphic biotite. Those micas usually have a hexagonal habit, a characteristic reddish-brown color, preferential intergrown at {001}, and several rutile inclusions. Those inclusions fill the sagenic texture; that is, the rutile needles follow biotite {001} crystallographic plane and are parallel to the {011} crystallographic axis (Shau et al., 1991). The reddish-pleochroism from biotite usually is related to high Ti content. The enrichment of this element is indicative of high-grade rocks, usually related to granulite terranes. The sagenitic texture, however, is indicative of retrogressive metamorphism back to green-schist facies (Shau et al., 1991).

Calcite occurs only close to the disconformity, between grain aggregates, as a product of plagioclase weathering or recrystallization. The presence of this mineral attests a subaerial period in which MEBC rocks were exposed, a fact already postulated by Tarney (1977).

3.1.2 Pre-, syn- to tardi-, and post-deformational granitoids

We classify the granitoid rocks into three units, due to their petrographic characteristics: i) pre-deformational; ii) syn- to tardi- deformational; iii) post-deformational. The term proposed by Tarney (1977; e.g., $\sigma 1$, $\sigma 2$, and so forth) will be excluded to avoid jargon misunderstandings. The pre- and syn- to tardi-deformational rocks are placed according to the primary foliation of the paragneiss. The post-deformational, albeit, does not. Still, pre-deformational and syn- to tardi-deformational have a distinctive mineral lineation that coincides with those observed in the gneissic rocks, which was partially obliterated due to static recrystallization processes. The post-deformational granitoids, again, do not have this preferential alignment. Therefore, pre-, syn- to tardi-granitoids are in essence metamorphic; whilst post-deformational granitoids are igneous.

The quantity of each mineral is variable. Nonetheless, the rocks have an evolutionary trend ranging from granites and sienogranites (pre-deformational and syn- to tardi-deformational) to sienites (post-deformational). All granitoids but post-deformational, are composed by potassium feldspar, plagioclase, quartz, and biotites. The post-deformational lacks plagioclase, being only constituted by potassium feldspar, quartz, and biotite. Accessories minerals, disregarding their lithofacies, are zircon, apatite, ilmenite, and monazite.

Alkali feldspars range in size from fine- to medium-grained, in pre-deformational and tardi-deformational to very-coarse in post-deformational. Usually hypidiomorphic, they have two distinct populations: microcline and sanidine. This contrast is related to fractures regions. Microcline only occurs at high-strained locations. Plagioclases, usually with albite twinning, are dominantly hypidiomorphic, ranging from fine to medium grained. Commonly, they are sericitized. Plagioclases from pre-deformational and tardi- post-deformational have different compositions. The pre-deformational has a slightly more sodic composition, whereas tardi- post-deformational, more calcic. Quartz crystals vary from very fine to coarse and are usually allotriomorphic with undulose extinction. Biotite is the only mafic forming mineral identified in all granitoids. The biotites crystals share those characteristics identified in paragneisses (i.g. hypidiomorphic, reddish pleochroism, sagenitic texture).

Unlike post-deformational granitoids, pre-deformational meta-granitoid has tabular sillimanite and acicular fibrolite. Still, both pre- and syn- to tardi-deformational have granoblastic garnet inserted in a matrix that was affected by some extend to ductile processes. These data suggest that the metamorphic peak affected not only paragneisses but also those two granitoid units.

3.1.3 Melanosome

This lithofacies dominantly consists of relict idiomorphic biotites. Today, biotite crystals are weathered to a greenish-clay mineral and unweathered reddish-brown biotites. The relict idiomorphic biotites usually have a hexagonal habit, a characteristic green color, and preferential intergrown at {001}. The reddish-brown biotites share the characteristics from other units (e.g., sagenitic texture). Thus, acicular rutile is a common accessory. There are no expansive clay minerals identified in this lithofacies. However, the greenish-clay mineral identified by Tarney (1977) consists of corrensite, a chlorite mineral (Supplementary Material 5).

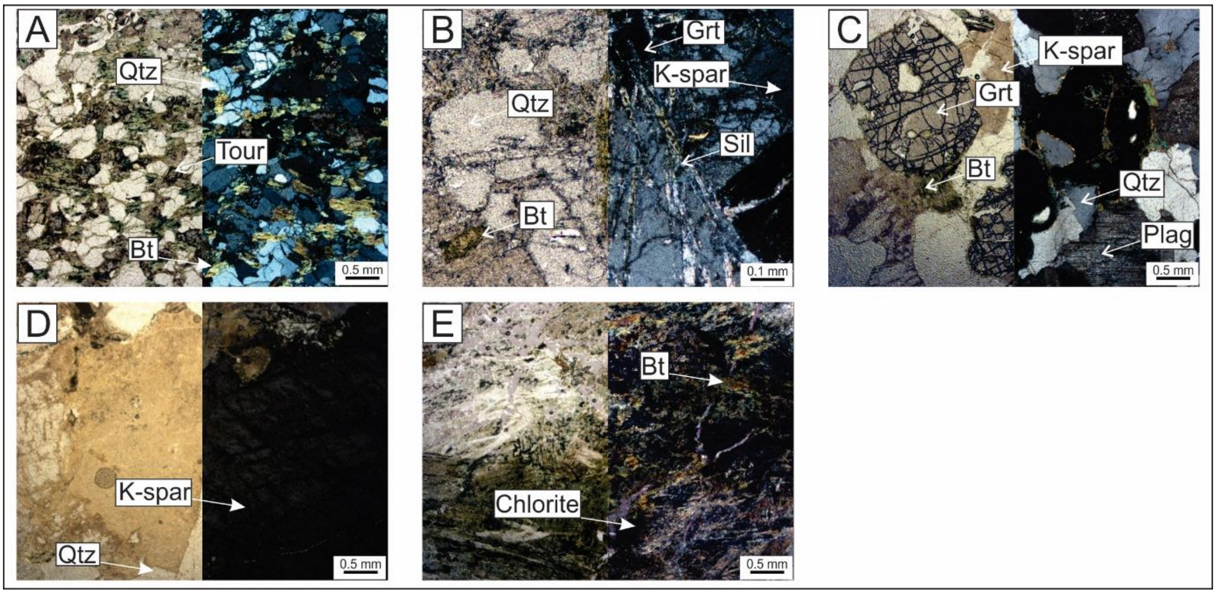

Figure 3 – Thin section of Maurice Ewing Bank Complex lithofacies. A – Paragneiss; B- Pre-deformational metagranite; C – Syn- to Tardi-deformational metagranite; D – Post-deformational sienite; E – Melanosome.

3.2 Geochemistry

Sample preparation and rock chemical analyses were made at Activation Labs for major, and trace elements. The acquired geochemistry results obtained by Tarney (1977) were assembled to our database to build a better statistical framework (Supplementary Material 6). The statistical sample was made using GCDKit software (JanoušEk et al., 2006) as well as the plotting of several geochemical diagrams. When applicable, all samples were prepared considering a volatile free environment, normalized to 100% total (Verma and Armstrong-Altrin, 2013). We utilized diagrams proposed by Herron (1988), Roser and Korsch (1988), and Verma and Armstrong-Altrin (2013) to understand the composition of protolith, in the rocks that have sedimentary derivation (e.g., paragneisses and weathered paragneisses). Those diagrams consist of the analysis of major and trace element concentrations to infer, respectively, the initial sedimentary composition, the provenance, type of source-area, and the geotectonic environment.

The criteria for lithofacies identification was based on major and trace element analysis (e.g., chondrite REE normalized diagram from Boynton, 1984). As petrography analysis, we interpreted 5 classes consisting of: i) paragneiss (non-weathered and weathered); ii) pre-deformational metagranite; iii) tardi-deformational granite; iv) post-deformational granite; and v) melanosome.

3.2.1 Paragneisses

The paragneisses share most of the oxide composition, despite being separated into two sub-groups. They have high SiO_2 content ranging from 58 to 82 wt%. The Al_2O_3 content is highly variable, ranging from 6 to 18.4 wt%. The TiO_2 is low (0.591 to 1.31 wt%), as well as FeO (0.68 to 4.1 wt%), Fe_2O_3 (1.7 to 5.87 wt%), MgO (0.28 to 2.16 wt%), MnO (0.01 to 0.16 wt%). The alkalis are relatively low. NaO ranges from 0.6 to 2.02 wt%, and K_2O from 1.23 to 6.58 wt%. CaO ranges from 0.24 to 9.55. We classify the paragneisses with high CaO content as weathered paragneiss sub-group, following Tarney (1977).

The chondrite normalized patterns of REEs showed enrichment of LREEs over HREEs with LaN/YbN = 3.82 – 6.30. All analyzed samples have a strong enrichment in light rare elements (LREE; LaN/SmN = 2.69 – 3.02), flat HREE (GdN/YbN =1.21 – 1.52), and subtle Eu anomaly (Eu/Eu* = 0.65 – 0.78; Figure 4 - A).

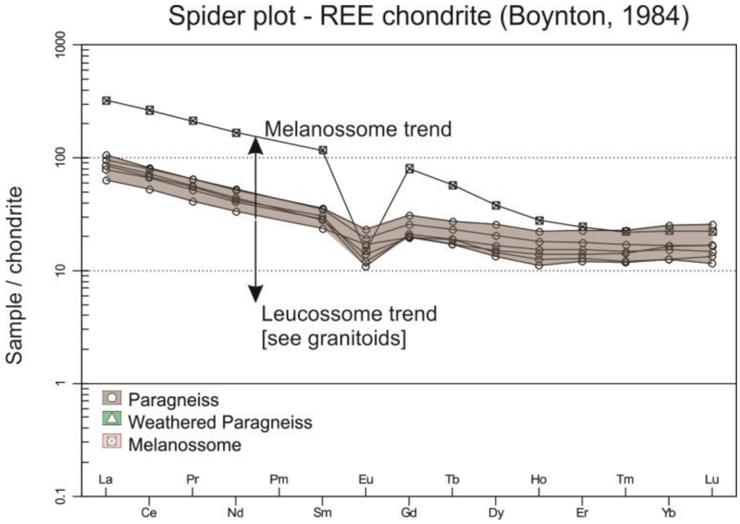

Figure 4 – REE Chondrite (Boynton, 1984) for MEBC paragneisses and melanosome.

In a broad sense, the paragneisses are related to immature rocks. The protolith varies in composition from psammitic to pelitic in composition. There is a predominance of wackes, litharenites, and arkoses (Figure 5 – A). Also, by using the major element analysis diagram from Roser and Korsch (1988; Figure 5 – B), all paragneisses fit into the recycled-orogenic field, whereas in tectonic discriminant diagram, the samples fit into the arc/collisional environment (Figure 5 – C).

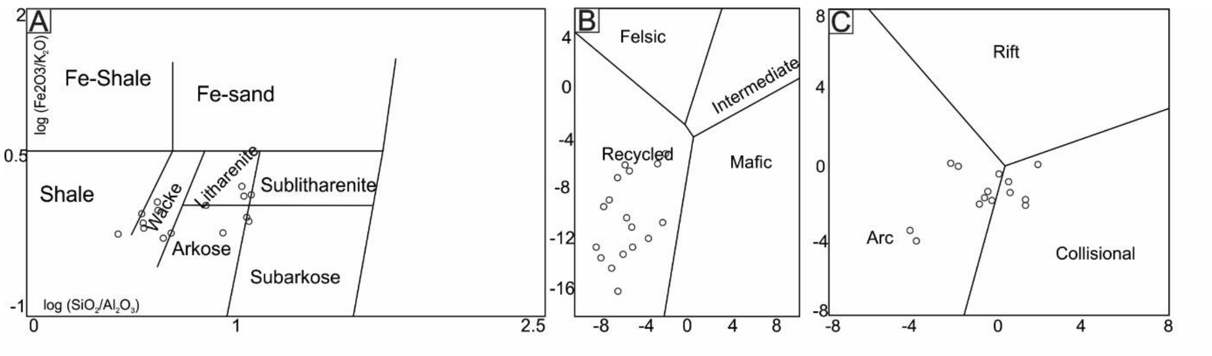

Figure 5 – Protolith initial composition diagrams. A) Diagram to discriminate the protolith composition (Herron, 1988); B) Provenance diagram based on the distribution of major elements (Roser and Korsch, 1988); C) Diagram to discriminant the geotectonic environment, based on major element analysis, prior to Cambrian period, for rocks with >63 wt% SiO_2 (Verma and Armstrong-Altrin, 2013).

3.2.2 Granitoids

We discriminate three classes of granitoids based on geochemistry, following petrography analyses. They are pre-, syn- to tardi-, and post-deformational. The SiO_2 from pre-deformational ranges from 70.1 to 71.88 wt. %. The tardi-deformational granites are slightly richer in SiO_2 content, with values ranging from 66.3 to 73.9 wt. %. In the post-deformational, similar values for SiO_2 are present, from 63 to 72.83 wt. %. TiO_2 tends to have lower values in pre-deformational granites than others. Al_2O_3 has values that range from 12.98 to 14.3 wt.%, 11.86 to 15.6 wt. % and 7.05 to 21.6 wt. % in pre-, tardi-, and post-deformational, respectively. K_2O tends to become enriched according to the fractioning varying from 5.65 to 5.92 wt% in the pre-deformational, 6.42 to 8.61 wt.% in the tardi-deformational, and 4.39 to 10.94 wt% in the post-deformational granite. The CaO has a composition from 0.31 to 0.52 wt. %, 0.27 to 1.00 wt% (with an outlier of 6.72) and 0.51 to 0.77 wt%.

The chondrite-normalized REE pattern for the pre-deformational metagranite is similar to paragneisses (Figure 6 – A). There is an enrichment of LREE over HREE (La_N/Yb_N = 4.74) as well as enrichment in LREE (La_N/Sm_N = 3.16), flat behavior in HREE (Gd_N/Yb_N =1.13), and subtle Eu anomaly (Eu/Eu* = 0.63). In tardi-deformational granites, the LREE pattern and Eu anomaly are similar to either paragneisses or pre-deformational meta granites (La_N/Sm_N = 2.39 – 2.66; Eu/Eu* = 0.5 – 0.88); however, there is a strong enrichment of LREE over HREE (37.08 – 106-52) and HREE depletion (Gd_N/Yb_N = 10.29 – 25.02). The post-deformational granite has the lowest LREE normalized values. Despite the overall low LREE content, this unit follows the trend of MEBC (La_N/Sm_N = 2.81 – 3.22). However, two main contrasting characteristics emerge i) lack of Eu anomaly (Eu/Eu* = 1.04 – 1.13) and ii) moderate HREE depletion (Eu_N/Yb_N = 3.98 - 5.97). We interpret that the REE pattern has similarities of arc granitoids, being generated during the first anatectic pulses. Therefore, pre-deformational metagranite is probably the older migmatized unit in the complex. Both sin- to tardi-deformational have a REE pattern similar to sin- to post-orogenic granitoids. In post-deformational granite, the strong HREE depletion probably reflects the lack of metamorphic minerals (e.g., garnets) in the assemblage, and thus the absence of metamorphism. We interpret the lack of Eu anomaly and the depletion of HREE as generated due to pegmatitic placement (Tarney, 1977). Thus, post-deformational granite is the youngest rock of the unit, probably generated close to the liquidus-out in the system.

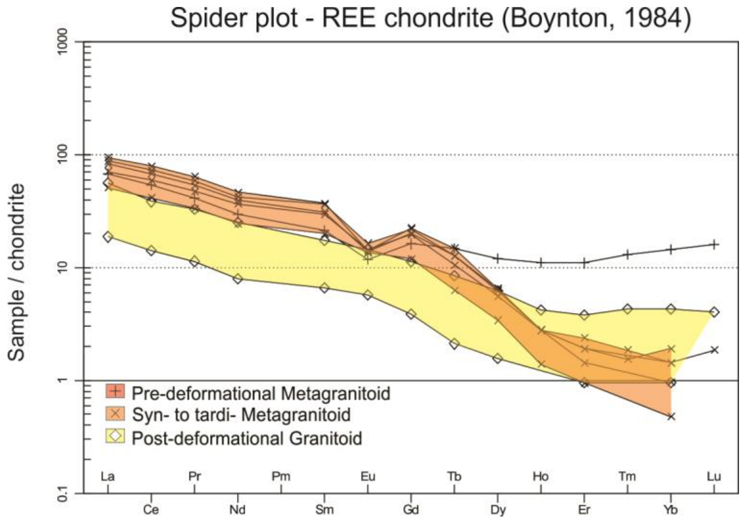

Figure 6 - REE Chondrite (Boynton, 1984) for MEBC granitoids.

There is a compositional evolution pattern from pre- to post-deformational granites. According to Middlemost (1994) classification diagram (Figure 7 – A), we classify the pre- and tardi-deformational granitoid as granites. The post-deformational granite, however, ranges from granite to syenite. In the Rb vs. Y+Nb diagram, pre-deformational metagranite falls into VAG field; whereas the other granites in the syn-COLG field (Figure 7 - B1). On the other hand, all granites fall into Volcanic Arc Granites (VAG) + syn- to tardi-collisional granite (syn-COLG) in Pearce Y-Nb tectonic discrimination diagram (Figure 7 – B2). Therefore, pre-deformational metagranitoid was generated in an arc environment; whereas, syn- to tardi-, and post-deformational were generated in a collisional setting. There is an agreement between geochemical and petrological description, thereby validating the interpretation. The granite samples preserved the expected characteristics of thermal/anatectic pulses, being useful markers for the tectono-thermal evolution of the complex (Chemale Jr. et al., 2018).

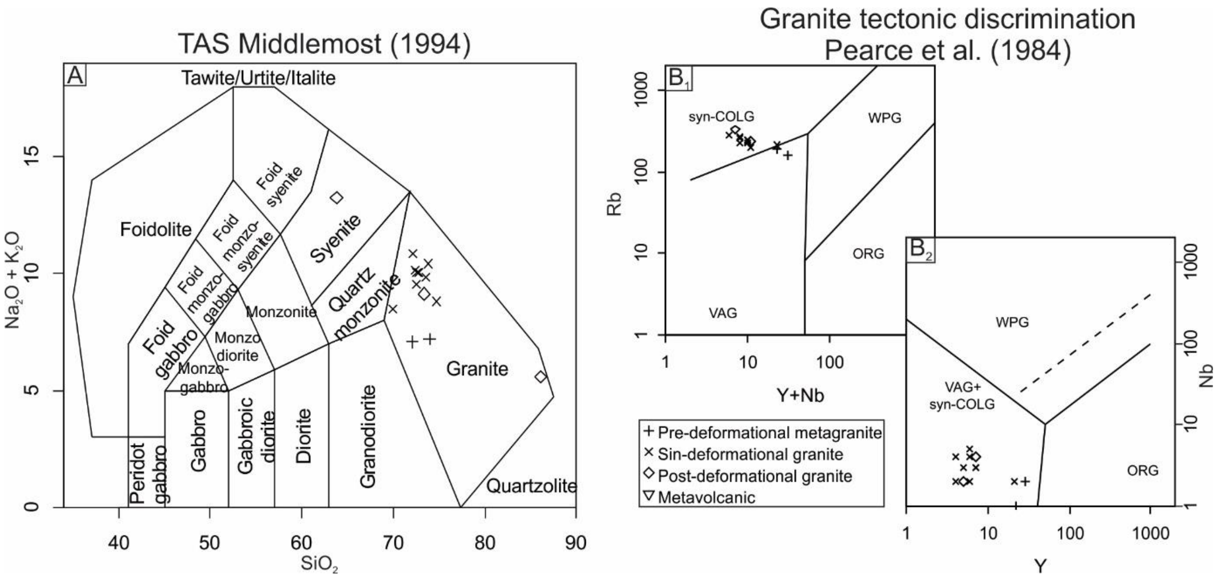

Figure 7- TAS classification diagram (Middlemost, 1994) and Granite discrimination diagram (Pearce et al., 1984) for MEBC granitoid rocks.

3.2.3 Melanosome

The melanosome lithofacies has a composition that suggests a high incompatible enrichment. SiO_2 is low, with a value of 39.15 wt%, whereas Al_2O_3 is high (22.03 wt.%). TiO_2 is also high, with 2.21 wt%, as well as Fe_2O_3 (17.05 wt%) and MgO (2.97 wt%). CaO and NaO have respectively low values of 0.29 and 0.54. K_2O is high with a value of 5.14. Al_2O_3, K_2O, and TiO_2 enrichment are mainly due to the quantity of Ti-rich biotites. The lack of sialic minerals, such as feldspars, reflects the SiO2 abundance.

There is a fractionated pattern with the highest identified REE abundances (La_N/Yb_N = 14.34) compared to the other rocks of the MEBC. The unit has a strong enrichment in LREE (La_N/Sm_N = 2.78), moderate enrichment in HREE (Gd_N/Yb_N = 3.55), and strong Eu anomaly (Eu/Eu* = 0.15) when compared to paragneiss. The normalized chondrite patterns of REEs of this unit is somewhat similar to the paragneisses but enriched in all aspects. Additionally, it has a strong Eu anomaly (Figure 4). Both data confirms that this lithofacies is indeed a melanosome, being enriched in LREE and MREE, in this case liquidus incompatible, and highly depleted in Eu.

3.3 Mineral Chemistry

Mineral chemical data were obtained with an electron microprobe JEOL JXA-8230 with one EDS and five WDS spectrometers, at the Instituto de Geociências da Universidade de Brasilia, operating at 15kV and 15nA. Major elements were calculated in garnet, white mica and biotite, plagioclase, alkali feldspar, opaques (e.g., mostly magnetite and ilmenite), chlorite, and tourmaline, despite the rock unit. The garnet was normalized to 12 oxygens. Additionally, a stoichiometric calculation was done to convert Fe_{total} to Fe_2O_3 and FeO. The mica group minerals were normalized to 11 oxygens, and its H_2O amount in the system estimated considering that OH + Cl + F = 2. The feldspars group were normalized to 8 oxygens. The software WinCCac (Yavuz et al., 2015) processed the data regarding chlorite minerals. The software calculated the amount of H_2O in each sampling, considering 14 oxygens in chlorite structural formula. Fe^{3+} was not calculated. We applied the Al_{IV} geothermometer proposed by Kranidiotis and MacLean (1987), widely used when chlorites that are associated with other alumino-silicates (Yavuz et al., 2015; Supplementary Material 7). The software WinTCal (Yavuz et al., 2014) processed the data acquired for tourmaline group minerals. The data was normalized to have either 15 cations at T + Z + Y position or the sum of OH + F + Cl = 4. The software estimated either Fe^{3+} content according to the normalization to $O_{24.5}$ or H_2O content (Supplementary Material 8). The calculation for end-members was made according the following formulas: (i) Garnet $X_{Alm} = Fe_{2+} / (Fe_{2+}+Mg+Mn+Ca)$, $X_{Py} = Mg / (Fe_{2+}+Mg+Mn+Ca)$; $X_{Gr} = Ca / (Fe_{2+}+Mg+Mn+Ca)$; $X_{Sps} = Mn / (Fe_{2+}+Mg+Mn+Ca)$; (ii) Feldspars: $X_{An} = Ca / (Ca+Na+K)$; $X_{Ab} = Na / (Ca+Na+K)$; $X_{Kfs} = K/(Ca+Na+K)$.

3.3.1 Garnet

The garnets from MEBC have mean composition of $Fe^{2+}_{2.26}Mn_{<0.01}Mg_{0.62}Ca_{0.06}Al_{2.03}Fe^{3+}_{<0.01}(SiO_4)_3$ (n=179) and a homogeneous composition. This homogeneity is unit independent; that is, it occurs in all lithological units, except those that do not have garnets in the system (e.g., melanosome and post-deformational granitoid). The crystals are almandine rich, with mean $X_{alm} = 77 \pm 0.12$ (2σ; Supplementary Material 9). There is no distinct Zoning from the core to the rim

(Figure 8A and 8B). The garnet composition fits well the garnets derived from granulite terranes (Supplementary Material 10).

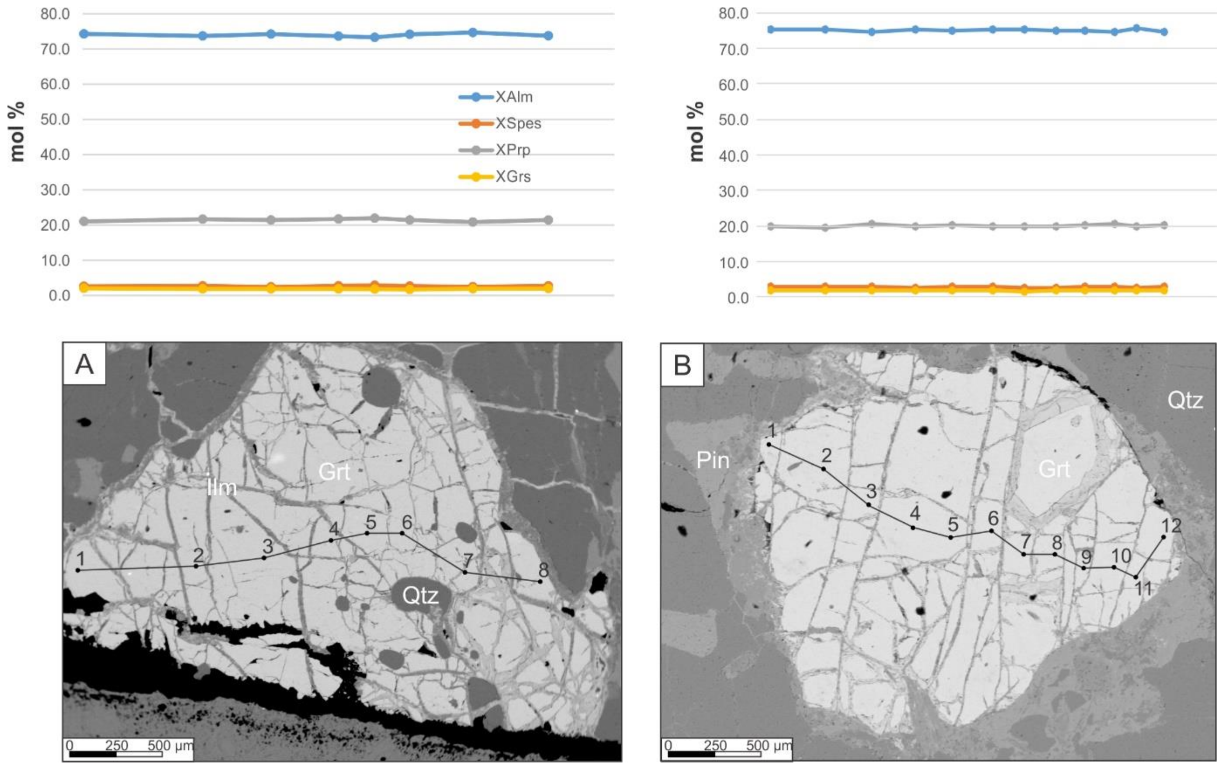

Figure 8 – Compositional profile of two idioblastic garnets. A) Pre-deformational metagranite: fractured garnet porphyroblast with elliptic-shaped quartz inclusions, and microinclusions of ilmenite. Additionally, there is a subtle reaction rim formed by pinite, a tardi-mineral phase (see text for discussions). B) Tardi-deformational granitoid– Fractured garnet porphyroblast with thicker pinite reaction-rim. Note the lack of quartz blobs and the presence of micro-ilmenites.

3.3.2 Feldspars

The analyzed feldspars are divided into four groups, three representing the alkali feldspars series and one representing the plagioclase series (Figure 9 - A). Each group is lithology dependent; that is, formed in a certain lithotype or a combination of lithotypes. Feldspars with X_{or} range from 74 to 99, with a mean (n=38) of 83 ± 2 (2σ), compose the first group, restrictedly occurring at paragneiss samples. The second group occurs in weathered paragneiss and mostly consists of X_{or} ranging from 58.7 to 96.9 with arithmetic mean of (n=9) 77 ± 10 (2σ). The third group has an arithmetic mean (n=20) of 85 ± 3 (2σ), with X_{or} ranging from 77 to 99, coinciding with pre-deformational granites. Rarely, do extreme X_{or} values occur in this specific group.

If all alkali feldspars samples are analyzed (n=67). For X_{or}, the arithmetic mean of 85 ± 2 (2σ) is obtained.

The plagioclases range in composition from anorthoclase to albite/oligoclase with An_{01-20} and Or_{21-23}. $An_{06 \pm 01}$ and $Ab_{83 \pm 02}$ (2σ; n=35) composes the arithmetic mean. The high variance observed in the plagioclase composition suggests crystal instability. Additionally, the low Anorthite content might suggest late albitization, related to greenschist-facies retrograde metamorphism (Moody et al., 1985; Supplementary Material 11).

3.3.3 Mica

We identified three distinct classes for micas (Figure 9 - B): i) Mg-rich biotites to Biotites; ii) Fe-Muscovite micas, and iii) lattice deficient micas. Each group is lithology-dependent. The Mg-rich Biotite to Biotite group mostly occurs in paragneiss (n=149), whether weathered or not. They have an X_{Mg} arithmetic mean of 0.46 ± 0.01 (2σ). The Ti (apfu) is considerably high, ranging from near zero to 0.92, with $\bar{x}$=0.40 ± 0.03 (2σ). On the other hand, in the pre-deformational granites (n=10) does only occurs "Fe-rich Muscovites", with X_{Mg} ranges from 0.22 to 0.37 and $\bar{x}$=0.33 ± 0.001 (2σ; Supplementary Material 12). Despite of being characterized as "Fe-rich Muscovites", the micas from pre-deformational metagranite are indeed biotites in either petrographical or chemical aspects. However, their high Ti content pushes their composition to another field. The compositional contrast between groups I and ii demonstrates two distinct phases of crystallization. We interpreted the former as metamorphosed by high-temperature metamorphic processes. The Ti content present in Biotite crystal lattice might suggest, among other things, high temperature conditions (Henry, 2005; Henry and Guidotti, 2002). Whilst, the latter (tardi-deformational granite) is a product of anactetic pulses. The Ti (apfu) varies from close to zero values to 0.87 with $\bar{x}$=0.3 ± 0.16 (2σ). Micas found in the melanossome lithofacies (n=26) have a different composition, while compared to other lithotypes found in the MEBC. X_{Mg} varies from 0.15 to 0.54, with $\bar{x}$=0.35 ± 0.04 (2σ). This broad range confirms the phlogopite composition identified in DRX analysis (Supplementary Material 5). Additionally, the Ti (apfu) ranges from close to zero values to 0.52 with $\bar{x}$=0.16 ± 0.07 (2σ). This difference in composition is largely due to weathering effects. In this case, relict biotites weathered to either chlorites or mica with deficient lattices (Rieder et al., 1998).

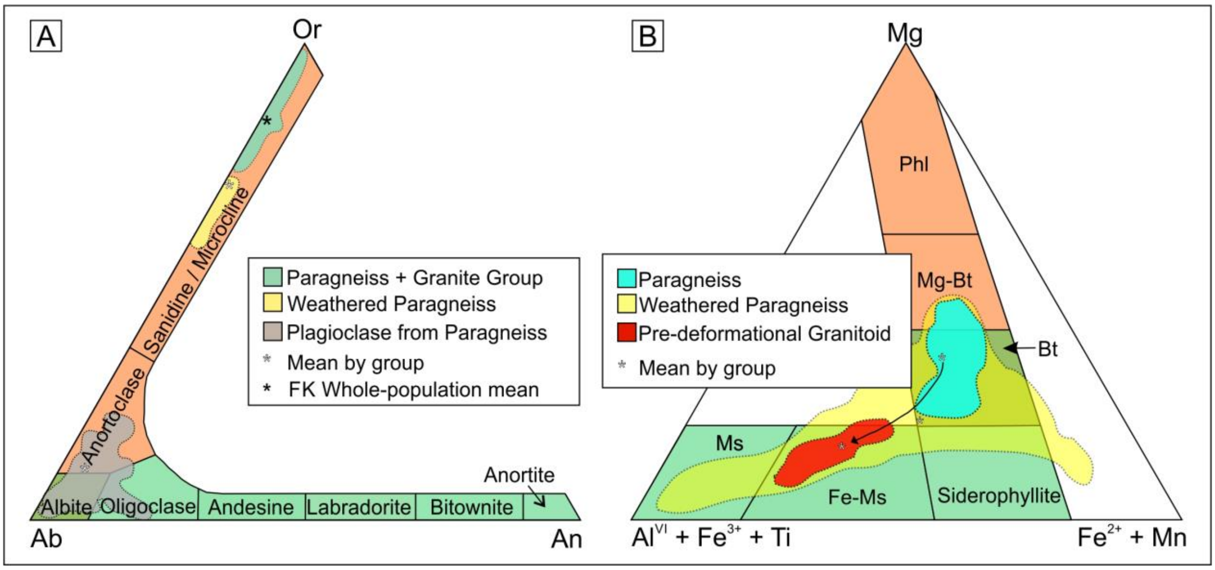

Figure 9 A –Ternary feldspar diagram classification (Smith and Brown, 1988). Note three populations, two composed by alkali feldspars and one by plagioclase. A color field represents each zone. B - Mica classification. Ternary diagram, as proposed by Foster (1960). Note three distinct group populations, partially limited by lithological units. The group I composes the acquired samples from paragneisses, classified as biotites. Group II composes the pre-deformational granitoid samples, mainly composed by Fe-Muscovites. Group III composes the mica with deficient lattice samples, mostly found in the melanosome lithofacies. Asterisc represents the arithmetic mean of each group.

3.3.4 Chlorite

Three distinct groups of chlorites were identified related with the MEBC lithofacies: i) weathered paragneiss, ii) pre-deformational meta-granitoid, and iii) paragneiss. The weathered paragneiss chlorites (n=4) have greater values of H2O when compared to others. Additionally, they have distinct values of Fe^{2+}, Mg, while almost negligible Mn. Pre-deformational meta-granitoid chlorites (n=5) lacks Mn in their lattice; also, they have more Fe^{2+} by the spend of less Mg. Chlorites from paragneiss have two characteristics: they lack Mg and have moderate values of Fe^{2+}, while compared to other lithofacies. Following the scheme proposed by Zane and Weiss (1998), all chlorites are tri-trioctahedral, because they have R_{10-12} (sum of octahedral cations), and ❑$_{2-0}$ (sum of vacant crystal lattice) According to Yavuz et al. (2015) classification scheme, they are considered Chamosites. Noteworthy is the variance in Al_{IV} content, that results in contrasting temperatures of stability. The weathered paragneiss has values varying from 0.23 to 0.48, whereas the pre-deformational meta-granitoid chlorites and paragneisses have values ranging from 0.42 to 0.65, and 0.85 to 1.05. As a result, the first group has the lowest modeled temperatures, ranging from 132 to 177ºC. The second group has similar temperatures, varying from 176 to 225ºC; whereas the chlorites from the latter have the greatest temperatures, ranging from 273 to 316ºC. We interpret that diagenetic processes generated the first two group of chlorites. On the other hand, anchi-metamorphic conditions generated the chlorites from non-weathered paragneiss (Supplementary Material 6).

3.3.5 Trace elements in zircon

Trace elements in zircons were determined at Universidade de Ouro Preto by LA microprobe Photon-machines ArF excimer Laser 193 (λ = 193 nm) coupled to Thermo-Fisher Element II sector field (HR-SF-ICP-MS). For a detailed description of the method, the reader is referred to Andrade et al. (2014). Twenty-six crystals were analyzed in the paragneiss unit (#17-R2-A from Chemale Jr. et al., 2018). Ti-in thermometer from Watson et al. (2006) was used to infer the temperature of metamorphism. We interpret that samples above 1057ºC are outliers; probably originated by magmatic processes. Thus they were disregarded from descriptive statistics. Mean confidence interval was calculated, assuming a 95% confidence level. The acquired 207/206Pb ages (2σ) follows Chemale Jr. et al. (2018) analysis. Detailed values of elements and isotopic ratio are in Supplementary Material 13.

Four zircon ages groups were identified (n=26; Figure 10): i) detrital derived from Calymmian rocks (n = 2); ii) detrital derived from Stenian rocks (n=17); iii) metamorphic zircon from Stenian-Tonian (n = 5) and iv) post-tectonic zircon (n=1) from Stenian. Due to the nature of the region (i.g. deposition age concordant with metamorphism), group ii and iii were combined for this interpretation. Groups i and iv were discarded for this analysis.

After combining all groups, the Ti-in thermometer gave a mean temperature of 762 ± 42 ºC (n = 25), with maximum and minimum of respectively 1021ºC and 642 ºC. By combining only group ii and iii, the mean temperature is 765 ± 21 ºC (n = 22) with maximum and minimum of respectively 1021ºC and 642ºC. If only the metamorphic zircons were considered, the temperature is 762 ± 48 ºC (n = 5) with maximum and minimum of respectively 666ºC and 881ºC. For the latter, we interpret the maximum temperature as peak metamorphism temperature, whereas we interpret the minimum as the liquidus-out. Likewise, we interpret the mean temperature as representative of syn to tardi-tectonic metamorphism; as a result, probably related to sin-deformational granite generation.

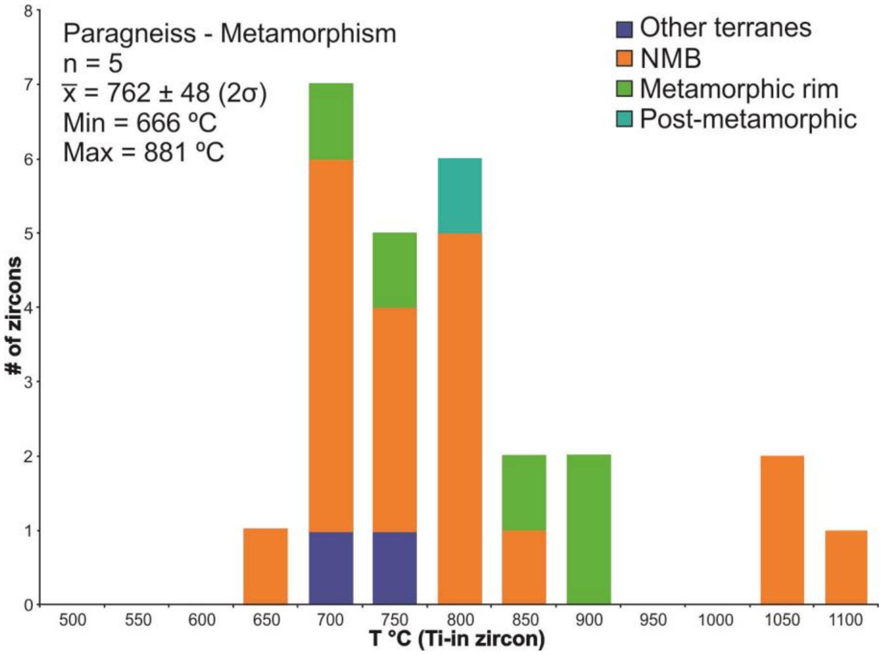

Figure 10 – Ti-in zircon histogram from paragneiss. Four classes were identified according to their ages, our data is concordant with data acquired by Chemale Jr. et al. (2018) interpretation. By considering only the data from the metamorphic rim, there is an agreement with liquidus-in trajectory throughout metamorphism.

4 MINERAL EQUILIBRIA MODELING

Pseudosection was made using the software Theriak-Domino to get, besides the PT grids, geothermobarometric interpretation by the isoplet intersection (de Capitani and Brown, 1987; de Capitani and Petrakakis, 2010). The data-entry was based on geochemical analysis representing pre-deformational metagranite lithofacies. The conversion from wt. % to chemical formula was done disregarding Mn. As a complexing agent, however, Fe^{3+} was considered. Besides, O_2 was modeled to be free to come and go of the system. Water, on the other hand, was steady through time, according to the values obtained in the whole rock chemistry formula.

The thermodynamic equilibrium model here utilized was K_2O-FeO-MgO-Al_2O_3-SiO_2-H_2O-TiO_2-Fe_2O_3 (KFMASHTO) proposed by White, Powell e Clarke (2002). Thermodynamics from plagioclase was according to Holland and Powell (2003). Epidote, cordierite, staurolite, and chlorite was according to Holland and Powell (1998). Garnet, biotite, and ilmenite-magnetite were according to White et al. (2007). Next, garnet and feldspar isoplets were calculated. A mean crustal density of 2.8 x 10^3 kg/m^3 was used to calculate the geothermal gradient.

The correlation between observed textures and microstructures (e.g., two distinct sillimanite habits, S-C fabric, granoblastic habit, to cite a few), coupled with homogeneous garnet crystals with pinite rims are indicative of clockwise progressive metamorphism (Figure 11). Each episode will be characterized in detail in the subsequent section.

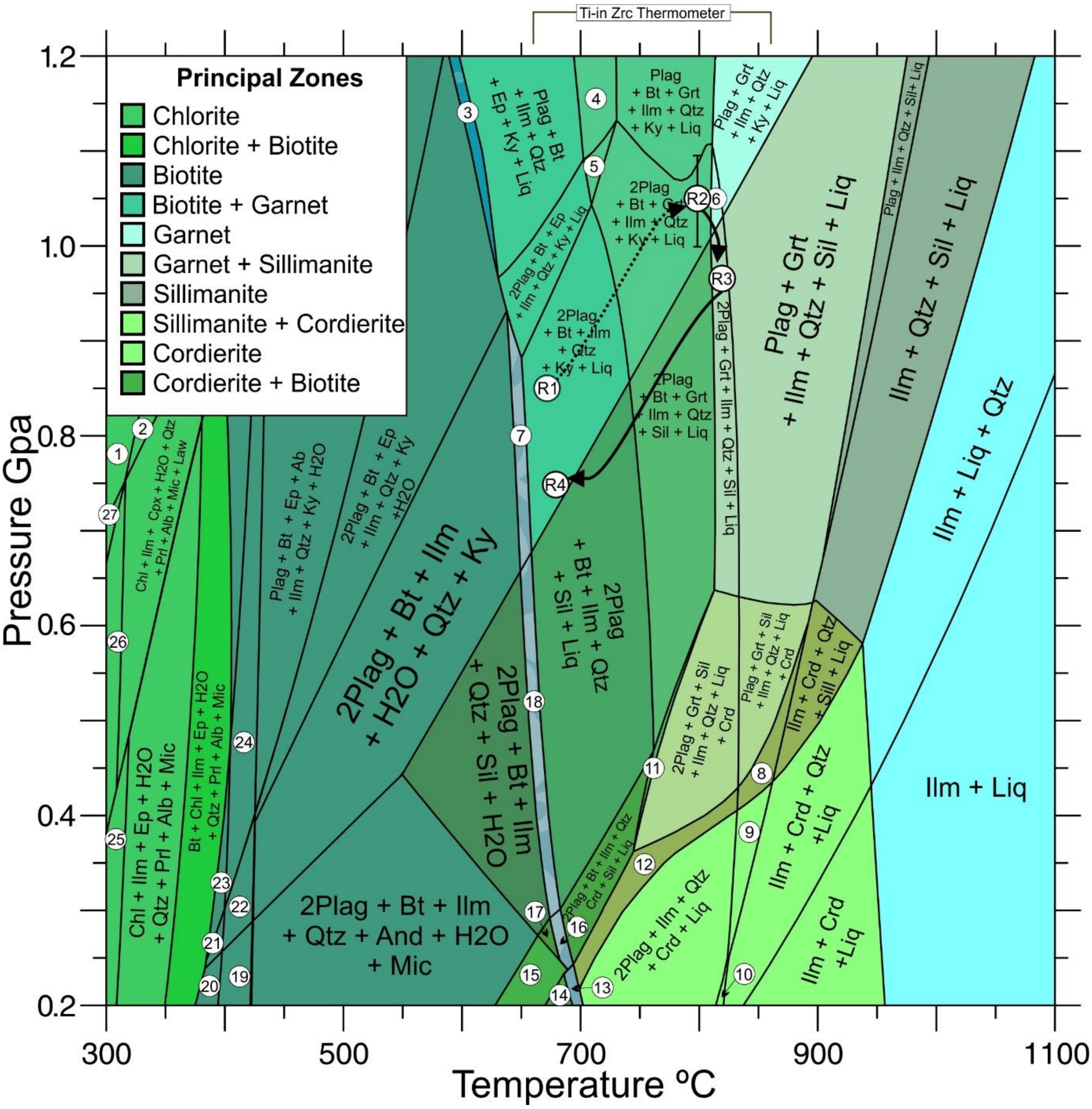

1271 Figure 11 – Pseudo-section based on the whole rock composition of sample 16R2-5B pre-deformational meta granitoid according to Tarney (1977). It has a composition of Si60.47 Ti0.05 Al14.54 Fe2+1.75 Fe3+1.32 Mg0.62 Mn0 Ca0.48 Na1.61 K6.54 H12.66 O?. It consists of a leucossome with posterior metamorphic recrystallization (see petrography section for more information). Its genesis coincides with the first anatectic pulse at R1. To check the paragenesis of small fields, please consult Supplementary Material 14.

4.1 Metamorphic zones

The rock has five distinct zones. Exothermic processes of high entropy characterize the transition between zones (Spear, 1993; Fig. 14). Nonetheless, the isogrades may have a negative slope, characteristic of endothermic processes, mainly when processes of mineral-in or mineral-out occur in the system (e.g., liquidus-in, garnet-in, biotite-out; Spear, 1993).

The zones of pseudosection are, from low to high T: chlorite, biotite, garnet, cordierite, and sillimanite. The chlorite zone is characterized by < 400ºC temperatures. The biotite zone ranges from 375ºC to 800ºC. In this model, due to its high amplitude, the biotite zone is not a useful PT index (Spear and Peacock, 1989). The garnet-in occurs above 0.35 GPa and 750ºC, and the garnet-out in T conditions above 900ºC. In a broad sense, the garnet zone occurs after the liquidus-in in the system. The liquidus increases the intergranular pressure, leading to garnet nucleation and growth (Ague and Carlson, 2013). Sillimanite zone occurs above 550ºC, and 1050ºC, being partially dependent on pressure. There is no evidence of cordierite zone assemblage, nor relict structures related to it. Thus, the complex has not reached Barrovian type metamorphism during its evolution (Spear, 1993). All other zones occur and are related to specific recrystallization event.

Table 2 – Summary of PT conditions of each recrystallization episode from MEBC as well as Depth and Geothermal gradient. Note that the geothermal gradient, even with the associated error, fits a collisional setting.

	P (GPa)	Depth (km)	T (ºC)	Geothermal Gradient (ºC*km^{-1})
R1	0.3-0.9	10.9	700	21-64
R2	1.05	38.3	800	21
R3	0.7-0.9	25.5	830-930	25-32
R4	0.3-0.9	10.9	700	21-64

4.2 Liquidus-in and first recrystallization episodes (R1)

This episode has a primary foliation and, when applicable, partially obliterated C-S fabric as characteristic textures. The former is result of a dominant pure shear condition; whilst the latter is a product of progressive strain circumstances (Passchier and Trouw, 2005). Nonetheless, both fabrics were partially obliterated during subsequences recrystallization episodes. Therefore, it is not recognizable whether the primary foliation cleavage obliterated the depositional strata or coincided with it. Additionally, R1 is coinciding with the first anatectic pulses, related to the formation of pre-deformational meta-granitoid. This specific rock is concordant with the primary paragneiss foliation and has direct evidence of ductile deformation generated before the static recrystallization. Thus, we interpreted that the first anatectic pulse might be generated around 700ºC and between not less than 0.3 nor high than 0.9 GPa. These PT conditions generate a geothermal gradient ranging from 21 to 64 ºC*km-1, which might be expected by either arc or continental orogenic belts (Spear, 1993; Table 02).

4.3 Maximum pressure event (R2)

The maximum pressure event has two main petrographical textures. The granoblastic pattern on minerals (i.g. quartz, plagioclases, and so on) from paragneisses to tardi-deformational granite suggests that after the R1 event, the minerals stayed in a quasi-steady temperature x stress for long periods. Thereby generating *static recrystallization textures* (Passchier and Trouw, 2005). The static recrystallization directly affects the geometric interface of grains boundaries, and can obliterate any prior preferential mineral orientation created due to stress fields (Otani and Wallis, 2006); thus, justifying the lack of foliation proposed to R1. Additionally, the occurrence and quasi-homogeneity of garnets in almost all complex units mark the maximum pressure event. Quasi-homogeneous garnets are time-temperature dependent processes (=> 700ºC; Spear and Peacock, 1989). The subtle compositional variation of garnets reflects not only long periods of crustal residence but also low uplifting rates (Jiang and Lasaga, 1990; Spear, 1991), as expected by collisional granulites (Bohlen, 2015). The garnet isoplet intersection suggests a crystal stabilization around 1.05 ± 0.05 GPa and 800ºC, coinciding with the textures and proposed zones (Supplementary Material 15). These PT conditions generate a geothermal gradient of 21ºC*km-1, which is expected to continental orogenic belts (Spear, 1993; Table 02).

4.4 Metamorphic climax (R3) event and isothermal decompression

Sillimanite and fibrolite characterize the metamorphic episode R3. The presence of sillimanite attests high-grade metamorphism with associated partial melting, as expected in Granulite Terranes (Spear, 1993). Usually, this aluminum polymorph is associated with aluminum-rich sedimentary derived protolith (White et al., 2002). The two distinct sillimanite habits demonstrate environmental contrasts. We interpret that an isomorphic reaction with a preterit R2 kyanite probably formed the sillimanite with blade habit. Fibrolite, on the other hand, is usually related to either anisotropy or process of a chemical reaction during the progressive strain (Musumeci, 2002). The presence of fibrolite suggests reactions with the presence of fluids and deformation (Digel et al., 1998; Musumeci, 2002; Vernon, 1979; Wintsch and Andrews, 1988). The necessary fluid to fibrolite generation was available after Biotite breakdown, that generates punctuate H_2O enrichment.

As observed in thin section, fibrolite as well as ilmenite, alkali feldspar, and melt are a product of the terminal reaction of Ti-rich biotite with garnet and plagioclase (Equation 01).

Ti-rich Bt + Grt + Plag= Kspar + Grt + Sil + Ilm + Qtz + liq (Equation 01)

Alkali-feldspar, the by-product of Equation 01, has a strict composition that suggests pressure of equilibrium around 0.8 ± 0.1 GPa and the temperature around 880 ± 50ºC (see Supplementary Material 15). These PT conditions generate a geothermal gradient ranging from 25 to 32ºC*km^{-1}, which is expected to orogenic belts exposed to high exhumation rates (Bohlen, 2015; Harley, 1989; Harlov, 2012; Spear, 1993; Table 02). According to the modeled pseusection, temperatures close to 900ºC are characteristic of Biotite-out reaction, validating Eq. 01. Even after the Biotite-out event, several biotites still occur in the analyzed sample. We interpret two main possibilities: i) time-dependent terminal reactions between biotites and other minerals, coinciding with fibrolite occurrence; ii) non-uniform temperature throughout the complex, resulting in punctuate zones of dehydration, and thus, mineral absence (e.g. biotite-out zone, "*incipient charnockitization"*), as expected in granulite terranes exposed to partial melting (Frost and Frost, 2008; Grantham et al., 2012; Mendonidis et al., 2015b; Mikhalsky et al., 2006).

4.5 Liquidus-out event and CO_2 rich liquidus(R4)

Post-deformational granitoid (1006 ± 13 Ma; Chemale Jr. et al., 2018); marks the end-of Rodinia-forming orogen at MEBC. This unit indicates the very last anatectic pulses that occurred in the complex. The lack of garnets, in opposition to observed in the pre- and tardi-deformational granitoids, demonstrates that the melting genesis occurred below the Garnet zone <750ºC. Still, it suggests that this lithofacies did not undergo high-grade metamorphic recrystallization events. The modeled liquidus-out isochore indicate a temperature between 700ºC. The lack of garnets suggests temperatures below 750ºC. Several textures corroborate to this observation. In post-tectonic granitoid, there are several occurrences of randomly arranged mineral (e.g., mostly alkali-feldspar) that suggest an isostatic stress field during their generation, in opposition to aligned minerals present in paragneisses, pre-, and syn- to tardi-deformational counterparts. These data demonstrate a change in the stress vector, probably related to the end of the collisional cycle. Igneous coarse-grained feldspars are associated with the late stage of crystallization, as a product of late-stage magmatic liquidus (Higgins, 1999; Johnson and Glazner, 2010). Bohlen (2015) suggests that there is a CO_2 enrichment related to last episodes of granulite terranes evolution, mostly associated with the final chapter of an orogenic cycle. CO_2 enrichment is a rule in Natal-Maud orogen. There are several occurrences of charnockites in Natal, Dronning Maud, and Falkland (Malvinas) Island that were interpreted as generated by CO2 saturated liquidus (Grantham et al., 2012; Mikhalsky et al., 2006; Thomas et al., 1997 and references therein). Thus, we interpret that a late-stage magmatic liquidus with a probable high CO_2 content might generate coarse-grained feldspars present in post-deformation granitoid. However, specific studies to prove this assertion must be done. This CO_2 concentration, as well as the lack of garnets, and the preferential mineral lineation in post-deformational granitoid might be related to the end of the Stenian orogenic cycle at MEBC.

5 DISCUSSIONS

Even with lack of regional mapping data (e.g., mineral lineation, rock fabrics, meso- and macro-scale structures, and so on), the lithostratigraphic history of a unit, and therefore, its tectonic environment, can be determined by using pseudosection analysis and PT trajectory through time interpretation (Bohlen, 2015; Girelli et al., 2018; Passchier and Trouw, 2005; Spear, 1993, 1993, 1991). MEBC consists of a polyphasic metamorphic terrain with at least two metamorphic cycles. The first cycle related to Rodinia forming orogen consists of a granulite-facies peak with a Stenian age (Chemale Jr. et al., 2018). It comprises recrystallization events R1 through R4, with a clockwise path. Granulite facies metamorphism with this trend is usually related to collisional tectonics (Harley, 1989; Harlov, 2012; Rudnick and Fountain, 1995). The normal geothermal gradient for each episode suggests a continental orogenic belt evolution (Table 2). All episodes (i.g., sedimentary deposition R0, and recrystallization events R1 through R4) share their best age estimation with several units throughout Natal-Maud Belt. At MEBC, we interpret these events as caused by progressive regional metamorphism, related to the amalgamation of the Rodinia supercontinent (Roberts et al., 2015). Except when specified, all ages consist of U-Pb in zircon.

The other events are related to retrograde low-grade metamorphism from other tectonic cycles. Retrograde metamorphism is tied to tectonic pulses dated from the Neoproterozoic-Paleozoic transition such as Pan-African, Pan-Antarctican, West-African Orogeny, among others (Pankhurst et al., 2006) or even younger events such as Gondwanides and Gondwana break-up (Chemale Jr. et al., 2018; Ramos et al., 2017). Those events will not be emphasized in this current study.

5.1 R0 – Sedimentary Basin evolution

The sedimentary deposition at R0 has detrital zircon with ages varying from 1745 ± 10 (Peak 1), 1186 ± 4.8 Ma (Peak 2), and a Peak 3 concordant with metamorphic age, due to the tectonic context of the unit (Chemale Jr. et al., 2018). Peak 3 ages probably derived from Kaapvaal-Grunehogna craton. It is important to emphasize that either Peak 2 or Peak 3 group predominates, suggesting a juvenile source. Peak 2 ages occur in adjacent Mesoproterozoic terranes such as Haag Nunataks (1176 ± 76 Rb-Sr, Millar, and Pankhurst, 1987), East Antarctica (e.g., Heimefrontfjella, ca. 1170 Ma leuco-gneisses; Jacobs et al., 2003). Additionally, in Natal Province, Thomas (2003) identified gneissic rocks with 1185 ± 15 Ma from Margate Terrane. Still, in Margate Terrane, there are garnet biotite gneisses with ages of 1169 ± 14 Ma (Mendonidis et al., 2015; Figure 12). Both rock units are related to arc magmatism (McCourt et al., 2006; Spencer et al., 2015b; Thomas, 1989), generated due to a N-S (present coordinates) subduction system. It was hypothesized a back-arc basin southern of this arc (Grantham et al., 2012; McCourt et al., 2006; Mendonidis et al., 2015b; Mendonidis and Grantham, 2003; Spencer et al., 2015b).

It is important to emphasize that there are several occurrences of metasedimentary gneisses at Heimefrontfjella, with kernel density probability plot similar with that obtained by MEBC paragneisses by Chemale Jr. et al. (2018; see Arndt et al., 1991; Johnston et al., 2001; Ksienzyk et al., 2007; Ross and Villeneuve, 2003; Spencer et al., 2015). These metasedimentary gneisses were deposited in Sivorg back-arc basin, due to the erosion of Kottas arc rocks (Bauer et al., 2003b, 2003a; Jacobs, 2009 and references therein).

The integration of geochemical and provenance age data from MEBC paragneisses suggests that, by the time of deposition, the protoliths were close to the source area. The source area probably consisted of a volcanic arc, herein considered Maurice Ewing Bank (MEB) Arc. Orogenic dynamics, related to arc tectonics, exposed the source area. The arc-signature identified in paragneisses geochemistry herein presented also endorse this hypothesis, as well as the predominance of juvenile age zircons against others (see Chemale Jr. et al., 2018; Figure 13 - A). We interpret that MEBC paragneisses were deposited in the same back-arc basin system of Mzumbe-Margate, and Sivorg terranes.

In the Falkland (Malvinas) Islands, there are no occurrences of such ages (Thomas et al., 2000; Figure 12). However, as postulated by Thomas et al. (1997), Big Cape Fm. is composed by amphibolites interspersed with paragneisses. The U-Pb in zircon ages of these two units are still unknown. The arc system of CMC, which generates “felsic orthogneisses” only developed during ca. 1120 Ma (Jacobs et al., 1999; Thomas et al., 2000, 1997).

5.2 R1 and R2– Fold- and thrust-belt

The R1 and R2 are herein interpreted as caused by a fold- and thrust-belt event. This event corresponds to a continent-continent collision and is related to the first anatectic pulses at ca. 700ºC and high-pressure, as well as a recrystallization event around 1 GPa and 800ºC. Negative εHf signatures (Chemale Jr. et al., 2018), protolith with a back-arc sedimentary deposition, followed by synchronous metamorphism with high-pressure and temperature, as well as syn-orogenic melting, validate this interpretation. The primary foliation, as well as the partially obliterated C-S fabric coincides with the deformation processes between R1 and R2. R2, according to our interpretation (e.g., static recrystallization, garnet homogenation, and so on), represents the orogenic climax. The R2 events is interpreted as generated by the 1068 ± 16 Ma ages obtained by Chemale Jr. et al. (2018), as the older syn- to tardi-deformational granitoid. This age coincides with the sinorogenic climax of Natal-Maud belt (ca. 1080-1020 Ma). As a result, there are several age occurrences found in *sensu latu* Natal-Maud belt (e.g., Natal, and Dronning Maud Land Terranes) and other near blocks (e.g., Falkland Islands, Agulhas Plateau, and Coats Land).

In Margate Terrane, southernmost Natal terrane, several coinciding magmatism occurrences vary from ca. 1052 to ca. 1088 Ma (Mendonidis and Armstrong, 2016; Spencer et al., 2015 and references therein). Granulite facies metamorphism is usual, occurring at Margate Granite Suite (1044 ± 11 and 1034 ± 26 Ma), and Leisure Bay Granulites (1047 ± 17 and 1046 ± 19 Ma; Mendonidis and Armstrong, 2016; Spencer et al., 2015). This dynamism also occurs at Mzumbe Terrane, where magmatic rocks ranging from ca. 1100 to 1045 Ma coincides with granulite facies metamorphism (Eglington et al., 2010, 2003, 1989). Tugela Terrane has compatible ages at Khomo Formation (1181 ± 126 Ma; Rb-Sr whole-rock) and Ngoye Granite (1067 ± 20 Ma; Barton, 1983; Figure 12). All these geological features led McCourt et al., (2006 and references therein) to interpret that Natal Province, by this time, as a thrust- and fold-belt environment due to the interaction between Kaapvaal craton and an unknown block.

In Dronning Maud Land, there are several occurrences of synchronous magmatism and metamorphism with MEBC fold and thrust belt. Jacobs et al. (1998) identified a migmatite Augen gneiss with 1076 ± 14 Ma. Jacobs et al. (2003) and

Bisnath and Frimmel (2004) also identified high-grade metamorphic overgrowth with respectively ca. 1080 and ca. 1070. Kirwanveggen has a migmatite Augen gneiss with 1074 ± 11 Ma (Jackson, 1999), as well as leucogranites with 1007 ± 57 Ma and orthogneisses with 1035 ± 18 Ma (Wolmarans and Kent, 1982). The metamorphism in the region is high grade and dated as 1081 ± 4 Ma by Jackson (1999) and 1061 ± 14 Ma by Bisnath and Frimmel (2005). In Heimefrontfjella, several magmato-metamorphic units occur from ca. 984 to 1090 Ma (Jacobs, 2009 and references therein). Noteworthy is the occurrence of amphibolite facies metamorphism, dating as 1031 ± 27, 1060 ± 8, and 1062 ± 11 Ma (Arndt et al., 1991; Jacobs et al., 2003c). H.U Sverdrupfjella has several magmato-metamorphic units dated from ca. 1040 to ca. 1085 Ma (Grantham et al., 2008 and references therein). A paragneiss with 1044 ± 47 Ma coincides with “D2” recrystallization event of Board et al. (2005); Also, there are zircon overgrowths dated as 1035 ± 21 Ma, being a product of “D3” deformational event. Generically, by this time, Western Dronning Maud Land terranes were involved in a complete fold- and thrust belt evolution (Bauer et al., 2016, 2003b). Additionally, a destral transcurrent system, related to tardi collisional processes had already been developed (Bauer et al., 2016, 2003b).

Microterranes that might be part of Natal-Maud orogens, such as Agulhas Plateau, Cape Meredith, and Coats Land, also have coinciding ages of magmatism/metamorphism. Allen and Tucholke (1981) had analyzed a quartz-biotite gneiss from Agulhas Plateau, using K-Ar in biotite, and obtained an isochron age of 1105 ± 36 Ma for the unit. We interpret this data as metamorphic age of this unit. G1 granodiorite and G2 mega crystal Augen gneiss from Cape Meredith Complex have ages ranging from ca. 1090 and 1067 ± 9 Ma, respectively (Jacobs et al., 1999). Chemale Jr. et al. (2018) already correlated the herein considered MEBC fold and thrust belt event with Cape Meredith Complex G1 and G2. In Coats Land, undeformed granophyre rhyolite and diabase from Coats Land were dated as 1078 ± 7 Ma by Storey et al. (1994).

The plethora of contemporary geological events points toward a regional orogenic climax. The event of ca. 1080 – 1040 Ma in which Natal and Dronning Maud Land are players, is related to Rodinia forming orogeny (Roberts et al., 2015). H.U. Sverdrupfjella, Kirwanveggen, Heimefrontfjella, Margate, and MEBC, by this time, stood right in the middle between Kalahari, “*East Antarctica”* craton collision (Bauer et al., 2003a) and an unknown cratonic mass (Cornell et al., 2006; McCourt et al., 2006). Jacobs et al. (2015) and references therein credited that the metamorphism and granitoid generation from DML are caused due to the collision between Kaapval and Coats Land craton. Loewy et al. (2011) hypothesized that Coats Land Craton and Grenville terrane, at Laurentia, have isotopic affinities; thus, being relatively close to each other by the time of their development. We interpret that MEBC, and thus its fold-and-thrust belt related metamorphism have strong age affinities not only to Western Dronning Maud Land (Bauer et al., 2003b), but also to Natal Province (McCourt et al., 2006). Cape Meredith Complex anatetic events could be related to MEBC collisional event; nonetheless, it is possible that the Falkland (Malvinas) basement represents a peripheric extension of collisional front (Figure 13 - B). The synchronous geological activity of Agulhas Plateau should be investigated in other studies to diminish the degrees of freedom about Rodinia evolution.

5.3 R3 – Orogeny exhumation and regional anatexis event

The R3 event marks the metamorphic climax in MEBC. A near-isothermal decompression curve, and therefore, a clockwise path diagnosis, characterizes this episode (Harley, 1989). We interpret that an over-thickened crust, followed by a rapid exhumation process might generate this condition (Bohlen, 2015; Harley, 1989; Rudnick and Fountain, 1995; Figure 13). Either erosion or rapid thinning, related to the tectonic exhumation, causes the decompression event (Harley, 1989). Thermodynamically, because of decompression at isothermal conditions, anatexis is a typical process, generating significant volumes of *liquidus*. MEBC shares the typical collisional granulites, which are felsic composition, correlation with paragneisses, and relation with upper crustal levels (Rudnick and Fountain, 1995). Additionally, MEBC fills the high-temperature granulite classification, being the first identified high-temperature-pressure granulite in Natal-Maud belt. We agree that the syn- to tardi-deformational granitoid age of 1032 ± 12 Ma, obtained by Chemale Jr. et al. (2018), represents this recrystallization event.

There is a reduction in synchronous magmato-metamorphic ages from Natal-Maud belt related to this episode; however, the ages related to this event are associated with plutons of regional extent, and thus, a regional anatectic event. In Margate Terrane, Oribi Gorge has ages of 1049 ± 14, 1037 ± 14, and 1025 ± 8 Ma (Eglington et al., 2003; Spencer et al., 2015b; Thomas, 1989). On the contrary, the age of metamorphism is 1029 ± 8 (Eglington et al., 2003). Port Edward Pluton has magmatic ages of 1034.4 ± 0.6, 1039 ± 18, and 1025 ± 8 Ma (Eglington et al., 2003; Spencer et al., 2015b). Magmatic ages are ranging from 1042.6 ± 4.4, and 1057 ± 27 Ma at Margate Suite. (Mendonidis and Armstrong, 2016; Mendonidis and Grantham, 2003). Still, in Margate Suite, there are cataloged metamorphic ages of 1044 ± 11 and 1037 ± 13 (Mendonidis et al., 2015b; Mendonidis and Armstrong, 2016). Mbzana and Margate “D2” granites have ages of 1026 ± 3, and 1042 ± 10 Ma (Grantham et al., 2012; Mendonidis and Armstrong, 2016). Leisure Bay and Turtle Bay (mafic unit) only have metamorphic ages that fit R3. They are 1047 ± 17, 1046 ± 16 Ma from Leisure Bay, and 1042 ± 7 Ma from Turtle Bay (Spencer et al., 2015b). There is only one occurrence in Mzumbe Terrane from Fafa Pluton, which has 1037 ± 10 Ma as an igneous placement age (Eglington et al., 2003; Figure 12).

In Heimefrontfjella, there are several occurrences of monzonites (1045 ± 8 Ma), amphibolites (1048 ± 8 Ma), granodiorites (1045 ± 9 Ma; Arndt et al., 1991). Also, Bauer et al. (2003) identified a dike with 1033 ± 7 Ma. Arndt et al. (1991) identified that the rocks from Heimefrontfjella underwent a clockwise path, suggesting continent vs. continent collision. In H.U. Sverdrupfjella, Jackson (1999), and Moyes and Barton (1990) obtained an age of crystallization of 1050 ± 10 and 1015 ± 24 Ma (Rb-Sr) for a leuco-pegmatite and an orthogneiss. Still in H.U. Sverdrupfjella, zircon overgrowth with ca. 1044 and 1031 Ma were obtained and interpreted as the age of peak metamorphism up to granulite facies (Board et al., 2005; Figure 12).

There is no age occurrence from Cape Meredith Complex, nor Agulhas Plateau, nor Coats Land. However, it is noteworthy that Coats Land and Agulhas Plateau are still unknown territories, being only dated by old methods. For example, of 12 recovered lithofacies at Agulhas Plateau, only two gave results consistent with Mesoproterozoic. Coats land has an extensive area to be mapped; however, of critical access (Gose et al., 1997).

5.4 The end of Rodinia-forming orogen at Maurice Ewing Bank (R4) and tardi-anatectic processes

The R4 event marks the end of Stenian-Tonian orogeny at MEBC. This event is characterized by a retrograde metamorphism curve still on the liquidus-in zone, result of an orogenic collapse at F2MT, as well as Natal-Maud belt (Figure 13). We agree that the post-deformational granitoid age of 1003 ± 16 Ma, obtained by Chemale Jr. et al. (2018), represents this episode. There is an increase in post-deformational ages from Natal-Maud belt. Additionally, rapid cooling processes are usual, being characteristic of the whole belt (Jacobs, 2009; Jacobs et al., 1999; Mendonidis et al., 2015b; Spencer et al., 2015b; Will et al., 2010, 2009). However, several portions of Dronning Maud Land, Shackeleton Range, Natal, and Maurice Ewing Bank underwent thermal resetting due to posterior events (Jacobs, 2009; Jacobs et al., 1999; Spencer et al., 2015b; Will et al., 2010).

In Natal Province, there is a dominant occurrence of low-grade metamorphism. In Mzumbe Terrane, there are occurrences,at Melville Thrust Zone of mylonitic Equeefa Dyke with Ar-Ar and K-Ar (Hornblende) ages of 988 ± 3 Ma. Their undeformed occurrences have ages of 1005 ± 4 Ma (Ar-Ar; K-Ar in hornblende). In the Jolivet, Shear zone occurs mylonitic amphibolites with ages of 1004 ± 2 and 1002 ± 4 Ma (K-Ar, Ar-Ar in hornblende). In Lilani-Matigulu Shear zone, there are occurrences of gabbros with Ar-Ar in Hbl of 1003 ± 5 and 1009 ± 5 Ma (Jacobs et al., 1997, 1995; Figure 12).

There are occurrences in Heimefrondfjella of ages is varying from 972 to 1019 Ma. Jackson (1999) identified, at H.U. Sverdrupfjella and Kirwanveggen, a banded gneiss with 994 ± 22 Ma, a leucogranite with 990 ± 12 and a porphyritic granite with 1011 ± 8 Ma. Moyes and Harris (1996), identified a late felsic dike with 1011 ± 8 Ma. In Sivorg Terrane, there are muscovites derived from pegmatites with ca. 987 Ma (K-Ar Muscovite). Ar-Ar in Muscovite, with ages of 987 ± 21 Ma suggests that some of the Heimefrontfjella rocks probably underwent a rapid cooling process (Jacobs et al., 1998; Figure 12).

There are several age occurrences in Cape Meredith Complex, mostly related to G3 group. Leucogranites have crystallization ages of 1003 ± 14 Ma, while G3 granite has an age of 1003 ± 16 Ma (Jacobs et al. 1999). Cape Meredith Complex rocks also underwent a rapid cooling process, as demonstrated by Ar-Ar in Hornblende in amphibolites with ages of 1015 ± 6 and 1009 ± 14 Ma, as well as Ar-Ar Muscovite ages of 989 ± 3 and 989.2 ± 3.4 Ma and Ar-Ar Biotite ages of 989 ± 7 and 989 ± 6.5 Ma occurring at G3 granitoids(Jacobs et al., 1995; Figure 12).

Eastin and Faure (1971) by using whole rock Rb-Sr had dated the rhyolite unit at Littlewood Nunataks, Coats Land, obtained 1001 ± 16 Ma. This data suggest that the Littlewood Nunataks may also played a role in Natal-Maud event (Figure 12).

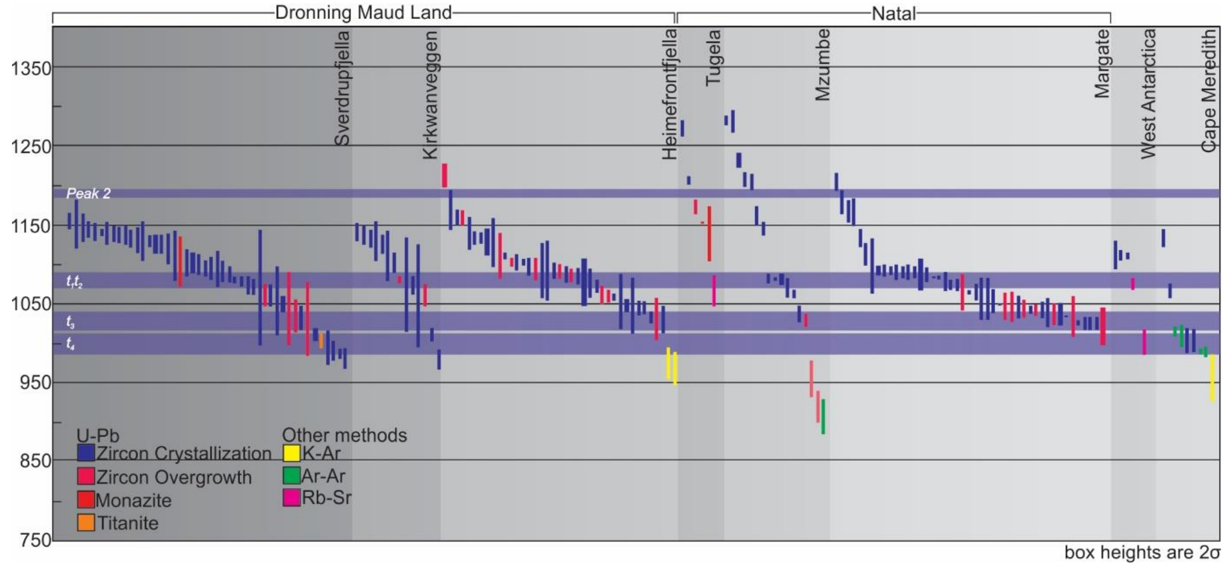

Figure 12 – Ages of magmatism and metamorphism of Natal-Maud belt, including West Antarctica + Coats Land and Cape Meredith Complex (Falkland-Malvinas Islands) occurrences. Rb-Sr with high uncertainty was disregarded. Blue stripes symbolize the events identified at MEBC. For a complete work reference, please check Supplementary Material 16.

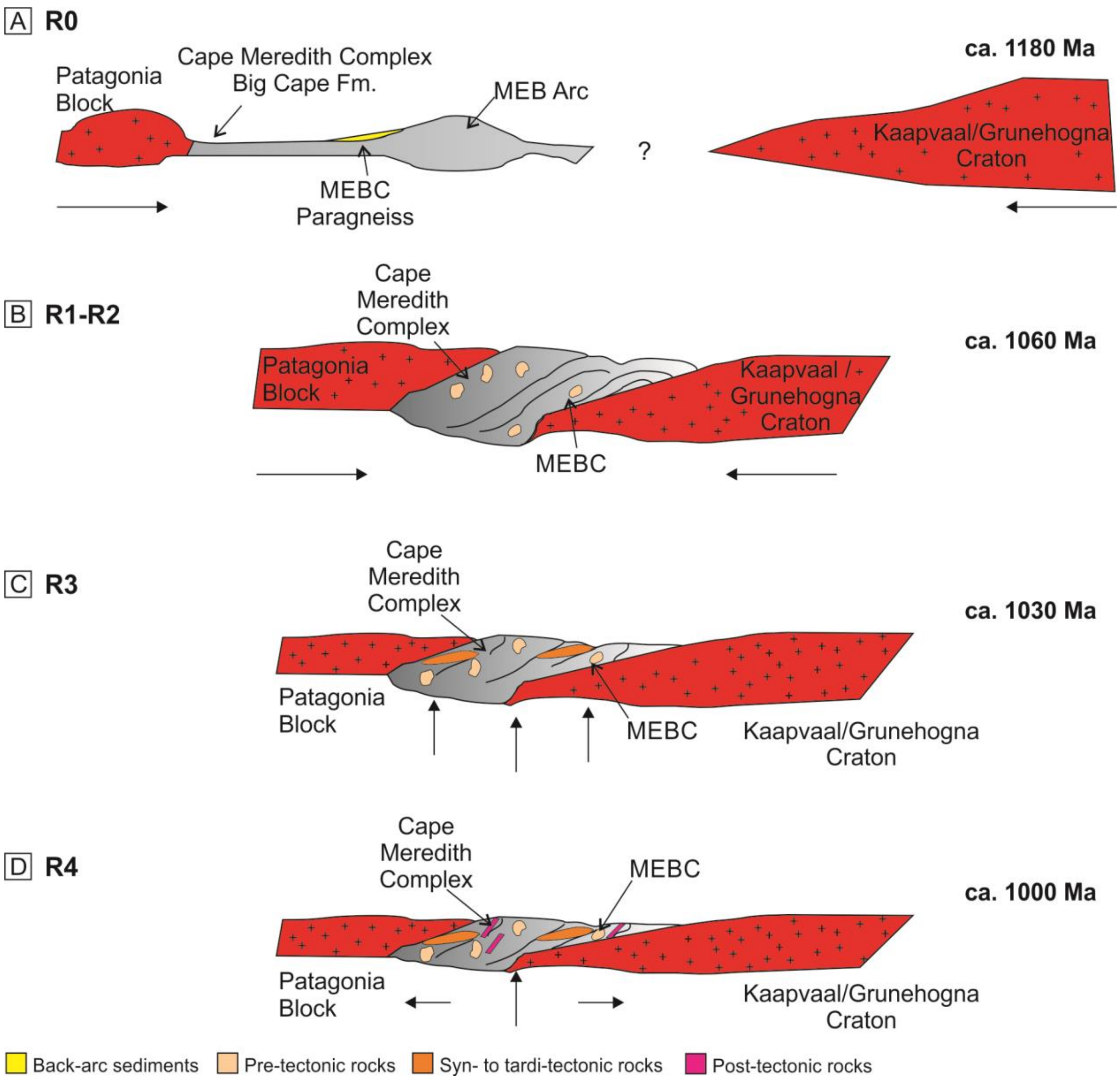

Figure 13 – Tectonic environment of F2MT. A) The deposition of immature sediments that generated MEBC paragneisses at ca. 1180 Ma; B) Orogenic climax coinciding with R2 static recrystalliozation event at ca. 1060 Ma; C) Metamorphic climax, isothermal decompression and generation of MEBC Tardi-metagranitoids. D) Orogenic collapse, and post-deformational granitoids related to a extensional field at ca. 1000 Ma.

5.5 Which terranes generate Natal-Maurice-Maud metamorphism

MEBC is part of Natal-Maud belt; therefore, it constitutes a missing fragment of Kalahari Craton *sensu* Jacobs et al. (2008). However, the extent of Natal-Maud belt orogeny might be more significant than previously thought and is possibly related to Beattie-A magnetic anomaly, a subsurface structure that extends 1000 km E-W of South Africa (Beattie, 1909; Thomas et al., 1992). Quesnel et al. (2009) interpreted that granulite-facies mid-crustal rocks caused the anomaly. Lindeque et al. (2011)

added that those rocks have a distinct north-dipping, relating them with Natal Province. Additionally, the authors suggest a south-dipping subduction zone during the Rodinia-forming orogen. Scheiber-Enslin et al. (2014), hypothesized that the Beattie-A's strong signal is due to the high susceptibility of granulite facies supracrustal rocks. The regional metamorphism of up to granulite facies is a distinctive characteristic of Natal-Maud belt, being identified at Natal Province (Cornell et al., 2006; Mendonidis et al., 2015b; Mendonidis and Armstrong, 2016; Mendonidis and Grantham, 2003; Spencer et al., 2015b; Thomas et al., 2003), Maud Belt (Bauer, 1995; Bauer et al., 2003a; Jacobs et al., 2015, 2003a, 2003c; Jacobs and Thomas, 1999; Ksienzyk et al., 2007), Falkland (Malvinas) Islands (Jacobs et al., 1999; Rex and Tanner, 1982; Thomas et al., 2000, 1997), MEBC (Chemale Jr. et al., 2018; Tarney, 1977; this work). Henceforth, we suggest that Beattie-A anomaly is a suture zone related to the collision between Kaapvaal and an unknown craton.

We disagree with the actual consensus of Falkland (Malvinas) Island, and its 180º rotation back to Rodinia amalgamation (e.g. (Jacobs and Thomas, 1999; Ksienzyk et al., 2007, and several references therein).There is actually no need to rotate Falkland (Malvinas) Island 180º to fit Falkland (Malvinas) Islands with regional data, nor limit their correlation with outcropping Mesoproterozoic units in Natal Province. Cape Meredith Complex can be considered as an eastward prolongation of Mesoproterozoic rocks that causes Beattie-A anomaly and as a northward prolongation of Coats-Patagonia Craton. By considering this assertion, Falkland (Malvinas) Islands structures such as metamorphic foliation, and mineral lineation coincides with those observed in Natal, thereby also demonstrating an SW-NE collision (Thomas et al., 1997, 1992). Also, Cape Meredith Complex has lithologies that are related to meta-volcanic-sedimentary arc (Jacobs et al., 1999; Thomas et al., 2000, 1997) that underwent collisional metamorphism. In specific, the Big Cape Formation is composed of layered gneisses, mostly consisting of amphibolites, felsic gneisses, calc-silicates, and metapelites (Thomas et al., 1997). The latter is composed by sillimanite, generated after a muscovite breakdown, suggesting high-grade peak metamorphism. This stratigraphic succession is usual in volcanic arcs, which partially justifies the Natal-Cape correlation. Jacobs et al. (1997) obtained 1118 ± 8 Ma and 1135 ± 11 Ma (U-Pb in zircon) for the felsic gneisses and inherited zircons from G2 granites. However, the Margate-Vardeklattene arc was experiencing a partial melting event. The partial-melting event registered at Cape Meredith

Complex is somewhat younger than its northern counterparts, only occurring at Maurice Ewing Bank due to peak metamorphism conditions. Recently, Chemale Jr. et al. (2018) and this work found evidences that MEBC and Cape Meredith Complex were indeed a single block in the Stenian-Tonian transition (F2MT). Schilling et al. (2017) pointed out that Deseado Massif, southern Patagonia, and Falkland (Malvinas) Islands still constitute a single block, named Patagonia-Malvinas terrane. Therefore, Deseado Massif, Falkland (Malvinas) Islands and MEBC were a single terrane since its generation, back to Meso-Neoproterozoic transition to Mesozoic. Any reconstruction should be aware of this fact.

The continental margin that collided to Kaapval to generate Margate, Maurice Ewing Bank, Cape Meredith, and Beattie-A metamorphism and granitogenesis is still unknown. Nonetheless, there is a specific terrane that might fit this interpretation: The Patagonian Geological Province (Ramos, 2008; Ramos et al., 2004). Despite the lack of crystallization and metamorphism age from Mesoproterozoic, the province has T_{DM} ranging from 1.7 Ga to 854 Ma, as well as $^{87}Sr/^{86}Sr$, and εNd data suggest that Patagonian rocks derived from young Mesoproterozoic crust related with Rodinia-forming orogens (Pankhurst et al., 2006; Wareham et al., 1998). T_{DM} data from Martínez Dopico et al. (2011) derived from North Patagonian massif also supports this interpretation. Additionally, Schilling et al. (2008), suggest that xenoliths recovered close to North Patagonian Massif are the roots from Cuyania Terrane. Cuyania is currently interpreted as an allochthonous terrane related to Mesoproterozoic units in Laurentia (Ramos, 2010, 2008; Ramos and Naipauer, 2014). Additionally, samples from the Deseado Massif gave depletion ages ranging from 1.34 to 2.11 Ga (Schilling et al., 2008). Recently, Mundl et al. (2015), by doing isotopic studies on mantle xenoliths, interpreted that rocks beneath Deseado Massif are similar to Natal-Namaqua belt rocks; thus, being directly related to the assembly of Rodinia. The rocks beneath the southernmost part of Deseado Massif has idiosyncrasies that point toward an Archean to the mid-Paleoproterozoic signature (Mundl et al., 2015; Schilling et al., 2008). Mundl et al. (2015) related them with the Shackleton Range in east Antarctica. Nonetheless, they might also be related to the still unknown Coats Land Block. We agree with the hypothesis postulate by Schilling et al. (2008), which propose that Deseado Massif is related to Falkland (Malvinas) Islands.

During Stenian-Tonian transition, Patagonia was a missing-link between Coats Land, in Antarctica, and Grenville orogen, in North America. This interpretation aligns with data presented by Loewy et al. (2011) and this work, who identified similarities between Coats Land and Laurentia. Moreover, we propose that Patagonia's southernmost part is related not only with F2MT (Schilling et al., 2017) but also to Coats Land and Shackleton Range rocks (Will et al., 2010, 2009). The Northern Patagonia Massif , together with Cuyania-Chilenia terrane (Benedetto, 2004; Casquet et al., 2001; Kay et al., 1996; Mundl et al., 2015; Sato et al., 2004; Schilling et al., 2008; Thomas and Astini, 1996), is connected to Laurentia Llano Uplift (Nelis et al., 1989; Ramos, 2004; Sato et al., 2004). Coats-Patagonia craton has the characteristics to fit the regional geology found in the region. collided to Kaapvaal, generating the continent vs. continent metamorphism in Natal-Maud-belt. By considering this interpretation, Mesoproterozoic Patagonia, consisting from Chilenia-Cuyania rocks, as well as Northern and southern Massif basement consequently becomes part of Grenville orogeny (Martínez Dopico et al., 2011; Ramos, 2010; Ramos and Naipauer, 2014; Schilling et al., 2017, 2008).

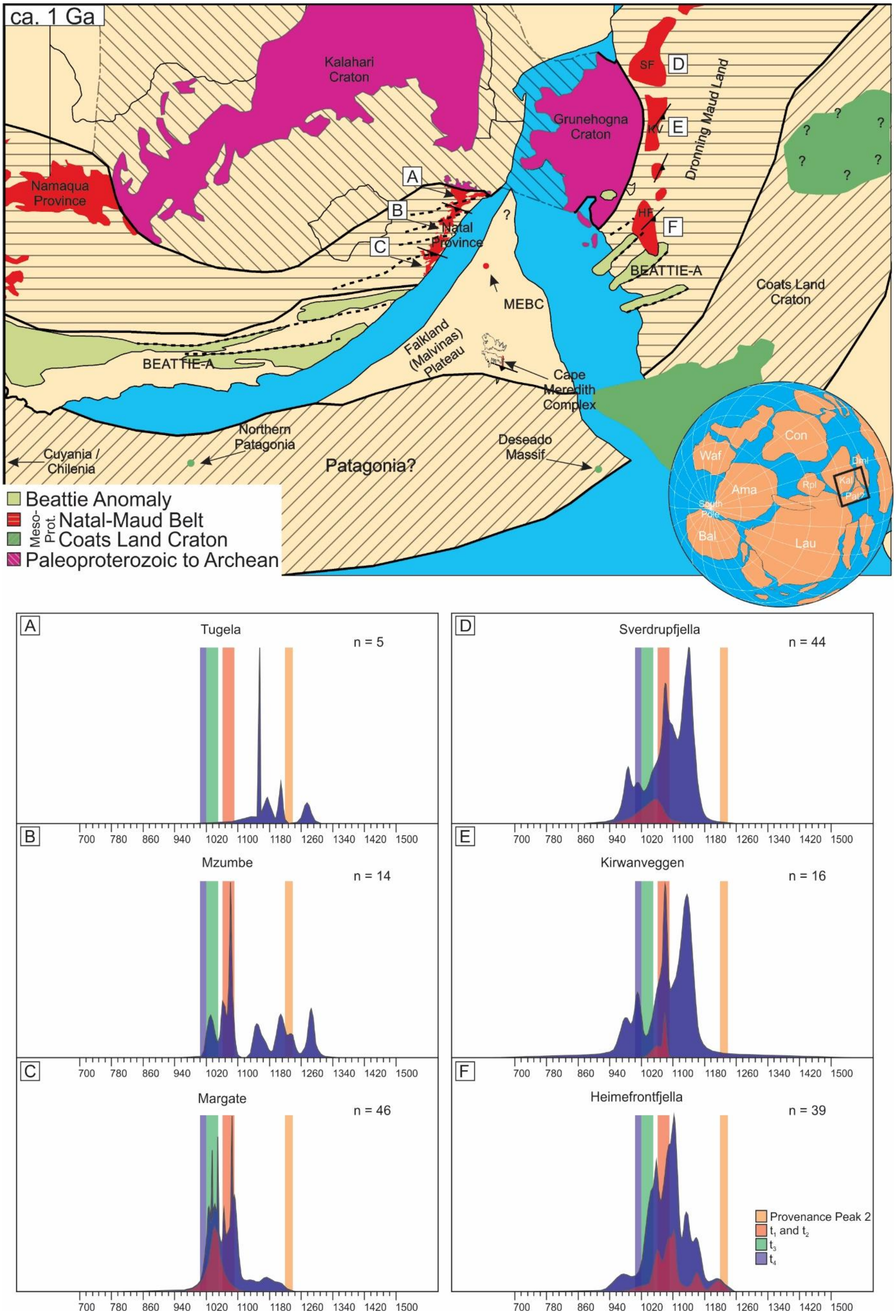

Figure 14 – Africa-Antarctica is setting at ca. 1 Ga, during Stenian-Tonian transition. This reconstruction follows Li et al. (2008) interpretation and adds Patagonia as a

hypothetical landmass that collided to Kalahari Cráton. Beattie-A anomaly and extension to Antarctica according to Scheiber-Enslin et al. (2014). Kalahari Craton extension according to Jacobs et al. (2008). Western Dronning Maud Land regional foliation according to Groenewald et al. (1995). Natal Province regional foliation according to Thomas et al. (1992). Cape Meredith Complex regional foliation according to Thomas et al. (1997). Probably density plot (PDP) of the adjacent Natal Province A) Tugela; B) Mzumbe; C) Margate, and Western Dronning Maud Land D) Sverdrupfjella; E) Kirwanveggen; F) Heimefrontfjella. For a complete work reference used for PDP, please check Supplementary Material 16. Legend: SF – Sverdrupfjella; KV – Kirwanveggen; HF – Heimefrontfjella.

5.6 The printing of other tectonic cycles at MEBC

Several textures indicate a posterior low-grade retrograde metamorphism, as already pointed out by Chemale Jr. et al. (2018) and Tarney (1977). The garnet minerals usually have a late fluid phase (Pinite) in its edges. The substitution of garnet by both chlorite and pinite, common in MEBC, is also an indication of retrometamorphism processes. Albitization in plagioclases is conventional, related to retrograde metamorphism in greenschist facies conditions (Moody et al., 1985 and references therein) and might be related to the opening of the Rb-Sr system. Thus, we interpret the whole rock Rb-Sr ages of 533 ± 65 Ma, obtained by Beckinsale et al. (1977) in paragneisses, as generated by a greenschist facies retrometamorphism as already suggested by Wareham et al. (1998), which associated the Rb-Sr resetting with Panafrican-Panantarctican thermal anomaly field. Biotite substitution to muscovite, chlorite, or mica with deficient lattices, as well as the presence of sagenitic texture also foment this interpretation (Henry, 2005; Henry and Guidotti, 2002). The later suggests conditions of metamorphism similar to those observed in Greenschist Facies (300-500ºC; Shau et al., 1991). This temperature range is also a requirement to open K-Ar in the rock system. Beckinsale et al. (1977), obtained ages of 287 ± 7 and 399 ± 10 Ma (whole-rock K-Ar) in granites and paragneisses, relating these results with *"several Paleozoic thermal reactivation events"* related to Argon loss. We agree with Beckinsale`s interpretation.

The late anchi-metamorphic to a diagenetic event cataloged in MEBC is probably related with a Jurassic pre- to syn-rift episode at Falkland Plateau. Calcrete paleosols (weathered paragneiss; Barker et al., 1977a) suggests a subaerial exposition within dry conditions back to its development, and thus a regional sequence boundary. Sediments deposited after this disconformity demonstrate a fluvial to lacustrine environment of Oxfordian age (Late Jurassic; Barker et al., 1977a), probably related to a syn-rift setting. These sediments have also been found in site 550 (de Graciansky et al., 1985) and seismically extended into the Falkland Plateau Basin (Marshall, 1994b). Similarly, syn-rift fluvio-lacustrine Jurassic sediments are also found at North Falkland Basin (Jones et al., 2019; Richards and Hillier, 2000), South Malvinas Basin (Foschi and Cartwright, 2016) and Agulhas zone (Stanca et al., 2019). It is prone that the same event that caused the rifting in those localities, also catalyzed the same process in MEBC during the Jurassic. In Falkland (Malvinas) Islands, there is also a record of rifting event of Jurassic age; however, not as sedimentation, but as mafic dykes placement. Mussett and Taylor (1994) dated an NWW, and NE dikes, using whole-rock Ar-Ar, and obtained 188, and 193 Ma, respectively. Posteriorly, Stone et al. (2008), using whole-rock Ar-Ar, obtained an age of 179 Ma for NE dike. However, specific information such as timing and magnitude of Paleozoic through Mezozoic events still need more research.

CONCLUDING REMARKS

The Maurice Ewing Bank Complex consists of igneous-metamorphic rocks that experienced polyphasic metamorphism related to at least two orogenic cycles. In a broad sense, we identified five lithofacies that represents a usual assemblage associated with collisional granulitic terranes. Due to high-grade conditions, the events of partial melting coexist with the metamorphism; thereby, generating igneous rocks pre, syn-, tardi, and post-deformational.

The most abundant lithofacies consists of paragneisses. Their preterit detritus was deposited in a back-arc environment. The source area is widely linked with juvenile rocks derived from an exposed island arc. Paraderivated metamorphic rocks of similar age and Genesis are found either on Natal Province (mostly Margate) or Dronning Maud Land (mostly Kirvanveggen, Sverdrupfjella, and Heimefrontfjella).

The first metamorphic cycle comprehends four episodes of recrystallization. It is interpreted as generated by the collision between the cratons of Kaapvaal and Coats-Patagonia. It is also correlated with the Rodinia forming events (R). The metamorphic evolution experienced by MEBC represents all normal orogenic cycles.

We interpret that R1 (ca. 700ºC, between 0.3 to 0.9 GPa) and R2 (800ºC; 1.05GPa) events as related to a fold-and-thrust belt evolution, product of compressional tectonics that had its climax at R2, around 1068 ± 16 Ma. Besides the paragneisses lithofacies, the pre-, and syn- to tardi-metagranitoids also represents this episode; we interpreted as caused by granulitization/partial melting, generated by collisional processes related to arc-continent, and mostly continent-continent collision. There are events of comparable magnitude and genesis in Mzumbe-Margate, Natal Province, as well as Sivorg-Vardeklattene, Dronning Maud Land.

The event R3 is interpreted as caused by a thermometric decompression (ca. 0.8GPa, and 880ºC), which occurred around 1032 ± 12 Ma (age of syn-deformational metagranitoid). It represents the metamorphic climax related to the generator of Natal-Maud orogen. In a broad sense, it is associated with a regional exhumation event where there is an increase in geothermal gradient at the expense of decrease in pressure. Regions that experienced events of comparable conditions are characterized by possessing significant volumes of intrusive magma generated by partial melting. Thus, the diagnostic lithofacies of R3 is tardi-deformational granitoids.

This decompression event is also correlated with large plutons located at Mzumbe-Margate, Natal Province, and Dronning Maud Land.

The R4 event, occurred still at liquidus-in zone but below garnet zone, between 700-750ºC. It occurred during 1003 ± 16 Ma, being correlated with post-orogenic processes. Thus, R4 diagnostic lithofacies comprises post-deformational granitoid. This event marks the end of the metamorphic cycle related to Rodinia forming orogens at MEBC. Pegmatites, coarse-grained dykes, and alkaline stocks have processes and genesis alike throughout Natal-Maud key players. Despite those terranes, there is also significant volumes of partial melting related to Cape Meredith Complex, Falkland-Malvinas Islands.

The MEBC, due to geological likelihood, constitute a parcel of Kalahari Craton. During its generation and evolution, the complex stands between the Margate and Heimefrontfjella terranes. The collisional event, consistent with those events that occurred in the Antarctica (e.g., Western Dronning Maud Land) and South Africa (e.g., Natal Province) counterparts, is interpreted as caused by the interaction of Kaapvaal and Coats-Patagonia margins. The latter has geological characteristics that match with Grenville orogen, located in Laurentia. Henceforth, MEBC is not only part of Natal-Maud Belt, but also constitutes a crucial role in the understanding of intercontinental Grenvillian orogeny.

Several indicators suggest retrometamorphism up to greenschist facies, correlated with the second metamorphic cycle in which MEBC underwent. The retrometamorphism experienced by MEBC is related to Rb-Sr, and K-Ar isotopic system reset. The former occurred during 533 ± 65 Ma, being interpreted as generated by far-field anomalies associated with Panantarctican-Panafrican orogenies. Neoproterozoic metamorphic/granitogenesis events are widely found not only in East and West Antarctica but also as outcropping basement of Cape Fold-Thrust Belt and Patagonia. The closure of the K-Ar system occurred in two stages, 287 ± 7 and 399 ± 10 Ma, being correlated with “several reactivations during the Paleozoic.”

There are events of recrystallization below 300ºC. We interpret them as generated due to the thermal instability catalyzed by Mesozoic rifting. Two rifting events occur in or close to the MEBC, with Jurassic and Cretaceous age. Nonetheless, their timing and reasons are yet uncomprehend. Therefore, we suggest a profound study in the retrometamorphic-anchimetamorphic processes in MEBC to fathom the interplay between low-temperature metamorphism-diagenesis and the evolution of Falkland-Malvinas Plateau.

This work shed light between Mesoproterozoic terranes of Natal-Maud, the interaction with adjacent terranes, including Patagonia-Coats Land and Grenville orogen. However, there are still several questions that remain unresolved, such as i) the role of Haag Nunataks and Agulhas Plateau in the Mesoproterozoic; ii) Is the easternmost portion of Maurice Ewing Bank Terrane part of Paleozoic-Archean crust of Kaapvaal Craton? iii) What is the evolution of the Falkland Plateau and what implications does it have to the positioning of Falkland (Malvinas) Islands during Mesozoic? iv) The movement of the Patagonia Province, since its generation, back to Mesoproterozoic until the present configuration.

REFERENCES

Adie, R.J., 1952a. The position of the Falkland Islands in a reconstruction of Gondwanaland. Geol. Mag. 89, 401–410.

Adie, R.J., 1952b. Representatives of the Gondwana System in the Falkland Islands, in: Teichert, C. (Ed.), Symposium Sur Ler Series de Gondwana. Presented at the XIXth International Geological Congress, IUGS, Algiers, pp. 385–392.

Ague, J.J., Carlson, W.D., 2013. Metamorphism as Garnet Sees It: The Kinetics of Nucleation and Growth, Equilibration, and Diffusional Relaxation. Elements 9, 439–445. https://doi.org/10.2113/gselements.9.6.439

Allen, R.B., Tucholke, B.E., 1981. Petrography and implications of continental rocks from the Agulhas Plateau, southwest Indian Ocean. Geology 9, 463. https://doi.org/10.1130/0091-7613(1981)9<463:PAIOCR>2.0.CO;2

Andrade, S., Ulbrich, H.H., Gomes, C. de B., Martins, L., 2014. Methodology for the Determination of Trace and Minor Elements in Minerals and Fused Rock Glasses with Laser Ablation Associated with Quadrupole Inductively Coupled Plasma Mass Spectrometry (LA-Q-ICPMS). Am. J. Anal. Chem. 2014. https://doi.org/10.4236/ajac.2014.511079

Arndt, N.T., Todt, W., Chauvel, C., Tapfer, M., Weber, K., 1991. U–Pb zircon age and Nd isotopic composition of granitoids, charnockites and supracrustal rocks from Heimefrontfjella. Antarct. Geol. Rundsch. 80, 759–777.

Baker, H.A., 1924. Final Report on Geological Investigations in the Falkland Islands. U.S. Government Printing Office.

Barker, P.F., 1977. Correlations between sites on the eastern Falkland Plateau by means of seismic reflection profiles, Leg 36, DSDP, in: Initial Reports of DSDP. U.S. Government Printing Office, Washington, D. C.

Barker, P.F., Dalziel, I.W.D., Dinkelman, M.G., Elliot, D.H., Gombos, A.M., Lonardi, A., Plafker, G., Tarney, J., Thompson, R.W., Tjalsma, R.C., Borch, C.C. von der, Wise, S.W., 1977a. 6. Site 330. Initial Rep. Deep Sea Drill. Proj. XXXVI, 207–257. https://doi.org/10.2973/dsdp.proc.36.106.1977

Barker, P.F., Dalziel, I.W.D., Wise, S.W., 1977b. 1. Introduction. Initial Rep. Deep Sea Drill. Proj. XXXVI, 5–15. https://doi.org/10.2973/dsdp.proc.36.101.1977

Barton, E.S., 1983. The geochronology of the frontal zones of the Namaqua-Natal mobile belt (Ph. D.). University of Witwatersrand, South Africa.

Bauer, W., 1995. Strukturentwicklung und Petrogenese des metamorphen Grundgebirges der nördlichen Heimefrontfjella (westliches Dronning Maud Land/Antarktika) = Structural evolution and petrogenesis of the metamorphic basement complex of the northern Heimefrontfjella (western Dronning Maud Land/Antarctica). Berichte Zur Polarforsch. Rep. Polar Res. 191, 222. https://doi.org/10.2312/BzP_0171_1995

Bauer, W., Fielitz, W., Jacobs, J., Fanning, C.M., Spaeth, G., 2003. Mafic Dykes from Heimefrontfjella and implications for the post-Grenvillian to pre-Pan-African geological evolution of western Dronning Maud Land, Antarctica. Antarct. Sci. 15, 379–391. https://doi.org/10.1017/S0954102003001391

Beattie, J.C., 1909. Report of a magnetic survey of South Africa., Royal Society of London Publication. Cambridge University Press, United Kingdom.

Beckinsale, R.D., Tarney, J., Darbyshire, D.P.., Humm, M.J., 1977. 24. Re-Sr and K-Ar age determinations on samples of the Falkland Plateau basement at site 330, DSDP. Initial Rep. Deep Sea Drill. Proj. XXXVI, 923–927. https://doi.org/10.2973/dsdp.proc.36.124.1977

Bisnath, A., Frimmel, H., 2005. Metamorphic evolution of the Maud Belt: P-T-t Path for high-grade gneisses in Gjelsvikfjella, Dronning Maud Land, East Antarctica. J. Afr. Earth Sci. - J AFR EARTH SCI 43, 505–524. https://doi.org/10.1016/j.jafrearsci.2005.09.007

Bisnath, A., Frimmel, H.E., 2004. Age and tectonothermal evolution of Gjelsvikfjella, Maud Belt, East Antarctica., in: Abstract Volume. Presented at the Geoscience Africa 2004, University of Witwatersrand, Johannesburg, South Africa, pp. 60–61.

Bisnath, A., Frimmel, H.E., Armstrong, R.A., Board, W.S., 2006. Tectono-thermal evolution of the Maud Belt: New SHRIMP U–Pb zircon data from Gjelsvikfjella, Dronning Maud Land, East Antarctica. Precambrian Res. 150, 95–121. https://doi.org/10.1016/j.precamres.2006.06.009

Board, W.S., Frimmel, H.E., Armstrong, R.A., 2005. Pan-African Tectonism in the Western Maud Belt: P–T–t Path for High-grade Gneisses in the H.U. Sverdrupfjella, East Antarctica. J. Petrol. 46, 671–699. https://doi.org/10.1093/petrology/egh093

Boger, S.D., 2011. Antarctica — Before and after Gondwana. Gondwana Res. 19, 335–371. https://doi.org/10.1016/j.gr.2010.09.003

Bohlen, S.R., 2015. Pressure-Temperature-Time Paths and a Tectonic Model for the Evolution of Granulites. J. Geol. https://doi.org/10.1086/629159

Borello, A.V., 1963. Sobre la geología de las Islas Malvinas. Ediciones Culturales Argentinas, Ministerio de Educación y Justicia, Dirección General de Cultura.

Boynton, W.V., 1984. Chapter 3 - Cosmochemistry of the Rare Earth Elements: Meteorite Studies, in: Henderson, P. (Ed.), Developments in Geochemistry, Rare Earth Element Geochemistry. Elsevier, pp. 63–114. https://doi.org/10.1016/B978-0-444-42148-7.50008-3

Chemale Jr., F., Ramos, V.A., Naipauer, M., Girelli, T.J., Vargas, M., 2018. Age of basement rocks from the Maurice Ewing Bank and the Falkland/Malvinas Plateau. Precambrian Res. 314, 28–40. https://doi.org/10.1016/j.precamres.2018.05.026

Cornell, D.H., Thomas, Robert J., Gibson, R., Moen, H.F.G., Reid, D.L., Moore, J.M., Gibson, R.L., 2006. The Namaqua-Natal Province, in: Johnson, M.R., Anhauesser, C.R., Thomas, Robert James (Eds.), The Geology of South Africa. Geological Society of South Africa, Johannesburg, South Africa, pp. 325–379.

Coutinho, J., Kräutner, H., Sassi, F., Schmid, R., Sen, S., 2007. 8. Amphibolite and Granulite, in: Metamorphic Rocks: A Classification and Glossary of Terms. Cambridge University Press, Cambridge.

de Capitani, C., Brown, T.H., 1987. The computation of chemical equilibrium in complex systems containing non-ideal solutions. Geochim. Cosmochim. Acta 51, 2639–2652. https://doi.org/10.1016/0016-7037(87)90145-1

de Capitani, C., Petrakakis, K., 2010. The computation of equilibrium assemblage diagrams with Theriak/Domino software. Am. Mineral. 95, 1006–1016. https://doi.org/10.2138/am.2010.3354

de Graciansky, P.C., Poag, C.W., et al., 1985. Initial Reports of the Deep Sea Drilling Project, 80, Initial Reports of the Deep Sea Drilling Project. U.S. Government Printing Office. https://doi.org/10.2973/dsdp.proc.80.1985

Digel, S.G., Ghent, E.D., Carr, S.D., Simony, P.S., 1998. Early Cretaceous kyanite-sillimanite metamorphism and Paleocene sillimanite overprint near Mount Cheadle, southeastern British Columbia: geometry, geochronology, and metamorphic implications. Can. J. Earth Sci. 35, 1070–1087. https://doi.org/10.1139/cjes-35-9-1070

Du Toit, 1927. A geological comparison of South America with South Africa. Carnegie Inst. Wash. Publ. 381, 1–157.

Du Toit, A.L., 1937. Our Wandering Continents; An Hypothesis of Continental Drifting, First Edition edition. ed. Oliver and Boyd.

Eastin, R., Faure, G., 1971. The Age of the Littlewood Volcanics of Coats Land, Antarctica. J. Geol. 79, 241–245. https://doi.org/10.1086/627612

Eglington, B.M., Harmer, R.E., Kerr, A., 1989. Isotope and geochemical constraints on Proterozoic crustal evolution in south-eastern Africa. Precambrian Res., Papers from the Meeting on Proterozoic Geochemistry 45, 159–174. https://doi.org/10.1016/0301-9268(89)90037-5

Eglington, B.M., Thomas, R.J., Armstrong, R.A., 2010. U-PB SHRIMP ZIRCON DATING OF MESOPROTEROZOIC MAGMATIC ROCKS FROM THE SCOTTBURGH AREA, CENTRAL MZUMBE TERRANE, KWAZULU-NATAL, SOUTH AFRICA. South Afr. J. Geol. 113, 229–235. https://doi.org/10.2113/gssajg.113.2.229

Eglington, B.M., Thomas, R.J., Armstrong, R.A., Walraven, F., 2003. Zircon geochronology of the Oribi Gorge Suite, KwaZulu-Natal, South Africa: constraints on the timing of trans-current shearing in the Namaqua–Natal Belt. Precambrian Res. 123, 29–46. https://doi.org/10.1016/S0301-9268(03)00016-0

Ewing, M., Hayes, D.E., 1970. Deep Sea Drilling in Antarctic waters. Geotimes 5, 15–16.

Foschi, M., Cartwright, J.A., 2016. South Malvinas/Falkland Basin: Hydrocarbon migration and petroleum system. Mar. Pet. Geol. 77, 124–140. https://doi.org/10.1016/j.marpetgeo.2016.06.002

Foster, M.D., 1960. Interpretation of the composition of trioctahedral micas. Geol. Surv. Prof. Pap. 354, 49.

Frimmel, H.E., 2004. Formation of a late Mesoproterozoic supercontinent: the South Africa–East Antarctica connection, in: The Precambrian Earth: Tempos and Events. Elsevier.

Frost, B.R., Frost, C.D., 2008. On charnockites. Gondwana Res. 13, 30–44. https://doi.org/10.1016/j.gr.2007.07.006

Fuck, R.A., Brito Neves, B.B., Schobbenhaus, C., 2008. Rodinia descendants in South America. Precambrian Res., Testing the Rodinia Hypothesis: Records in its Building Blocks 160, 108–126. https://doi.org/10.1016/j.precamres.2007.04.018

Gose, W.A., Helper, M.A., Connelly, J.N., Hutson, F.E., Dalziel, I.W.D., 1997. Paleomagnetic data and U-Pb isotopic age determinations from Coats Land, Antarctica: Implications for late Proterozoic plate reconstructions. J. Geophys. Res. Solid Earth 102, 7887–7902. https://doi.org/10.1029/96JB03595

Grantham, G.H., Macey, P.H., Ingram, B.A., Roberts, M.P., Armstrong, R.A., Hokada, T., Shiraishi, K., Jackson, C., Bisnath, A., Manhica, V., 2008. Terrane correlation between Antarctica, Mozambique and Sri Lanka; comparisons of geochronology, lithology, structure and metamorphism and possible implications for the geology of southern Africa and Antarctica. Geol. Soc. Lond. Spec. Publ. 308, 91–119. https://doi.org/10.1144/SP308.4

Grantham, G.H., Mendonidis, P., Thomas, R.J., Satish-Kumar, M., 2012. Multiple origins of charnockite in the Mesoproterozoic Natal belt, Kwazulu-Natal, South Africa. Geosci. Front., Charnockites and Charnockites 3, 755–771. https://doi.org/10.1016/j.gsf.2012.05.006

Groenewald, P.B., Moyes, A.B., Grantham, G.H., Krynauw, J.R., 1995. East Antarctic crustal evolution: geological constraints and modelling in western Dronning Maud Land. Precambrian Res. 75, 231–250. https://doi.org/10.1016/0301-9268(95)80008-6

Harley, S.L., 1989. The origins of granulites: a metamorphic perspective. Geol. Mag. 126, 215–247. https://doi.org/10.1017/S0016756800022330

Harlov, D.E., 2012. The potential role of fluids during regional granulite-facies dehydration in the lower crust. Geosci. Front., Charnockites and Charnockites 3, 813–827. https://doi.org/10.1016/j.gsf.2012.03.007

Henry, D.J., 2005. The Ti-saturation surface for low-to-medium pressure metapelitic biotites: Implications for geothermometry and Ti-substitution mechanisms. Am. Mineral. 90, 316–328. https://doi.org/10.2138/am.2005.1498

Henry, D.J., Guidotti, C.V., 2002. Titanium in biotite from metapelitic rocks: Temperature effects, crystal-chemical controls, and petrologic applications. Am. Mineral. 87, 375–382. https://doi.org/10.2138/am-2002-0401

Herron, M.M., 1988. Geochemical Classification of Terrigenous Sands and Shales from Core or Log Data. SEPM J. Sediment. Res. Vol. 58. https://doi.org/10.1306/212F8E77-2B24-11D7-8648000102C1865D

Higgins, M.D., 1999. Origin of megacrysts in granitoids by textural coarsening: a crystal size distribution (CSD) study of microcline in the Cathedral Peak Granodiorite, Sierra Nevada, California. Geol. Soc. Lond. Spec. Publ. 168, 207–219. https://doi.org/10.1144/GSL.SP.1999.168.01.14

Holland, T., Powell, R., 2003. Activity composition relations for phases in petrological calculations: an asymmetric multicomponent formulation. Contrib. Mineral. Petrol. 145, 492–501. https://doi.org/10.1007/s00410-003-0464-z

Holland, T.J.B., Powell, R., 1998. An internally consistent thermodynamic data set for phases of petrological interest: AN INTERNALLY CONSISTENT THERMODYNAMIC DATA SET. J. Metamorph. Geol. 16, 309–343. https://doi.org/10.1111/j.1525-1314.1998.00140.x

Ivanov, A.V., Meffre, S., Thompson, J., Corfu, F., Kamenetsky, V.S., Kamenetsky, M.B., Demonterova, E.I., 2017. Timing and genesis of the Karoo-Ferrar large igneous province: New high precision U-Pb data for Tasmania confirm short duration of the major magmatic pulse. Chem. Geol. 455, 32–43. https://doi.org/10.1016/j.chemgeo.2016.10.008

Jackson, C., 1999. Characterization of Mesoproterozoic to Palaeozoic crustal evolution of Western Dronning Maud Land. Unpubl. Rep. South Afr. Natl. Antarct. Program Study 534, 80.

Jacobs, J., 2009. A review of two decades (1986 – 2008) of geochronological work in Heimefrontfjella, and geotectonic Interpretation of western Dronning Maud Land, East Antarctica. Polarforschung 79, 47–57.

Jacobs, J., Ahrendt, H., Kreutzer, H., Weber, K., 1995. K-Ar, 40Ar/39Ar and apatite fission-track evidence for Neoproterozoic and Mesozoic basement rejuvenation events in the Heimefrontfjella and Mannefallknausane (East Antarctica). Precambrian Res. 75, 251–262. https://doi.org/10.1016/0301-9268(95)80009-7

Jacobs, J., Bauer, W., Fanning, C., 2003a. New age constraints for Grenville-age metamorphism in western central Dronning Maud Land (East Antarctica), and implications for the palaeogeography of Kalahari in Rodinia. Int. J. Earth Sci. 92, 301–315. https://doi.org/10.1007/s00531-003-0335-x

Jacobs, J., Bauer, W., Spaeth, G., Thomas, R.J., Weber, K., 1996. Litholog and structure of the Grenville-aged (≈1.1 Ga) basement of heimefrontfjella (East Antarctica). Geol. Rundsch. 85, 800–821. https://doi.org/10.1007/BF02440112

Jacobs, J., Elburg, M., Läufer, A., Kleinhanns, I.C., Henjes-Kunst, F., Estrada, S., Ruppel, A.S., Damaske, D., Montero, P., Bea, F., 2015. Two distinct Late Mesoproterozoic/Early Neoproterozoic basement provinces in central/eastern Dronning Maud Land, East Antarctica: The missing link, 15–21° E. Precambrian Res., The structural, metamorphic and magmatic evolution of Mesoproterozoic orogens 265, 249–272. https://doi.org/10.1016/j.precamres.2015.05.003

Jacobs, J., Falter, M., Thomas, B., Kunz, J., Jessberger, E., 1997. 40Ar39Ar Thermochronological constraints on the structural evolution of the Mesoproterozoic Natal Metamorphic Province, SE Africa. Precambrian Res. 75, 71–92. https://doi.org/10.1016/S0301-9268(97)00042-9

Jacobs, J., Fanning, C.., Bauer, W., 2003b. Timing of Grenville-age vs. Pan-African medium- to high grade metamorphism in western Dronning Maud Land (East Antarctica) and significance for correlations in Rodinia and Gondwana. Precambrian Res. 125, 1–20. https://doi.org/10.1016/S0301-9268(03)00048-2

Jacobs, J., Fanning, C.M., Henjes-Kunst, F., Olesch, M., Paech, H.-J., 1998. Continuation of the Mozambique Belt Into East Antarctica: Grenville-Age Metamorphism and Polyphase Pan-African High-Grade Events in Central Dronning Maud Land. J. Geol. 106, 385–406. https://doi.org/10.1086/516031

Jacobs, J., Pisarevsky, S., Thomas, B., Fullgraf, T., 2008. The Kalahari Craton during the assembly and dispersal of Rodinia. Precambrian Res. 160, 142–158. https://doi.org/10.1016/j.precamres.2007.04.022

Jacobs, J., Thomas, B., 1999. From Rodinia to Gondwana, the East-Antarctic Perspective. Gondwana Res. 2, 567–567. https://doi.org/10.1016/S1342-937X(05)70198-2

Jacobs, J., Thomas, R.J., Armstrong, R.A., Henjes-Kunst, F., 1999. Age and thermal evolution of the Mesoproterozoic Cape Meredith Complex, West Falkland. J. Geol. Soc. 156, 917–928. https://doi.org/10.1144/gsjgs.156.5.0917

Jacobs, J., Thomas, R.J., Weber, K., 1993. Accretion and indentation tectonics at the southern edge of the Kaapvaal craton during the Kibaran (Grenville) orogeny. Geology 21, 203–206. https://doi.org/10.1130/0091-7613(1993)021<0203:AAITAT>2.3.CO;2

JanoušEk, V., Farrow, C.M., Erban, V., 2006. Interpretation of Whole-rock Geochemical Data in Igneous Geochemistry: Introducing Geochemical Data Toolkit (GCDkit). J. Petrol. 47, 1255–1259. https://doi.org/10.1093/petrology/egl013

Jiang, J., Lasaga, A.C., 1990. The effect of post-growth thermal events on growth-zoned garnet: implications for metamorphic P-T history calculations. Contrib. Mineral. Petrol. 105, 454–459. https://doi.org/10.1007/BF00286832

Johnson, B.R., Glazner, A.F., 2010. Formation of K-feldspar megacrysts in granodioritic plutons by thermal cycling and late-stage textural coarsening. Contrib. Mineral. Petrol. 159, 599–619. https://doi.org/10.1007/s00410-009-0444-z

Jokat, W., Miller, H., Hübscher, C., 1996. Crustal structure of the Antarctic continental margin in the eastern Weddell Sea. Geol. Soc. Lond. Spec. Publ. 108, 165–174. https://doi.org/10.1144/GSL.SP.1996.108.01.12

Jones, D.J.R., McCarthy, D.J., Dodd, T.J.H., 2019. Tectonostratigraphy and the petroleum systems in the Northern sector of the North Falkland Basin, South Atlantic. Mar. Pet. Geol. https://doi.org/10.1016/j.marpetgeo.2019.02.020

Kimbell, G.S., Richards, P.C., 2008. The three-dimensional lithospheric structure of the Falkland Plateau region based on gravity modelling. J. Geol. Soc. 165, 795–806. https://doi.org/10.1144/0016-76492007-114

Kranidiotis, P., MacLean, W.H., 1987. Systematics of chlorite alteration at the Phelps Dodge massive sulfide deposit, Matagami, Quebec. Econ. Geol. 82, 1898–1911. https://doi.org/10.2113/gsecongeo.82.7.1898

Ksienzyk, A., Jacobs, J., Košler, J., Sircombe, K., 2007. A comparative provenance study of the late Mesoproterozoic Maud Belt (East Antarctica) and the Pinjarra Orogen (Western Australia): implications for a possible Mesoproterozoic Kalahari-Western Australia connection.

Kudryavtzev, G.A., Butzenko, V.V., Kadmina, I.N., 1991. Crustal section across western Dronning Maud Land continental margin, in: Yoshida, Y., Kaminuma, K., Shiraishi, K. (Eds.), Abstracts.

Presented at the Proceedings of the Sixth International Symposium on Antarctic Earth Science, National Institute for Polar Research, Tokyo, pp. 330–335.

Li, Z.X., Bogdanova, S.V., Collins, A.S., Davidson, A., De Waele, B., Ernst, R.E., Fitzsimons, I.C.W., Fuck, R.A., Gladkochub, D.P., Jacobs, J., Karlstrom, K.E., Lu, S., Natapov, L.M., Pease, V., Pisarevsky, S.A., Thrane, K., Vernikovsky, V., 2008. Assembly, configuration, and break-up history of Rodinia: A synthesis. Precambrian Res., Testing the Rodinia Hypothesis: Records in its Building Blocks 160, 179–210. https://doi.org/10.1016/j.precamres.2007.04.021

Lindeque, A., Wit, M.J.D., Ryberg, T., Weber, M., Chevallier, L., 2011. DEEP CRUSTAL PROFILE ACROSS THE SOUTHERN KAROO BASIN AND BEATTIE MAGNETIC ANOMALY, SOUTH AFRICA: AN INTEGRATED INTERPRETATION WITH TECTONIC IMPLICATIONS. South Afr. J. Geol. 114, 265–292. https://doi.org/10.2113/gssajg.114.3-4.265

Loewy, S.L., Dalziel, I.W.D., Pisarevsky, S., Connelly, J.N., Tait, J., Hanson, R.E., Bullen, D., 2011. Coats Land crustal block, East Antarctica: A tectonic tracer for Laurentia? Geology 39, 859–862. https://doi.org/10.1130/G32029.1

Ludwig, W.J., Rabinowitz, P.D., 1982. The collision complex of the North Scotia Ridge. J. Geophys. Res. Solid Earth 87, 3731–3740. https://doi.org/10.1029/JB087iB05p03731

Marshall, J.E.A., 1994. The Falkland Islands and the early fragmentation of Gondwana: implications for hydrocarbon exploration in the Falkland Plateau. Mar. Pet. Geol. 11, 631–636. https://doi.org/10.1016/0264-8172(94)90073-6

Martínez Dopico, C.I., López de Luchi, M.G., Rapalini, A.E., Kleinhanns, I.C., 2011. Crustal segments in the North Patagonian Massif, Patagonia: An integrated perspective based on Sm–Nd isotope systematics. J. South Am. Earth Sci. 31, 324–341. https://doi.org/10.1016/j.jsames.2010.07.009

McMenamin, M.A.S., McMenamin, D.L., 1990. The Emergence of Animals: The Cambrian Breakthrough. Columbia University Press.

Mendonidis, P., Armstrong, R.A., 2016. U–Pb Zircon (SHRIMP) ages of granite sheets and timing of deformational events in the Natal Metamorphic Belt, southeastern Africa: Evidence for deformation partitioning and implications for Rodinia reconstructions. Precambrian Res. 278, 22–33. https://doi.org/10.1016/j.precamres.2016.03.003

Mendonidis, P., Grantham, G.H., 2003. Petrology, Origin and Metamorphic History of Proterozoic-aged Granulites of the Natal Metamorphic Province, Southeastern Africa. Gondwana Res. 6, 607–628. https://doi.org/10.1016/S1342-937X(05)71011-X

Mendonidis, P., Thomas, R.J., Grantham, G.H., Armstrong, R.A., 2015a. Geochronology of emplacement and charnockite formation of the Margate Granite Suite, Natal Metamorphic Province, South Africa: Implications for Natal-Maud belt correlations. Precambrian Res., The structural, metamorphic and magmatic evolution of Mesoproterozoic orogens 265, 189–202. https://doi.org/10.1016/j.precamres.2015.02.013

Mendonidis, P., Thomas, R.J., Grantham, G.H., Armstrong, R.A., 2015b. Geochronology of emplacement and charnockite formation of the Margate Granite Suite, Natal Metamorphic Province, South Africa: Implications for Natal-Maud belt correlations. Precambrian Res., The structural, metamorphic and magmatic evolution of Mesoproterozoic orogens 265, 189–202. https://doi.org/10.1016/j.precamres.2015.02.013

Middlemost, E.A.K., 1994. Naming materials in the magma/igneous rock system. Earth-Sci. Rev. 37, 215–224. https://doi.org/10.1016/0012-8252(94)90029-9

Mikhalsky, E.V., Sheraton, J.W., Hahne, K., 2006. Charnockite composition in relation to the tectonic evolution of East Antarctica. Gondwana Res. 9, 379–397. https://doi.org/10.1016/j.gr.2005.11.007

Millar, I.L., Pankhurst, R.J., 1987. Rb-Sr geochronology of the region between the Antarctic Peninsula and the Transantarctic Mountains: Haag nunataks and Mesozoic granitoids, in: McKenzie, G.D. (Ed.), Geophysical Monograph Series. American Geophysical Union, Washington, D. C., pp. 151–160.

Moody, J.B., Jenkins, J.E., Meyer, D., 1985. An experimental investigation of the albitization of plagioclase. Can. Mineral. 23, 583–596.

Moyes, A.B., Barton, J.M., 1990. A review of isotopic data from western Dronning Maud Land, Antarctica. Zentralblatt Geol. Palaeontol. Teil 1 1.

Mundl, A., Ntaflos, T., Ackerman, L., Bizimis, M., Bjerg, E.A., Hauzenberger, C.A., 2015. Mesoproterozoic and Paleoproterozoic subcontinental lithospheric mantle domains beneath southern Patagonia: Isotopic evidence for its connection to Africa and Antarctica. Geology 43, 39–42. https://doi.org/10.1130/G36344.1

Mussett, A.E., Taylor, G.K., 1994. 40Ar-39Ar ages for dykes from the Falkland Islands with implications for the break-up of southern Gondwanaland. J. Geol. Soc. 151, 79–81. https://doi.org/10.1144/gsjgs.151.1.0079

Musumeci, G., 2002. Sillimanite-bearing shear zones in syntectonic leucogranite: fluid-assisted brittle–ductile deformation under amphibolite facies conditions. J. Struct. Geol. 24, 1491–1505. https://doi.org/10.1016/S0191-8141(01)00153-5

Nance, R.D., Murphy, J.B., Santosh, M., 2014. The supercontinent cycle: A retrospective essay. Gondwana Res. 25, 4–29. https://doi.org/10.1016/j.gr.2012.12.026

Otani, M., Wallis, S., 2006. Quartz lattice preferred orientation patterns and static recrystallization: Natural examples from the Ryoke belt, Japan. Geology 34, 561–564. https://doi.org/10.1130/G22430.1

Pankhurst, R.J., Rapela, C.W., Fanning, C.M., Márquez, M., 2006. Gondwanide continental collision and the origin of Patagonia. Earth-Sci. Rev. 76, 235–257. https://doi.org/10.1016/j.earscirev.2006.02.001

Passchier, C.., Trouw, R.A.J., 2005. Microtectonics, 2nd ed. Springer, New York.

Pearce, J.A., Harris, N.B.W., Tindle, A.G., 1984. Trace Element Discrimination Diagrams for the Tectonic Interpretation of Granitic Rocks. J. Petrol. 25, 956–983. https://doi.org/10.1093/petrology/25.4.956

Quesnel, Y., Weckmann, U., Ritter, O., Stankiewicz, J., Lesur, V., Mandea, M., Langlais, B., Sotin, C., Galdéano, A., 2009. Simple models for the Beattie Magnetic Anomaly in South Africa. Tectonophysics, Magnetic Anomalies 478, 111–118. https://doi.org/10.1016/j.tecto.2008.11.027

Rabinowitz, P.D., LaBrecque, J.L., 1979. The Mesozoic South Atlantic Ocean and evolution of its continental margins. J. Geophys. Res. Solid Earth 84, 5973–6002. https://doi.org/10.1029/JB084iB11p05973

Ramos, V.A., 2010. The Grenville-age basement of the Andes. J. South Am. Earth Sci., The Grenville Orogen in Central and South America 29, 77–91. https://doi.org/10.1016/j.jsames.2009.09.004

Ramos, V.A., 2008. Patagonia: A paleozoic continent adrift? J. South Am. Earth Sci. 26, 235–251. https://doi.org/10.1016/j.jsames.2008.06.002

Ramos, V.A., Cingolani, C., Junior, F.C., Naipauer, M., Rapalini, A., 2017. The Malvinas (Falkland) Islands revisited: The tectonic evolution of southern Gondwana based on U-Pb and Lu-Hf detrital zircon isotopes in the Paleozoic cover. J. South Am. Earth Sci. 76, 320–345. https://doi.org/10.1016/j.jsames.2016.12.013

Ramos, V.A., Naipauer, M., 2014. Patagonia: where does it come from? J. Iber. Geol. 40, 367–379. https://doi.org/10.5209/rev_JIGE.2014.v40.n2.45304

Ramos, V.A., Riccardi, A.C., Rolleri, E.O., 2004. Límites naturales del norte de la Patagonia. Rev. Asoc. Geológica Argent. 59, 785–786.

Rex, D.C., Tanner, P.W.G., 1982. Precambrian age for gnaisses at Cape Meredith in the Falkland Islands, in: Craddock, C. (Ed.), Antarctic Geoscience, B. University of Wisconsin Press, International Union of Geological Sciences, pp. 107–108.

Richards, P.C., Hillier, B.V., 2000. Post-Drilling Analysis of the North Falkland Basin— Part 1: Tectono-Stratigraphic Framework. J. Pet. Geol. 23, 253–272. https://doi.org/10.1111/j.1747-5457.2000.tb01019.x

Rieder, M., Cavazzini, G., D'Yakonov, Y., Kamenetskii, V.A., Gottardi, G., Guggenheim, S., Koval, P., Müller, G., Neiva, A.M.R., Radolosvich, E.W., Robert, J.L., Sassi, F., Takeda, T., Weiss, Z., Wones, D.R., 1998. Nomenclature of the micas. Can. Mineral. 36, 1–7.

Roberts, N.M.W., 2013. The boring billion? – Lid tectonics, continental growth and environmental change associated with the Columbia supercontinent. Geosci. Front., Thematic Section: Antarctica – A window to the far off land 4, 681–691. https://doi.org/10.1016/j.gsf.2013.05.004

Roberts, N.M.W., Slagstad, T., Viola, G., 2015. The structural, metamorphic and magmatic evolution of Mesoproterozoic orogens. Precambrian Res., The structural, metamorphic and magmatic evolution of Mesoproterozoic orogens 265, 1–9. https://doi.org/10.1016/j.precamres.2015.05.031

Roser, B.P., Korsch, R.J., 1988. Provenance signatures of sandstone-mudstone suites determined using discriminant function analysis of major-element data. Chem. Geol. 67, 119–139. https://doi.org/10.1016/0009-2541(88)90010-1

Ross, G.M., Villeneuve, M., 2003. Provenance of the Mesoproterozoic (1.45 Ga) Belt basin (western North America): Another piece in the pre-Rodinia paleogeographic puzzle. GSA Bull. 115, 1191–1217. https://doi.org/10.1130/B25209.1

Rudnick, R.L., Fountain, D.M., 1995. Nature and composition of the continental crust: A lower crustal perspective. Rev. Geophys. 33, 267–309. https://doi.org/10.1029/95RG01302

Scheiber-Enslin, S., Ebbing, J., Webb, S.J., 2014. An integrated geophysical study of the Beattie Magnetic Anomaly, South Africa. Tectonophysics 636, 228–243. https://doi.org/10.1016/j.tecto.2014.08.021

Schilling, M.E., Carlson, R.W., Conceição, R.V., Dantas, C., Bertotto, G.W., Koester, E., 2008. Re–Os isotope constraints on subcontinental lithospheric mantle evolution of southern South America. Earth Planet. Sci. Lett. 268, 89–101. https://doi.org/10.1016/j.epsl.2008.01.005

Schimschal, C.M., Jokat, W., 2019. The Falkland Plateau in the context of Gondwana breakup. Gondwana Res. 68, 108–115. https://doi.org/10.1016/j.gr.2018.11.011

Schimschal, C.M., Jokat, W., 2018. The crustal structure of the continental margin east of the Falkland Islands. Tectonophysics 724–725, 234–253. https://doi.org/10.1016/j.tecto.2017.11.034

Schmid, R., Fettes, D., Harte, B., Eleutheria, D., Desmons, J., 2007. 1. How to name a metamorphic rock, in: Metamorphic Rocks: A Classification and Glossary of Terms. Cambridge University Press, Cambridge.

Schulze, P., 1992. Petrogenese des metamorphen Grundgebirges der zentralen Heimefrontfjella (westliches Dronning Maud Land / Antarktis) = Petrogenesis of the metamorphic basement complex of the central Heimefrontfjella mountains (western Dronning Maud Land / Antarctica). Berichte Zur Polarforsch. Rep. Polar Res. 117, 321. https://doi.org/10.2312/BzP_0117_1992

Shau, Y.-H., Yang, H.-Y., Peacor, D.R., 1991. On oriented titanite and rutile inclusions in sagenitic biotite. Am. Mineral. 76, 1205–1217.

Smith, J.V., Brown, W.L., 1988. Feldspar Minerals. Springer Berlin Heidelberg, Berlin, Heidelberg.

Spear, F.S., 1993. Metamorphic Phase Equilibria and Pressure-Temperature-Time Paths. Mineralogical Society of America, Washington, D. C.

Spear, F.S., 1991. On the interpretation of peak metamorphic temperatures in light of garnet diffusion during cooling. Metamorph. Geol. 9, 379–388. https://doi.org/10.1111/j.1525-1314.1991.tb00533.x

Spear, F.S., Peacock, S.M. (Eds.), 1989. Petrologic determination of metamorphic pressure-temperature-time paths, in: Metamorphic Pressure-Temperature-Time Paths, American Geophysical Union Short Course In Geology. AGU, Boulder, Colorado, pp. 1–55.

Spencer, C.J., Thomas, R.J., Roberts, N.M.W., Cawood, P.A., Millar, I., Tapster, S., 2015a. Crustal growth during island arc accretion and transcurrent deformation, Natal Metamorphic Province, South Africa: New isotopic constraints. Precambrian Res., The structural, metamorphic and magmatic evolution of Mesoproterozoic orogens 265, 203–217. https://doi.org/10.1016/j.precamres.2015.05.011

Spencer, C.J., Thomas, R.J., Roberts, N.M.W., Cawood, P.A., Millar, I., Tapster, S., 2015b. Crustal growth during island arc accretion and transcurrent deformation, Natal Metamorphic Province, South Africa: New isotopic constraints. Precambrian Res., The structural, metamorphic and magmatic evolution of Mesoproterozoic orogens 265, 203–217. https://doi.org/10.1016/j.precamres.2015.05.011

Stanca, R.M., Paton, D.A., Hodgson, D.M., McCarthy, D.J., Mortimer, E.J., 2019. A revised position for the rotated Falkland Islands microplate. J. Geol. Soc. jgs2018-163. https://doi.org/10.1144/jgs2018-163

Stone, P., Richards, P.C., Kimbell, G.S., Esser, R.P., Reeves, D., 2008. Cretaceous dykes discovered in the Falkland Islands: implications for regional tectonics in the South Atlantic. J. Geol. Soc. 165, 1–4. https://doi.org/10.1144/0016-76492007-072

Storey, B.C., Pankhurst, R.J., Johnson, A.C., 1994. The Grenville Province within Antarctica: a test of the SWEAT hypothesis. J. Geol. Soc. 151, 1–4. https://doi.org/10.1144/gsjgs.151.1.0001

Tarney, J., 1977. 23. Petrology, Mineralogy, and Geochemistry of the Falkland Plateau basement Rocks, site 330, Deep Sea Drilling Project. Initial Rep. Deep Sea Drill. Proj. XXXVI. https://doi.org/10.2973/dsdp.proc.36.123.1977

Thomas, R.J., 1989. A tale of two tectonic terranes. South Afr. J. Geol. 92, 306–321.

Thomas, R.J., Agenbacht, A.L.D., Cornell, D.H., Moore, J.M., 1994. The Kibaran of southern Africa: Tectonic evolution and metallogeny. Ore Geol. Rev., Kibaran (Mid-Proterozoic) Metallogeny in Central and Southern Africa 9, 131–160. https://doi.org/10.1016/0169-1368(94)90025-6

Thomas, R.J., Armstrong, R.A., Eglington, B.M., 2003. Geochronology of the Sikombe Granite, Transkei, Natal Metamorphic Province, South Africa. South Afr. J. Geol. 106, 403–408. https://doi.org/10.2113/106.4.403

Thomas, R.J., Du Plessis, A.J., Fitch, F., Marshall, C.G.A., Miller, J.A., Von Brunn, V., Watkeys, M.K., 1992. Geological studies in southern Natal and Transkei: implications for the Cape Orogen, in:

De Wit, M.J., Ransome, I.G.. (Eds.), Inversion Tectonics of the Cape Fold Belt, Karoo and Cretaceous Basins of Southern Africa. pp. 229–236.

Thomas, R.J., Jacobs, J., Eglington, B.M., 2000. Geochemistry and isotopic evolution of the Mesoproterozoic Cape Meredith Complex, West Falkland. Geol. Mag. 137, 537–553.

Thomas, R.J., Jacobs, J., Weber, K., 1997. Geology of the Mesoproterozoic Cape Meredith Complex, West Falkland, in: Ricci, C.A. (Ed.), The Antarctic Region: Geological Evolution and Processes. Terra Antarctica, Siena, pp. 21–30.

Thompson, R.N., 1982. Magmatism of the British Tertiary Volcanic Province. Scott. J. Geol. 18, 49–107. https://doi.org/10.1144/sjg18010049

Veevers, J.J., 2012. Reconstructions before rifting and drifting reveal the geological connections between Antarctica and its conjugates in Gondwanaland. Earth-Sci. Rev. 111, 249–318. https://doi.org/10.1016/j.earscirev.2011.11.009

Verma, S.P., Armstrong-Altrin, J.S., 2013. New multi-dimensional diagrams for tectonic discrimination of siliciclastic sediments and their application to Precambrian basins. Chem. Geol. 355, 117–133. https://doi.org/10.1016/j.chemgeo.2013.07.014

Vernon, R.H., 1979. Formation of late sillimanite by hydrogen metasomatism (base-leaching) in some high-grade gneisses. Lithos 12, 143–152. https://doi.org/10.1016/0024-4937(79)90045-8

Wareham, C.D., Pankhurst, R.J., Thomas, R.J., Storey, B.C., Grantham, G.H., Jacobs, J., Eglington, B.M., 1998. Pb, Nd, and Sr Isotope Mapping of Grenville-Age Crustal Provinces in Rodinia. J. Geol. 106, 647–660. https://doi.org/10.1086/516051

Watson, E.B., Wark, D.A., Thomas, J.B., 2006. Crystallization thermometers for zircon and rutile. Contrib. Mineral. Petrol. 151, 413. https://doi.org/10.1007/s00410-006-0068-5

White, R.W., Powell, R., Clarke, G.L., 2002. The interpretation of reaction textures in Fe-rich metapelitic granulites of the Musgrave Block, central Australia: constraints from mineral equilibria calculations in the system K2O-FeO-MgO-Al2O3-SiO2-H2O-TiO2-Fe2O3: REACTION TEXTURES, MUSGRAVE BLOCK GRANULITES. J. Metamorph. Geol. 20, 41–55. https://doi.org/10.1046/j.0263-4929.2001.00349.x

White, R.W., Powell, R., Holland, T.J.B., 2007. Progress relating to calculation of partial melting equilibria for metapelites. J. Metamorph. Geol. 25, 511–527. https://doi.org/10.1111/j.1525-1314.2007.00711.x

Wintsch, R.P., Andrews, M.S., 1988. Deformation induced growth of sillimanite: ' stress' minerals revisited. J. Geol. 96, 143–161.

Wolmarans, L.G., Kent, A., 1982. Geological investigations in western Dronning Maud Land, Antarctica, a synthesis. South African Scientific Committee for Antarctic Research.

Yavuz, F., Karakaya, N., Yıldırım, D.K., Karakaya, M.Ç., Kumral, M., 2014. A Windows program for calculation and classification of tourmaline-supergroup (IMA-2011). Comput. Geosci. 63, 70–87. https://doi.org/10.1016/j.cageo.2013.10.012

Yavuz, F., Kumral, M., Karakaya, N., Karakaya, M.Ç., Yıldırım, D.K., 2015. A Windows program for chlorite calculation and classification. Comput. Geosci. 81, 101–113. https://doi.org/10.1016/j.cageo.2015.04.011

Zane, A., Weiss, Z., 1998. A procedure for classifying rock-forming chlorites based on microprobe data. Rendiconti Lincei 9, 51–56.

SUPPLEMENTARY MATERIAL

SUPPLEMENTARY MATERIAL 1 – SAMPLING AND LOGGING INFORMATION

Table 3 – Sampling and logging information of DSDP Site 330. Lithofacies according to this work. Bold letter in classification refers to classification according to Tarney (1977). Italic letters in classification refers to classification according to this work.

Core	Section	Interval	Code	Geochemistry Tarney + Farid	Lithofacies	Classification	Thin Section A	Thin Section B Code
15	2	130-132	1		Peat / Coal / Black Shale			
15	2	132-135	2		Organic medium sandstone			
15	2	135-137	3		Peat / Coal / Black Shale			
15	2	137-141	4		Medium Sandstone w/ pebbles			
15	2	141-143	5		Peat / Coal / Black Shale			
15	2	143-145	6		Peat / Coal / Black Shale			
15	2	145-150	7		Medium Sandstone w/ pebbles			
16	1	26-31	1	#01 (18-22)	Weathered Paragneiss	**Calcite-impregnated metassedimentary gneiss**		
16	1	31-37	2	#02 (30-38)	Weathered Paragneiss	**Calcite impregnated metasedimentary gneiss with large poikilitic calcites**		
16	1	40-46	3		Weathered Paragneiss			
16	1	46-53	4	#03 (52-55)	Syn- to tardi-deformational granite	**Coarse K-feldspar-rich pegmatitic vein (S2)**		
16	1	55-58	5		Weathered Paragneiss			
16	1	58-61	6		Weathered Paragneiss			
16	1	63-69	7		Weathered Paragneiss			

16	1	69-77	8	#04 (71-78)	Weathered Paragneiss	**Quartz-rich granular gneiss**		
16	1	77-92	9		Weathered Paragneiss			
16	1	87-94	10	16R1-10	Weathered Paragneiss	*Chlorite-calcte bearing epidote-biotite-gneiss*	16R1-10A	16R1-10B
16	1	94-97	11		Weathered Paragneiss			
16	1	97-105	12		Weathered Paragneiss			
16	1	105-106	13	#05 (100-108)	Weathered Paragneiss	**Quartz-rich metasedimentary gneiss with K-feldspar, biotite, ore, siderite, and garnet**		
16	1	106-113	14		Weathered Paragneiss			
16	1	113-118	15		Weathered Paragneiss			
16	1	118-123	16		Paragneiss / Syn- to tardi-deformational granite			
16	1	123-126	17		Paragneiss			
16	1	126-129	18		Paragneiss / Syn- to tardi-deformational granite			
16	1	129-134	19		Paragneiss			
16	1	134-137	20		Paragneiss / Syn- to tardi-deformational granite			
16	1	137-139	21		Paragneiss / Syn- to tardi-deformational granite			
16	1	139-142	22		Paragneiss			
16	1	142-146	23	#06 (142-146)	Paragneiss	**Metassedimentary gneiss with quartz, plagioclase, K-feldspar, biotite, and ore**		

16	2	0-6	1	#07 (1-11)	Restite	**Pelitic gneiss, mainly biotite and garnet variably replaced by chlorite -** *garnet-calcite-chlorite bearing biotite-gneiss; Restite*	16R2-01	
16	2	9-12	2	#07 (1-11)	Restite	**Pelitic gneiss, mainly biotite and garnet variably replaced by chlorite**		
16	2	12-17	3		Paragneiss / Syn- to tardi-deformational granite	*Ep bearing Plag-Qtz Paragneiss*	16R2-03A	16R2-03B
16	2	17-19	4		Post-deformational granite / paragneiss			
16	2	19-21	5		Post-deformational granite / paragneiss			
16	2	21-26	6		Post-deformational granite			
16	2	23-26	7		Syn- to tardi-deformational metagranitoid			
16	2	50-56	8	#08 (43-50)	Pre-deformational metagranitoid	**Deformed early sigma01 K-feldspar pegmatite vein, with garnet, quartz, plagioclase, and biotite -** *chlorite-sillimanite-garnet bearing calcite-biotite-metagranite s1*	16R1-08A	16R1-08B
16	2	58,5-63	9		Paragneiss			
16	2	63-67	10		Restite / Paragneiss			

16	2	77-69	11		Restite	**Biotitite**		
16	2	69-70,5	12		Paragneiss / Restite			
16	2	70,5-73	13	16R2-13	Restite	*13A - Chlorite-rutile bearing biotitite; (Restite) 13B - Quartzolite*	16R2-13A	16R2-13B
16	2	73-78	14	#09 (74-78)	Restite / Post-deformational granite	**Banded semipelitic gneiss, with quartz, biotite, K-feldspar, and plagioclase / Granite s3**		
16	2	82-84	15		Paragneiss			
16	2	84-87	16		Paragneiss / Syn- to tardi-deformational granite			
16	2	87-90	17		Paragneiss			
16	2	90-99	18		Paragneiss			
16	2	99-100	19		Post-deformational granite			
16	2	100-104	20		Paragneiss			
16	2	104-105	21	#10 (104-108)	Paragneiss	**Banded semipelitic gneiss, with quartz, biotite, K-feldspar, plagioclase, and garnet**		
16	2	118-121	22	#11 (117-124)	Paragneiss	**Metassedimentary gneiss with quartz, K-feldspar, biotite, garnet, and tourmaline**		
16	2	123-129	23		Post-deformational granite			
16	2	129-133	24		Paragneiss to Syn- to Tardi deformational granite	*A - Bt Monzogranite; B - Chlorite-Calcite-Sillimanite-Biotite Gneiss;*	16R2-24A	16R2-24b

16	2	136-138	25	#12 (136-144)	Paragneiss	**Banded semipelitic gneiss with quartz, biotite, plagioclase, and K-feldspar**		
16	2	138-141	26	#12 (136-144)	Paragneiss	**Banded semipelitic gneiss with quartz, biotite, plagioclase, and K-feldspar**		
16	2	141-145	27	#12 (136-144)	Paragneiss	**Banded semipelitic gneiss with quartz, biotite, plagioclase, and K-feldspar**		
16	2	145-150	28		Paragneiss			
17	cc	04-11	1	#24	Syn- to tardi-deformational granite	**Granite Pegmatite sigma2**		
17	cc	19-24	2	17RCC-02	Paragneiss	*Ep bearing Plag-Qtz Paragneiss*	17RCC-02A	17RCC-02A
17	cc	24-25	3	#25 & 17RCC-03	Paragneiss	**Fine-grained microsyenite, with some quartz and granite xenoliths. Sericitized groundmass. Secondary thin veins filled with calcite and quartz.**	17RCC-03	n
17	1	57-61	1	#13 (46-52) Abaixo desta	Paragneiss	**Garnet-bearing quartz rich granular gneiss with plagioclase and biotite**		
17	1	63-69	2	#14 (58-63)	Paragneiss	**Metassedimentary gneiss with quartz, K-feldspar, biotite, plagioclase, garnet, and tourmaline**		
17	1	69-72	3		Paragneiss to Syn- to Tardi deformational granite			
17	1	72-75	4		Paragneiss			

17	1	75-78	5		Paragneiss to Syn- to Tardi deformational granite	
17	1	78-81	6	#15 (78-83)	Paragneiss to Syn- to Tardi deformational granite	**Quartz-rich metasedimentary gneiss**
17	1	83-89	7	#15 (78-83)	Paragneiss	**Quartz-rich metasedimentary gneiss**
17	1	93,5-101	8	#16 (93-102)	Paragneiss	**Quartz-rich metassedimentary gneiss**
17	1	101-104	9		Paragneiss	
17	1	104-107	10		Paragneiss	
17	1	107-113	11		Paragneiss	
17	1	113-119	12		Paragneiss	
17	1	119-126	13		?	
17	1	126-132	14		Paragneiss	
17	1	132-136	15		Paragneiss to Syn- to Tardi deformational granite	
17	1	136-139	16		Paragneiss to Syn- to Tardi deformational granite	
17	1	139-141	17		Paragneiss to Syn- to Tardi deformational granite	
17	1	141-149	18		Paragneiss to Syn- to Tardi deformational granite	
17	2	01-06	1		Paragneiss to Syn- to Tardi deformational granite	
17	2	08-10	2	#17 (8-16)	Paragneiss	**Foliated metasedimentary gneiss with garnet**

17	2	10-11	3	#17 (8-16)	Paragneiss	**Foliated metasedimentary gneiss with garnet**		
17	2	11-13	4	#17 (8-16)	Paragneiss	**Foliated metasedimentary gneiss with garnet**		
17	2	26-31	5		Paragneiss			
17	2	33-40	6	#18 (37-45)	Paragneiss	**Foliated semipelitic gneiss with garnet**		
17	2	52-55	7		Paragneiss			
17	2	55-57	8		Paragneiss			
17	2	59-62	9		Paragneiss			
17	2	62-68	10	17R2-10	Paragneiss to Syn- to Tardi deformational granite	*10A - Chlorite-Calcite-Sillimanite-Biotite Gneiss; 10B - Rutile-bearing Biotitite*	17R2-10A	17R2-10B
17	2	73-74	11	#19 (68-71)	Paragneiss	**Foliated semipelitic gneiss with garnet**		
17	2	74-79	12		Paragneiss to Syn- to Tardi deformational granite			
17	2	79-87	13	17R2-13	Paragneiss	*13A - Sillimanite-Garnet-Calcite bearing Biotite-Gneiss; 13B - Garnet-Sillimanite-Calcite bearing Biotite Gneiss*	17R2-13A	17R2-13B
17	2	87-96	14	17R2-14	Paragneiss	*Sillimanite-Calcite-Biotite Gneiss*	17R2-14A	17R2-14B
17	2	96-99	15		Paragneiss			
17	2	99-102	16		Paragneiss			
17	2	102-16	17		Paragneiss			
17	2	106-112	18		Paragneiss to Syn- to Tardi deformational granite			
17	2	112-115	19		Paragneiss			
17	2	115-121	20		Paragneiss			

17	2	121-125	21	#20 (122-129)	Paragneiss	**Foliated semipelitic gneiss**		
17	2	125-128	22	#20 (122-129)	Paragneiss	**Foliated semipelitic gneiss**		
17	2	128-132	23		Paragneiss			
17	2	132-136	24		Paragneiss			
17	2	136-143	25		Paragneiss			
17	2	143-146	26		Paragneiss			
17	2	146-149	27		Paragneiss			
17	3	01-07	1		Paragneiss			
17	3	07-12	2		Paragneiss			
17	3	12-15	3		Paragneiss			
17	3	15-18	4		Paragneiss			
17	3	18-20	5		Paragneiss			
17	3	20-26	6		Paragneiss			
17	3	26-29	7		Paragneiss			
17	3	31-36	8		Syn- to tardi-deformational granite			
17	3	42-50	9		Syn- to tardi-deformational granite			
17	3	50-55	10		Syn- to tardi-deformational granite			
17	3	59-65	11		Syn- to tardi-deformational granite			
17	3	65-72	12	#21 (65-74)	Syn- to tardi-deformational granite	**Granite pegmatite sigma2**		
17	3	75-83	13		Syn- to tardi-deformational granite			
17	3	83-90	14		Syn- to tardi-deformational granite	*A and B - Bt Granite*	17R3-14A	17R3-14B
17	3	90-92	15	#22 (90-100)	Syn- to tardi-deformational granite	**Granite pegmatite sigma2**		
17	3	121-130	16	#23 (107-118) Abaixo desta	Post-deformational granite	**Granite pegmatite sigma2 coarse-grained K-feldspar rich facies**		

17	3	130-141	17	Syn- to tardi-deformational granite

SUPPLEMENTARY MATERIAL 2 – STATISTICAL MODE FROM EACH SAMPLE

Table 4 – Mineral counting per sample

	Quantity															
Sample	Qtz	Kfs	Pl	Grt	Bt	Sil	Ep	Chl	Cal	Tour	Ap	Rut	Zrc	Nat	Op	Total
16R1-10A	165	3	34	0	32	0	0	8	18	28	1	4	1	0	6	300
16R1-10B	194	2	33	9	14	0	0	2	14	23	1	0	3	0	5	300
16R2-01	188	35	14	10	22	0	0	14	13	0	0	0	0	0	4	300
17R2-10A	94	65	9	17	64	13	0	2	22	4	0	4	0	0	6	300
17R2-10B	140	59	8	16	36	9	0	0	24	3	0	1	0	0	4	300
17R2-13A	70	61	9	14	108	10	0	1	18	3	3	2	1	0	0	300
17R2-13B	105	58	7	13	60	26	0	0	22	2	1	3	1	0	2	300
17R2-14A	71	51	11	2	95	20	0	0	35	6	0	4	1	0	4	300
17R2-14B	130	10	30	1	71	9	0	10	25	2	1	0	2	0	9	300
16R2-08A	91	86	10	18	49	10	0	2	25	0	3	1	3	2	0	300
16R2-08B	125	171	14	10	33	12	0	3	22	0	2	1	4	3	0	400
16R1-10A	8	63	6	0	14	0	0	3	4	0	0	0	2	0	0	100
16R2-24A	87	113	41	0	32	0	0	2	5	0	6	0	10	4	0	300
16R2-24B	75	115	43	0	44	0	0	6	0	0	2	0	12	3	0	300
17RCC-01A	25	213	18	0	19	0	0	0	4	0	0	0	17	4	0	300
17RCC-01B	34	206	25	0	17	0	0	0	0	0	0	0	11	7	0	300
17RCC-02	125	41	0	0	12	0	29	15	7	0	0	0	0	16	55	300
17RCC-03	101	27	0	0	8	0	32	33	17	0	0	0	0	9	73	300
16R2-13A	0	0	0	0	245	0	12	16	0	0	0	27	0	0	0	300
16R2-13B	287	0	0	0	0	0	0	0	13	0	0	0	0	0	0	300
17R2-10B	15	0	0	0	236	0	3	10	17	0	0	15	4	0	0	300

	Percentual															Classification
Sample	Qtz	Kfs	Pl	Grt	Bt	Sil	Ep	Chl	Cal	Tour	Ap	Rut	Zrc	Nat	Op	
16R1-10A	55	1	11	0	11	0	0	3	6	9	0	1	0	0	2	Chl-Cal bearing Tour-Gneiss
16R1-10B	65	1	11	3	5	0	0	1	5	8	0	0	1	0	2	Chl-Cal bearing Tour-Gneiss
16R2-01	63	12	5	3	7	0	0	5	4	0	0	0	0	0	1	Grt-Cal-Chl bearing Gneiss
17R2-10A	31	22	3	6	21	4	0	1	7	1	0	1	0	0	2	Tour-Sil bearing Grt-Cal-Gneiss
17R2-10B	47	20	3	5	12	3	0	0	8	1	0	0	0	0	1	Tour-Sil bearing Grt-Cal-Gneiss
17R2-13A	23	20	3	5	36	3	0	0	6	1	1	1	0	0	0	Sil-Grt-Cal bearing Gneiss
17R2-13B	35	19	2	4	20	9	0	0	7	1	0	1	0	0	1	Grt-Sil-Cal bearing Gneiss
17R2-14A	24	17	4	1	32	7	0	0	12	2	0	1	0	0	1	Sil-Cal-Gneiss
17R2-14B	43	3	10	0	24	3	0	3	8	1	0	0	1	0	3	Chl-Sil bearing Cal-Gneiss
16R2-08A	30	29	3	6	16	3	0	1	8	0	1	0	1	1	0	FK-Metagranite
16R2-08B	31	43	4	3	8	3	0	1	6	0	1	0	1	1	0	FK-Metagranite
16R1-10A	8	63	6	0	14	0	0	3	4	0	0	0	2	0	0	Bt Qtz-FK-Syenite
16R2-24A	29	38	14	0	11	0	0	1	2	0	2	0	3	1	0	Bt Syenogranite
16R2-24B	25	38	14	0	15	0	0	2	0	0	1	0	4	1	0	Bt Syenogranite
17RCC-01A	8	71	6	0	6	0	0	0	1	0	0	0	6	1	0	Zrc-Bt Qtz-FK-Syenite
17RCC-01B	11	69	8	0	6	0	0	0	0	0	0	0	4	2	0	Bt Quartzsienite
17RCC-02	42	14	0	0	4	0	10	5	2	0	0	0	0	5	18	Paragneiss
17RCC-03	34	9	0	0	3	0	11	11	6	0	0	0	0	3	24	Paragneiss
16R2-13A	0	0	0	0	82	0	4	5	0	0	0	9	0	0	0	Ep-Chl beating Rut Biotitite
16R2-13B	96	0	0	0	0	0	0	0	4	0	0	0	0	0	0	Cal bearing Quartzite
17R2-10B	5	0	0	0	79	0	1	3	6	0	0	5	1	0	0	Ep bearing Rut-Qtz-Cal Biotitite

SUPPLEMENTARY MATERIAL 3 – COMPARISON BETWEEN PETROLOGICAL INTERPRETATION FROM TARNEY (1977), CHEMALE ET AL. (2008) AND THIS WORK

Table 5 – Comparison between petrological interpretation

Tarney (1977)	Chemale Jr. et al (2008)	This work
Metasedimentary Gneiss	Granulite Paragneiss	Paragneiss
Deformed Pegmatitic Gneiss	Not observed	Pre-deformational Metagranite
Granite Pegmatite T1	Pink granite	Tardi-deformational Granitoid
Granite Pegmatite T2	Post-kinematic pink granite	Post-deformational Granite
Microsyenite Intrusion	Not observed	Paragneiss
Thin Basic Veins	Biotite layer	Melanossome

SUPPLEMENTARY MATERIAL 4 - MICROTECTONICS

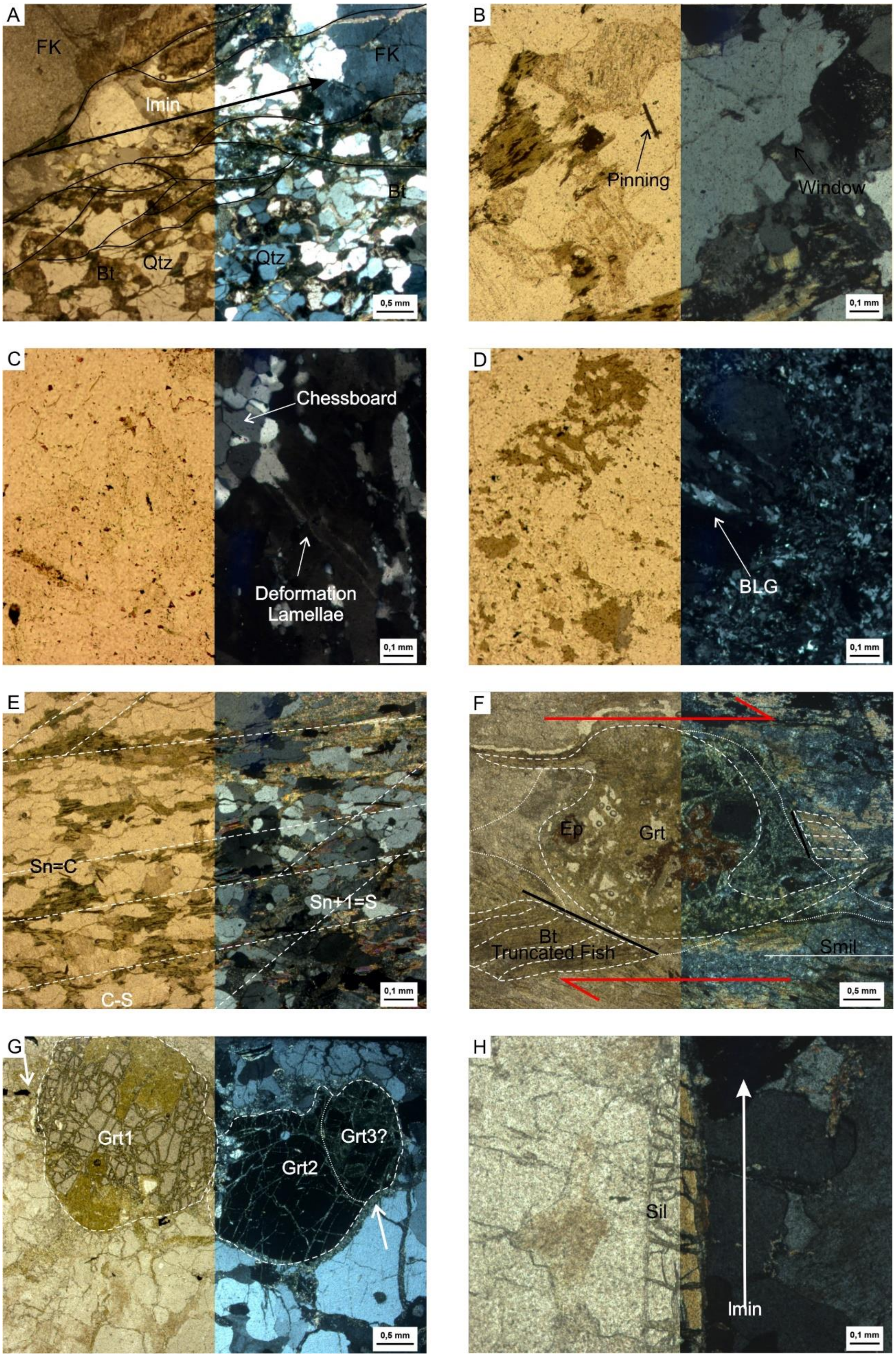

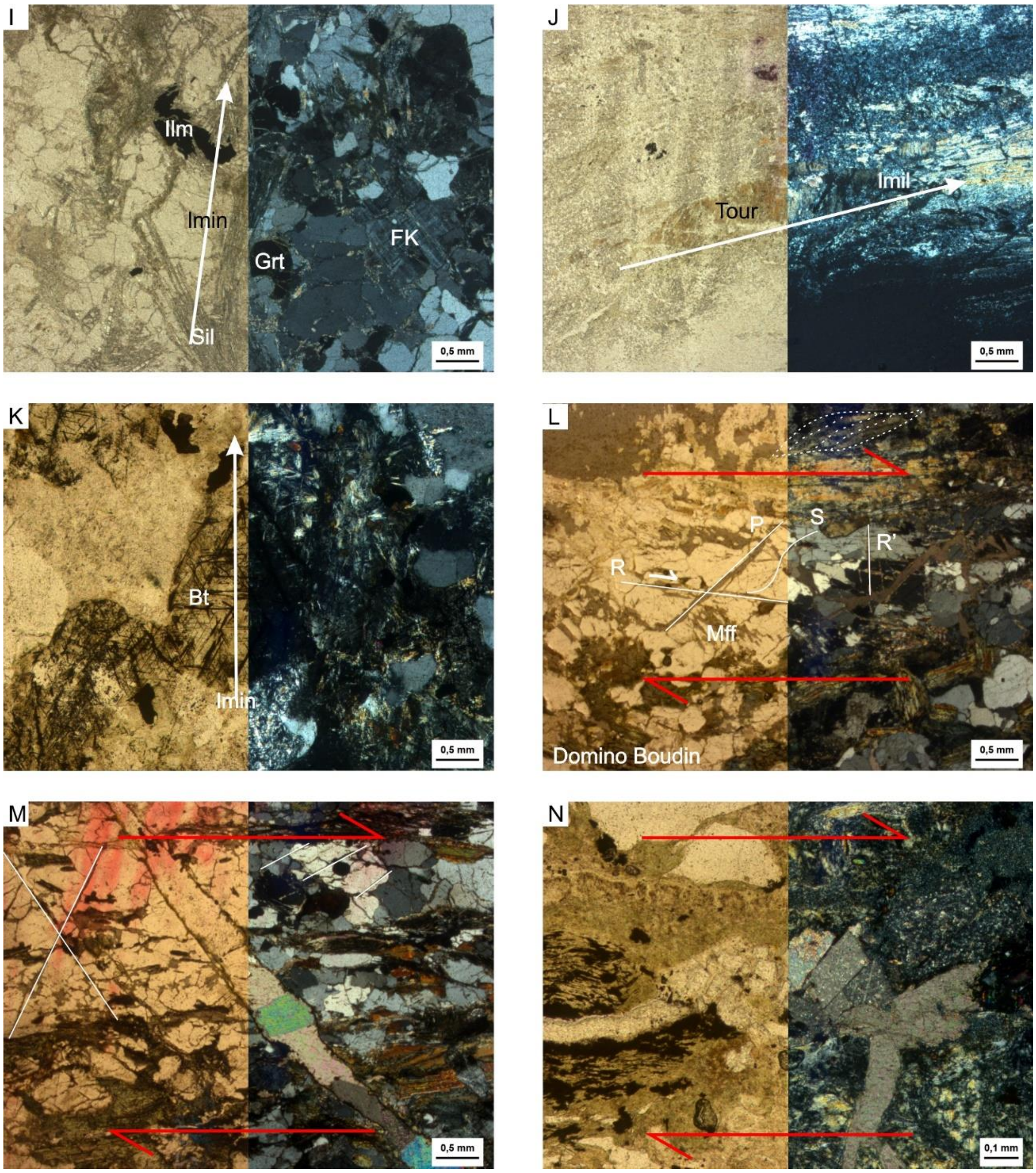

Figure 15 - Main textural and mineral features observed in the studied thin section. **A –** 16R2-10A (0.63-0.67m) Contact between the Syn-to tardi-deformational granitoid and Paragneiss. Note the trachytic texture, according to I_{min}. Also notice the granoblastic texture of quartz in both rocks, demonstrating time spam of static recrystallization. Between the lithological interface, that is, the zone of weakness, it was generated a cataclastic zone with horse-tailing structures. **B –** 17R2-14A (0.87-0.96m) Evidence of dynamic recrystallization – Pinning and window indicative of grain boundary migration (GBM), and therefore high-temperature processes; **C –** 17RCC-03 (0.34-0.35m) – Paragneiss - Chessboard and deformation lamellae microtextures, demonstrating the momentum of overlapping during the first episode of progressive deformation in quartz crystals. The former is indicative of superposing factors such as high temperature, strain rates, differential stresses, and water content in either crystal lattice or grain vs. grain interface. The latter is indicative of a progressive attenuation of those factors. The overlap of those contrasting features suggests processes of retrometamorphism that mitigate the crystal recovery. **D -** 17RCC-03 (0.34-0.35m) – Paragneiss – Bulging (BLG) and undulose quartz extinction. superposing of low-

temperature/low-grade dynamic recrystallization microstructures; **E –** 17R2-14B (0.87-0.96m) – Foliation planes of paragneisses and C-S fabric, suggesting a progressive deformation that after the generation of an S_n plane, it was generated an oblique foliation S_{n+1}, followed by an event of static recrystallization; **F –** 16R2-01B (0.00-0.06m) Weathered Paragneiss generated after the nucleation and homogenisation of garnet. The highly fractured porphyroblast type δ has an eye-shaped pattern, indicative of high strain rates in a destral motion. The presence of truncated biotite fishes also corroborates to a destral movement, with the shearing band near the interface of porphyroblast mantle. **G –** 16R2-08A (0.50-0.56m) - Garnet porphyroblasts amalgamated within the lineation plane. This feature suggests that the Grt crystals superimposed each other, after the homogenization event and during the event of metamorphic climax. Probably, this fabric is related to a transtensional stress regime associated with the R3 episode; **H –** 16R2-08A (0.50-0.56m) Isomorphic bladed sillimanite aligned according to lmin; **I –** 16R2-08A (0.50-0.56m) fibrolite product of reaction Biotite + Garnet = Ilmenite+Fibrolite+Alkali Feldspar+Quartz+Water. Note that the Grt porphyroblast is partially consumed, whilst the Bt is entirely absent. This *in-situ* reaction validates the modeled pseudosection; **J –** 16R2-01B (0.00-0.06m) Idiomorphic Tabular tourmaline porphyroblast related to post-deformational events; **K –** 17R2-14A (0.87-0.96m) Sagenitic texture in Biotite, which represents low-grade metamorphism, typical of medium to superior green-schist facies. **L –** 17R2-13B (0.79-0.87m) Ruptile regime and cataclasis evidence – the presence of Riedel Shear indicator in quartz porphyroclast, suggesting a destral sense motion during ruptile-ductile episodes. Mff - microscopic feather features; **M –** 17R2-13B (0.79-0.87m) Extensional vein en-echelon filled by a tardi calcite mineral, with distinctive pressure twinning, suggesting a destral shear sense. Note in the superior right corner the presence of twin pair, suggesting deformational processes in the supracrustal regime. In the superior left corner, there are antithetical fractures in Qtz crystals, cogenetic with those of “M,” also indicative os destral sense; **N –** 17R2-14A (0.87-0.96m) Bookshelf microtexture in ptygmatic Cal vein, indicating a progressive destral deformation even in tardi-deformational low-temperature processes.

SUPPLEMENTARY MATERIAL 5 – X-RAY DIFFRACTOMETRY (XRD) OF MELANOSOME.

We made x-ray diffractometry (XRD) whole-rock analysis at Instituto de Geociências da Universidade de Brasília (UnB) in sample #16R2-11 to identify whether there is the presence of expansive clays or not. The sample was pulverized and compacted on the glass section. After the XRD analyses were conducted on a Rigaku Ultima IV coupled with DETEX, using Cukα radiation (λ = 1.5418 Å), a Be filter, a voltage of 35 kV, and a current of 15 mA. The scan speed was 2º/min, with steps of 0.05º, and the 2θ interval between 3° and 80°.

The minerals identified using this technique agree with the petrographical description of the melanosome. We interpret the peak in intensity at d=10 and d=3.34 as characteristic of biotite. Rutile is also present, with two distinct peaks at d≈3.3, and d=1.66. These paragenesis fits the sagenitic texture, characteristic of this lithofacies. Additionally, chlorites (i.g. corrensite) were also identified, with two peaks at d=31.49 and d=14.15. Thus, we suggest that the green-mineral pointed out by Tarney (1977) is corrensite. There are two late mineral phases in this lithofacies: i) calcite; ii) kaolinite. Their presence suggests low-temperature processes (Figure 16).

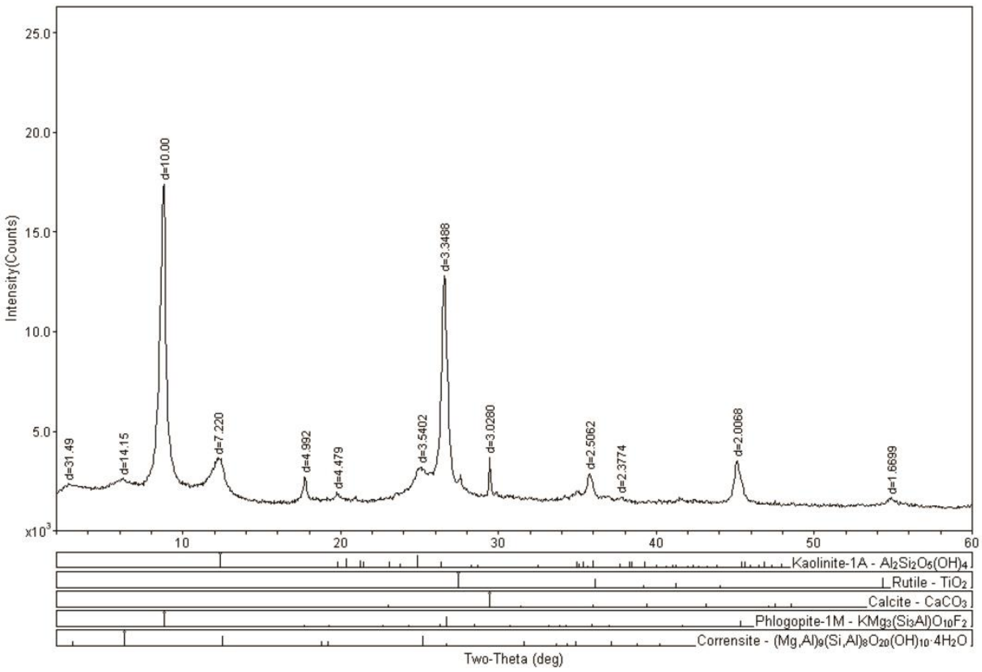

Figure 16 – RX Diffractogram of sample #16R2-11, which consists of melanosome lithofacies.

SUPPLEMENTARY MATERIAL 6 – WHOLE ROCK GEOCHEMISTRY OBTAINED BY TARNEY (1977) AND THIS WORK

Table 6 – Geochemistry from Paragneisse lithofacies. Bold letters refer to data acquired by this work. Samples with asterisc refer to data acquired by Tarney (1977)

Sample	17R1-2*	17R1-6*	17R1-8*	17R2-2*	17R2-6*	17R2-11*	17R2-21*	**17R2-10**	**17R2-13**	**17R2-14**	**16R1-10**	17RCC-3*	**17RCC-3**	**17RCC-2**
Major wt.%	Paragneisse													
SiO2	70.50	80.90	79.70	66.90	61.70	61.00	61.80	70.15	64.19	58.98	76.53	66.30	69.98	70.15
TiO2	1.19	0.82	0.78	1.23	1.13	1.15	1.19	0.59	0.82	0.68	0.88	0.87	0.64	0.72
Al2O3	13.00	7.00	7.10	13.60	15.40	15.20	15.30	11.43	14.37	11.72	7.44	13.30	11.86	12.04
Fe2O3	3.36	2.53	2.77	2.73	4.23	4.60	4.39	n.a.	n.a.	n.a.	n.a.	2.04	n.a.	n.a.
FeO	2.15	1.76	2.00	4.10	3.75	3.60	3.58	n.a.	n.a.	n.a.	n.a.	4.01	n.a.	n.a.
Fe2O3T	n.a.	n.a.	n.a.	n.a.	n.a.	n.a.	n.a.	5.89	6.49	7.61	4.71	n.a.	6.63	5.88
MnO	0.01	0.01	0.01	0.01	0.01	0.01	0.01	0.04	0.02	0.07	0.04	0.01	0.07	0.06
MgO	1.40	0.97	0.92	2.16	1.87	0.28	1.87	1.08	1.56	1.24	0.65	2.18	1.78	1.92
CaO	0.24	0.73	1.21	0.56	0.78	1.65	0.47	1.57	0.99	5.28	2.23	1.01	1.17	1.03
Na2O	0.74	1.75	1.83	1.09	1.13	1.04	1.08	1.88	1.21	1.36	0.92	1.23	1.93	1.66
K2O	4.62	1.50	1.32	4.12	4.59	4.29	5.29	3.62	5.57	3.55	2.97	4.65	3.48	3.85
P2O5	0.05	0.06	0.07	0.09	0.11	0.03	0.11	0.13	0.05	0.30	0.03	0.09	0.09	0.09
H2O	2.48	1.37	1.67	2.81	4.35	4.02	3.83	n.a.	n.a.	n.a.	n.a.	2.89	n.a.	n.a.
CO2	0.10	0.20	0.40	0.20	0.20	0.20	0.20	n.a.	n.a.	n.a.	n.a.	0.80	n.a.	n.a.
LOI	n.a.	n.a.	n.a.	n.a.	n.a.	n.a.	n.a.	3.78	4.38	8.11	4.11	n.a.	2.57	2.44
Total	99.90	99.80	99.90	99.50	98.50	99.00	99.30	100.20	99.64	98.90	100.50	99.50	100.20	99.82
Trace (ppm)														
S	106	98	128	325	95	115	103	n.a.	n.a.	n.a.	n.a.	522	n.a.	n.a.
Cl	180	200	290	160	680	540	720	n.a.	n.a.	n.a.	n.a.	190	n.a.	n.a.
Sc	n.a.	n.a.	n.a.	n.a.	n.a.	n.a.	n.a.	9	14	17	6	n.a.	12	11
Be	n.a.	n.a.	n.a.	n.a.	n.a.	n.a.	n.a.	2	3	2	< 1	n.a.	1	2
V	n.a.	n.a.	n.a.	n.a.	n.a.	n.a.	n.a.	85	112	140	67	n.a.	86	87
Ba	702	562	663	627	709	502	696	475	703	464	374	527	391	439
Sr	51	72	73	60	77	67	78	96	90	114	58	55	76	70
Y	20	20	18	21	28	23	27	28	32	38	24	22	24	20
Zr	230	281	235	206	174	164	163	205	201	194	493	170	244	167

Cr	95	74	61	106	114	103	103	80	100	90	90	80	90	90
Co	n.a.	n.a.	n.a.	n.a.	n.a.	n.a.	n.a.	12	17	18	10	n.a.	19	18
Ni	43	25	27	68	39	38	43	30	50	40	20	46	40	40
Cu	<5	<5	<5	14	95	90	73	70	50	80	20	115	100	70
Zn	111	106	119	164	199	166	176	100	130	120	40	555	200	190
Ga	n.a.	n.a.	n.a.	n.a.	n.a.	n.a.	n.a.	14	19	16	8	n.a.	17	18
Ge	n.a.	n.a.	n.a.	n.a.	n.a.	n.a.	n.a.	2	2	2	1	n.a.	1	1
As	n.a.	n.a.	n.a.	n.a.	n.a.	n.a.	n.a.	< 5	< 5	< 5	< 5	n.a.	< 5	< 5
Rb	159	66	57	127	135	138	158	141	227	153	102	178	161	184
Nb	14	11	13	14	9	10	9	7	10	9	8	16	13	13
Mo	n.a.	n.a.	n.a.	n.a.	n.a.	n.a.	n.a.	< 2	< 2	< 2	< 2	n.a.	2	< 2
Ag	n.a.	n.a.	n.a.	n.a.	n.a.	n.a.	n.a.	0.9	0.9	0.9	2.3	n.a.	1.1	0.5
In	n.a.	n.a.	n.a.	n.a.	n.a.	n.a.	n.a.	< 0.2	< 0.2	< 0.2	< 0.2	n.a.	< 0.2	< 0.2
Sn	n.a.	n.a.	n.a.	n.a.	n.a.	n.a.	n.a.	2	2	1	2	n.a.	2	2
Sb	n.a.	n.a.	n.a.	n.a.	n.a.	n.a.	n.a.	< 0.5	< 0.5	< 0.5	< 0.5	n.a.	< 0.5	< 0.5
Cs	n.a.	n.a.	n.a.	n.a.	n.a.	n.a.	n.a.	5.4	9.3	14.8	2.6	n.a.	1.5	2
La	20	16	19	25	21	22	27	19.8	32.7	30	27.7	28	24	26.3
Ce	32	24	33	44	37	35	49	42.6	66.1	64.7	57.8	50	53.2	55.1
Pr	n.a.	n.a.	n.a.	n.a.	n.a.	n.a.	n.a.	5.09	7.94	7.85	6.9	n.a.	6.32	6.75
Nd	n.a.	n.a.	n.a.	n.a.	n.a.	n.a.	n.a.	20.2	31.6	30.8	26.4	n.a.	24.5	25.1
Sm	n.a.	n.a.	n.a.	n.a.	n.a.	n.a.	n.a.	4.6	6.8	7	5.5	n.a.	5.6	5.9
Eu	n.a.	n.a.	n.a.	n.a.	n.a.	n.a.	n.a.	1.24	1.43	1.72	1.02	n.a.	0.8	0.89
Gd	n.a.	n.a.	n.a.	n.a.	n.a.	n.a.	n.a.	5.1	6.6	8	5.1	n.a.	5.4	5.2
Tb	n.a.	n.a.	n.a.	n.a.	n.a.	n.a.	n.a.	0.9	1.1	1.3	0.8	n.a.	0.9	0.8
Dy	n.a.	n.a.	n.a.	n.a.	n.a.	n.a.	n.a.	5.4	6.6	8.3	4.9	n.a.	4.7	4.3
Ho	n.a.	n.a.	n.a.	n.a.	n.a.	n.a.	n.a.	1.1	1.3	1.6	1	n.a.	0.9	0.8
Er	n.a.	n.a.	n.a.	n.a.	n.a.	n.a.	n.a.	3.2	3.7	4.8	2.9	n.a.	2.7	2.5
Tm	n.a.	n.a.	n.a.	n.a.	n.a.	n.a.	n.a.	0.48	0.55	0.73	0.46	n.a.	0.39	0.38
Yb	n.a.	n.a.	n.a.	n.a.	n.a.	n.a.	n.a.	3.2	3.5	5.3	3.4	n.a.	2.6	2.6
Lu	n.a.	n.a.	n.a.	n.a.	n.a.	n.a.	n.a.	0.48	0.54	0.82	0.54	n.a.	0.43	0.37
Hf	n.a.	n.a.	n.a.	n.a.	n.a.	n.a.	n.a.	4.2	4.5	4.2	10	n.a.	5.4	4
Ta	n.a.	n.a.	n.a.	n.a.	n.a.	n.a.	n.a.	0.5	0.7	0.7	0.7	n.a.	0.9	1
W	n.a.	n.a.	n.a.	n.a.	n.a.	n.a.	n.a.	6	3	5	7	n.a.	10	< 1
Tl	n.a.	n.a.	n.a.	n.a.	n.a.	n.a.	n.a.	0.9	1.3	1	0.6	n.a.	1.2	1.2
Pb	29	13	11	34	45	24	37	19	24	17	8	33	20	19
Bi	n.a.	n.a.	n.a.	n.a.	n.a.	n.a.	n.a.	< 0.4	< 0.4	< 0.4	< 0.4	n.a.	< 0.4	< 0.4
Th	8	8	6	9	6	6	6	6.1	9.7	9	8.9	12	20.5	10.9
U	n.a.	n.a.	n.a.	n.a.	n.a.	n.a.	n.a.	3.8	4.6	5.9	3.5	n.a.	5.8	4.2

Table 7 - – Geochemistry from Weathered Paragneisse lithofacies. Bold letters refer to data acquired by this work. Samples with asterisc refer to data acquired by Tarney (1977)

Sample	16R1-0*	16R1-2*	16R1-8*	16R1-13*	16R1-23*	16R2-14*	16R2-21*	16R2-22*	16R2-25*	17R1-0*
Major wt. %	Weathered Paragneisses									
SiO2	67.10	71.20	79.60	78.90	70.90	63.40	59.80	58.00	64.60	81.30
TiO2	0.76	0.68	0.92	1.25	0.89	1.16	1.27	1.31	1.21	0.88
Al2O3	7.30	6.00	6.60	6.40	9.10	13.70	15.30	18.70	13.70	7.00
Fe2O3	1.70	2.36	2.65	3.71	4.48	5.42	5.87	4.56	4.58	2.67
FeO	1.54	1.36	0.68	2.37	2.26	3.74	3.53	3.62	3.46	1.38
Fe2O3T	n.a.	n.a.	n.a.	n.a.	n.a.	n.a.	n.a.	n.a.	n.a.	n.a.
MnO	0.15	0.16	0.11	0.12	0.12	0.11	0.12	0.11	0.12	0.12
MgO	0.65	0.59	0.69	0.96	1.20	1.85	1.76	1.59	1.66	0.80
CaO	9.55	8.62	2.32	0.98	2.16	0.83	1.34	0.32	0.80	0.62
Na2O	0.83	0.60	1.02	0.85	1.29	0.86	1.41	0.78	1.56	2.02
K2O	2.35	2.24	2.72	2.15	3.32	3.74	4.08	6.58	3.73	1.23
P2O5	0.04	0.01	0.34	0.01	0.03	0.01	0.38	0.11	0.07	0.06
H2O	1.97	1.82	1.69	2.65	3.15	4.23	4.12	3.76	3.43	1.60
CO2	5.94	4.70	1.00	0.40	0.90	0.60	0.70	0.10	0.27	0.10
LOI	n.a.	n.a.	n.a.	n.a.	n.a.	n.a.	n.a.	n.a.	n.a.	n.a.
Total	99.80	100.30	100.30	100.70	99.80	99.60	99.70	99.50	99.20	99.80
Trace (ppm)										
S	129	193	108	158	115	67	86	79	121	103
Cl	570	490	260	360	750	470	730	350	390	410
Sc	n.a.	n.a.	n.a.	n.a.	n.a.	n.a.	n.a.	n.a.	n.a.	n.a.
Be	n.a.	n.a.	n.a.	n.a.	n.a.	n.a.	n.a.	n.a.	n.a.	n.a.
V	n.a.	n.a.	n.a.	n.a.	n.a.	n.a.	n.a.	n.a.	n.a.	n.a.
Ba	306	421	574	608	518	354	489	688	527	574
Sr	67	64	62	42	63	47	85	73	78	66
Y	30	31	46	19	21	17	56	27	28	22
Zr	256	271	428	549	336	172	195	179	189	335
Cr	68	66	77	117	61	106	101	113	91	71
Co	n.a.	n.a.	n.a.	n.a.	n.a.	n.a.	n.a.	n.a.	n.a.	n.a.
Ni	30	31	24	28	39	55	56	49	91	29

Cu	115	180	<5	20	19	36	<5	<5	8	<5
Zn	54	56	39	72	80	137	119	141	138	86
Ga	n.a.	n.a.	n.a.	n.a.	n.a.	n.a.	n.a.	n.a.	n.a.	n.a.
Ge	n.a.	n.a.	n.a.	n.a.	n.a.	n.a.	n.a.	n.a.	n.a.	n.a.
As	n.a.	n.a.	n.a.	n.a.	n.a.	n.a.	n.a.	n.a.	n.a.	n.a.
Rb	56	57	96	68	93	127	119	189	118	53
Nb	7	8	11	14	11	18	14	11	12	14
Mo	n.a.	n.a.	n.a.	n.a.	n.a.	n.a.	n.a.	n.a.	n.a.	n.a.
Ag	n.a.	n.a.	n.a.	n.a.	n.a.	n.a.	n.a.	n.a.	n.a.	n.a.
In	n.a.	n.a.	n.a.	n.a.	n.a.	n.a.	n.a.	n.a.	n.a.	n.a.
Sn	n.a.	n.a.	n.a.	n.a.	n.a.	n.a.	n.a.	n.a.	n.a.	n.a.
Sb	n.a.	n.a.	n.a.	n.a.	n.a.	n.a.	n.a.	n.a.	n.a.	n.a.
Cs	n.a.	n.a.	n.a.	n.a.	n.a.	n.a.	n.a.	n.a.	n.a.	n.a.
La	13	14	20	20	35	21	51	33	30	15
Ce	26	35	46	35	59	38	98	57	54	33
Pr	n.a.	n.a.	n.a.	n.a.	n.a.	n.a.	n.a.	n.a.	n.a.	n.a.
Nd	n.a.	n.a.	n.a.	n.a.	n.a.	n.a.	n.a.	n.a.	n.a.	n.a.
Sm	n.a.	n.a.	n.a.	n.a.	n.a.	n.a.	n.a.	n.a.	n.a.	n.a.
Eu	n.a.	n.a.	n.a.	n.a.	n.a.	n.a.	n.a.	n.a.	n.a.	n.a.
Gd	n.a.	n.a.	n.a.	n.a.	n.a.	n.a.	n.a.	n.a.	n.a.	n.a.
Tb	n.a.	n.a.	n.a.	n.a.	n.a.	n.a.	n.a.	n.a.	n.a.	n.a.
Dy	n.a.	n.a.	n.a.	n.a.	n.a.	n.a.	n.a.	n.a.	n.a.	n.a.
Ho	n.a.	n.a.	n.a.	n.a.	n.a.	n.a.	n.a.	n.a.	n.a.	n.a.
Er	n.a.	n.a.	n.a.	n.a.	n.a.	n.a.	n.a.	n.a.	n.a.	n.a.
Tm	n.a.	n.a.	n.a.	n.a.	n.a.	n.a.	n.a.	n.a.	n.a.	n.a.
Yb	n.a.	n.a.	n.a.	n.a.	n.a.	n.a.	n.a.	n.a.	n.a.	n.a.
Lu	n.a.	n.a.	n.a.	n.a.	n.a.	n.a.	n.a.	n.a.	n.a.	n.a.
Hf	n.a.	n.a.	n.a.	n.a.	n.a.	n.a.	n.a.	n.a.	n.a.	n.a.
Ta	n.a.	n.a.	n.a.	n.a.	n.a.	n.a.	n.a.	n.a.	n.a.	n.a.
W	n.a.	n.a.	n.a.	n.a.	n.a.	n.a.	n.a.	n.a.	n.a.	n.a.
Tl	n.a.	n.a.	n.a.	n.a.	n.a.	n.a.	n.a.	n.a.	n.a.	n.a.
Pb	11	7	8	9	19	14	15	32	17	7
Bi	n.a.	n.a.	n.a.	n.a.	n.a.	n.a.	n.a.	n.a.	n.a.	n.a.
Th	5	5	9	11	24	11	7	9	7	7
U	n.a.	n.a.	n.a.	n.a.	n.a.	n.a.	n.a.	n.a.	n.a.	n.a.

Table 8 - Geochemistry from Pre-, syn- to tardi-, and post-deformational granitoid lithofacies. Bold letters refer to data acquired by this work. Samples with asterisc refer to data acquired by Tarney (1977)

Sample	16R2-8*	**16R2-08**	16R1-4*	17R3-12*	17R3-15*	17RCC-1*	**17R3-14**	**17RCC-1**	**17R3-12**	**17R3-09**	**17R3-14**	17R3-16*	16R2-18	**16R2-07**
Major wt. %	Pre-deformational Metagranite		Syn- to tardi-deformational Granite									Post-deformational Granite		
SiO_2	70.10	71.88	66.30	71.60	71.50	73.90	70.85	72.28	71.63	72.77	71.61	63.00	71.17	84.43
TiO_2	0.08	0.09	0.02	0.14	0.19	0.35	0.22	0.19	0.15	0.16	0.21	0.01	0.33	0.01
Al_2O_3	14.30	12.98	12.30	15.40	15.60	13.30	13.37	13.41	14.00	13.81	14.58	21.60	12.76	7.05
Fe_2O_3	2.03	n.a.	0.95	0.66	0.86	1.37	n.a.	n.a.	n.a.	n.a.	n.a.	0.10	n.a.	n.a.
FeO	2.42	n.a.	0.03	0.02	0.10	0.22	n.a.	n.a.	n.a.	n.a.	n.a.	0.05	n.a.	n.a.
Fe_2O_3T	n.a.	4.80	n.a.	n.a.	n.a.	n.a.	1.98	1.67	1.93	0.96	1.35	n.a.	2.92	0.49
MnO	0.12	0.05	0.12	0.01	0.01	0.01	0.02	0.02	0.01	0.00	0.01	0.01	0.02	0.01
MgO	0.48	0.44	0.19	0.28	0.39	0.54	0.36	0.42	0.31	0.30	0.37	0.04	0.38	0.07
CaO	0.52	0.31	6.72	0.67	0.44	0.32	1.00	0.58	0.51	0.27	0.34	0.73	0.77	0.51
Na_2O	0.96	1.34	1.37	2.27	2.70	2.29	2.28	2.58	2.53	1.99	2.16	2.14	1.20	1.07
K_2O	5.92	5.65	6.68	7.77	6.72	6.42	7.54	7.08	7.38	8.30	8.61	10.94	7.66	4.39
P_2O_5	0.30	0.14	0.06	0.13	0.13	0.12	0.16	0.18	0.16	0.18	0.17	0.15	0.05	0.08
H_2O	2.20	n.a.	0.90	0.72	0.79	0.79	n.a.	n.a.	n.a.	n.a.	n.a.	0.46	n.a.	n.a.
CO_2	0.20	n.a.	4.50	0.10	0.10	0.10	n.a.	n.a.	n.a.	n.a.	n.a.	0.10	n.a.	n.a.
LOI	n.a.	1.96	n.a.	n.a.	n.a.	n.a.	1.33	0.84	0.71	0.60	0.66	n.a.	1.49	0.53
Total	99.60	99.63	100.10	99.80	99.60	99.80	99.11	99.26	99.32	99.34	100.10	99.40	98.76	98.65
Trace (ppm)														
S	64	n.a.	395	117	87	90	n.a.	n.a.	n.a.	n.a.	n.a.	72	n.a.	n.a.
Cl	290	n.a.	260	390	340	400	n.a.	n.a.	n.a.	n.a.	n.a.	440	n.a.	n.a.
Sc	n.a.	7	n.a.	n.a.	n.a.	n.a.	< 1	2	< 1	< 1	< 1	n.a.	3	< 1
Be	n.a.	< 1	n.a.	n.a.	n.a.	n.a.	< 1	< 1	< 1	< 1	< 1	n.a.	< 1	< 1
V	n.a.	9	n.a.	n.a.	n.a.	n.a.	7	14	8	8	8	n.a.	26	< 5
Ba	641	564	594	599	558	627	480	455	469	515	569	610	563	405
Sr	83	87	125	104	113	96	96	106	108	100	108	126	101	60
Y	29	22	21	7	5	6	6	7	6	4	4	5	7	4
Zr	72	90	11	85	99	103	99	114	99	29	75	8	43	5
Cr	13	20	17	10	1	90	< 20	20	30	20	30	9	40	30
Co	n.a.	6	n.a.	n.a.	n.a.	n.a.	3	4	4	3	3	n.a.	6	< 1

Ni	18	< 20	8	<2	4	2	< 20	< 20	< 20	< 20	< 20	<2	< 20	< 20
Cu	5	10	1400	<5	<5	<5	< 10	10	< 10	< 10	< 10	<5	20	< 10
Zn	32	< 30	29	28	32	72	< 30	< 30	40	30	30	6	< 30	< 30
Ga	n.a.	18	n.a.	n.a.	n.a.	n.a.	15	13	16	16	16	n.a.	14	6
Ge	n.a.	2	n.a.	n.a.	n.a.	n.a.	< 1	< 1	1	< 1	1	n.a.	1	1
As	n.a.	< 5	n.a.	n.a.	n.a.	n.a.	< 5	< 5	< 5	< 5	< 5	n.a.	< 5	< 5
Rb	161	189	214	252	229	201	244	230	257	279	274	331	234	151
Nb	2	1	2	3	3	5	4	3	2	2	4	2	4	< 1
Mo	n.a.	< 2	n.a.	n.a.	n.a.	n.a.	< 2	< 2	< 2	< 2	< 2	n.a.	< 2	< 2
Ag	n.a.	< 0.5	n.a.	n.a.	n.a.	n.a.	< 0.5	< 0.5	< 0.5	< 0.5	< 0.5	n.a.	< 0.5	< 0.5
In	n.a.	< 0.2	n.a.	n.a.	n.a.	n.a.	< 0.2	< 0.2	< 0.2	< 0.2	< 0.2	n.a.	< 0.2	< 0.2
Sn	n.a.	1	n.a.	n.a.	n.a.	n.a.	2	2	2	1	3	n.a.	1	< 1
Sb	n.a.	< 0.5	n.a.	n.a.	n.a.	n.a.	< 0.5	< 0.5	< 0.5	< 0.5	< 0.5	n.a.	< 0.5	< 0.5
Cs	n.a.	6.7	n.a.	n.a.	n.a.	n.a.	1.5	1.3	1.7	1.9	1.8	n.a.	2.6	0.9
La	10	21.1	6	13	11	22	25.8	22	29.3	15.8	27.4	2	17.4	5.8
Ce	20	43.4	12	24	24	42	55.2	48.2	64.1	33.5	59	4	31.1	11.5
Pr	n.a.	5.04	n.a.	n.a.	n.a.	n.a.	6.52	5.77	7.81	4.09	7.18	n.a.	4.04	1.39
Nd	n.a.	17.7	n.a.	n.a.	n.a.	n.a.	23.6	22	27.9	14.7	25.5	n.a.	15.1	4.8
Sm	n.a.	4.2	n.a.	n.a.	n.a.	n.a.	6.1	5.8	7.2	3.9	7.1	n.a.	3.4	1.3
Eu	n.a.	0.86	n.a.	n.a.	n.a.	n.a.	1.02	1.06	1.05	1	1.2	n.a.	1.07	0.42
Gd	n.a.	4.2	n.a.	n.a.	n.a.	n.a.	5.2	5.1	5.8	3.1	5.7	n.a.	2.9	1
Tb	n.a.	0.7	n.a.	n.a.	n.a.	n.a.	0.6	0.5	0.7	0.3	0.6	n.a.	0.4	0.1
Dy	n.a.	3.9	n.a.	n.a.	n.a.	n.a.	2.1	1.8	2.1	1.1	2	n.a.	2	0.5
Ho	n.a.	0.8	n.a.	n.a.	n.a.	n.a.	0.2	0.2	0.2	0.1	0.2	n.a.	0.3	< 0.1
Er	n.a.	2.3	n.a.	n.a.	n.a.	n.a.	0.5	0.4	0.4	0.2	0.3	n.a.	0.8	0.2
Tm	n.a.	0.42	n.a.	n.a.	n.a.	n.a.	0.06	0.05	< 0.05	< 0.05	< 0.05	n.a.	0.14	< 0.05
Yb	n.a.	3	n.a.	n.a.	n.a.	n.a.	0.3	0.4	0.3	0.1	0.2	n.a.	0.9	0.2
Lu	n.a.	0.52	n.a.	n.a.	n.a.	n.a.	0.06	< 0.01	< 0.01	< 0.01	< 0.01	n.a.	0.13	< 0.01
Hf	n.a.	2.4	n.a.	n.a.	n.a.	n.a.	2.3	3	2.4	0.7	2.8	n.a.	1.2	0.2
Ta	n.a.	< 0.1	n.a.	n.a.	n.a.	n.a.	0.2	0.2	0.1	0.9	0.2	n.a.	0.3	< 0.1
W	n.a.	3	n.a.	n.a.	n.a.	n.a.	3	2	< 1	< 1	< 1	n.a.	< 1	< 1
Tl	n.a.	1.3	n.a.	n.a.	n.a.	n.a.	1.7	1.7	1.7	1.9	2.1	n.a.	1.2	0.6
Pb	49	27	36	76	69	66	39	40	51	50	57	108	39	14
Bi	n.a.	< 0.4	n.a.	n.a.	n.a.	n.a.	< 0.4	< 0.4	< 0.4	< 0.4	< 0.4	n.a.	< 0.4	< 0.4
Th	6	14.8	1	9	11	17	12.9	10	18.1	9.4	15.7	1	8.4	2.1
U	n.a.	6.7	n.a.	n.a.	n.a.	n.a.	3.5	4.2	4.3	2.5	3.7	n.a.	1.4	0.3

Table 9 - Geochemistry from Melanossome lithofacies. Bold letters refer to data acquired by this work. Samples with asterisc refer to data acquired by Tarney (1977)

Sample	16R2-1*	**16R2-1**
Major wt.%	Melanossome	
SiO2	43.30	39.15
TiO2	2.41	2.21
Al2O3	20.40	22.03
Fe2O3	6.82	n.a.
FeO	7.84	n.a.
Fe2O3T	n.a.	17.05
MnO	0.13	0.04
MgO	2.28	2.97
CaO	1.06	0.29
Na2O	0.38	0.54
K2O	6.91	5.14
P2O5	0.01	0.04
H2O	7.58	n.a.
CO2	0.70	n.a.
LOI	n.a.	9.11
Total	99.80	98.56
Trace (ppm)		
S	31	n.a.
Cl	690	n.a.
Sc	n.a.	25
Be	n.a.	6
V	n.a.	275
Ba	698	695
Sr	44	81
Y	30	47

Zr	323	574
Cr	223	220
Co	n.a.	46
Ni	87	110
Cu	12	30
Zn	163	190
Ga	n.a.	49
Ge	n.a.	4
As	n.a.	< 5
Rb	214	306
Nb	26	44
Mo	n.a.	< 2
Ag	n.a.	2.7
In	n.a.	< 0.2
Sn	n.a.	2
Sb	n.a.	< 0.5
Cs	n.a.	17.6
La	28	100
Ce	56	213
Pr	n.a.	25.7
Nd	n.a.	99.8
Sm	n.a.	22.6
Eu	n.a.	1.09
Gd	n.a.	20.7
Tb	n.a.	2.7
Dy	n.a.	12.2
Ho	n.a.	2
Er	n.a.	5.1
Tm	n.a.	0.71
Yb	n.a.	4.7
Lu	n.a.	0.71
Hf	n.a.	13.6

Ta	n.a.	2.2
W	n.a.	< 1
Tl	n.a.	1.4
Pb	13	13
Bi	n.a.	< 0.4
Th	14	29.8
U	n.a.	17

SUPPLEMENTARY MATERIAL 7 – CHLORITE CHEMICAL DATA

Table 10 – Chlorite mineral analyses

	Paragneiss n= 12			Weathered Paragneiss n=4			Pre-deformational metagranitoid n=5		
wt. %	x̄	σ	CI (2σ)	x̄	σ	CI (2σ)	x̄	σ	CI (2σ)
SiO_2	25.61	0.59	0.38	36.16	1.71	2.72	30.62	1.14	1.42
TiO_2	0.03	0.02	0.01	0.03	0.03	0.05	0.01	0.01	0.02
Al_2O_3	18.42	0.50	0.32	19.42	3.08	4.90	15.96	0.42	0.52
V_2O_3	0.08	0.03	0.02	0.01	0.01	0.02	0.03	0.01	0.01
Cr_2O_3	0.06	0.06	0.04	0.01	0.02	0.04	0.07	0.04	0.05
FeO	32.65	2.26	1.44	33.45	0.43	0.68	37.19	0.75	0.93
MnO	8.76	1.53	0.97	0.84	0.46	0.74	0.03	0.01	0.02
MgO	0.25	0.06	0.04	4.74	0.99	1.57	2.04	0.06	0.08
Na_2O	0.01	0.01	0.01	0.05	0.07	0.11	0.06	0.02	0.02
K2O	0.05	0.03	0.02	0.21	0.34	0.55	0.53	0.09	0.11
F	0.02	0.02	0.01	0.02	0.02	0.04	0.00	0.01	0.01
O=Cl	0.00	0.00	0.00	0.00	0.00	0.00	0.00	0.00	N.A.
Total	83.58	0.86	0.55	93.00	5.83	9.28	84.00	1.10	1.36
H_2O	9.93	0.14	0.09	11.98	0.86	1.36	10.36	0.23	0.28
apfu									
Si	3.04	0.07	0.04	3.59	0.10	0.16	3.50	0.08	0.10
Ti	0.00	0.00	N.A.	0.00	0.00	N.A	0.00	0.00	N.A
Al	2.54	0.07	0.04	2.23	0.20	0.32	2.10	0.05	0.06
Fe^{2+}	3.25	0.25	0.16	2.80	0.21	0.34	3.55	0.14	0.18
Mn	0.86	0.14	0.09	0.06	0.04	0.06	0.00	0.00	N.A
Mg	0.00	0.00	N.A.	0.63	0.09	0.14	0.31	0.07	0.09
F	0.00	0.00	N.A.	0.00	0.00	N.A	0.00	0.00	N.A
Cl	0.00	0.00	N.A.	0.00	0.00	N.A	0.00	0.00	N.A
OH	8.00	0.00	N.A.	8.00	0.00	N.A	8.00	0.00	N.A
Tetrahedral									
Si	3.04	0.07	0.04	3.59	0.10	0.16	3.50	0.08	0.10

Al_{IV}	0.96	0.07	0.04	0.41	0.10	0.16	0.50	0.08	0.10
Total Tetrahedral	4.00	0.00	N.A.	4.00	0.00	N.A	4.00	0.00	N.A.
Octahedral									
Al_{VI}	1.58	0.07	0.04	1.81	0.10	0.16	1.60	0.08	0.10
Fe^{2+}	3.25	0.25	0.16	2.80	0.21	0.34	3.55	0.14	0.18
Mn	0.86	0.14	0.09	0.06	0.04	0.06	0.00	0.00	N.A
Mg	0.00	0.00	N.A.	0.63	0.09	0.14	0.31	0.07	0.09
Total Octahedral	5.69	0.06	0.04	5.30	0.00	0.01	5.45	0.08	0.10
Octahedral vacant	0.31	0.06	0.04	0.70	0.00	0.01	0.55	0.08	0.10
OH	8.00	0.00	N.A.	8.00	0.00	N.A	8.00	0.00	N.A

SUPPLEMENTARY MATERIAL 8 – TOURMALINE CHEMICAL DATA

Tourmaline group minerals were analyzed using the software WinTCal (Yavuz et al., 2014). They were normalized to have either 15 cations at T + Z + Y position or the sum of OH + F + Cl=4. The Fe^{3+} content was estimated according to the normalization to $O_{24.5}$ and stoichiometric calculation of H_2O content made on software.

All crystals fit the alkaline tourmaline zone with two distinctive populations (hydroxy- and fluor). They have a significant amount of $^{Y}Mg^{2+}$ in comparison with other elements that can fit Y-site. Also, there is an exotism of the allocated element in the X-site (i.g. K^{1+}). According to Henry et al. (2011) classification scheme they are classified as Potassium Rich (Fluor)-Dravites (Figure 17).

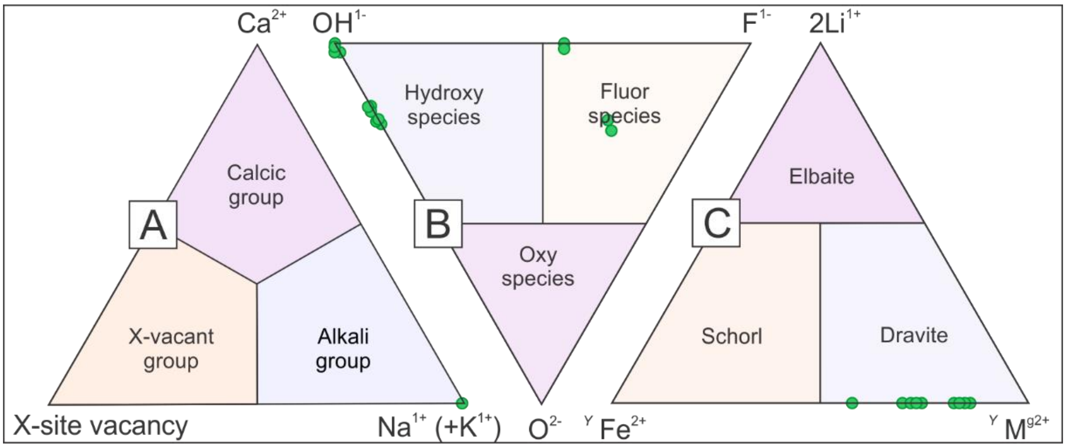

Figure 17 - Tourmaline classification according to Henry et al. (2011). A – Ternary diagram of Tourmaline Primary Group, according to the element that fits the X-site vacancy. Note that K1+ occupies the vacancy, instead of Na1+. B – Ternary diagram of tourmaline species, according to the element that fits the W-site vacancy. Note two distinct populations: OH1- rich near the crystal center, and F1- near the crystal rim. C- Ternary diagram of alkali elements that fit the Y-site. Note that the analyses have a trend from Mg-rich nucleus to Fe-rich borders.

A variety of environments can generate tourmalines. The tourmaline crystals have a wide stability range using PT, fluid composition, and whole rock composition (van Hinsberg et al., 2011). Here, we interpret the tourmaline as generated during the post-kinematic event (e.g., the post-kinematic blade shape of its crystals). Additionally, it is identifiable that the tourmaline has a metamorphic origin; thereby, being related to metapelites, Ca-poor metapelites, and metapsamites (Figure 18 - A e B). There is no relationship with the tourmalines and greisenization processes or contact metamorphism (Figure 19 - C). Thus, the tourmalines were generated by tardi-fluid-rich metamorphism. This data suggests that, by the time of tourmaline generation, the metamorphism generated the granitogenesis, not the opposite.

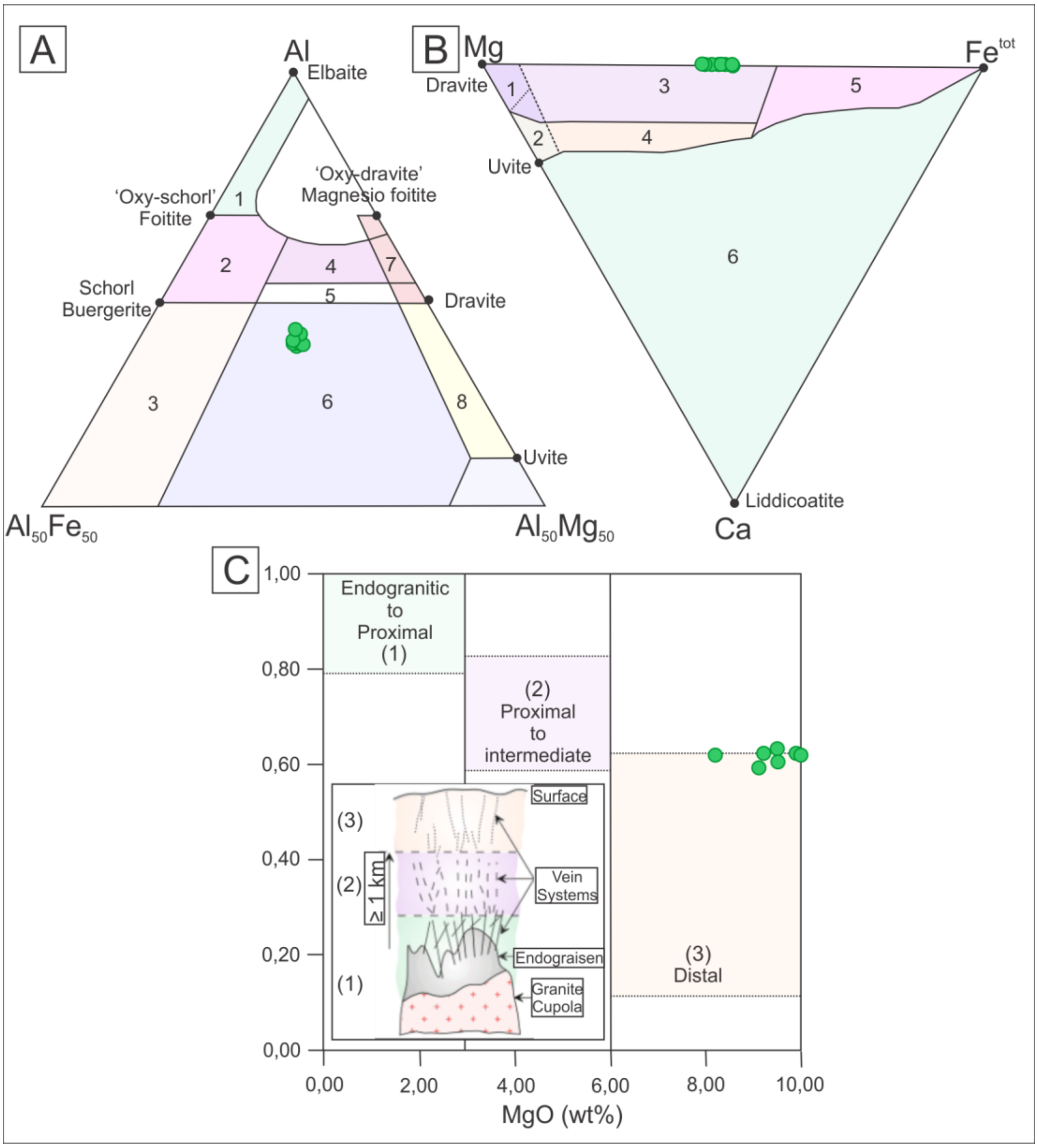

Figure 18 - Tourmaline classification. A and B) Ternary diagrams proposed by Henry and Guidotti (1985) to predict the geotectonic environment in which the tourmaline were generated. Legend: A) 1–Li-rich granitoid pegmatites and aplites; 2–Li-poor granitoids and their associated pegmatites and aplites; 3–Ferric iron-rich quartz-tourmaline rocks (hydrothermally altered granites); 4–Metapelites and metapsammites coexisting with an Al-saturating phase; 5–Metapelites and metapsammites not coexisting with an Al-saturating phase; *6–Ferric iron-rich quartz-tourmaline rocks, calc-silicate rocks, and metapelites;* 7–Low-Ca meta ultramafics and Cr, V-rich metasediments; B) 1-Li-rich granitoid pegmatites and aplites; 2-Li-poor granitoids and associated pegmatites and aplites; *3-Ca-rich metapelites, metapsammites, and calc-silicate rocks.* 4-Ca-poor metapelites, metapsammites, and quartz-tourmaline rocks; 5-Metacarbonates; 6-Metaultramafics. C) Binary diagram proposed by Pirajno and Smithies (1992) to estimate the proximity with a granitic source, based on major elements. Modified from Yavuz et al. (2014).

Cited references:

Henry, D.J., Guidotti, C.V., 1985. Tourmaline as a petrogenetic indicator mineral: an example from the staurolite-grade metapelites of NW Maine. Am. Mineral. 70, 1–15.

Henry, D.J., Novak, M., Hawthorne, F.C., Ertl, A., Dutrow, B.L., Uher, P., Pezzotta, F., 2011. Nomenclature of the tourmaline-supergroup minerals. Am. Mineral. 96, 895–913. https://doi.org/10.2138/am.2011.3636

Pirajno, F., Smithies, R.H., 1992. The FeO/(FeO+MgO) ratio of tourmaline: A useful indicator of spatial variations in granite-related hydrothermal mineral deposits. J. Geochem. Explor. 42, 371–381. https://doi.org/10.1016/0375-6742(92)90033-5

van Hinsberg, V.J., Henry, D.J., Marschall, H.R., 2011. Tourmaline: an ideal indicator of its host environment. Can. Mineral. 49, 1–16. https://doi.org/10.3749/canmin.49.1.1

Yavuz, F., Karakaya, N., Yıldırım, D.K., Karakaya, M.Ç., Kumral, M., 2014. A Windows program for calculation and classification of tourmaline-supergroup (IMA-2011). Comput. Geosci. 63, 70–87. https://doi.org/10.1016/j.cageo.2013.10.012

Table 11 – Tourmaline mineral analyses

	SiO2	TiO2	Al2O3	V2O3	Cr2O3	FeO	MnO	MgO	CaO	Na2O	K2O	F	H2O	B2O3	F	Total
Weight Percent	36,738	3,49	19,28	0,174	0	15	0.022	9.5040	0.08	0,374	8,812	0,904	3.245	9.938	0	102.183
	36,526	3,912	19,222	0,194	0	15	0.064	9.2070	0.229	0,28	9,004	0,781	3.453	10.035	0	104.488
	36,116	4,286	18,359	0,202	0,009	16.29	0.03	9.4850	0.033	0,311	9,05	0,933	3.461	10.083	0	105.544
	35,878	4,105	17,891	0,202	0	16	0.067	9.9220	0.043	0,328	9,221	0,823	3.417	9.83	0	103.248
	35,85	3,834	17,956	0,198	0,032	16	0.058	9.9780	0.087	0,343	8,978	0,999	3.211	9.743	0	100.954
	35,908	3,739	18,168	0,193	0,036	16.33	0.077	10.4040	0,044	0,354	9,308	1,044	2.981	10.052	0.421	104.613
	36,209	3,569	18,353	0,188	0	15	0.036	10.8880	0,036	0,311	8,89	1,04	2.793	10.071	0.421	103.444
	35,983	3,849	17,904	0,206	0,136	15	0.064	10.3880	0,099	0,327	8,724	0,884	3.207	9.722	0	99.929
	36,958	3,143	20,087	0,17	0,134	13	0.03	9.1120	0,085	0,314	8,934	0,898	3.251	9.978	0	102.23
	37,444	3,649	21,006	0,205	0	13	0.025	8.1930	0,078	0,249	9,19	0,583	3.456	10.058	0	104.514
	36,333	3,121	17,89	0,187	0,153	16	0.039	10.9160	0,082	0,318	9,037	1,064	2.961	9.935	0.421	103.475
	35,162	3,272	17,633	0,186	0,091	16	0.095	10.6620	0,107	0,354	8,916	1,212	2.767	9.916	0.421	102.262

	Si	Ti	Al	Fe(3+)	Fe(2+)	Mg	K	F	B	(%) H2O	OH	F	Total
apfu	6.296	0.395	3.916	1.394	0.654	2.346	1.785	0	2.996	3.245	3.785	0	3.785
	6.235	0.391	3.878	1.496	0.676	2.324	1.988	0	2.994	3.453	3.989	0	3.989
	6.205	0.519	3.657	1.619	0.687	2.313	1.979	0	2.996	3.461	3.979	0	3.979
	6.188	0.532	3.542	1.738	0.628	2.372	2.03	0	2.999	3.417	4.03	0	4.03
	6.243	0.402	3.574	1.78	0.607	2.393	1.821	0	3.016	3.211	3.821	0	3.821
	6.051	0.39	3.668	1.891	0.423	2.577	1.985	0.547	3.024	2.981	3.438	0.547	3.985
	6.212	0.389	3.661	1.737	0.427	2.573	1.761	0.546	3.019	2.793	3.215	0.546	3.761
	6.257	0.403	3.582	1.758	0.335	2.665	1.824	0	3.014	3.207	3.825	0	3.825
	6.271	0.393	4.106	1.231	0.663	2.337	1.778	0	2.989	3.251	3.778	0	3.778
	6.394	0.39	4.277	0.94	0.939	2.061	1.984	0	2.958	3.456	3.984	0	3.984
	6.298	0.395	3.505	1.802	0.392	2.608	2.009	0.553	3.005	2.961	3.455	0.553	4.009
	6.135	0.395	3.512	1.958	0.387	2.613	1.789	0.554	3.033	2.767	3.235	0.554	3.789

X Sites	K(X)	Total(X)	Y Sites	Ti(Y)	Fe2+(Y)	Mg(Y)	Total(Y)	Z Sites	Al(Z)	Fe3+(Z)	Mg(Z)	Total(Z)	T Sites	Si(T)	Total(T)	V+W Sites	OH (V)	OH (W)	OH (V+W)	F (W)	O (W)	Total (V+W)
	1.785	1.785		0.395	0.654	1.656	2.704		3.916	1.394	0.69	6		6.296	6.296		3	0.785	3.785	0	0.215	4
	1.988	1.989		0.391	0.676	1.698	2.765		3.878	1.496	0.626	6		6.235	6.235		3	0.989	3.989	0	0.011	4
	1.979	1.979		0.519	0.687	1.589	2.795		3.657	1.619	0.724	6		6.205	6.205		3	0.979	3.979	0	0.021	4
	2.03	2.03		0.532	0.628	1.652	2.812		3.542	1.738	0.72	6		6.188	6.188		3	1	4.03	0	0	4
	1.821	1.821		0.402	0.607	1.748	2.757		3.574	1.78	0.646	6		6.243	6.243		3	0.821	3.821	0	0.179	4
	1.985	1.985		0.39	0.423	2.136	2.949		3.668	1.891	0.441	6		6.051	6.051		3	0.438	3.438	0.547	0.015	4
	1.761	1.761		0.389	0.427	1.971	2.788		3.661	1.737	0.602	6		6.212	6.212		3	0.215	3.215	0.546	0.239	4
	1.824	1.825		0.403	0.335	2.005	2.743		3.582	1.758	0.66	6		6.257	6.257		3	0.825	3.825	0	0.175	4
	1.778	1.778		0.393	0.663	1.673	2.729		4.106	1.231	0.664	6		6.271	6.271		3	0.778	3.778	0	0.222	4
	1.984	1.984		0.39	0.939	1.277	2.606		4.277	0.94	0.784	6		6.394	6.394		3	0.984	3.984	0	0.016	4
	2.009	2.009		0.395	0.392	1.915	2.702		3.505	1.802	0.693	6		6.298	6.298		3	0.447	3.455	0.553	0	4
	1.789	1.789		0.395	0.387	2.083	2.865		3.512	1.958	0.53	6		6.135	6.135		3	0.235	3.235	0.554	0.211	4

Group name (X-site)	Species series (W-site)	Dominant cation (X-site)	OH/(OH+O) (V-site)	Dominant anion (V-site)	Si/(Si+B+Al) (T-site)	Dominant cation (T-site)	Total divalent cation (Y+Z sites)	Dominant divalent cation (Y+Z sites)	Total divalent cation (Y-site)	Dominant divalent cation (Y-site)	Total divalent cation (Z-site)	Dominant divalent cation (Z-site)	Total trivalent cation (YZ sites)	Dominant trivalent cation (YZ sites)	Total trivalent cation (Y-site)	Dominant trivalent cation (Y-site)	Total trivalent cation (Z-site)	Dominant trivalent cation (Z-site)	Total quad. cation (YZ sites)	Dominant quad. cation (YZ sites)
Alkali	Hydroxy-	K	1	OH	1	Si4+	3	Mg2+	2.31	Mg2+	0.69	Mg2+	5.31	Al3+	0	n.a.	5.31	Al3+	0.395	Ti4+
Alkali	Hydroxy-	K	1	OH	1	Si4+	3	Mg2+	2.374	Mg2+	0.626	Mg2+	5.374	Al3+	0	n.a.	5.374	Al3+	0.391	Ti4+
Alkali	Hydroxy-	K	1	OH	1	Si4+	3	Mg2+	2.276	Mg2+	0.724	Mg2+	5.276	Al3+	0	n.a.	5.276	Al3+	0.519	Ti4+
Alkali	Hydroxy-	K	1	OH	1	Si4+	3	Mg2+	2.28	Mg2+	0.72	Mg2+	5.28	Al3+	0	n.a.	5.28	Al3+	0.532	Ti4+
Alkali	Hydroxy-	K	1	OH	1	Si4+	3	Mg2+	2.354	Mg2+	0.646	Mg2+	5.354	Al3+	0	n.a.	5.354	Al3+	0.402	Ti4+
Alkali	Fluor-	K	1	OH	1	Si4+	3	Mg2+	2.559	Mg2+	0.441	Mg2+	5.559	Al3+	0	n.a.	5.559	Al3+	0.39	Ti4+
Alkali	Fluor-	K	1	OH	1	Si4+	3	Mg2+	2.398	Mg2+	0.602	Mg2+	5.398	Al3+	0	n.a.	5.398	Al3+	0.389	Ti4+
Alkali	Hydroxy-	K	1	OH	1	Si4+	3	Mg2+	2.34	Mg2+	0.66	Mg2+	5.34	Al3+	0	n.a.	5.34	Al3+	0.403	Ti4+
Alkali	Hydroxy-	K	1	OH	1	Si4+	3	Mg2+	2.336	Mg2+	0.664	Mg2+	5.336	Al3+	0	n.a.	5.336	Al3+	0.393	Ti4+
Alkali	Hydroxy-	K	1	OH	1	Si4+	3	Mg2+	2.216	Mg2+	0.784	Mg2+	5.216	Al3+	0	n.a.	5.216	Al3+	0.39	Ti4+

Alkali	Fluor-	K	1	OH	1	Si4+	3	Mg2+	2.307	Mg2+	0.693	Mg2+	5.307	Al3+	0	n.a.	5.307	Al3+	0.395	Ti4+
Alkali	Fluor-	K	1	OH	1	Si4+	3	Mg2+	2.47	Mg2+	0.53	Mg2+	5.47	Al3+	0	n.a.	5.47	Al3+	0.395	Ti4+

	R1	R2	R3		R+	R2+	R3+		Mg*	Al*	Na*	OH*		T-site	Z-site	Y-site	X-site	Total Cation charge
Cation Proportion	0	4.394	4.441	**Cation Propostion**	1.785	3	5.836	**Element Ratio**	2.605	6.099	1.785	0.785	**Site Charge**	25.183	17.31	6.198	1.785	50.475
	0	4.496	4.398		1.989	3	5.895		2.609	6.156	1.989	0.989		24.939	17.374	6.312	1.989	50.614
	0	4.619	4.346		1.979	3	5.967		2.481	6.313	1.979	0.979		24.822	17.276	6.626	1.979	50.703
	0	4.738	4.25		2.03	3	5.989		2.468	6.344	2.03	1		24.752	17.28	6.688	2.03	50.75
	0	4.78	4.109		1.821	3	5.891		2.598	6.159	1.821	0.821		24.973	17.354	6.318	1.821	50.466
	0	4.891	4.187		1.985	3	6.079		2.61	6.339	1.985	0.985		24.205	17.559	6.678	1.985	50.426
	0	4.737	4.179		1.761	3	5.917		2.611	6.177	1.761	0.761		24.85	17.398	6.354	1.761	50.363
	0	4.758	4.118		1.825	3	5.878		2.597	6.146	1.825	0.825		25.028	17.34	6.293	1.825	50.485
	0	4.231	4.628		1.778	3	5.86		2.607	6.122	1.778	0.778		25.082	17.336	6.245	1.778	50.441
	0	3.94	4.795		1.984	3	5.736		2.61	5.996	1.984	0.984		25.575	17.216	5.992	1.984	50.768
	0	4.802	4.03		2.009	3	5.834		2.605	6.097	2.009	1		25.191	17.307	6.194	2.009	50.701
	0	4.958	4.038		1.789	3	5.997		2.605	6.261	1.789	0.789		24.538	17.47	6.522	1.789	50.319

	T-site	Z-site	Y-site	X-site	Fe(tot) / (Fe (tot) +Mg)	Na/(Na+Ca)	Al/(Al+Mg)	Al/(Al+Si)	Al/(Al+Fe (tot)+Mg)	Ca/(Ca+Fe (tot)+Mg)	O / (O + OH + F) (W-site)	Al / (Al + Fe3 + Cr) (Z-site)	Fe3+ / (Al + Fe3 + Cr) (Z-site)	Si excess	Normalizat.	Total (Z+Y sites)	Total (T+Z+Y sites)	Total (T+Z+Y+X sites)	Subgroup	Tourmaline species
Site Allocation	Full	Full	Deficiency	Full	0.466	1	0.625	0.383	0.471	0	0.215	0.738	0.262	0.296	15 cations (T+Z+Y)	8.704	15	16.785	subgroup 1	Potassium-dravite
	Full	Full	Deficiency	Full	0.483	1	0.625	0.383	0.463	0	0.011	0.722	0.278	0.235	15 cations (T+Z+Y)	8.765	15	16.989	subgroup 1	Potassium-dravite
	Full	Full	Deficiency	Full	0.499	1	0.613	0.371	0.442	0	0.021	0.693	0.307	0.205	15 cations (T+Z+Y)	8.795	15	16.979	subgroup 1	Potassium-dravite
	Full	Full	Deficiency	Full	0.499	1	0.599	0.364	0.428	0	0	0.671	0.329	0.188	15 cations (T+Z+Y)	8.812	15	17.03	subgroup 1	Potassium-dravite
	Full	Full	Deficiency	Full	0.499	1	0.599	0.364	0.428	0	0.179	0.668	0.332	0.243	15 cations (T+Z+Y)	8.757	15	16.821	subgroup 1	Potassium-dravite
	Full	Full	Deficiency	Full	0.473	1	0.587	0.377	0.429	0	0.015	0.66	0.34	0.051	15 cations (T+Z+Y)	8.949	15	16.985	subgroup 1	Potassium-dravite
	Full	Full	Deficiency	Full	0.457	1	0.587	0.371	0.436	0	0.239	0.678	0.322	0.212	15 cations (T+Z+Y)	8.788	15	16.761	subgroup 1	Potassium-dravite
	Full	Full	Deficiency	Full	0.44	1	0.573	0.364	0.429	0	0.175	0.671	0.329	0.257	15 cations (T+Z+Y)	8.743	15	16.825	subgroup 1	Potassium-dravite
	Full	Full	Deficiency	Full	0.448	1	0.637	0.396	0.493	0	0.222	0.769	0.231	0.271	15 cations (T+Z+Y)	8.729	15	16.778	subgroup 1	Potassium-dravite
	Full	Full	Deficiency	Full	0.477	1	0.675	0.401	0.521	0	0.016	0.82	0.18	0.394	15 cations (T+Z+Y)	8.606	15	16.984	subgroup 1	Potassium-dravite
	Full	Full	Deficiency	Full	0.457	1	0.573	0.358	0.422	0	0	0.66	0.34	0.298	15 cations (T+Z+Y)	8.702	15	17.009	subgroup 1	Potassium-dravite
	Full	Full	Deficiency	Full	0.473	1	0.573	0.364	0.415	0	0.211	0.642	0.358	0.135	15 cations (T+Z+Y)	8.865	15	16.789	subgroup 1	Potassium-dravite

SUPPLEMENTARY MATERIAL 9 – COMPOSITION OF GARNETS FROM MEBC

Table 12 – Garnet mineral analyses

	All = 179			Paragneiss n=58			Pre-deformational metagranite n=52			Syn- to tardi-deformational granite n=69		
wt. %	x̄	σ	CI (2σ)	x̄	σ	CI (2σ)	x̄	σ	CI (2σ)	x̄	σ	CI (2σ)
SiO_2	37.49	0.44	0.06	37.50	0.28	0.07	37.32	0.68	0.19	37.59	0.24	0.06
TiO_2	0.02	0.02	0	0.02	0.02	0	0.01	0.02	0	0.02	0.02	0
$Al2O_3$	21.51	0.28	0.04	21.53	0.19	0.05	21.40	0.41	0.11	21.57	0.19	0.04
Cr_2O_3	0.03	0.05	0.01	0.03	0.06	0.01	0.03	0.05	0.01	0.03	0.05	0.01
Fe_2O_3	<0.01	<0.01	<0.01	<0.01	<0.01	<0.01	<0.01	<0.01	<0.01	<0.01	<0.01	<0.01
FeO	33.78	0.33	0.05	33.77	0.37	0.10	33.75	0.28	0.08	33.82	0.31	0.07
MgO	5.21	0.21	0.03	5.20	0.21	0.05	5.16	0.16	0.04	5.26	0.23	0.05
CaO	0.70	0.10	0.01	0.68	0.08	0.02	0.79	0.08	0.02	0.65	0.08	0.02
TOTAL	98.73	0.82	0.12	98.73	0.57	0.15	98.45	1.26	0.34	98.95	0.44	0.10
apfu												
Si	3.00	0.01	0	3.00	0.01	0	3.00	0.02	0.00	3.00	0.01	0.0
Ti	0.00	0.00	0	0.00	0	0	0.0	0.0	0.0	0.0	0.0	0.0
Al	2.03	0.01	0	2.03	0.01	0	2.03	0.02	0.0	2.03	0.01	0.0
Cr	0.00	0.00	0	0.00	0	0	0.0	0.0	0.0	0.0	0.0	0.0
Fe^{3+}	<0.01	0.01	0.01	<0.01	0.01	0.01	<0.01	0.01	0.01	<0.01	0.01	0.01
Fe^{2+}	2.26	0.02	0	2.26	0.02	0.01	2.27	0.03	0.01	2.26	0.02	0.01
Mg	0.62	0.02	0	0.62	0.02	0.01	0.62	0.02	0.0	0.63	0.03	0.01
Ca	0.06	0.01	0	0.06	0.01	0	0.07	0.01	0.0	0.06	0.01	0.0
Total	7.98	0.01	0	7.98	0	0	7.98	0.0	0.0	7.98	0.0	0.0
Mole fractions												

XFe^2 (VIII)	0.77	0.01	<0.01	0.77	0.01	<0.01	0.77	0.01	<0.01	0.77	0.01	<0.01
XMg (VIII)	0.21	0.01	<0.01	0.21	0.01	<0.01	0.21	0.01	<0.01	0.21	0.01	<0.01
XCa (VIII)	0.02	<0.01	<0.01	0.02	<0.01	<0.01	0.02	<0.01	<0.01	0.02	<0.01	<0.01
XFe^3 (VI)	<0.01	<0.01	<0.01	<0.01	<0.01	<0.01	<0.01	<0.01	0.01	<0.01	<0.01	<0.01
XCr (VI)	<0.01	<0.01	<0.01	<0.01	<0.01	<0.01	<0.01	<0.01	<0.01	<0.01	<0.01	<0.01
End-members												
Almandine	77	0.80	0.12	77	0.79	0.20	77	0.72	0.20	77	0.84	0.20
Pyrope	21	0.84	0.12	21	0.86	0.22	21	0.59	0.16	21	0.95	0.22
Grossular	2	0.29	0.04	2	0.22	0.06	2	0.25	0.07	2	0.22	0.05
Andradite	0	0.04	0.01	0	0.03	0.01	0	0.05	0.01	0	0.03	0.01
Uvarovite	0	0.00	0.00	0	0.00	0.00	0	0.00	0.00	0	0.00	0.00

SUPPLEMENTARY MATERIAL 10 – GARNET DERIVATION ACCORDING TO ITS CHEMISTRY

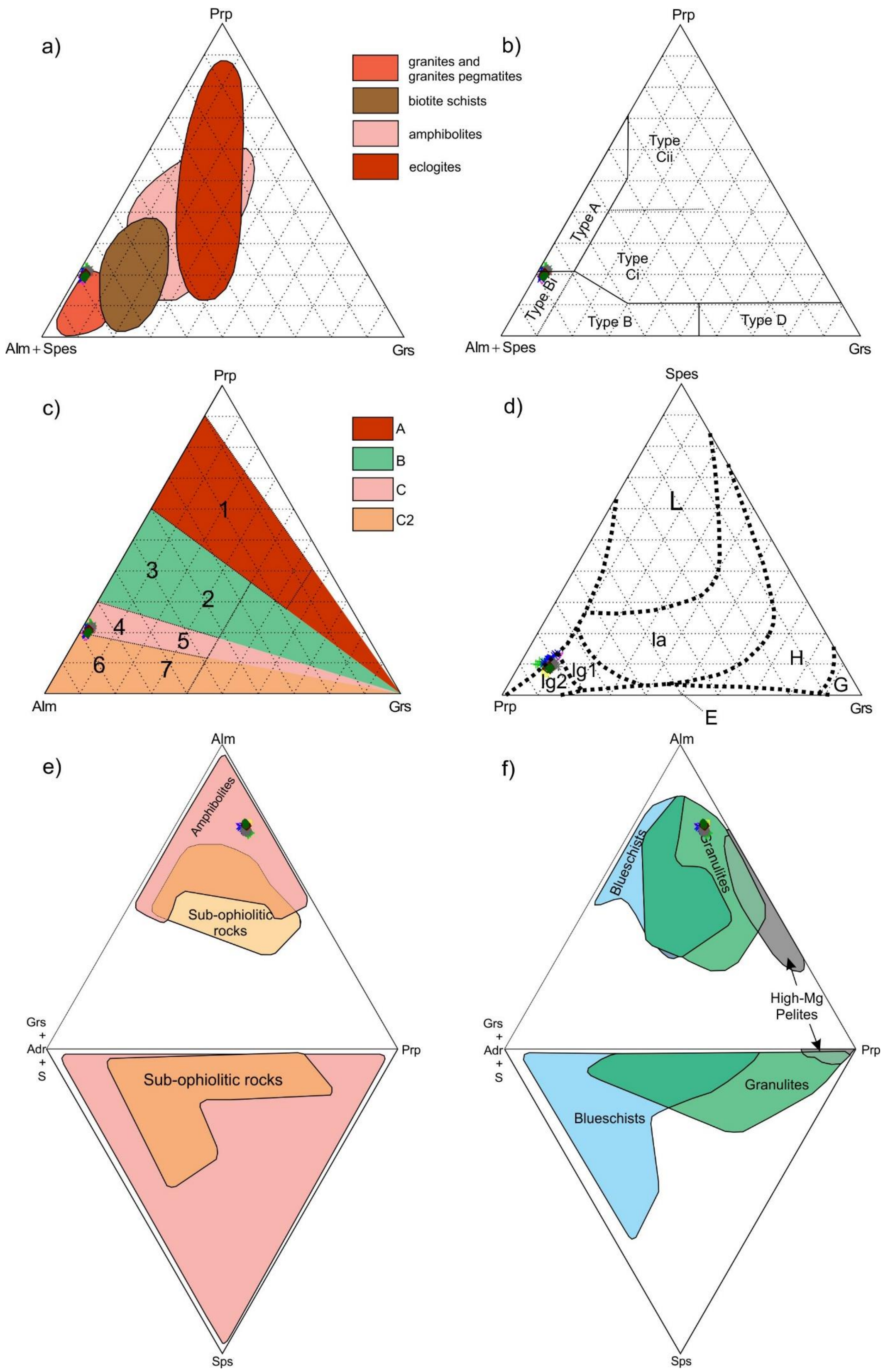

Figure 19 - Ternary Diagrams utilized by Krippner et al. (2014) to discriminate which rock the garnets derived from a) Diagram proposed by Wright (1938). Maurice Ewing Bank Garnets fall into granite and granites pegmatites garnets.

b) Diagram proposed by Mange and Morton (2007) where A - High-grade rocks, mainly granulite or charnockites and igneous intermediate or felsic rocks; B – Metasedimentary rock that underwent to amphibolite facies; Bi – igneous intermediate or felsic rocks; Ci – high-grade metamorphic mafic rocks; Cii – High-Mg rocks such as metapyroxenites and metaperidotites; D – metasomatic rock, very low-grade rocks and calc-silicates from ultra-high-temperature metamorphism. Note that garnets from MEBC fall into either field A or B, being related to granulites or igneous intermediate or felsic rocks.

c) Diagram proposed by Aubrecht et al. (2009). A – High pressure terranes and ultra-high pressure terranes; B – Eclogite or Granulite facies rocks; C – Amphibolite rocks. C1 – from upper amphibolite to granulite transition; C2 – Amphibolites but also blue-schists, skarns, serpentinites, and igneous rocks. The lithologies where garnets came from are: 1 – ultra-high eclogite terranes or peridotites; 2 – high-pressure eclogite and high-pressure mafic granulite; 3 – intermediate to felsic granulite; 4 – garnets from gneisses of upper amphibolite to granulite facies; 5 – garnets from amphibolites of upper amphibolite to granulite facies; 6 – garnets from gneisses of upper amphibolite facies. Note that MEBC garnets fall into field 4, suggesting a gneiss as host rock, metamorphosed in upper-amphibolite to granulite facies metamorphism.

d) Diagram proposed by Teraoka et al. (1998, 1997). L – low-grade rocks; Ia – intermediate grade rocks (amphibolite facies); H – high-grade rocks; Ig1 and Ig2 - intermediate grade rocks (granulite facies); E – eclogites, G – granodiorites. Note that garnets fall into granulite facies rocks.

e and f) Diagram proposed by Suggate and Hall (2014). Note that either in e or f, garnets do fill intermediate facies derivatives.

Cited references:

Aubrecht, R., Méres, S., Sýkora, M., Mikus, T., 2009. Provenance of the detrital garnets and spinels from the Albian sediments of the Czorsztyn Unit (Pieniny Klippen Belt, Western Carpathians, Slovakia). Geol. Carpathica 60, 463–483.

Krippner, A., Meinhold, G., Morton, A.C., von Eynatten, H., 2014. Evaluation of garnet discrimination diagrams using geochemical data of garnets derived from various host rocks. Sediment. Geol. 306, 36–52. https://doi.org/10.1016/j.sedgeo.2014.03.004

Mange, M.A., Morton, A.C., 2007. Geochemistry of heavy minerals, in: Wright, D.T., Mange, M.A. (Eds.), Heavy Minerals in Use, Developments in Sedimentology. Elsevier, Amsterdam, pp. 345–391.

Suggate, S.M., Hall, R., 2014. Using detrital garnet compositions to determine provenance: a new compositional database and procedure. Geol. Soc. Lond. Spec. Publ. 386, 373–393. https://doi.org/10.1144/SP386.8

Teraoka Y., Suzuki M., Hayashi T., Kawakami K., 1997. Detrital Garnets from Paleozoic and Mesozoic snadstones in the Onogawa area, East Kyushu, Southwest Japan. Bull. Fac. Sch. Educ. Hiroshima Univ. 19, 87–101.

Teraoka, Y., Suzuki, M., Kawakami, K., 1998. Provenance of Cretaceous and Paleogene sediments in the Median Zone of Southwest Japan. Bull. Geol. Soc. Jpn. 49, 394–411.

Wright, W.I., 1938. The composition and ocurrence of garnets. Am. Mineral. 23, 436–449

SUPPLEMENTARY MATERIAL 11 – COMPOSITION OF FELDSPAR GROUP MINERALS

Table 13 – Feldspars mineral analyses

	Alkali Feldspars												Plagioclase		
	All units n=77			Paragneiss n=38			Weathered Paragneiss n=9			Pre-deformational Granitoids n=20			Paragneiss n=35		
wt. %	x̄	σ	CI (2σ)	x̄	σ	CI (2σ)	x̄	σ	CI (2σ)	x̄	σ	CI (2σ)	x̄	σ	CI (2σ)
SiO_2	64.39	0.63	0.15	64.29	0.47	0.15	63.89	1.02	0.67	64.82	0.45	0.20	64.15	2.48	0.82
TiO_2	<0.01	<0.01	<0.01	0	0	N.A.	0	0	N.A.	<0.01	<0.01	<0.01	0.01	0.02	0.01
Al_2O_3	18.81	0.35	0.08	18.79	0.24	0.07	18.89	0.58	0.38	18.82	0.40	0.18	21.23	1.33	0.44
FeO	0.09	0.17	0.04	0.10	0.22	0.07	0.10	0.08	0.05	0.07	0.07	0.03	0.71	0.86	0.28
MnO	0.01	0.01	<0.01	0.01	0.01	0.00	0.02	0.02	0.01	0.01	0.01	0.00	0.01	0.02	0.01
MgO	0.01	0.03	0.01	0.01	0.03	0.01	0.01	0.02	0.01	0.01	0.01	0.00	0.14	0.23	0.07
CaO	0.13	0.11	0.03	0.11	0.08	0.02	0.17	0.11	0.07	0.14	0.15	0.07	1.15	0.73	0.24
Na_2O	1.78	0.83	0.20	1.71	0.50	0.16	2.50	1.69	1.10	1.60	0.66	0.29	9.03	0.83	0.27
K_2O	14.11	1.25	0.30	14.29	0.77	0.25	12.79	2.53	1.66	14.38	0.77	0.34	1.82	0.77	0.26
TOTAL	99.34	0.72	0.17	99.31	0.54	0.17	98.38	0.42	0.27	99.84	0.66	0.29	98.25	1.41	0.47
apfu															
Si	2.98	0.02	<0.01	2.98	0.01	<0.01	2.97	0.03	0.02	2.98	0.02	0.01	2.89	0.07	0.02
Ti	<0.01	<0.01	<0.01	0	0	0	0	0	0	0	0	0	0	0	0
Al	1.03	0.02	<0.01	1.03	0.01	<0.01	1.04	0.03	0.02	1.02	0.02	0.01	1.13	0.07	0.02
Fe	<0.01	0.01	<0.01	<0.01	0.01	<0.01	<0.01	<0.01	<0.01	<0.01	0.00	<0.01	0.03	0.04	0.01
Mn	<0.01	<0.01	<0.01	<0.01	<0.01	<0.01	<0.01	<0.01	<0.01	<0.01	<0.01	<0.01	<0.01	<0.01	0.00
Mg	<0.01	<0.01	<0.01	<0.01	<0.01	<0.01	<0.01	<0.01	<0.01	<0.01	<0.01	0.00	0.01	0.02	0.01
Ca	0.01	0.01	<0.01	0.01	<0.01	<0.01	0.01	0.01	<0.01	0.01	<0.01	<0.01	0.06	0.04	0.01
Na	0.16	0.07	0.02	0.15	0.04	0.01	0.22	0.15	0.10	0.14	0.06	0.03	0.79	0.06	0.02
K	0.83	0.08	0.02	0.84	0.05	0.01	0.76	0.16	0.10	0.84	0.05	0.02	0.11	0.05	0.01
TOTAL	5.01	0.01	<0.01	5.01	0.01	<0.01	5.00	0.01	0.01	5.00	0.01	0.01	5.00	0.02	0.01
Or	84.64	8.38	1.84	82.70	8.34	2.38	76.53	15.62	10.21	85.01	6.01	2.63	11.15	4.84	1.60
Ab	14.78	8.13	1.78	16.70	8.06	2.30	22.62	15.26	9.97	14.29	5.90	2.58	83.01	5.27	1.75
An	0.58	0.52	0.11	0.60	0.43	0.12	0.85	0.53	0.34	0.69	0.73	0.32	5.84	3.63	1.20

SUPPLEMENTARY MATERIAL 12 –MICA MINERAL ANALYSES

Table 14 – Mica mineral analyses

	Paragneiss n=149			Syn- to Tardi-deformational Granitoids n=10			Melanossome n=26		
wt. %	x̄	σ	CI (2σ)	x̄	σ	CI (2σ)	x̄	σ	CI (2σ)
SiO_2	36.77	2.29	0.37	40.18	3.74	2.32	39.56	4.74	1.82
TiO_2	3.44	1.52	0.24	2.58	2.08	1.29	1.39	1.55	0.6
Al_2O_3	18.1	2.64	0.42	24.49	3.07	1.9	21.22	6.42	2.47
FeO	16.14	2.28	0.37	12.5	4.05	2.51	16.65	8.27	3.18
MnO	0.03	0.02	0	0.02	0.03	0.02	0.04	0.03	0.01
MgO	8.01	1.92	0.31	3.37	0.75	0.46	4.87	2.69	1.03
CaO	0.11	0.11	0.02	0.09	0.03	0.02	0.35	0.23	0.09
Na_2O	0.16	0.06	0.01	0.13	0.06	0.03	0.22	0.12	0.05
K_2O	7.79	1.87	0.3	4.21	1.15	0.71	6.38	2.71	1.04
F	0.56	0.26	0.04	0.04	0.03	0.02	0.23	0.23	0.09
Cr_2O_3	0.07	0.08	0.01	0.02	0.04	0.02	0.05	0.08	0.03
H_2O*	3.63	0.19	0.03	3.83	0.23	0.15	3.74	0.36	0.14
Subtotal	94.77	2.83	0.45	91.48	2.11	1.31	94.7	3.29	1.26
O=F,Cl	0.21	0.13	0.02	0.13	0.1	0.06	0.18	0.12	0.05
TOTAL	94.56	2.85	0.46	91.35	2.13	1.32	94.52	3.33	1.28

apfu									
Si	5.71	0.24	0.04	6.04	0.33	0.2	6	0.31	0.12
Al^{IV}	2.29	0.24	0.04	1.96	0.33	0.2	2	0.31	0.12
Al^{VI}	1.03	0.62	0.1	2.38	0.7	0.44	1.75	1.07	0.41
Al total	3.31	0.41	0.07	4.34	0.41	0.25	3.74	0.81	0.31
Ti	0.4	0.18	0.03	0.3	0.26	0.16	0.16	0.18	0.07
Cr	0.01	0.01	0	0.01	0.01	0.01	0.01	0.01	0
Fe	2.1	0.32	0.05	1.6	0.63	0.39	2.21	1.2	0.46
Mn	0	0	0	0	0	0	0.01	0	0
Mg	1.86	0.44	0.07	0.76	0.18	0.11	1.13	0.63	0.24
Ca	0.02	0.02	0	0.01	0.01	0	0.06	0.04	0.01
Na	0.05	0.02	0	0.04	0.01	0.01	0.06	0.03	0.01
K	1.55	0.37	0.06	0.81	0.2	0.13	1.22	0.49	0.19
OH*	3.76	0.15	0.02	3.85	0.12	0.07	3.79	0.14	0.05
F	0.24	0.15	0.02	0.15	0.12	0.07	0.21	0.14	0.05
Y total	5.41	0.2	0.03	5.05	0.29	0.18	5.26	0.67	0.26
X total	1.61	0.37	0.06	0.86	0.22	0.14	1.34	0.47	0.18
Total Al	3.31	0.41	0.07	4.34	0.41	0.25	3.74	0.81	0.31
TOTAL	19.02	0.45	0.07	17.91	0.33	0.21	18.6	0.54	0.21
$Al^{VI} + Fe^{3+} + Ti$	1.43	0.48	0.08	2.68	0.49	0.3	1.91	0.96	0.37
$Fe^{2+} + Mn$	2.11	0.32	0.05	1.6	0.63	0.39	2.21	1.2	0.46

SUPPLEMENTARY MATERIAL 13 – ZIRCON TRACE ANALYSES

Table 15 – Trace elements analyses from zircon

Spot	Event	Age	2s	Th/U	206Pb	208Pb	Th (ppm)	U (ppm)	Ti (ppm)	T °C
1	Post-met?	866.10	20.57	0.58	1131.65	62.60	734.10	1272.36	29.31	845
2	Rodinia Event Metamorphism / Vulcanic Arc	981.46	11.86	0.01	452.50	1.45	3.31	630.21	5.00	683
3		1019.77	20.19	0.03	887.16	6.73	26.56	873.40	6.32	702
4		1033.17	20.95	0.28	453.43	16.96	140.14	496.07	3.97	666
5		1058.83	20.01	0.02	742.25	2.49	16.58	880.62	40.04	880
6		1059.36	19.95	0.44	666.94	17.24	361.62	820.86	40.68	881
7		1060.44	22.90	0.02	294.33	3.90	10.12	447.12		
8	NMB Derived	1139.21	19.20	0.37	536.89	21.47	229.52	621.99	10.34	744
9		1142.28	19.16	0.89	728.80	69.85	826.65	928.69	104.84	
10		1146.36	19.62	0.01	742.67	4.27	12.17	980.48	3.98	666
11		1146.87	19.36	0.04	322.21	3.00	19.59	460.45	2.86	642
12		1149.16	20.35	0.72	923.79	69.80	693.66	969.36	200.73	
13		1150.69	19.31	0.06	926.81	7.13	71.68	1195.70	5.56	692
14		1159.05	19.96	0.28	272.87	11.92	95.12	342.01	5.57	692
15		1171.88	19.05	0.31	785.21	24.25	264.14	853.53	12.67	762
16		1172.89	19.03	0.50	504.19	14.23	409.05	825.92	18.07	796
17		1181.13	19.93	0.34	351.58	16.17	140.57	416.05	6.80	708
18		1183.37	19.65	0.69	314.06	32.37	292.46	420.84	12.56	761
19		1197.23	19.47	0.33	294.67	14.01	121.28	362.42	3.78	662
20		1239.29	18.95	0.20	915.73	4.64	256.82	1287.06	12.87	764
21		1270.86	20.67	0.19	262.01	6.06	80.62	428.92	13.72	770
22		1277.85	28.05	0.33	147.41	7.44	54.65	164.33	9.49	736
23		1288.13	19.28	0.44	214.42	13.96	126.82	287.14	121.73	1021
24		1307.02	18.72	0.40	888.46	26.98	490.86	1231.16	24.89	828
25	Other Terranes Derived	1466.56	18.59	0.08	521.32	6.50	34.66	446.94	4.21	670
26		1630.82	41.41	0.54	146.96	10.46	66.45	124.08	8.35	725

SUPPLEMENTARY MATERIAL 14 – REACTION BOXES DESCRIPTION

1 Chl + Ilm + Cpx + Liq + Qtz + Phl + Mic + Rut + Law
2 Chl + Ilm + Cpx + H2O + Qtz + Prl + Mic + Rut + Law
3 Plag + Bt + ilm + Qtz + Ep + Ky + Liq + H2O
4 Plag + Grt + Ilm + Qtz + Ep + Ky + Liq
5 2Plag + Bt + Ep + Ilm + Qtz + Ky + Liq + Grt
6 2Plag + Grt + Ilm + Liq + Qtz + Ky
7 2 Plag + Bt + Ilm + H2O + Qtz + Ky + Liq
8 Plag + Ilm + Crd + Liq + Qtz + Sil
9 Plag + Ilm + Qtz + Crd + Liq
10 Plag + Ilm + Qtz + Crd + Liq
11 2Plag + Grt + Bt + Ilm + Crd + Liq + Qtz + Sil
12 2Plag + Ilm + Qtz + Crd + Sil + Liq
13 2Plag + Bt + Ilm + Qtz + And + Crd + H2O + Liq
14 2Plag + Ilm + Crd + H2O + Qtz + And
15 2Plag + Bt + Ilm + Qtz + And + Crd + H2O
16 2Plag + Bt + Ilm + Crd + Liq + H2O + Qtz + Sil
17 2Plag + Bt + Ilm + Crd + H2O + Qtz + Sil
18 2Plag + Bt + Ilm + Qtz + Sil + H2O + Liq
19 Plag + Bt + Ilm + H2O + Qtz + And + Ab + Mic
20 Plag + Bt + Chl + Ilm + H2O + Qtz + And + Ab + Mic
21 Plag + Bt + Chl + Ilm + H2O + Qtz + Ky + Ab + Mic
22 Plag + Bt + Ilm + H2O + Qtz + Ky + Ab + Mic
23 Bt + Chl + Ilm + Ep + H2O + Qtz + Ky + Ab + Mic
24 Bt + Ilm + Ep + H2O + Qtz + Ab + Mic
25 Chl + Ilm + Ep + H2O + Qtz + Prl + Alb + Mic + Rut
26 Chl + Ilm + H2O + Qtz + Prl + Alb + Mic + Rut + Law
27 Chl + Ilm + Liq + Qtz + Prl + Ab + Mic + Rut + Law

Figure 20 – Reaction boxes from Pseudosection analyses.

SUPPLEMENTARY MATERIAL 15 – GARNET AND ALKALI FELDSPAR ISOPLETS

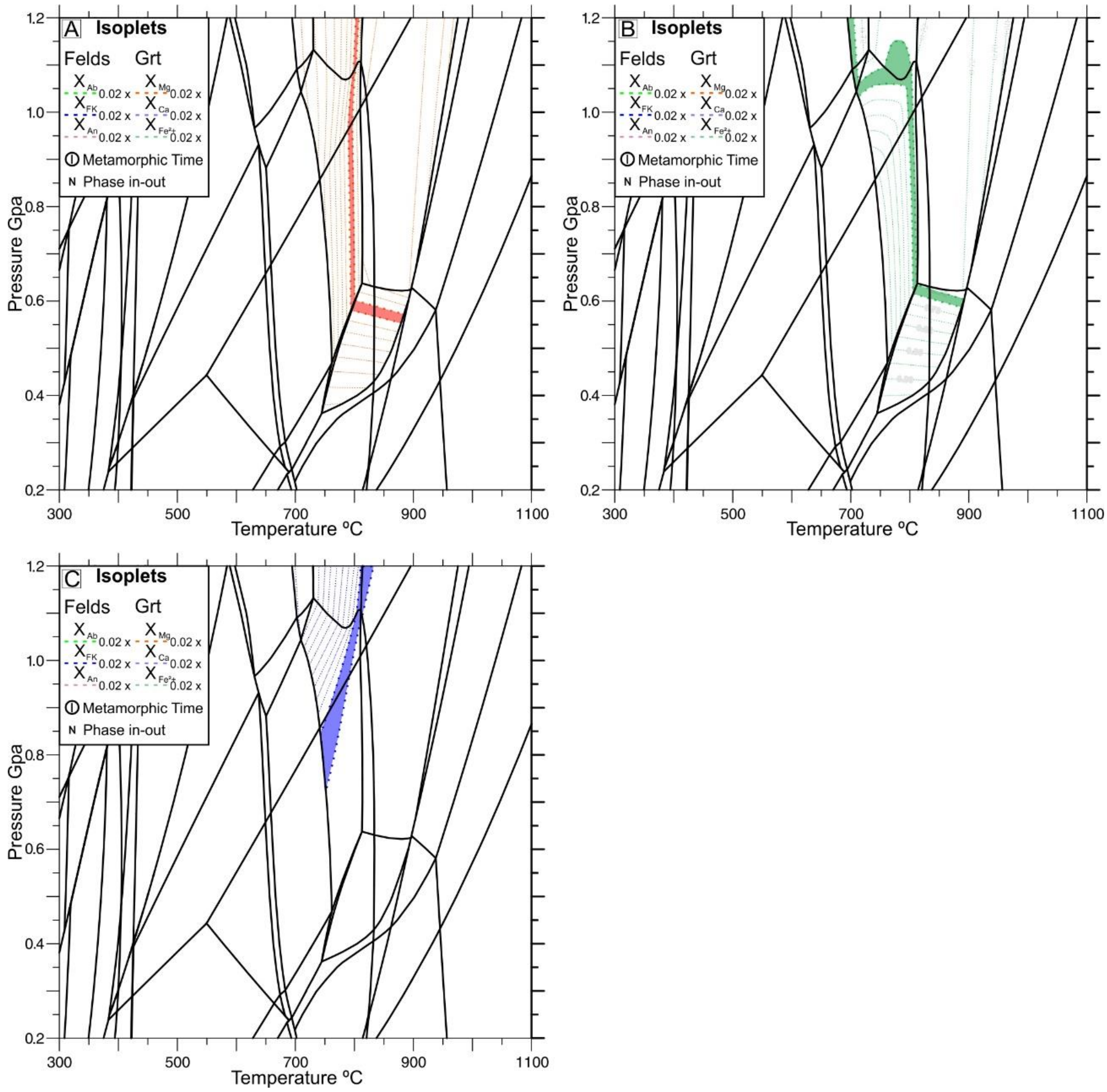

Figure 21 – Garnet isoplets. A - X_{Fe} isoplets, demonstrating a high-temperature inverse proportionality with almandine series; B - X_{Mg} component, demonstrating a PxT direct proportional relationship with pyrope series. C - X_{Ca} suggesting either an inverse proportion between grossular series. Numbers represent recrystallization events. Arrows represent a simplified P x T trajectory.

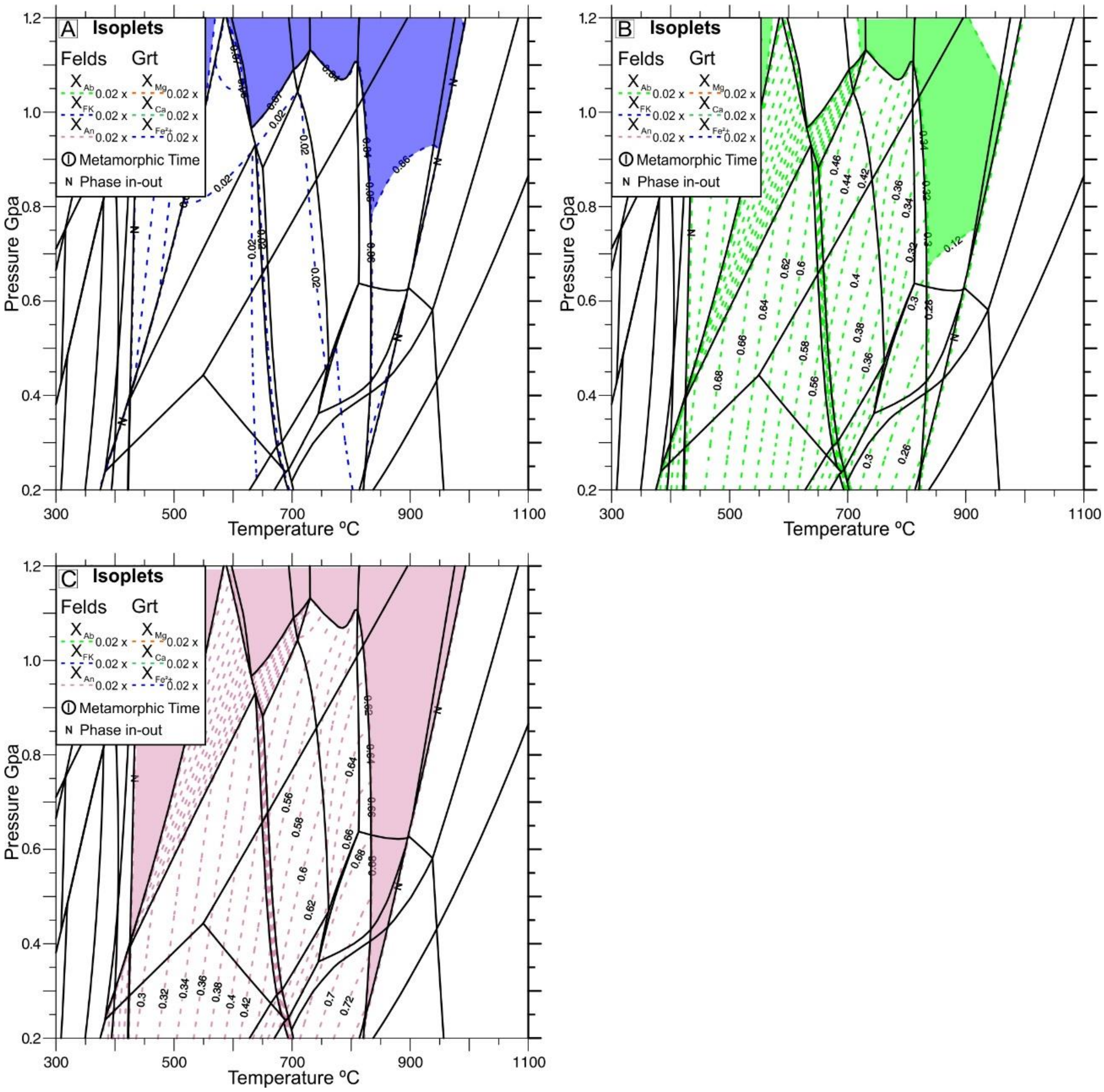

Figure 22 – Alkali-feldspar isoplets. A – X_{FK}; B – X_{Ab}; C - X_{An}.

Table 16– Alkali feldspars close to Bt-out reaction identified in #16R2-08.

#16R2-08B						
Number	1	2	3	4	5	6
SiO2	64.99	64.84	64.57	64.99	64.38	64.48
TiO2	0.00	0.00	0.00	0.00	0.00	0.00
Al2O3	18.78	18.76	19.01	18.79	18.75	18.90
FeO	0.01	0.08	0.13	0.07	0.15	0.01
MnO	0.02	0.00	0.00	0.00	0.00	0.00
MgO	0.01	0.01	0.01	0.01	0.00	0.00
CaO	0.08	0.20	0.12	0.08	0.27	0.66
Na2O	1.59	1.35	1.44	1.45	1.54	1.51
K2O	14.51	14.93	14.90	14.68	14.41	14.39
TOTAL	99.99	100.18	100.19	100.06	99.51	99.94
Si	2.99	2.98	2.97	2.99	2.98	2.97
Al	1.02	1.02	1.03	1.02	1.02	1.03
Fe	0.00	0.00	0.00	0.00	0.01	0.00
Mn	0.00	0.00	0.00	0.00	0.00	0.00
Mg	0.00	0.00	0.00	0.00	0.00	0.00
Ca	0.00	0.01	0.01	0.00	0.01	0.03
Na	0.14	0.12	0.13	0.13	0.14	0.13
K	0.85	0.88	0.87	0.86	0.85	0.85
Total	5.00	5.01	5.02	5.00	5.01	5.01
XOr	85.35	87.09	86.64	86.58	84.86	83.48
XAb	14.25	11.92	12.76	13.04	13.80	13.31
XAn	0.40	0.98	0.61	0.39	1.35	3.20

SUPPLEMENTARY MATERIAL 16 – AUTHOR REFERENCES

We made the Natal-Maud Belt age distribution chart using the software Isoplot (Ludwig, 2012). The ages from Agulhas Plateau are according to Allen and Tucholke (1981). Coasts Lands and West Antarctica ages are according to Eastin and Faure (1971), Gose et al. (1997), Millar and Pankhurst (1987), and Storey et al. (1994). Meredith Complex ages are according to Jacobs et al. (1999), and Rex and Tanner (1982). The ages from Sverdupfjella Terrane are according Bisnath and Frimmel (2005), Board et al. (2005), Grantham et al. (2008), Groenewald et al. (1995, 1991), Harris (1999), Harris et al. (1995), Jackson (1999), Moyes et al. (1993), Moyes and Barton (1990), and Moyes and Harris (1996). The ages from Kirwanveggen Terrane are according Bisnath and Frimmel (2005), Groenewald et al. (1995), Harris (1999), Jackson (1999), and Wolmarans and Kent (1982). Heimefrontfjella ages are according to Arndt et al. (1991), Bauer et al. (2003a, 2003c, 2003b, 2016), Gose et al. (1997), Groenewald et al. (1995), Jacobs et al. (1996, 2003a, 2003c, 2003b), and Jacobs (2009). The ages from Natal Province are according Barton (1983), Cornell and Thomas (2006), Eglington et al. (2010, 2003), Evans et al. (2007), Grantham et al. (2012), Harmer (1979); Jacobs and Thomas (1996), Johnston et al. (2001); Mendonidis et al. (2015, 2002); Mendonidis and Armstrong (2016, 2009), Spencer et al. (2015), Thomas (1989), Thomas et al. (2003, 1996), and Thomas and Eglington (1990).

Cited references:

Allen, R.B., Tucholke, B.E., 1981. Petrography and implications of continental rocks from the Agulhas Plateau, southwest Indian Ocean. Geology 9, 463. https://doi.org/10.1130/0091-7613(1981)9<463:PAIOCR>2.0.CO;2

Arndt, N.T., Todt, W., Chauvel, C., Tapfer, M., Weber, K., 1991. U–Pb zircon age and Nd isotopic composition of granitoids, charnockites and supracrustal rocks from Heimefrontfjella. Antarct. Geol. Rundsch. 80, 759–777.

Barton, E.S., 1983. The geochronology of the frontal zones of the Namaqua-Natal mobile belt (Ph. D.). University of Witwatersrand, South Africa.

Bauer, W., Fielitz, W., Jacobs, J., Fanning, C.M., Spaeth, G., 2003a. Mafic Dykes from Heimefrontfjella and implications for the post-Grenvillian to pre-Pan-African geological evolution of western Dronning Maud Land, Antarctica. Antarct. Sci. 15, 379–391. https://doi.org/10.1017/S0954102003001391

Bauer, W., Jacobs, J., Fanning, C.M., Schmidt, R., 2003b. Late Mesoproterozoic Arc and Back-arc Volcanism in the Heimefrontfjella (East Antarctica) and Implications for the Palaeogeography at the Southeastern Margin of the Kaapvaal-Grunehogna Craton. Gondwana Res. 6, 449–465. https://doi.org/10.1016/S1342-937X(05)70998-9

Bauer, W., Siemes, H., Spaeth, G., Jacobs, J., 2016. Transpression and tectonic exhumation in the Heimefrontfjella, western orogenic front of the East African/Antarctic Orogen, revealed by quartz textures of high strain domains. Polar Res. 35, 25420. https://doi.org/10.3402/polar.v35.25420

Bauer, W., Thomas, R.J., Jacobs, J., 2003c. Proterozoic-Cambrian history of Dronning Maud Land in the context of Gondwana assembly. Geol. Soc. Lond. Spec. Publ. 206, 247–269. https://doi.org/10.1144/GSL.SP.2003.206.01.13

Bisnath, A., Frimmel, H., 2005. Metamorphic evolution of the Maud Belt: P-T-t Path for high-grade gneisses in Gjelsvikfjella, Dronning Maud Land, East Antarctica. J. Afr. Earth Sci. - J AFR EARTH SCI 43, 505–524. https://doi.org/10.1016/j.jafrearsci.2005.09.007

Board, W.S., Frimmel, H.E., Armstrong, R.A., 2005. Pan-African Tectonism in the Western Maud Belt: P–T–t Path for High-grade Gneisses in the H.U. Sverdrupfjella, East Antarctica. J. Petrol. 46, 671–699. https://doi.org/10.1093/petrology/egh093

Cornell, D.H., Thomas, R.J., 2006. Age and tectonic significance of the Banana Beach Gneiss, KwaZulu-Natal South Coast, South Africa. South Afr. J. Geol. 109, 335–340. https://doi.org/10.2113/gssajg.109.3.335

Eastin, R., Faure, G., 1971. The Age of the Littlewood Volcanics of Coats Land, Antarctica. J. Geol. 79, 241–245. https://doi.org/10.1086/627612

Eglington, B.M., Thomas, R.J., Armstrong, R.A., 2010. U-PB SHRIMP ZIRCON DATING OF MESOPROTEROZOIC MAGMATIC ROCKS FROM THE SCOTTBURGH AREA, CENTRAL MZUMBE TERRANE, KWAZULU-NATAL, SOUTH AFRICA. South Afr. J. Geol. 113, 229–235. https://doi.org/10.2113/gssajg.113.2.229

Eglington, B.M., Thomas, R.J., Armstrong, R.A., Walraven, F., 2003. Zircon geochronology of the Oribi Gorge Suite, KwaZulu-Natal, South Africa: constraints on the timing of trans-current shearing in the Namaqua–Natal Belt. Precambrian Res. 123, 29–46. https://doi.org/10.1016/S0301-9268(03)00016-0

Evans, D.M., Windrim, D.P., Armstrong, R.A., 2007. Age of Metavolcanic rocks at the northern margin of the Namaqua-Natal Metamorphic Province in the Karas Mountains, Namibia, defined by SHRIMP U-Pb dating of zircons. South Afr. J. Geol. 110, 47–54. https://doi.org/10.2113/gssajg.110.1.47

Gose, W.A., Helper, M.A., Connelly, J.N., Hutson, F.E., Dalziel, I.W.D., 1997. Paleomagnetic data and U-Pb isotopic age determinations from Coats Land, Antarctica: Implications for late Proterozoic plate reconstructions. J. Geophys. Res. Solid Earth 102, 7887–7902. https://doi.org/10.1029/96JB03595

Grantham, G.H., Macey, P.H., Ingram, B.A., Roberts, M.P., Armstrong, R.A., Hokada, T., Shiraishi, K., Jackson, C., Bisnath, A., Manhica, V., 2008. Terrane correlation between Antarctica, Mozambique and Sri Lanka; comparisons of geochronology, lithology, structure and metamorphism and possible implications for the geology of southern Africa and Antarctica. Geol. Soc. Lond. Spec. Publ. 308, 91–119. https://doi.org/10.1144/SP308.4

Grantham, G.H., Mendonidis, P., Thomas, R.J., Satish-Kumar, M., 2012. Multiple origins of charnockite in the Mesoproterozoic Natal belt, Kwazulu-Natal, South Africa. Geosci. Front., Charnockites and Charnockites 3, 755–771. https://doi.org/10.1016/j.gsf.2012.05.006

Groenewald, P.B., Grantham, G.H., Watkeys, M.K., 1991. Geological evidence for a Proterozoic to

Mesozoic link between southeastern Africa and Dronning Maud Land, Antarctica. J. Geol. Soc. 148, 1115–1123. https://doi.org/10.1144/gsjgs.148.6.1115

Groenewald, P.B., Moyes, A.B., Grantham, G.H., Krynauw, J.R., 1995. East Antarctic crustal evolution: geological constraints and modelling in western Dronning Maud Land. Precambrian Res. 75, 231–250. https://doi.org/10.1016/0301-9268(95)80008-6

Harmer, R., 1979. Pre-cape geology of the Tugela valley north of Kranskop, Natal (M. Sc.). University of Natal.

Harris, P.D., 1999. The geological evolution of Neumayerskarvet in the Northern Kirwanveggen, Western Dronning Maud Land, Antartica (Ph.D. Thesis). Rand Afrikaans University, Johannesburg.

Harris, P.D., Moyes, A.B., Fanning, C.M., Armstrong, R.A., Barton, J.M., Copperthwaite, Y.E., 1995. Zircon ion microprobe results from the Maudheim high-grade gneiss terrane, western Dronning Maud Land, Antarctica. Centen. Geocongress 3–7.

Jackson, C., 1999. Characterization of Mesoproterozoic to Palaeozoic crustal evolution of Western Dronning Maud Land. Unpubl. Rep. South Afr. Natl. Antarct. Program Study 534, 80.

Jacobs, J., 2009. A review of two decades (1986 – 2008) of geochronological work in Heimefrontfjella, and geotectonic Interpretation of western Dronning Maud Land, East Antarctica. Polarforschung 79, 47–57.

Jacobs, J., Bauer, W., Fanning, C.., 2003a. Late Neoproterozoic/Early Palaeozoic events in central Dronning Maud Land and significance for the southern extension of the East African Orogen into East Antarctica. Precambrian Res. 126, 27–53. https://doi.org/10.1016/S0301-9268(03)00125-6

Jacobs, J., Bauer, W., Fanning, C., 2003b. New age constraints for Grenville-age metamorphism in western central Dronning Maud Land (East Antarctica), and implications for the palaeogeography of Kalahari in Rodinia. Int. J. Earth Sci. 92, 301–315. https://doi.org/10.1007/s00531-003-0335-x

Jacobs, J., Bauer, W., Spaeth, G., Thomas, R.J., Weber, K., 1996. Litholog and structure of the Grenville-aged (≈1.1 Ga) basement of heimefrontfjella (East Antarctica). Geol. Rundsch. 85, 800–821. https://doi.org/10.1007/BF02440112

Jacobs, J., Fanning, C.., Bauer, W., 2003c. Timing of Grenville-age vs. Pan-African medium- to high grade metamorphism in western Dronning Maud Land (East Antarctica) and significance for correlations in Rodinia and Gondwana. Precambrian Res. 125, 1–20. https://doi.org/10.1016/S0301-9268(03)00048-2

Jacobs, J., Thomas, R.J., 1996. Pan-African rejuvenation of the c. 1.1 Ga Natal Metamorphic Province(South Africa):K–Ar muscovite and titanite fission track evidence. J. Geol. Soc. 153, 971–978. https://doi.org/10.1144/gsjgs.153.6.0971

Jacobs, J., Thomas, R.J., Armstrong, R.A., Henjes-Kunst, F., 1999. Age and thermal evolution of the Mesoproterozoic Cape Meredith Complex, West Falkland. J. Geol. Soc. 156, 917–928. https://doi.org/10.1144/gsjgs.156.5.0917

Johnston, S.T., Armstrong, R., Arima, M., 2001. Preliminary U-Pb geochronology of the Tugela terrane, Natal belt, eastern South Africa. Mem. Natl. Inst. Polar Res. 55, 40–58.

Ludwig, K.R., 2012. Users Manual for ISOPLOT/EX, Version 3. A Geochronological Toolkit for Microsoft Excel, Berkeley Geochronological Centre Special Publication.

Mendonidis, P., Armstrong, R.A., 2016. U–Pb Zircon (SHRIMP) ages of granite sheets and timing of deformational events in the Natal Metamorphic Belt, southeastern Africa: Evidence for deformation partitioning and implications for Rodinia reconstructions. Precambrian Res. 278, 22–33. https://doi.org/10.1016/j.precamres.2016.03.003

Mendonidis, P., Armstrong, R.A., 2009. A new U-Pb zircon age for the Portobello Granite from the southern part of the Natal Metamorphic Belt. South Afr. J. Geol. 112, 197–208. https://doi.org/10.2113/gssajg.112.2.197

Mendonidis, P., Armstrong, R.A., Eglington, B.M., Grantham, G.H., Thomas, R.J., 2002. Metamorphic history and U-Pb Zircon (SHRIMP) geochronology of the Glenmore Granite: Implications for the tectonic evolution of the Natal Metamorphic Province. South Afr. J. Geol. 105, 325–336. https://doi.org/10.2113/1050325

Mendonidis, P., Thomas, R.J., Grantham, G.H., Armstrong, R.A., 2015. Geochronology of emplacement and charnockite formation of the Margate Granite Suite, Natal Metamorphic Province, South Africa: Implications for Natal-Maud belt correlations. Precambrian Res., The structural, metamorphic and magmatic evolution of Mesoproterozoic orogens 265, 189–202. https://doi.org/10.1016/j.precamres.2015.02.013

Millar, I.L., Pankhurst, R.J., 1987. Rb-Sr geochronology of the region between the Antarctic Peninsula and the Transantarctic Mountains: Haag nunataks and Mesozoic granitoids, in: McKenzie, G.D. (Ed.), Geophysical Monograph Series. American Geophysical Union, Washington, D. C., pp. 151–160.

Moyes, A.B., Barton, J.M., 1990. A review of isotopic data from western Dronning Maud Land, Antarctica. Zentralblatt Geol. Palaeontol. Teil 1 1.

Moyes, A.B., Barton, J.M., Groenewald, P.B., 1993. Late Proterozoic to Early Palaeozoic tectonism in Dronning Maud Land, Antarctica: supercontinental fragmentation and amalgamation. J. Geol. Soc. 150, 833–842. https://doi.org/10.1144/gsjgs.150.5.0833

Moyes, A.B., Harris, P.D., 1996. Geological evolution of western Dronning Maud Land within a Gondwana framework. (South African National Antarctic Programme Final Report), Radiogenic Isotope Geology Project 1991-1996. Johannesburg.

Rex, D.C., Tanner, P.W.G., 1982. Precambrian age for gnaisses at Cape Meredith in the Falkland Islands, in: Craddock, C. (Ed.), Antarctic Geoscience, B. University of Wisconsin Press, International Union of Geological Sciences, pp. 107–108.

Spencer, C.J., Thomas, R.J., Roberts, N.M.W., Cawood, P.A., Millar, I., Tapster, S., 2015. Crustal growth during island arc accretion and transcurrent deformation, Natal Metamorphic Province, South Africa: New isotopic constraints. Precambrian Res., The structural, metamorphic and magmatic evolution of Mesoproterozoic orogens 265, 203–217. https://doi.org/10.1016/j.precamres.2015.05.011

Storey, B.C., Pankhurst, R.J., Johnson, A.C., 1994. The Grenville Province within Antarctica: a test of the SWEAT hypothesis. J. Geol. Soc. 151, 1–4. https://doi.org/10.1144/gsjgs.151.1.0001

Thomas, R.J., 1989. A tale of two tectonic terranes. South Afr. J. Geol. 92, 306–321.

Thomas, R.J., Armstrong, R.A., Eglington, B.M., 2003. Geochronology of the Sikombe Granite, Transkei, Natal Metamorphic Province, South Africa. South Afr. J. Geol. 106, 403–408. https://doi.org/10.2113/106.4.403

Thomas, R.J., De Beer, C.H., Bowring, S.A., 1996. A comparative study of the Mesoproterozoic late orogenic porphyritic granitoids of southwest Namaqualand and Natal, South Africa. J. Afr. Earth Sci., IGCP 348 (Mozambique and Related Belts) 23, 485–508. https://doi.org/10.1016/S0899-5362(97)00014-6

Thomas, R.J., Eglington, B.M., 1990. A Rb-Sr, Sm-Nd and U-Pb zircon isotopic study of the Mzumbe Suite, the oldest intrusive granitoid in southern Natal, South Africa. South Afr. J. Geol. 93, 761–765.

Wolmarans, L.G., Kent, A., 1982. Geological investigations in western Dronning Maud Land, Antarctica, a synthesis. South African Scientific Committee for Antarctic Research.

FIM DO MANUSCRITO

CONCLUSÕES

- As rochas do embasamento de Maurice Ewing Bank consistem de um complex formado por rochas metamórficas polifásicas e contrapartes ígneos intrusivos.
- Cinco litofácies magmato-metamórficas foram descritas em detalhe, representando uma assembléia comum de terrenos granulíticos colisionais, onde processos ígneos e metamórficos coexistem em uma intrínseca relação.
- Mesmo com a carência de elementos de mapeamento, os dados obtidos e interpretados coincidem com dados de terrenos adjacentes como Província Natal (majoritariamente Margate) e Dronning Maud Land (majoritariamente Kirvanveggen, Sverdrupfjella e Heimefrontfjella).
- Os protólitos da litofácies paragneiss foram depositados próximos a fonte, em um context de *back-arc*. Os detritos derivaram de rochas juvenis expostas devido a tectônica collisional em uma elongação do arco meta-vulcanossedimentar de Margate-Sivorg.
- A primeira fase de recristalização, relacionada com os eventos Grenvillianos, é dividida em 4 episódios de recristalização / deformação. A evolução experienciada pelo MEBC contempla o espectro esperado de um ciclo orogênico.
- Os eventos Rodínia 1 (R1) e R2 são relacionados com um episódio de dobramento e cavalgamento Gerado pela colisão de duas massas cratônicas. Esse evento gerou os granitos pré- e sin-deformacionais. Mzumbe e Margate, na província de Natal, e Sivorg-Vardeklettane, em Dronning Maud Land, também registraram eventos de gênese similar, relacionado com granolitização e geração de fusão parcial.
- O evento R3 é interpretado como o climax metamórfico, chegando a fácies Granulito. Entre R2 e R3 há um episódio de descompressão termométrica, interpretada como gerada por exumação tectônica. Como resultado da descompressão, granitóides sin- a tardi-deformacionais, produto de expressivos volumes de fusão parcial, são a litofácies característica. Este evento descompressivo também é registrado, através da ocorrência de grandes plutons em Mzumbe-Margate e Dronning Maud Land.

- O evento R4 é correlacionável com processos tardi-anatéticos e possui como litofácies característica os granitóides pós-deformacionais. Este evento marca o fim da orogênese formadora do Rodínia no MEBC. Nas regiões adjacentes há diversas ocorrências de pegmatites, diques de grão-grosso e stocks alcalinos interpretados como gerados por processos pós-tectônicos.
- Portanto, nós interpretamos que MEBC é originalmente derivado do cráton de Kalahari, estando entre os terrenos de Margate e Heimefrontfjella da Província de Natal e Maud Land, respectivamente.
- Nós propomos que as duas massas cratônicas que geraram o evento collisional formados da orogenia Natal-Maud consistiu do cráton de Kaapvaal e cráton de Coats-Patagonia. Em especial, o cráton de Coats-Patagonia representava uma extensão da orogenia Grenville, localizada no Laurentia. Portanto, MEBC é não somente parte do cinturão de Natal-Maud, mas também o cinturão Natal-Maud é parte da orogenia Grenville.
- O segundo ciclo tectônico é relacionado com o resseting dos sistemas Rb-Sr e K-Ar nas rochas de MEBC. De maneira geral, o complex possui evidências que apontam a eventos de retrometamorfismo na fácies xisto-verde. O reset do Sistema Rb-Sr é interpretado como Gerado por anomalias térmicas *far-field* relacionadas com a orogenia Ross, amplamente distribuído nos blocos da Antártica Leste e Oeste, além do embasamento aflorante do cinturão de Cabo e Patagônia. O reset do Sistema K-Ar é interpretado como produto de “diversas reativações termais durante o Paleozóico”.
- Há eventos de recristalização relacionados com temperaturas abaixo de 300ºC e , como consequencia, regime rúptil. Nós os interpretamos como produto da instabilidade termal ocasionada por eventos de rifteamento Mesozóico. Nas adjacências de MEBC há um evento extensional do Jurássico e um do Cretáceo; no entanto, os processos catalizadores e seus *timings* ainda não são compreendidos.
- Ainda há diversas questões que mantém-se não resolvidas: i) Qual o papel de outros micro-blocos, tais como Haag Nunataks e Agulhas Plateau no Mesoproterozóico? Seria o extremo leste do alto de Maurice Ewing Bank pertencente a uma crosta Paleoproterozóica-Arqueana do cráton de Kaapvaal? iii) Qual a evolução do Platô de Falkland e quais as implicações sobre o posicionamento das Ilhas Falkland (Malvinas) durante o Mesozóico? iv) Qual a

cinemática da Província da Patagônia entre sua geração, no Mesoproterozóico e posicionamento próximo ao atual, no Mesozóico?

REFERÊNCIAS BIBLIOGRÁFICAS:

Adie, R.J., 1952a. The position of the Falkland Islands in a reconstruction of Gondwanaland. Geol. Mag. 89, 401–410.

Adie, R.J., 1952b. Representatives of the Gondwana System in the Falkland Islands, in: Teichert, C. (Ed.), Symposium Sur Ler Series de Gondwana. Presented at the XIXth International Geological Congress, IUGS, Algiers, pp. 385–392.

Ague, J.J., Carlson, W.D., 2013. Metamorphism as Garnet Sees It: The Kinetics of Nucleation and Growth, Equilibration, and Diffusional Relaxation. Elements 9, 439–445. https://doi.org/10.2113/gselements.9.6.439

Alessandretti, L., Philipp, R.P., Chemale, F., Brückmann, M.P., Zvirtes, G., Matté, V., Ramos, V.A., 2013. Provenance, volcanic record, and tectonic setting of the Paleozoic Ventania Fold Belt and the Claromecó Foreland Basin: Implications on sedimentation and volcanism along the southwestern Gondwana margin. J. South Am. Earth Sci. 47, 12–31. https://doi.org/10.1016/j.jsames.2013.05.006

Allen, R.B., Tucholke, B.E., 1981. Petrography and implications of continental rocks from the Agulhas Plateau, southwest Indian Ocean. Geology 9, 463. https://doi.org/10.1130/0091-7613(1981)9<463:PAIOCR>2.0.CO;2

Andrade, S., Ulbrich, H.H., Gomes, C. de B., Martins, L., 2014. Methodology for the Determination of Trace and Minor Elements in Minerals and Fused Rock Glasses with Laser Ablation Associated with Quadrupole Inductively Coupled Plasma Mass Spectrometry (LA-Q-ICPMS). Am. J. Anal. Chem. 2014. https://doi.org/10.4236/ajac.2014.511079

Archibald, D.B., Collins, A.S., Foden, J.D., Payne, J.L., Macey, P.H., Holden, P., Razakamanana, T., 2018. Stenian–Tonian arc magmatism in west–central Madagascar: the genesis of the Dabolava Suite. J. Geol. Soc. 175, 111–129. https://doi.org/10.1144/jgs2017-028

Arima, M., Johnston, S.T., 2001. Crustal Evolution of the Tugela Terrane, Natal Belt, South Africa. Gondwana Res. 4, 563–564. https://doi.org/10.1016/S1342-937X(05)70367-1

Arndt, N.T., Todt, W., Chauvel, C., Tapfer, M., Weber, K., 1991. U–Pb zircon age and Nd isotopic composition of granitoids, charnockites and supracrustal rocks from Heimefrontfjella. Antarct. Geol. Rundsch. 80, 759–777.

Aubrecht, R., Méres, S., Sýkora, M., Mikus, T., 2009. Provenance of the detrital garnets and spinels from the Albian sediments of the Czorsztyn Unit (Pieniny Klippen Belt, Western Carpathians, Slovakia). Geol. Carpathica 60, 463–483.

Baker, H.A., 1924. Final Report on Geological Investigations in the Falkland Islands. U.S. Government Printing Office.

Barker, P.F., 1999. Falkland Plateau evolution and a mobile southernmost South America, in: Cameron, N.R., Bate, R.H., Clure, V.S. (Eds.), Geological Society, London, Special Publications. Geological Society of London, London, pp. 403–408.

Barker, P.F., Dalziel, I.W.D., Dinkelman, M.G., Elliot, D.H., Gombos, A.M., Lonardi, A., Plafker, G., Tarney, J., Thompson, R.W., Tjalsma, R.C., Borch, C.C. von der, Wise, S.W., 1977a. 6. Site 330. Initial Rep. Deep Sea Drill. Proj. XXXVI, 207–257. https://doi.org/10.2973/dsdp.proc.36.106.1977

Barker, P.F., Dalziel, I.W.D., Wise, S.W., 1977b. 1. Introduction. Initial Rep. Deep Sea Drill. Proj. XXXVI, 5–15. https://doi.org/10.2973/dsdp.proc.36.101.1977

Barrett, D.M., 1977. Agulhas Plateau off southern Africa: A geophysical study. Geol. Soc. Am. Bull. 88, 749. https://doi.org/10.1130/0016-7606(1977)88<749:APOSAA>2.0.CO;2

Barton, E.S., 1983. The geochronology of the frontal zones of the Namaqua-Natal mobile belt (Ph. D.). University of Witwatersrand, South Africa.

Basei, M.A., Varela, R., Passarelli, C., Jr, O.S., Cingolani, C., Sato, A.M., González, P.D., 2005. The crystalline basement in the north of Patagonia: isotopic ages and regional characteristics. Presented at the Gondwana 12: Geological and Biological Heritage of Gondwana., Academia Nacional de Ciencias, Córdoba, p. 62.

Basei, M.A.S., Neves, B.B.B., Varela, R., Teixeira, W., Jr, O.S., Sato, A.M., Cingolani, C., 1999. Isotopic dating on the crystalline basement rocks of the Bariloche region, Río Negro, Argentina, in: Anales. Presented at the 2 Simposio Sudamericano de Geología Isotópica (Carlos Paz), Servicio Geológico Minero Argentino, Buenos Aires, pp. 15–18.

Bauer, W., 1995. Strukturentwicklung und Petrogenese des metamorphen Grundgebirges der nördlichen Heimefrontfjella (westliches Dronning Maud Land/Antarktika) = Structural evolution and petrogenesis of the metamorphic basement complex of the northern Heimefrontfjella (western Dronning Maud Land/Antarctica). Berichte Zur Polarforsch. Rep. Polar Res. 191, 222. https://doi.org/10.2312/BzP_0171_1995

Bauer, W., Fielitz, W., Jacobs, J., Fanning, C.M., Spaeth, G., 2003a. Mafic Dykes from Heimefrontfjella and implications for the post-Grenvillian to pre-Pan-African geological evolution of western Dronning Maud Land, Antarctica. Antarct. Sci. 15, 379–391. https://doi.org/10.1017/S0954102003001391

Bauer, W., Jacobs, J., Fanning, C.M., Schmidt, R., 2003b. Late Mesoproterozoic Arc and Back-arc Volcanism in the Heimefrontfjella (East Antarctica) and Implications for the Palaeogeography at the Southeastern Margin of the Kaapvaal-Grunehogna Craton. Gondwana Res. 6, 449–465. https://doi.org/10.1016/S1342-937X(05)70998-9

Bauer, W., Siemes, H., Spaeth, G., Jacobs, J., 2016. Transpression and tectonic exhumation in the Heimefrontfjella, western orogenic front of the East African/Antarctic Orogen, revealed by quartz textures of high strain domains. Polar Res. 35, 25420. https://doi.org/10.3402/polar.v35.25420

Bauer, W., Thomas, R.J., Jacobs, J., 2003c. Proterozoic-Cambrian history of Dronning Maud Land in the context of Gondwana assembly. Geol. Soc. Lond. Spec. Publ. 206, 247–269. https://doi.org/10.1144/GSL.SP.2003.206.01.13

Beattie, J.C., 1909. Report of a magnetic survey of South Africa., Royal Society of London Publication. Cambridge University Press, United Kingdom.

Beckinsale, R.D., Tarney, J., Darbyshire, D.P.F., Humm, M.J., 1977. 24. Re-Sr and K-Ar age determinations on samples of the Falkland Plateau basement at site 330, DSDP. Initial Rep. Deep Sea Drill. Proj. XXXVI, 923–927. https://doi.org/10.2973/dsdp.proc.36.124.1977

Bell, R.T., Jefferson, C.W., 1987. An hypothesis for an Australian-Canadian connection in the Late Proterozoic and the birth of the Pacific Ocean, in: Proceeding on Pacific Rim International Congress. Presented at the Pacific Rim International Congress 87, Queensland, Australia, p. 29.

Ben-Avraham, Z., Hartnady, C.J.H., Malan, J.A., 1993. Early tectonic extension between the Agulhas Bank and the Falkland Plateau due to the rotation of the Lafonia microplate. Earth Planet. Sci. Lett. 117, 43–58. https://doi.org/10.1016/0012-821X(93)90116-Q

Benedetto, J.L., 2004. The Allochthony of the Argentine Precordillera Ten Years Later (1993–2003): A New Paleobiogeographic Test of the Microcontinental Model. Gondwana Res. 7, 1027–1039. https://doi.org/10.1016/S1342-937X(05)71082-0

Bisnath, A., Frimmel, H., 2005. Metamorphic evolution of the Maud Belt: P-T-t Path for high-grade gneisses in Gjelsvikfjella, Dronning Maud Land, East Antarctica. J. Afr. Earth Sci. - J AFR EARTH SCI 43, 505–524. https://doi.org/10.1016/j.jafrearsci.2005.09.007

Bisnath, A., Frimmel, H.E., 2004. Age and tectonothermal evolution of Gjelsvikfjella, Maud Belt, East Antarctica., in: Abstract Volume. Presented at the Geoscience Africa 2004, University of Witwatersrand, Johannesburg, South Africa, pp. 60–61.

Bisnath, A., Frimmel, H.E., Armstrong, R.A., Board, W.S., 2006. Tectono-thermal evolution of the Maud Belt: New SHRIMP U–Pb zircon data from Gjelsvikfjella, Dronning Maud Land, East Antarctica. Precambrian Res. 150, 95–121. https://doi.org/10.1016/j.precamres.2006.06.009

Board, W.S., Frimmel, H.E., Armstrong, R.A., 2005. Pan-African Tectonism in the Western Maud Belt: P–T–t Path for High-grade Gneisses in the H.U. Sverdrupfjella, East Antarctica. J. Petrol. 46, 671–699. https://doi.org/10.1093/petrology/egh093

Bohlen, S.R., 2015. Pressure-Temperature-Time Paths and a Tectonic Model for the Evolution of Granulites. J. Geol. https://doi.org/10.1086/629159

Borello, A.V., 1963. Sobre la geología de las Islas Malvinas. Ediciones Culturales Argentinas, Ministerio de Educación y Justicia, Dirección General de Cultura.

Borg, S.G., DePaolo, D.J., 1994. Laurentia, Australia, and Antarctica as a Late Proterozoic supercontinent: Constraints from isotopic mapping. Geology 22, 307–310. https://doi.org/10.1130/0091-7613(1994)022<0307:LAAAAA>2.3.CO;2

Boynton, W.V., 1984. Chapter 3 - Cosmochemistry of the Rare Earth Elements: Meteorite Studies, in: Henderson, P. (Ed.), Developments in Geochemistry, Rare Earth Element Geochemistry. Elsevier, pp. 63–114. https://doi.org/10.1016/B978-0-444-42148-7.50008-3

Brookfield, M.E., 1993. Neoproterozoic Laurentia-Australia fit. Geology 21, 683–686. https://doi.org/10.1130/0091-7613(1993)021<0683:NLAF>2.3.CO;2

Bruguier, O., Bosch, D., Pidgeon, R.T., Byrne, D.I., Harris, L.B., 1999. U-Pb chronology of the Northampton Complex, Western Australia – evidence for Grenvillian sedimentation, metamorphism and deformation and geodynamic implications. Contrib. Mineral. Petrol. 136, 258–272. https://doi.org/10.1007/s004100050537

Burrett, C., Berry, R., 2000. Proterozoic Australia–Western United States (AUSWUS) fit between Laurentia and Australia. Geology 28, 103–106. https://doi.org/10.1130/0091-7613(2000)28<103:PAUSAF>2.0.CO;2

Casquet, C., Baldo, E., Pankhurst, R.J., Rapela, C.W., Galindo, C., Fanning, C.M., Saavedra, J., 2001. Involvement of the Argentine Precordillera terrane in the Famatinian mobile belt: U-Pb SHRIMP and metamorphic evidence from the Sierra de Pie de Palo. Geology 29, 703–706. https://doi.org/10.1130/0091-7613(2001)029<0703:IOTAPT>2.0.CO;2

Chemale Jr., F., Ramos, V.A., Naipauer, M., Girelli, T.J., Vargas, M., 2018. Age of basement rocks from the Maurice Ewing Bank and the Falkland/Malvinas Plateau. Precambrian Res. 314, 28–40. https://doi.org/10.1016/j.precamres.2018.05.026

Cingolani, C., Varela, R., 1976. Investigaciones geologicas y geochronologicas en el extremo sur de la isla Gran Malvina, sector do Cabo Belgrano (Cabo Meredith), Islas Malvinas. Actas Sexto Congr. Geol. Argent. 457–473.

Clarke, J.M., 1913. Fósseis Devonianos do Paraná. Monogr. Serviço Geológico E Miner. Bras. 1–27, 1–353.

Cobb, M.M., Cawood, P.A., Kinny, P.D., Fitzsimons, I.C.W., 2001. SHRIMP U-Pb zircon ages from the Mullingarra Complex, Western Australia: Isotopic evidence for allochthonous blocks in the Pinjarra Orogen and implications for East Gondwana assembly, in: Geological Society of Australia Abstracts 64. Presented at the Geological Society of Australia Conference: a structural odyssey, Ulverstone, Australia, pp. 21–22.

Cornell, D.H., Thomas, R.J., 2006. Age and tectonic significance of the Banana Beach Gneiss, KwaZulu-Natal South Coast, South Africa. South Afr. J. Geol. 109, 335–340. https://doi.org/10.2113/gssajg.109.3.335

Cornell, D.H., Thomas, Robert J., Gibson, R., Moen, H.F.G., Reid, D.L., Moore, J.M., Gibson, R.L., 2006. The Namaqua-Natal Province, in: Johnson, M.R., Anhauesser, C.R., Thomas, Robert James (Eds.), The Geology of South Africa. Geological Society of South Africa, Johannesburg, South Africa, pp. 325–379.

Coutinho, J., Kräutner, H., Sassi, F., Schmid, R., Sen, S., 2007. 8. Amphibolite and Granulite, in: Metamorphic Rocks: A Classification and Glossary of Terms. Cambridge University Press, Cambridge.

Dalziel, I.W.D., 1991. Pacific margins of Laurentia and East Antarctica-Australia as a conjugate rift pair: Evidence and implications for an Eocambrian supercontinent. Geology 19, 598–601. https://doi.org/10.1130/0091-7613(1991)019<0598:PMOLAE>2.3.CO;2

de Capitani, C., Brown, T.H., 1987. The computation of chemical equilibrium in complex systems containing non-ideal solutions. Geochim. Cosmochim. Acta 51, 2639–2652. https://doi.org/10.1016/0016-7037(87)90145-1

de Capitani, C., Petrakakis, K., 2010. The computation of equilibrium assemblage diagrams with Theriak/Domino software. Am. Mineral. 95, 1006–1016. https://doi.org/10.2138/am.2010.3354

de Graciansky, P.C., Poag, C.W., et al., 1985. Initial Reports of the Deep Sea Drilling Project, 80, Initial Reports of the Deep Sea Drilling Project. U.S. Government Printing Office. https://doi.org/10.2973/dsdp.proc.80.1985

Digel, S.G., Ghent, E.D., Carr, S.D., Simony, P.S., 1998. Early Cretaceous kyanite-sillimanite metamorphism and Paleocene sillimanite overprint near Mount Cheadle, southeastern British Columbia: geometry, geochronology, and metamorphic implications. Can. J. Earth Sci. 35, 1070–1087. https://doi.org/10.1139/cjes-35-9-1070

Direen, N.G., Crawford, A.J., 2003. The Tasman Line: where is it, what is it, and is it Australia's Rodinian breakup boundary? Aust. J. Earth Sci. 50, 491–502.

Du Toit, 1927. A geological comparison of South America with South Africa. Carnegie Inst. Wash. Publ. 381, 1–157.

Du Toit, A.L., 1937. Our Wandering Continents; An Hypothesis of Continental Drifting, First Edition edition. ed. Oliver and Boyd.

du Toit, A.L., 1927. Our Wandering Continents, Publs Carnegie Instn. Oliver & Boyd.

Eastin, R., Faure, G., 1971. The Age of the Littlewood Volcanics of Coats Land, Antarctica. J. Geol. 79, 241–245. https://doi.org/10.1086/627612

Eglington, B.M., Harmer, R.E., Kerr, A., 1989. Isotope and geochemical constraints on Proterozoic crustal evolution in south-eastern Africa. Precambrian Res., Papers from the Meeting on Proterozoic Geochemistry 45, 159–174. https://doi.org/10.1016/0301-9268(89)90037-5

Eglington, B.M., Thomas, R.J., Armstrong, R.A., 2010. U-PB SHRIMP ZIRCON DATING OF

MESOPROTEROZOIC MAGMATIC ROCKS FROM THE SCOTTBURGH AREA, CENTRAL MZUMBE TERRANE, KWAZULU-NATAL, SOUTH AFRICA. South Afr. J. Geol. 113, 229–235. https://doi.org/10.2113/gssajg.113.2.229

Eglington, B.M., Thomas, R.J., Armstrong, R.A., Walraven, F., 2003. Zircon geochronology of the Oribi Gorge Suite, KwaZulu-Natal, South Africa: constraints on the timing of trans-current shearing in the Namaqua–Natal Belt. Precambrian Res. 123, 29–46. https://doi.org/10.1016/S0301-9268(03)00016-0

Eisbacher, G.H., 1985. Late proterozoic rifting, glacial sedimentation, and sedimentary cycles in the light of windermere deposition, Western Canada. Palaeogeogr. Palaeoclimatol. Palaeoecol., Proceedings of the Till Mauretania ’83 Symposium 51, 231–254. https://doi.org/10.1016/0031-0182(85)90087-2

Emmel, B., Jacobs, J., Crowhurst, P., Austegard, A., Schwarz-Schampera, U., 2008. Apatite single-grain (U-Th)/He data from Heimefrontfjella, East Antarctica: Indications for differential exhumation related to glacial loading? Tectonics 27. https://doi.org/10.1029/2007TC002220

Emmel, B., Jacobs, J., Daszinnies, M., 2009. Combined titanite and apatite fission-track data from Gjelsvikfjella, East Antarctica - another piece of a concealed intracontinental Permo-Triassic Gondwana rift basin? Geol. Soc. Lond. Spec. Publ. 324, 317–330. https://doi.org/10.1144/SP324.21

Evans, D.M., Windrim, D.P., Armstrong, R.A., 2007. Age of Metavolcanic rocks at the northern margin of the Namaqua-Natal Metamorphic Province in the Karas Mountains, Namibia, defined by SHRIMP U-Pb dating of zircons. South Afr. J. Geol. 110, 47–54. https://doi.org/10.2113/gssajg.110.1.47

Ewing, M., Hayes, D.E., 1970. Deep Sea Drilling in Antarctic waters. Geotimes 5, 15–16.

Fitzsimons, I., 2002. Comparison of detrital zircon ages in the Pinjarra Orogen (WA) and Maud Province (Antarctica): evidence for collision of Western Australia with southern Africa at 1100 Ma, in: Geological Society of Australia, Abstracts. p. 228.

Fitzsimons, I.C.W., 2003. Mix and match: using zircon geochronology to correlate late Mesoproterozoic metamorphic belts in Antarctica and Western Australia, in: Geological Society of Australia Abstracts 72. p. 69.

Fortey, R., Pankhurst, R.J., Herve, F., 1992. Devonian Trilobites at Buill, Chile (42°S). Andean Geol. 19, 133–143. https://doi.org/10.5027/andgeoV19n2-a01

Foschi, M., Cartwright, J.A., 2016. South Malvinas/Falkland Basin: Hydrocarbon migration and petroleum system. Mar. Pet. Geol. 77, 124–140. https://doi.org/10.1016/j.marpetgeo.2016.06.002

Foster, M.D., 1960. Interpretation of the composition of trioctahedral micas. Geol. Surv. Prof. Pap. 354, 49.

Franzese, J., Martino, R., 1998. Aspectos cinemáticos y tectónicos de la zona de cizalla de Gastre en la sierra de Calcapatul, provincia de Chubut, Argentina, in: Actas 2. Presented at the 10º Congreso Latinoamericanode Geologíay 6º Congreso Nacional de Geología Económica, Argentina, p. 3.

Frimmel, H.E., 2004. Formation of a late Mesoproterozoic supercontinent: the South Africa–East Antarctica connection, in: The Precambrian Earth: Tempos and Events. Elsevier.

Frost, B.R., Frost, C.D., 2008. On charnockites. Gondwana Res. 13, 30–44. https://doi.org/10.1016/j.gr.2007.07.006

Fuck, R.A., Brito Neves, B.B., Schobbenhaus, C., 2008. Rodinia descendants in South America. Precambrian Res., Testing the Rodinia Hypothesis: Records in its Building Blocks 160, 108–126. https://doi.org/10.1016/j.precamres.2007.04.018

Girelli, T.J., Chemale, F., Lavina, E.L.C., Laux, J.H., Bongiolo, E.M., Lana, C., 2018. Granulite accretion to Rio de la Plata Craton, based on zircon U-Pb-Hf isotopes: Tectonic implications for Columbia Supercontinent reconstruction. Gondwana Res. 56, 105–118. https://doi.org/10.1016/j.gr.2017.12.010

Gohl, K., Uenzelmann-Neben, G., 2001. The crustal role of the Agulhas Plateau, southwest Indian Ocean: evidence from seismic profiling. Geophys. J. Int. 144, 632–646. https://doi.org/10.1046/j.1365-246x.2001.01368.x

Goodge, J.W., Myrow, P., Williams, I.S., Bowring, S.A., 2002. Age and Provenance of the Beardmore Group, Antarctica: Constraints on Rodinia Supercontinent Breakup. J. Geol. 110, 393–406. https://doi.org/10.1086/340629

Gose, W.A., Helper, M.A., Connelly, J.N., Hutson, F.E., Dalziel, I.W.D., 1997. Paleomagnetic data and U-Pb isotopic age determinations from Coats Land, Antarctica: Implications for late Proterozoic plate reconstructions. J. Geophys. Res. Solid Earth 102, 7887–7902.

https://doi.org/10.1029/96JB03595
Grantham, G.H., Macey, P.H., Ingram, B.A., Roberts, M.P., Armstrong, R.A., Hokada, T., Shiraishi, K., Jackson, C., Bisnath, A., Manhica, V., 2008. Terrane correlation between Antarctica, Mozambique and Sri Lanka; comparisons of geochronology, lithology, structure and metamorphism and possible implications for the geology of southern Africa and Antarctica. Geol. Soc. Lond. Spec. Publ. 308, 91–119. https://doi.org/10.1144/SP308.4
Grantham, G.H., Mendonidis, P., Thomas, R.J., Satish-Kumar, M., 2012. Multiple origins of charnockite in the Mesoproterozoic Natal belt, Kwazulu-Natal, South Africa. Geosci. Front., Charnockites and Charnockites 3, 755–771. https://doi.org/10.1016/j.gsf.2012.05.006
Greentree, M.R., Li, Z.-X., Li, X.-H., Wu, H., 2006. Late Mesoproterozoic to earliest Neoproterozoic basin record of the Sibao orogenesis in western South China and relationship to the assembly of Rodinia. Precambrian Res. 151, 79–100. https://doi.org/10.1016/j.precamres.2006.08.002
Griffis, N.P., Montanez, I.P., Isbell, J., Gulbranson, E.L., Wimpenny, J., Yin, Q.Z., Cúneo, N.R., Pagani, M.A., Taboada, A.C., 2014. U-Pb Detrital Zircon Geochronologic Constraints on Depositional Age and Sediment Source Terrains of the Late Paleozoic Tepuel-Genoa Basin. AGU Fall Meet. Abstr. 21, EP21D-3566.
Groenewald, P.B., Grantham, G.H., Watkeys, M.K., 1991. Geological evidence for a Proterozoic to Mesozoic link between southeastern Africa and Dronning Maud Land, Antarctica. J. Geol. Soc. 148, 1115–1123. https://doi.org/10.1144/gsjgs.148.6.1115
Groenewald, P.B., Moyes, A.B., Grantham, G.H., Krynauw, J.R., 1995. East Antarctic crustal evolution: geological constraints and modelling in western Dronning Maud Land. Precambrian Res. 75, 231–250. https://doi.org/10.1016/0301-9268(95)80008-6
Harley, S.L., 1989. The origins of granulites: a metamorphic perspective. Geol. Mag. 126, 215–247. https://doi.org/10.1017/S0016756800022330
Harlov, D.E., 2012. The potential role of fluids during regional granulite-facies dehydration in the lower crust. Geosci. Front., Charnockites and Charnockites 3, 813–827. https://doi.org/10.1016/j.gsf.2012.03.007
Harmer, R., 1979. Pre-cape geology of the Tugela valley north of Kranskop, Natal (M. Sc.). University of Natal.
Harris, C., Watters, B.R., Groenewald, P.B., 1991. Geochemistry of the Mesozoic regional basic dykes of western Dronning Maud Land, Antarctica. Contrib. Mineral. Petrol. 107, 100–111. https://doi.org/10.1007/BF00311188
Harris, P.D., 1999. The geological evolution of Neumayerskarvet in the Northern Kirwanveggen, Western Dronning Maud Land, Antartica (Ph.D. Thesis). Rand Afrikaans University, Johannesburg.
Harris, P.D., Moyes, A.B., Fanning, C.M., Armstrong, R.A., Barton, J.M., Copperthwaite, Y.E., 1995. Zircon ion microprobe results from the Maudheim high-grade gneiss terrane, western Dronning Maud Land, Antarctica. Centen. Geocongress 3–7.
Henry, D.J., 2005. The Ti-saturation surface for low-to-medium pressure metapelitic biotites: Implications for geothermometry and Ti-substitution mechanisms. Am. Mineral. 90, 316–328. https://doi.org/10.2138/am.2005.1498
Henry, D.J., Guidotti, C.V., 2002. Titanium in biotite from metapelitic rocks: Temperature effects, crystal-chemical controls, and petrologic applications. Am. Mineral. 87, 375–382. https://doi.org/10.2138/am-2002-0401
Henry, D.J., Guidotti, C.V., 1985. Tourmaline as a petrogenetic indicator mineral: an example from the staurolite-grade metapelites of NW Maine. Am. Mineral. 70, 1–15.
Henry, D.J., Novak, M., Hawthorne, F.C., Ertl, A., Dutrow, B.L., Uher, P., Pezzotta, F., 2011. Nomenclature of the tourmaline-supergroup minerals. Am. Mineral. 96, 895–913. https://doi.org/10.2138/am.2011.3636
Herron, M.M., 1988. Geochemical Classification of Terrigenous Sands and Shales from Core or Log Data. SEPM J. Sediment. Res. Vol. 58. https://doi.org/10.1306/212F8E77-2B24-11D7-8648000102C1865D
Higgins, M.D., 1999. Origin of megacrysts in granitoids by textural coarsening: a crystal size distribution (CSD) study of microcline in the Cathedral Peak Granodiorite, Sierra Nevada, California. Geol. Soc. Lond. Spec. Publ. 168, 207–219. https://doi.org/10.1144/GSL.SP.1999.168.01.14
Hoffman, P.F., 1991. Did the breakout of laurentia turn gondwanaland inside-out? Science 252, 1409–1412. https://doi.org/10.1126/science.252.5011.1409
Hole, M.J., Ellam, R.M., MacDonald, D.I.M., Kelley, S.P., 2015. Gondwana break-up related magmatism in the Falkland Islands. J. Geol. Soc. 173, 108–126.

Holland, T., Powell, R., 2003. Activity composition relations for phases in petrological calculations: an asymmetric multicomponent formulation. Contrib. Mineral. Petrol. 145, 492–501. https://doi.org/10.1007/s00410-003-0464-z

Holland, T.J.B., Powell, R., 1998. An internally consistent thermodynamic data set for phases of petrological interest: AN INTERNALLY CONSISTENT THERMODYNAMIC DATA SET. J. Metamorph. Geol. 16, 309–343. https://doi.org/10.1111/j.1525-1314.1998.00140.x

Jackson, C., 1999. Characterization of Mesoproterozoic to Palaeozoic crustal evolution of Western Dronning Maud Land. Unpubl. Rep. South Afr. Natl. Antarct. Program Study 534, 80.

Jacobs, J., 2009. A review of two decades (1986 – 2008) of geochronological work in Heimefrontfjella, and geotectonic Interpretation of western Dronning Maud Land, East Antarctica. Polarforschung 79, 47–57.

Jacobs, J., Ahrendt, H., Kreutzer, H., Weber, K., 1995. K-Ar, 40Ar/39Ar and apatite fission-track evidence for Neoproterozoic and Mesozoic basement rejuvenation events in the Heimefrontfjella and Mannefallknausane (East Antarctica). Precambrian Res. 75, 251–262. https://doi.org/10.1016/0301-9268(95)80009-7

Jacobs, J., Bauer, W., Fanning, C., 2003a. New age constraints for Grenville-age metamorphism in western central Dronning Maud Land (East Antarctica), and implications for the palaeogeography of Kalahari in Rodinia. Int. J. Earth Sci. 92, 301–315. https://doi.org/10.1007/s00531-003-0335-x

Jacobs, J., Bauer, W., Fanning, C.M., 2003b. Late Neoproterozoic/Early Palaeozoic events in central Dronning Maud Land and significance for the southern extension of the East African Orogen into East Antarctica. Precambrian Res. 126, 27–53. https://doi.org/10.1016/S0301-9268(03)00125-6

Jacobs, J., Bauer, W., Spaeth, G., Thomas, R.J., Weber, K., 1996. Litholog and structure of the Grenville-aged (≈1.1 Ga) basement of heimefrontfjella (East Antarctica). Geol. Rundsch. 85, 800–821. https://doi.org/10.1007/BF02440112

Jacobs, J., Elburg, M., Läufer, A., Kleinhanns, I.C., Henjes-Kunst, F., Estrada, S., Ruppel, A.S., Damaske, D., Montero, P., Bea, F., 2015. Two distinct Late Mesoproterozoic/Early Neoproterozoic basement provinces in central/eastern Dronning Maud Land, East Antarctica: The missing link, 15–21° E. Precambrian Res., The structural, metamorphic and magmatic evolution of Mesoproterozoic orogens 265, 249–272. https://doi.org/10.1016/j.precamres.2015.05.003

Jacobs, J., Falter, M., Thomas, B., Kunz, J., Jessberger, E., 1997. 40Ar39Ar Thermochronological constraints on the structural evolution of the Mesoproterozoic Natal Metamorphic Province, SE Africa. Precambrian Res. 75, 71–92. https://doi.org/10.1016/S0301-9268(97)00042-9

Jacobs, J., Fanning, C.M., Bauer, W., 2003c. Timing of Grenville-age vs. Pan-African medium- to high grade metamorphism in western Dronning Maud Land (East Antarctica) and significance for correlations in Rodinia and Gondwana. Precambrian Res. 125, 1–20. https://doi.org/10.1016/S0301-9268(03)00048-2

Jacobs, J., Fanning, C.M., Henjes-Kunst, F., Olesch, M., Paech, H.-J., 1998. Continuation of the Mozambique Belt Into East Antarctica: Grenville-Age Metamorphism and Polyphase Pan-African High-Grade Events in Central Dronning Maud Land. J. Geol. 106, 385–406. https://doi.org/10.1086/516031

Jacobs, Joachim, Pisarevsky, S., Thomas, B., Fullgraf, T., 2008. The Kalahari Craton during the assembly and dispersal of Rodinia. Precambrian Res. 160, 142–158. https://doi.org/10.1016/j.precamres.2007.04.022

Jacobs, J., Pisarevsky, S., Thomas, R.J., Becker, T., 2008. The Kalahari Craton during the assembly and dispersal of Rodinia. Precambrian Res., Testing the Rodinia Hypothesis: Records in its Building Blocks 160, 142–158. https://doi.org/10.1016/j.precamres.2007.04.022

Jacobs, J., Thomas, B., 1999. From Rodinia to Gondwana, the East-Antarctic Perspective. Gondwana Res. 2, 567–567. https://doi.org/10.1016/S1342-937X(05)70198-2

Jacobs, J., Thomas, R.J., 1996. Pan-African rejuvenation of the c. 1.1 Ga Natal Metamorphic Province(South Africa):K–Ar muscovite and titanite fission track evidence. J. Geol. Soc. 153, 971–978. https://doi.org/10.1144/gsjgs.153.6.0971

Jacobs, J., Thomas, R.J., Armstrong, R.A., Henjes-Kunst, F., 1999. Age and thermal evolution of the Mesoproterozoic Cape Meredith Complex, West Falkland. J. Geol. Soc. 156, 917–928. https://doi.org/10.1144/gsjgs.156.5.0917

Jacobs, J., Thomas, R.J., Weber, K., 1993. Accretion and indentation tectonics at the southern edge of the Kaapvaal craton during the Kibaran (Grenville) orogeny. Geology 21, 203–206. https://doi.org/10.1130/0091-7613(1993)021<0203:AAITAT>2.3.CO;2

JanoušEk, V., Farrow, C.M., Erban, V., 2006. Interpretation of Whole-rock Geochemical Data in Igneous Geochemistry: Introducing Geochemical Data Toolkit (GCDkit). J. Petrol. 47, 1255–1259. https://doi.org/10.1093/petrology/egl013

Jiang, J., Lasaga, A.C., 1990. The effect of post-growth thermal events on growth-zoned garnet: implications for metamorphic P-T history calculations. Contrib. Mineral. Petrol. 105, 454–459. https://doi.org/10.1007/BF00286832

Johansson, Å., 2014. From Rodinia to Gondwana with the 'SAMBA' model—A distant view from Baltica towards Amazonia and beyond. Precambrian Res., Precambrian Supercontinents 244, 226–235. https://doi.org/10.1016/j.precamres.2013.10.012

Johansson, Å., 2009. Baltica, Amazonia and the SAMBA connection—1000 million years of neighbourhood during the Proterozoic? Precambrian Res. 175, 221–234. https://doi.org/10.1016/j.precamres.2009.09.011

Johnson, B.R., Glazner, A.F., 2010. Formation of K-feldspar megacrysts in granodioritic plutons by thermal cycling and late-stage textural coarsening. Contrib. Mineral. Petrol. 159, 599–619. https://doi.org/10.1007/s00410-009-0444-z

Johnston, S.T., Armstrong, R., Arima, M., 2001. Preliminary U-Pb geochronology of the Tugela terrane, Natal belt, eastern South Africa. Mem. Natl. Inst. Polar Res. 55, 40–58.

Jones, D.J.R., McCarthy, D.J., Dodd, T.J.H., 2019. Tectonostratigraphy and the petroleum systems in the Northern sector of the North Falkland Basin, South Atlantic. Mar. Pet. Geol. https://doi.org/10.1016/j.marpetgeo.2019.02.020

Karlstrom, K.E., Harlan, S.S., Williams, M.L., McLelland, J., Geissman, J.W., Åhäll, K.I., 1999. Refining Rodinia: Geologic evidence for the Australia-Western U.S. Connection in the Proterozoic. GSA Today 9, 2–7.

Kay, S.M., Orrell, S., Abbruzzi, J.M., 1996. Zircon and Whole Rock Nd-Pb Isotopic Evidence for a Grenville Age and a Laurentian Origin for the Basement of the Precordillera in Argentina. J. Geol. 104, 637–648.

Keidel, J., 1916. La geología de las sierras de la provincia de Buenos Aires y sus relaciones con las montañas de Sud Africa y los Andes. Dir. Gen. Minas Geol. E Hidrol. B. Aires An. 9, 1–78.

Keidel, J., 1913. Über das Alter, die Verbreitung und die gegenseitigen Beziehungen der verschiedenen tektonischen strukturen in den argentinischen Gebirgen. 12° Sess. Congrés Géologique Int. Tor. Compte Rendus 671–687.

Kimbell, G.S., Richards, P.C., 2008. The three-dimensional lithospheric structure of the Falkland Plateau region based on gravity modelling. J. Geol. Soc. 165, 795–806. https://doi.org/10.1144/0016-76492007-114

Kranidiotis, P., MacLean, W.H., 1987. Systematics of chlorite alteration at the Phelps Dodge massive sulfide deposit, Matagami, Quebec. Econ. Geol. 82, 1898–1911. https://doi.org/10.2113/gsecongeo.82.7.1898

Krippner, A., Meinhold, G., Morton, A.C., von Eynatten, H., 2014. Evaluation of garnet discrimination diagrams using geochemical data of garnets derived from various host rocks. Sediment. Geol. 306, 36–52. https://doi.org/10.1016/j.sedgeo.2014.03.004

Ksienzyk, A., Jacobs, J., Košler, J., Sircombe, K., 2007. A comparative provenance study of the late Mesoproterozoic Maud Belt (East Antarctica) and the Pinjarra Orogen (Western Australia): implications for a possible Mesoproterozoic Kalahari-Western Australia connection.

Ksienzyk, A.K., Jacobs, J., 2015. Western Australia-Kalahari (WAlahari) connection in Rodinia: Not supported by U/Pb detrital zircon data from the Maud Belt (East Antarctica) and the Northampton Complex (Western Australia). Precambrian Res., Supercontinental Cycles and Geodynamics 259, 207–221. https://doi.org/10.1016/j.precamres.2014.11.020

Ksienzyk, A.K., Jacobs, J., Boger, S.D., Košler, J., Sircombe, K.N., Whitehouse, M.J., 2012. U–Pb ages of metamorphic monazite and detrital zircon from the Northampton Complex: evidence of two orogenic cycles in Western Australia. Precambrian Res. Complete, 37–50. https://doi.org/10.1016/j.precamres.2011.12.011

Li, X.-H., Li, Z.-X., Ge, W., Zhou, H., Li, W., Liu, Y., Wingate, M.T.D., 2003. Neoproterozoic granitoids in South China: crustal melting above a mantle plume at ca. 825 Ma? Precambrian Res., Precambrian tectonics of East Asia and relevance to supercontintent evolution 122, 45–83. https://doi.org/10.1016/S0301-9268(02)00207-3

Li, Z.X., Bogdanova, S.V., Collins, A.S., Davidson, A., De Waele, B., Ernst, R.E., Fitzsimons, I.C.W., Fuck, R.A., Gladkochub, D.P., Jacobs, J., Karlstrom, K.E., Lu, S., Natapov, L.M., Pease, V., Pisarevsky, S.A., Thrane, K., Vernikovsky, V., 2008. Assembly, configuration, and break-up history of Rodinia: A synthesis. Precambrian Res., Testing the Rodinia Hypothesis: Records in its Building Blocks 160, 179–210. https://doi.org/10.1016/j.precamres.2007.04.021

Li, Z.X., Li, X.H., Kinny, P.D., Wang, J., 1999. The breakup of Rodinia: did it start with a mantle plume beneath South China? Earth Planet. Sci. Lett. 173, 171–181. https://doi.org/10.1016/S0012-821X(99)00240-X

Li, Z.-X., Zhang, L., Powell, C.M., 1995. South China in Rodinia: Part of the missing link between Australia–East Antarctica and Laurentia? Geology 23, 407–410. https://doi.org/10.1130/0091-7613(1995)023<0407:SCIRPO>2.3.CO;2

Lindeque, A., Wit, M.J.D., Ryberg, T., Weber, M., Chevallier, L., 2011. DEEP CRUSTAL PROFILE ACROSS THE SOUTHERN KAROO BASIN AND BEATTIE MAGNETIC ANOMALY, SOUTH AFRICA: AN INTEGRATED INTERPRETATION WITH TECTONIC IMPLICATIONS. South Afr. J. Geol. 114, 265–292. https://doi.org/10.2113/gssajg.114.3-4.265

Ling, W., Gao, S., Zhang, B., Li, H., Liu, Y., Cheng, J., 2003. Neoproterozoic tectonic evolution of the northwestern Yangtze craton, South China: implications for amalgamation and break-up of the Rodinia Supercontinent. Precambrian Res., Precambrian tectonics of East Asia and relevance to supercontintent evolution 122, 111–140. https://doi.org/10.1016/S0301-9268(02)00222-X

Llambías, E.J., Varela, R., Basei, M., Sato, A.M., 2002. Deformación dúctil y metamorfismo neopaleozoico en Yaminué y su relación con la fase orogénica San Rafael. 15 ° Congr. Geológico Argent. Actas 3, 123–128.

Loewy, S.L., Dalziel, I.W.D., Pisarevsky, S., Connelly, J.N., Tait, J., Hanson, R.E., Bullen, D., 2011. Coats Land crustal block, East Antarctica: A tectonic tracer for Laurentia? Geology 39, 859–862. https://doi.org/10.1130/G32029.1

Ludwig, K.R., 2012. Users Manual for ISOPLOT/EX, Version 3. A Geochronological Toolkit for Microsoft Excel, Berkeley Geochronological Centre Special Publication.

Ludwig, W.J., Krasheninnikov, V.A., Basov, I.A., Bayer, U., Bloemendal, J., Bornhold, B., Ciesielsky, P.F., Goldstein, E.H., Robert, C., Salloway, J., Usher, J.L., von der Hick, H., Weaver, F.M., Wise Jr, S.W., 1983. Initial Reports of the Deep Sea Drilling Project, 71, Initial Reports of the Deep Sea Drilling Project. U.S. Government Printing Office, Washington, D. C.

Ludwig, W.J., Rabinowitz, P.D., 1982. The collision complex of the North Scotia Ridge. J. Geophys. Res. Solid Earth 87, 3731–3740. https://doi.org/10.1029/JB087iB05p03731

Manceñido, M., Damborenea, S., 1984. Megafauna de invertebrados paleozoicos y mesozoicos, in: Geología Y Recursos Naturales De La Provincia De Río Negro. pp. 413–465.

Mange, M.A., Morton, A.C., 2007. Geochemistry of heavy minerals, in: Wright, D.T., Mange, M.A. (Eds.), Heavy Minerals in Use, Developments in Sedimentology. Elsevier, Amsterdam, pp. 345–391.

Marshall, J.E.A., 1994a. The Falkland Islands: A key element in Gondwana paleogeography. Tectonics 13, 499–514. https://doi.org/10.1029/93TC03468

Marshall, J.E.A., 1994b. The Falkland Islands and the early fragmentation of Gondwana: implications for hydrocarbon exploration in the Falkland Plateau. Mar. Pet. Geol. 11, 631–636. https://doi.org/10.1016/0264-8172(94)90073-6

Martínez Dopico, C.I., López de Luchi, M.G., Rapalini, A.E., Kleinhanns, I.C., 2011. Crustal segments in the North Patagonian Massif, Patagonia: An integrated perspective based on Sm–Nd isotope systematics. J. South Am. Earth Sci. 31, 324–341. https://doi.org/10.1016/j.jsames.2010.07.009

Masao, A., Kazuhiro, S., Mamoru, A., 1996. Monazite ages by the chemical Th-U-total Pb isochron method for pelitic gneisses from the eastern Sor Rondane Mountains, East Antarctica, in: Proceedings of the NIPR Symposium on Antarctic Geosciences 9. Presented at the Proceedings of the NIPR Symposium, National Institute of Polar Research, Tokyo, Japan, pp. 49–64.

McCourt, S., Armstrong, R.A., Grantham, G.H., Thomas, R.J., 2006. Geology and evolution of the Natal belt, South Africa. J. Afr. Earth Sci. 46, 71–92. https://doi.org/10.1016/j.jafrearsci.2006.01.013

McMenamin, Mark A. S., McMenamin, D.L., 1990. The Emergence of Animals: The Cambrian Breakthrough. Columbia University Press.

McMenamin, M.A.S., McMenamin, D.L.S., 1990. The Emergence of Animals: The Cambrian Breakthrough 217.

Mendonidis, P., Armstrong, R.A., 2016. U–Pb Zircon (SHRIMP) ages of granite sheets and timing of deformational events in the Natal Metamorphic Belt, southeastern Africa: Evidence for deformation partitioning and implications for Rodinia reconstructions. Precambrian Res. 278, 22–33. https://doi.org/10.1016/j.precamres.2016.03.003

Mendonidis, P., Armstrong, R.A., 2009. A new U-Pb zircon age for the Portobello Granite from the southern part of the Natal Metamorphic Belt. South Afr. J. Geol. 112, 197–208.

https://doi.org/10.2113/gssajg.112.2.197

Mendonidis, P., Armstrong, R.A., Eglington, B.M., Grantham, G.H., Thomas, R.J., 2002. Metamorphic history and U-Pb Zircon (SHRIMP) geochronology of the Glenmore Granite: Implications for the tectonic evolution of the Natal Metamorphic Province. South Afr. J. Geol. 105, 325–336. https://doi.org/10.2113/1050325

Mendonidis, P., Grantham, G.H., 2003. Petrology, Origin and Metamorphic History of Proterozoic-aged Granulites of the Natal Metamorphic Province, Southeastern Africa. Gondwana Res. 6, 607–628. https://doi.org/10.1016/S1342-937X(05)71011-X

Mendonidis, P., Thomas, R.J., Grantham, G.H., Armstrong, R.A., 2015a. Geochronology of emplacement and charnockite formation of the Margate Granite Suite, Natal Metamorphic Province, South Africa: Implications for Natal-Maud belt correlations. Precambrian Res., The structural, metamorphic and magmatic evolution of Mesoproterozoic orogens 265, 189–202. https://doi.org/10.1016/j.precamres.2015.02.013

Mendonidis, P., Thomas, R.J., Grantham, G.H., Armstrong, R.A., 2015b. Geochronology of emplacement and charnockite formation of the Margate Granite Suite, Natal Metamorphic Province, South Africa: Implications for Natal-Maud belt correlations. Precambrian Res., The structural, metamorphic and magmatic evolution of Mesoproterozoic orogens 265, 189–202. https://doi.org/10.1016/j.precamres.2015.02.013

Middlemost, E.A.K., 1994. Naming materials in the magma/igneous rock system. Earth-Sci. Rev. 37, 215–224. https://doi.org/10.1016/0012-8252(94)90029-9

Mikhalsky, E.V., Sheraton, J.W., Hahne, K., 2006. Charnockite composition in relation to the tectonic evolution of East Antarctica. Gondwana Res. 9, 379–397. https://doi.org/10.1016/j.gr.2005.11.007

Millar, I.L., Pankhurst, R.J., 1987. Rb-Sr geochronology of the region between the Antarctic Peninsula and the Transantarctic Mountains: Haag nunataks and Mesozoic granitoids, in: McKenzie, G.D. (Ed.), Geophysical Monograph Series. American Geophysical Union, Washington, D. C., pp. 151–160.

Mitchell, C., Taylor, G.K., Cox, K.G., Shaw, J., 1986. Are the Falkland Islands a rotated microplate? Nature 319, 131–134. https://doi.org/10.1038/319131a0

Moody, J.B., Jenkins, J.E., Meyer, D., 1985. An experimental investigation of the albitization of plagioclase. Can. Mineral. 23, 583–596.

Moores, E.M., 1991. Southwest U.S.-East Antarctic (SWEAT) connection: A hypothesis. Geology 19, 425–428. https://doi.org/10.1130/0091-7613(1991)019<0425:SUSEAS>2.3.CO;2

Moreira, P., Fernández, R., Hervé, F., Fanning, C.M., Schalamuk, I.A., 2013. Detrital zircons U-Pb SHRIMP ages and provenance of La Modesta Formation, Patagonia Argentina. J. South Am. Earth Sci. 47, 32–46. https://doi.org/10.1016/j.jsames.2013.05.010

Moyes, A.B., Barton, J.M., 1990. A review of isotopic data from western Dronning Maud Land, Antarctica. Zentralblatt Geol. Palaeontol. Teil 1 1.

Moyes, A.B., Barton, J.M., Groenewald, P.B., 1993. Late Proterozoic to Early Palaeozoic tectonism in Dronning Maud Land, Antarctica: supercontinental fragmentation and amalgamation. J. Geol. Soc. 150, 833–842. https://doi.org/10.1144/gsjgs.150.5.0833

Moyes, A.B., Harris, P.D., 1996. Geological evolution of western Dronning Maud Land within a Gondwana framework. (South African National Antarctic Programme Final Report), Radiogenic Isotope Geology Project 1991-1996. Johannesburg.

Mundl, A., Ntaflos, T., Ackerman, L., Bizimis, M., Bjerg, E.A., Hauzenberger, C.A., 2015. Mesoproterozoic and Paleoproterozoic subcontinental lithospheric mantle domains beneath southern Patagonia: Isotopic evidence for its connection to Africa and Antarctica. Geology 43, 39–42. https://doi.org/10.1130/G36344.1

Mussett, A.E., Taylor, G.K., 1994. 40Ar-39Ar ages for dykes from the Falkland Islands with implications for the break-up of southern Gondwanaland. J. Geol. Soc. 151, 79–81. https://doi.org/10.1144/gsjgs.151.1.0079

Musumeci, G., 2002. Sillimanite-bearing shear zones in syntectonic leucogranite: fluid-assisted brittle–ductile deformation under amphibolite facies conditions. J. Struct. Geol. 24, 1491–1505. https://doi.org/10.1016/S0191-8141(01)00153-5

Nance, R.D., Murphy, J.B., Santosh, M., 2014. The supercontinent cycle: A retrospective essay. Gondwana Res. 25, 4–29. https://doi.org/10.1016/j.gr.2012.12.026

Nelis, M., MOSHER, S., D. CARLSON, W., 1989. Grenville-age orogeny in the Llano Uplift of central Texas: Deformation and metamorphism of the Rough Ridge Formation. Geol. Soc. Am. Bull. - GEOL SOC AMER BULL 101, 876–883. https://doi.org/10.1130/0016-7606(1989)101<0876:GAOITL>2.3.CO;2

Otani, M., Wallis, S., 2006. Quartz lattice preferred orientation patterns and static recrystallization: Natural examples from the Ryoke belt, Japan. Geology 34, 561–564. https://doi.org/10.1130/G22430.1

Owada, M., Baba, S., Läufer, A., Elvevold, S., Shiraishi, K., Jacobs, J., 2003. Geology of eastern Mühlig-Hofmannfjella and Filchnerfjella in Dronning Maud Land, East Antarctica: A preliminary report on a Japan-Norway-Germany joint geological investigation. Polar 16, 108–136.

Pankhurst, R.J., Rapela, C.W., Fanning, C.M., Márquez, M., 2006. Gondwanide continental collision and the origin of Patagonia. Earth-Sci. Rev. 76, 235–257. https://doi.org/10.1016/j.earscirev.2006.02.001

Park, J.K., Buchan, K.L., Harlan, S.S., 1995. A proposed giant radiating dyke swarm fragmented by the separation of Laurentia and Australia based on paleomagnetism of ca. 780 Ma mafic intrusions in western North America. Earth Planet. Sci. Lett. 132, 129–139. https://doi.org/10.1016/0012-821X(95)00059-L

Parsiegla, N., Gohl, K., Uenzelmann-Neben, G., 2008. The Agulhas Plateau: structure and evolution of a Large Igneous Province. Geophys. J. Int. 174, 336–350. https://doi.org/10.1111/j.1365-246X.2008.03808.x

Passchier, C.W., Trouw, R.A.J., 2005. Microtectonics, 2nd ed. Springer, New York.

Pearce, J.A., Harris, N.B.W., Tindle, A.G., 1984. Trace Element Discrimination Diagrams for the Tectonic Interpretation of Granitic Rocks. J. Petrol. 25, 956–983. https://doi.org/10.1093/petrology/25.4.956

Pirajno, F., Smithies, R.H., 1992. The FeO/(FeO+MgO) ratio of tourmaline: A useful indicator of spatial variations in granite-related hydrothermal mineral deposits. J. Geochem. Explor. 42, 371–381. https://doi.org/10.1016/0375-6742(92)90033-5

Pisarevsky, S.A., Elming, S.-Å., Pesonen, L.J., Li, Z.-X., 2014. Mesoproterozoic paleogeography: Supercontinent and beyond. Precambrian Res., Precambrian Supercontinents 244, 207–225. https://doi.org/10.1016/j.precamres.2013.05.014

Pisarevsky, S.A., Wingate, M.T.D., Powell, C.M., Johnson, S., Evans, D.A.D., 2003. Models of Rodinia assembly and fragmentation. Geol. Soc. Lond. Spec. Publ. 206, 35–55. https://doi.org/10.1144/GSL.SP.2003.206.01.04

Powell, C.M., Li, Z.X., McElhinny, M.W., Meert, J.G., Park, J.K., 1993. Paleomagnetic constraints on timing of the Neoproterozoic breakup of Rodinia and the Cambrian formation of Gondwana. Geology 21, 889–892. https://doi.org/10.1130/0091-7613(1993)021<0889:PCOTOT>2.3.CO;2

Powell, C.M., Pisarevsky, S.A., 2002. Late Neoproterozoic assembly of East Gondwana. Geology 30, 3–6. https://doi.org/10.1130/0091-7613(2002)030<0003:LNAOEG>2.0.CO;2

Powell, C.McA., Pisarevsky, S., Wingate, M.T.D., 2001. A New Shape for Rodinia. Gondwana Res. 4, 736–737.

Quesnel, Y., Weckmann, U., Ritter, O., Stankiewicz, J., Lesur, V., Mandea, M., Langlais, B., Sotin, C., Galdéano, A., 2009. Simple models for the Beattie Magnetic Anomaly in South Africa. Tectonophysics, Magnetic Anomalies 478, 111–118. https://doi.org/10.1016/j.tecto.2008.11.027

Rabinowitz, P.D., LaBrecque, J.L., 1979. The Mesozoic South Atlantic Ocean and evolution of its continental margins. J. Geophys. Res. Solid Earth 84, 5973–6002. https://doi.org/10.1029/JB084iB11p05973

Ramos, V.A., 2010. The Grenville-age basement of the Andes. J. South Am. Earth Sci., The Grenville Orogen in Central and South America 29, 77–91. https://doi.org/10.1016/j.jsames.2009.09.004

Ramos, V.A., 2008. Patagonia: A paleozoic continent adrift? J. South Am. Earth Sci. 26, 235–251. https://doi.org/10.1016/j.jsames.2008.06.002

Ramos, V.A., 2004. Cuyania, an Exotic Block to Gondwana: Review of a Historical Success and the Present Problems. Gondwana Res. 7, 1009–1026. https://doi.org/10.1016/S1342-937X(05)71081-9

Ramos, V.A., Basei, M.A., 1997. The Basement of Chilenia: An Exotic Continental Terrane to Gondwana During the Early Paleozoic, in: Symposium on Terrane Dynamics. New Zealand, pp. 140–143.

Ramos, V.A., Cingolani, C., Junior, F.C., Naipauer, M., Rapalini, A., 2017. The Malvinas (Falkland) Islands revisited: The tectonic evolution of southern Gondwana based on U-Pb and Lu-Hf detrital zircon isotopes in the Paleozoic cover. J. South Am. Earth Sci. 76, 320–345. https://doi.org/10.1016/j.jsames.2016.12.013

Ramos, V.A., Jordan, T.E., Allmendinger, R.W., Mpodozis, C., Kay, S.M., Cortés, J.M., Palma, M., 1986. Paleozoic terranes of the central Argentine-Chilean Andes. Tectonics 5, 855–880. https://doi.org/10.1029/TC005i006p00855

Ramos, V.A., Naipauer, M., 2014. Patagonia: where does it come from? J. Iber. Geol. 40, 367–379. https://doi.org/10.5209/rev_JIGE.2014.v40.n2.45304

Ramos, V.A., Riccardi, A.C., Rolleri, E.O., 2004. Límites naturales del norte de la Patagonia. Rev. Asoc. Geológica Argent. 59, 785–786.

Rapalini, A.E., Astini, R.A., 1998. Paleomagnetic confirmation of the Laurentian origin of the Argentine Precordillera. Earth Planet. Sci. Lett. 155, 1–14. https://doi.org/10.1016/S0012-821X(97)00196-9

Rapela, C.W., Pankhurst, R.J., 1992. The granites of northern Patagonia and the Gastre Fault System in relation to the break -up of Gondwana, in: Storey, B.C., Alabaster, T., Pankhurst, R.J. (Eds.), Geological Society, London, Special Publications. Geological Society of London, London, pp. 209–220.

Rapela, C.W., Pankhurst, R.J., Oviedo, E.S., 1991. The Gastre Fault System: an intraplate boundary during the initial rifting Gondwana, in: Comunicaciones. Presented at the 5º International Circum-Pacific Terrane Conference, Departamento de Geología y Geofísica de la Universidad de Chile, Santiago, pp. 186–193.

Rex, D.C., Tanner, P.W.G., 1982. Precambrian age for gnaisses at Cape Meredith in the Falkland Islands, in: Craddock, C. (Ed.), Antarctic Geoscience, B. University of Wisconsin Press, International Union of Geological Sciences, pp. 107–108.

Richards, P.C., Hillier, B.V., 2000. Post-Drilling Analysis of the North Falkland Basin— Part 1: Tectono-Stratigraphic Framework. J. Pet. Geol. 23, 253–272. https://doi.org/10.1111/j.1747-5457.2000.tb01019.x

Richards, P.C., Stone, P., Kimbell, G.S., Mcintosh, W.C., Phillips, E.R., 2012. Mesozoic magmatism in the falkland islands (south atlantic) and their offshore sedimentary basins. J. Pet. Geol. 36, 61–73. https://doi.org/10.1111/jpg.12542

Richter, R., Richter, E., 1942. Die Trilobiten der Weismes-Schichten am Hohen Venn, mit Bemerkungen über die Malvinocaffrische Provinz. Senckenbergiana 25, 156–179.

Rieder, M., Cavazzini, G., D'Yakonov, Y., Kamenetskii, V.A., Gottardi, G., Guggenheim, S., Koval, P., Müller, G., Neiva, A.M.R., Radolosvich, E.W., Robert, J.L., Sassi, F., Takeda, T., Weiss, Z., Wones, D.R., 1998. Nomenclature of the micas. Can. Mineral. 36, 1–7.

Roberts, N.M.W., 2013. The boring billion? – Lid tectonics, continental growth and environmental change associated with the Columbia supercontinent. Geosci. Front., Thematic Section: Antarctica – A window to the far off land 4, 681–691. https://doi.org/10.1016/j.gsf.2013.05.004

Roberts, N.M.W., Slagstad, T., Viola, G., 2015. The structural, metamorphic and magmatic evolution of Mesoproterozoic orogens. Precambrian Res., The structural, metamorphic and magmatic evolution of Mesoproterozoic orogens 265, 1–9. https://doi.org/10.1016/j.precamres.2015.05.031

Roser, B.P., Korsch, R.J., 1988. Provenance signatures of sandstone-mudstone suites determined using discriminant function analysis of major-element data. Chem. Geol. 67, 119–139. https://doi.org/10.1016/0009-2541(88)90010-1

Ross, G.M., Parrish, R.R., Winston, D., 1992. Provenance and U-Pb geochronology of the Mesoproterozoic Belt Supergroup (northwestern United States): implications for age of deposition and pre-Panthalassa plate reconstructions. Earth Planet. Sci. Lett. 113, 57–76. https://doi.org/10.1016/0012-821X(92)90211-D

Ross, G.M., Villeneuve, M., 2003. Provenance of the Mesoproterozoic (1.45 Ga) Belt basin (western North America): Another piece in the pre-Rodinia paleogeographic puzzle. GSA Bull. 115, 1191–1217. https://doi.org/10.1130/B25209.1

Rudnick, R.L., Fountain, D.M., 1995. Nature and composition of the continental crust: A lower crustal perspective. Rev. Geophys. 33, 267–309. https://doi.org/10.1029/95RG01302

Ruppel, A., Jacobs, J., Eagles, G., Läufer, A., Jokat, W., 2018. New geophysical data from a key region in East Antarctica: Estimates for the spatial extent of the Tonian Oceanic Arc Super Terrane (TOAST). Gondwana Res. 59. https://doi.org/10.1016/j.gr.2018.02.019

Sato, A.M., Tickyj, H., Llambías, E.J., Stipp Basei, M.A., González, P.D., 2004. Las Matras Block, Central Argentina (37°S-67°W): the Southernmost Cuyania Terrane and its Relationship with the Famatinian Orogeny. Gondwana Res. 7, 1077–1087. https://doi.org/10.1016/S1342-937X(05)71085-6

Scheiber-Enslin, S., Ebbing, J., Webb, S.J., 2014. An integrated geophysical study of the Beattie Magnetic Anomaly, South Africa. Tectonophysics 636, 228–243. https://doi.org/10.1016/j.tecto.2014.08.021

Schilling, M.E., Carlson, R.W., Conceição, R.V., Dantas, C., Bertotto, G.W., Koester, E., 2008. Re–Os isotope constraints on subcontinental lithospheric mantle evolution of southern South America.

Earth Planet. Sci. Lett. 268, 89–101. https://doi.org/10.1016/j.epsl.2008.01.005

Schilling, M.E., Carlson, R.W., Tassara, A., Conceição, R.V., Bertotto, G.W., Vásquez, M., Muñoz, D., Jalowitzki, T., Gervasoni, F., Morata, D., 2017. The origin of Patagonia revealed by Re-Os systematics of mantle xenoliths. Precambrian Res. 294, 15–32. https://doi.org/10.1016/j.precamres.2017.03.008

Schimschal, C.M., Jokat, W., 2019. The Falkland Plateau in the context of Gondwana breakup. Gondwana Res. 68, 108–115. https://doi.org/10.1016/j.gr.2018.11.011

Schimschal, C.M., Jokat, W., 2018. The crustal structure of the continental margin east of the Falkland Islands. Tectonophysics 724–725, 234–253. https://doi.org/10.1016/j.tecto.2017.11.034

Schmid, R., Fettes, D., Harte, B., Eleutheria, D., Desmons, J., 2007. 1. How to name a metamorphic rock, in: Metamorphic Rocks: A Classification and Glossary of Terms. Cambridge University Press, Cambridge.

Schulze, P., 1992. Petrogenese des metamorphen Grundgebirges der zentralen Heimefrontfjella (westliches Dronning Maud Land / Antarktis) = Petrogenesis of the metamorphic basement complex of the central Heimefrontfjella mountains (western Dronning Maud Land / Antarctica). Berichte Zur Polarforsch. Rep. Polar Res. 117, 321. https://doi.org/10.2312/BzP_0117_1992

Scrutton, R.A., 1973. Structure and evolution of the sea floor south of South Africa. Earth Planet. Sci. Lett. 19, 250–256. https://doi.org/10.1016/0012-821X(73)90125-8

Shau, Y.-H., Yang, H.-Y., Peacor, D.R., 1991. On oriented titanite and rutile inclusions in sagenitic biotite. Am. Mineral. 76, 1205–1217.

Smith, J.V., Brown, W.L., 1988. Feldspar Minerals. Springer Berlin Heidelberg, Berlin, Heidelberg.

Spear, F.S., 1993. Metamorphic Phase Equilibria and Pressure-Temperature-Time Paths. Mineralogical Society of America, Washington, D. C.

Spear, F.S., 1991. On the interpretation of peak metamorphic temperatures in light of garnet diffusion during cooling. Metamorph. Geol. 9, 379–388. https://doi.org/10.1111/j.1525-1314.1991.tb00533.x

Spear, F.S., Peacock, S.M. (Eds.), 1989. Petrologic determination of metamorphic pressure-temperature-time paths, in: Metamorphic Pressure-Temperature-Time Paths, American Geophysical Union Short Course In Geology. AGU, Boulder, Colorado, pp. 1–55.

Spencer, C.J., Thomas, R.J., Roberts, N.M.W., Cawood, P.A., Millar, I., Tapster, S., 2015a. Crustal growth during island arc accretion and transcurrent deformation, Natal Metamorphic Province, South Africa: New isotopic constraints. Precambrian Res., The structural, metamorphic and magmatic evolution of Mesoproterozoic orogens 265, 203–217. https://doi.org/10.1016/j.precamres.2015.05.011

Spencer, C.J., Thomas, R.J., Roberts, N.M.W., Cawood, P.A., Millar, I., Tapster, S., 2015b. Crustal growth during island arc accretion and transcurrent deformation, Natal Metamorphic Province, South Africa: New isotopic constraints. Precambrian Res., The structural, metamorphic and magmatic evolution of Mesoproterozoic orogens 265, 203–217. https://doi.org/10.1016/j.precamres.2015.05.011

Stanca, R.M., Paton, D.A., Hodgson, D.M., McCarthy, D.J., Mortimer, E.J., 2019. A revised position for the rotated Falkland Islands microplate. J. Geol. Soc. jgs2018-163. https://doi.org/10.1144/jgs2018-163

Stone, P., Kimbell, G.S., Richards, P.C., 2009. Rotation of the Falklands microplate reassessed after recognition of discrete Jurassic and Cretaceous dyke swarms. Pet. Geosci. 15, 279–287. https://doi.org/10.1144/1354-079309-847

Stone, P., Richards, P.C., Kimbell, G.S., Esser, R.P., Reeves, D., 2008. Cretaceous dykes discovered in the Falkland Islands: implications for regional tectonics in the South Atlantic. J. Geol. Soc. 165, 1–4. https://doi.org/10.1144/0016-76492007-072

Storey, B.C., Curtis, M.L., Ferris, J.K., Hunter, M.A., Livermore, R.A., 1999. Reconstruction and break-out model for the Falkland Islands within Gondwana. J. Afr. Earth Sci., Gondwana-10: Event Stratigraphy of Gondwana, Proceedings volume 1 29, 153–163. https://doi.org/10.1016/S0899-5362(99)00086-X

Storey, B.C., Pankhurst, R.J., Johnson, A.C., 1994. The Grenville Province within Antarctica: a test of the SWEAT hypothesis. J. Geol. Soc. 151, 1–4. https://doi.org/10.1144/gsjgs.151.1.0001

Suggate, S.M., Hall, R., 2014. Using detrital garnet compositions to determine provenance: a new compositional database and procedure. Geol. Soc. Lond. Spec. Publ. 386, 373–393. https://doi.org/10.1144/SP386.8

Tarney, J., 1977. 23. Petrology, Mineralogy, and Geochemistry of the Falkland Plateau basement Rocks, site 330, Deep Sea Drilling Project. Initial Rep. Deep Sea Drill. Proj. XXXVI. https://doi.org/10.2973/dsdp.proc.36.123.1977

Taylor, G.K., Shaw, J., 1989. The Falkland Islands: New palaeomagnetic data and their origin as a displaced terrane from southern Africa, in: Hillhouse, J. W. (Ed.), Deep Structure and Past Kinematics of Accreted Terranes., Geophysical Monographs. AGU, Washington, D. C., pp. 59–72.

Teraoka Y., Suzuki M., Hayashi T., Kawakami K., 1997. Detrital Garnets from Paleozoic and Mesozoic snadstones in the Onogawa area, East Kyushu, Southwest Japan. Bull. Fac. Sch. Educ. Hiroshima Univ. 19, 87–101.

Teraoka, Y., Suzuki, M., Kawakami, K., 1998. Provenance of Cretaceous and Paleogene sediments in the Median Zone of Southwest Japan. Bull. Geol. Soc. Jpn. 49, 394–411.

Thistlewood, L., Leat, P.T., Millar, I.L., Storey, B.C., Vaughan, A.P.M., 1997. Basement geology and Palaeozoic–Mesozoic mafic dykes from the Cape Meredith Complex, Falkland Islands: a record of repeated intracontinental extension. Geol. Mag. 134, 355–367.

Thomas, R.J., 1989. A tale of two tectonic terranes. South Afr. J. Geol. 92, 306–321.

Thomas, R.J., Agenbacht, A.L.D., Cornell, D.H., Moore, J.M., 1994. The Kibaran of southern Africa: Tectonic evolution and metallogeny. Ore Geol. Rev., Kibaran (Mid-Proterozoic) Metallogeny in Central and Southern Africa 9, 131–160. https://doi.org/10.1016/0169-1368(94)90025-6

Thomas, R.J., Armstrong, R.A., Eglington, B.M., 2003. Geochronology of the Sikombe Granite, Transkei, Natal Metamorphic Province, South Africa. South Afr. J. Geol. 106, 403–408. https://doi.org/10.2113/106.4.403

Thomas, R.J., De Beer, C.H., Bowring, S.A., 1996. A comparative study of the Mesoproterozoic late orogenic porphyritic granitoids of southwest Namaqualand and Natal, South Africa. J. Afr. Earth Sci., IGCP 348 (Mozambique and Related Belts) 23, 485–508. https://doi.org/10.1016/S0899-5362(97)00014-6

Thomas, R.J., Du Plessis, A.J., Fitch, F., Marshall, C.G.A., Miller, J.A., Von Brunn, V., Watkeys, M.K., 1992. Geological studies in southern Natal and Transkei: implications for the Cape Orogen, in: De Wit, M.J., Ransome, I.G.D. (Eds.), Inversion Tectonics of the Cape Fold Belt, Karoo and Cretaceous Basins of Southern Africa. pp. 229–236.

Thomas, R.J., Eglington, B.M., 1990. A Rb-Sr, Sm-Nd and U-Pb zircon isotopic study of the Mzumbe Suite, the oldest intrusive granitoid in southern Natal, South Africa. South Afr. J. Geol. 93, 761–765.

Thomas, R.J., Henjes-Kunst, F., Jacobs, J., 1998. Pre-lamprophyre mafic dykes of the Cape Meredith Complex, West Falkland. Geol. Mag. 135, 495–500.

Thomas, R.J., Jacobs, J., Eglington, B.M., 2000. Geochemistry and isotopic evolution of the Mesoproterozoic Cape Meredith Complex, West Falkland. Geol. Mag. 137, 537–553.

Thomas, R.J., Jacobs, J., Weber, K., 1997. Geology of the Mesoproterozoic Cape Meredith Complex, West Falkland, in: Ricci, C.A. (Ed.), The Antarctic Region: Geological Evolution and Processes. Terra Antarctica, Siena, pp. 21–30.

Thomas, W.A., Astini, R.A., 1996. The Argentine Precordillera: A Traveler from the Ouachita Embayment of North American Laurentia. Science 273, 752–757. https://doi.org/10.1126/science.273.5276.752

Thomson, K., 1998. When did the Falklands rotate? Mar. Pet. Geol. 15, 723–736. https://doi.org/10.1016/S0264-8172(98)00050-6

Uenzelmann-Neben, G., Gohl, K., Ehrhardt, A., Seargent, M., 1999. Agulhas Plateau, SW Indian Ocean: New evidence for excessive volcanism. Geophys. Res. Lett. 26, 1941–1944. https://doi.org/10.1029/1999GL900391

Valentine, J.W., Moores, E.M., 1970. Plate-tectonic Regulation of Faunal Diversity and Sea Level: a Model. Nature 228, 657–659. https://doi.org/10.1038/228657a0

van Hinsberg, V.J., Henry, D.J., Marschall, H.R., 2011. Tourmaline: an ideal indicator of its host environment. Can. Mineral. 49, 1–16. https://doi.org/10.3749/canmin.49.1.1

Varela, R., Basei, M.A.S., Neves, B.B.B., Sato, A.M., Teixeira, W., Cingolani, C.A., Siga, O., 1999. Isotopic study of igneous and metamorphic rocks of Comallo-Paso Flores, Río Negro, Argentina, in: Anales. Presented at the 2 Simposio Sudamericano de Geología Isotópica (Carlos Paz), Servicio Geológico Minero Argentino, Buenos Aires, pp. 148–151.

Verma, S.P., Armstrong-Altrin, J.S., 2013. New multi-dimensional diagrams for tectonic discrimination of siliciclastic sediments and their application to Precambrian basins. Chem. Geol. 355, 117–133. https://doi.org/10.1016/j.chemgeo.2013.07.014

Vernon, R.H., 1979. Formation of late sillimanite by hydrogen metasomatism (base-leaching) in some high-grade gneisses. Lithos 12, 143–152. https://doi.org/10.1016/0024-4937(79)90045-8

von Gosen, W., 2003. Thrust tectonics in the North Patagonian Massif (Argentina): Implications for a Patagonia plate: THRUST TECTONICS IN THE NORTH PATAGONIAN MASSIF. Tectonics

22, 5–33. https://doi.org/10.1029/2001TC901039
von Gosen, W., Loske, W., 2004. Tectonic history of the Calcatapul Formation, Chubut province, Argentina, and the “Gastre fault system.” J. South Am. Earth Sci. - J AMER EARTH SCI 18, 73–88. https://doi.org/10.1016/j.jsames.2004.08.007
Wareham, C.D., Pankhurst, R.J., Thomas, R.J., Storey, B.C., Grantham, G.H., Jacobs, J., Eglington, B.M., 1998. Pb, Nd, and Sr Isotope Mapping of Grenville-Age Crustal Provinces in Rodinia. J. Geol. 106, 647–660. https://doi.org/10.1086/516051
Watson, E.B., Wark, D.A., Thomas, J.B., 2006. Crystallization thermometers for zircon and rutile. Contrib. Mineral. Petrol. 151, 413. https://doi.org/10.1007/s00410-006-0068-5
White, R.W., Powell, R., Clarke, G.L., 2002. The interpretation of reaction textures in Fe-rich metapelitic granulites of the Musgrave Block, central Australia: constraints from mineral equilibria calculations in the system K2O-FeO-MgO-Al2O3-SiO2-H2O-TiO2-Fe2O3: REACTION TEXTURES, MUSGRAVE BLOCK GRANULITES. J. Metamorph. Geol. 20, 41–55. https://doi.org/10.1046/j.0263-4929.2001.00349.x
White, R.W., Powell, R., Holland, T.J.B., 2007. Progress relating to calculation of partial melting equilibria for metapelites. J. Metamorph. Geol. 25, 511–527. https://doi.org/10.1111/j.1525-1314.2007.00711.x
Will, T.M., Frimmel, H.E., Zeh, A., Le Roux, P., Schmädicke, E., 2010. Geochemical and isotopic constraints on the tectonic and crustal evolution of the Shackleton Range, East Antarctica, and correlation with other Gondwana crustal segments. Precambrian Res. 180, 85–112. https://doi.org/10.1016/j.precamres.2010.03.005
Will, T.M., Zeh, A., Gerdes, A., Frimmel, H.E., Millar, I.L., Schmädicke, E., 2009. Palaeoproterozoic to Palaeozoic magmatic and metamorphic events in the Shackleton Range, East Antarctica: Constraints from zircon and monazite dating, and implications for the amalgamation of Gondwana. Precambrian Res. 172, 25–45. https://doi.org/10.1016/j.precamres.2009.03.008
Wingate, M.T.D., Campbell, I.H., Compston, W., Gibson, G.M., 1998. Ion microprobe U–Pb ages for Neoproterozoic basaltic magmatism in south-central Australia and implications for the breakup of Rodinia. Precambrian Res. 87, 135–159. https://doi.org/10.1016/S0301-9268(97)00072-7
Wintsch, R.P., Andrews, M.S., 1988. Deformation induced growth of sillimanite: ’ stress’ minerals revisited. J. Geol. 96, 143–161.
Wolmarans, L.G., Kent, A., 1982. Geological investigations in western Dronning Maud Land, Antarctica, a synthesis. South African Scientific Committee for Antarctic Research.
Wright, W.I., 1938. The composition and ocurrence of garnets. Am. Mineral. 23, 436–449.
Yavuz, F., Karakaya, N., Yıldırım, D.K., Karakaya, M.Ç., Kumral, M., 2014. A Windows program for calculation and classification of tourmaline-supergroup (IMA-2011). Comput. Geosci. 63, 70–87. https://doi.org/10.1016/j.cageo.2013.10.012
Yavuz, F., Kumral, M., Karakaya, N., Karakaya, M.Ç., Yıldırım, D.K., 2015. A Windows program for chlorite calculation and classification. Comput. Geosci. 81, 101–113. https://doi.org/10.1016/j.cageo.2015.04.011
Zane, A., Weiss, Z., 1998. A procedure for classifying rock-forming chlorites based on microprobe data. Rendiconti Lincei 9, 51–56.

Universidade de Brasília

Termo de Autorização para Publicação de Teses e Dissertações Eletrônicas no Repositório Institucional da UnB

1 IDENTIFICAÇÃO

Autor: Mateus Rodrigues de Vargas

RG: 2098112581 | CPF: 017 924 870-70 | Telefone: 51 992032277

E-mail: matvargas@unisinos.br

Afiliação (Instituição de vínculo empregatício): Universidade do Vale do Rio dos Sinos

Orientador: Farid Chemale Junior

Coorientador: —

Título do Trabalho: Estudos Petrológicos do Complexo de Maurice Ewing Bank

Data de Defesa: 17/05/2019 | Área do Conhecimento: Geologia Regional

Palavras-Chave: DSDP Sítio 330; Cráton Kalahari; Ilhas Falkland-Malvinas; Bloco Falkland-Malvinas-Maurice F2MT; Orogenia Natal-Maud; Orogenia Grenville; Supercontinente Rodínia.

Programa/Curso: Programa de Pós-Graduação em Geologia

Titulação: | Agência de Fomento: N/A

Tipo de material: ( ) Tese (V) Dissertação

2 INFORMAÇÃO DE ACESSO AO DOCUMENTO

Liberação para publicação: (V)Total ( )Parcial[1,2,3,4]

Em caso de publicação parcial, especifique os capítulos a serem retidos:

N/A

Observações:

[1] É imprescindível o envio do arquivo em formato digital do trabalho completo, mesmo se tratando de publicação parcial.

[2] A solicitação de publicação parcial deve ser feita mediante justificativa lícita e assinada pelo **autor do trabalho**, que deve ser entregue juntamente com o termo de autorização e documentos que comprovem a necessidade da restrição da parte do conteúdo do trabalho.

[3] A restrição poderá ser mantida por até um ano a partir da data de assinatura deste termo e a extensão deste prazo suscita justificativa formal à BCE e ao DPP.

[4] O resumo e os metadados ficarão sempre disponibilizados (exceções deverão ser devidamente justificadas).

3 LICENÇA DE PERMISSÃO DE USO

Na qualidade de titular dos direitos de autor da publicação, autorizo a Universidade de Brasília e o IBICT a disponibilizar por meio dos *sites* www.unb.br, www.ibict.br, www.ndltd.org sem ressarcimento dos direitos autorais, de acordo com a Lei nº 9610/98, o texto integral da obra abaixo citada, conforme permissões assinaladas, para fins de leitura, impressão e/ou *download*, a título de divulgação da produção científica brasileira, a partir desta data.

Brasília, 17/05/19

Local Data

Vargas

Assinatura do Autor